



**University of Strathclyde**  
Department of Electronic and Electrical Engineering

**Multimedia Services over Wireless Networks**  
**Using OFDM**

By  
**Ahmed Amin Ahmed Solyman**

A thesis presented in fulfilment of the requirements for the degree of  
Doctor of Philosophy

**2013**

# Dedication

---

*Dedicated to*

*My wife and my family for their love and support*

*Ahmed Amin*

# Declaration

---

This thesis is the result of the author's original research. It has been composed by the author and has not been previously submitted for examination which has led to the award of a degree. I have referenced the work of others where appropriate throughout the thesis.

Copyright © 2013 by Ahmed Solyman.

The copyright of this thesis belongs to the author under the terms of the United Kingdom Copyright Acts as qualified by University of Strathclyde Regulation 3.50. Due acknowledgement must always be made of the use of any material contained in, or derived from, this thesis.

# Acknowledgements

---

First of all, great thanks to ALLAH for his continuous support and guidance which without them none of this work would have been accomplished.

I am greatly indebted to my supervisors Prof. John Soraghan and Dr. Stephan Weiss for giving me an excellent opportunity to carry out a very innovating and challenging research. Their assistance and instructions during my time at University of Strathclyde have been invaluable. Prof. Soraghan provided me endless source of thoughts and inspiration. His enthusiasm in research, systematic organisation in work and positive attitude towards life confidently influenced my study and life.

I would like to extend my sincere gratitude to my sponsor, the Egyptian government, through MoD for giving me the opportunity to pursue my PhD in University of Strathclyde.

My deepest and sincere thanks are always to my parents, parent-in-laws, brothers, sisters, brother-in-laws and sister-in-laws for their constant support and prayers. I am so lucky and so proud to have such a wonderful family.

Lastly, and most importantly, I owe my loving thanks to my wife Mona and my sons Adham and Adam without their understanding, endless patience and encouragement it would have been impossible for me to finish this work.

# Abstract

---

This Thesis presents Multimedia systems based on Orthogonal Frequency Division Multiplexing (OFDM) multi carrier modulation system (MCM) architecture and signal processing techniques including discrete fractional Fourier transform (DFrFT), discrete fractional Cosine transform (DFrCT), and equalisation algorithms to mitigate the doubly dispersive channel effect on the OFDM communication systems. Equalisation algorithms are implemented for both the OFDM and the DFrFT orthogonal chirp division multiplexing (OCDM) systems. Mathematical formulae for the equalisation problem in doubly dispersive channel scenario are derived. A multimode system using both the OFDM and the DFrFT-OCDM depending on the communication channel characteristics and the system performance are presented. New low complexity equalisers based on the LSMR iterative algorithm are developed. The performance of these new equalisers is shown to be comparable to conventional low complexity equalisers however they require less complexity. A good improvement in the MCM systems under doubly dispersive channels is gained using the DFrCT transformation as bases for the MCM system with the new low complexity equalisers. Finally, extension to the previous work in multi input multi output (MIMO) is proposed including multi input single output (MISO) Alamouti space time block codes (STBCs), the extended orthogonal STBC (EO-STBC) MISO systems and the MIMO systems with the using of equalisation to improve the overall system performance under doubly dispersive fading channels.

# Contents

---

## Contents

Dedication .....	ii
Declaration .....	iii
Acknowledgements .....	iv
Abstract .....	v
Contents .....	vi
List of Figures .....	xi
List of Tables .....	xiv
Abbreviations .....	xv
List of Symbols .....	xix
<i>1. Introduction</i> .....	<i>1</i>
1.1 Preface .....	1
1.2 Motivation of Research .....	1
1.3 Summary of Original Contributions .....	2
1.4 Thesis Organization .....	3
<i>2. OFDM Fundamentals</i> .....	<i>6</i>
2.1 Introduction .....	6
2.2 OFDM History .....	7
2.3 The Concept of Multicarrier Transmission .....	11
2.4 Signal Orthogonality .....	16
2.4.1 Preliminary Concepts .....	18
2.4.2 Definition of Sub-Carriers .....	19
2.4.3 Mathematical Description of OFDM .....	20

2.5	Cyclic Prefix.....	21
2.5.1	CP Protection against Time Offset .....	22
2.5.2	CP Protection against ISI.....	23
2.5.3	CP effect in equalisation .....	24
2.6	Traditional OFDM Block Diagram.....	24
2.7	OFDM Equalisation .....	25
2.8	Multicarrier Systems based on different Transformations.....	26
2.8.1	Wavelet Transform .....	27
2.8.2	Discrete Cosine transform (DCT).....	30
2.8.3	Discrete Hartley transform (DHT).....	31
2.8.4	Discrete Fractional Fourier Transform (DFrFT) .....	33
2.9	OFDM advantages .....	38
2.9.1	Multipath Delay Spread Tolerance .....	38
2.9.2	Effectiveness against Channel Distortion .....	38
2.9.3	Throughput maximization.....	39
2.9.4	Computational Efficiency .....	40
2.9.5	Frequency Diversity.....	40
2.9.6	Robustness against Narrowband Interference.....	40
2.10	OFDM disadvantage .....	40
2.10.1	Peak to Average Power Ratio (PAPR) .....	41
2.10.2	Frequency offset .....	41
2.10.3	Sensitive to Doppler Shift.....	42
2.11	Examples of OFDM applications.....	42
2.11.1	Digital Audio Broadcasting (DAB-T) .....	43
2.11.2	Terrestrial Digital Video Broadcasting (DVB-T).....	43
2.11.3	Magic WAND.....	43
2.11.4	IEEE802.11a/HIPERLAN2 and MMAC Wireless LAN .....	43
2.11.5	WiMAX (Worldwide interoperability for Microwave Access).....	43
2.12	OFDM System Implementation on Real DSP Board.....	44
2.12.1	Equipment.....	45
2.12.2	Project Overview .....	45
2.13	Conclusion.....	46
3.	Novel MCM Equalisers for Doubly Dispersive Channels.....	47
3.1	Introduction.....	47
3.2	Doubly Dispersive channel .....	47
3.2.1	Rayleigh fading channel model .....	49
3.2.2	Rician fading channel .....	50
3.2.3	Jakes' Model.....	51

3.2.4	Fading Channels with Doppler Effect .....	52
3.3	Communication Channel Equalisation.....	54
3.4	OFDM and DFrFT-OCDM Equalisation Techniques under Doubly Dispersive Fading Channel.....	55
3.4.1	OFDM and DFrFT-OCDM systems under Doubly Dispersive Fading Channel .....	56
3.4.2	Zero Forcing and MMSE Block Equalisers.....	59
3.4.3	Low Complexity Equalisers.....	60
3.5	A Novel Multimode Transmission Method Using OFDM and DFrFT-OCDM .....	60
3.5.1	Performance Analysis .....	63
3.5.2	Multimode Scheme Conclusion.....	65
3.6	Low Complexity Band $LDL^H$ Factorization Equaliser for DFrFT-OCDM. (Linear equaliser).....	65
3.7	Low-Complexity LSMR Equalisation (Linear equaliser).....	69
3.7.1	LSMR Algorithm:.....	70
3.7.2	LSMR Complexity:.....	71
3.7.3	Linear Least Squares LSMR Equaliser.....	72
3.7.4	Regularized Least Squares LSMR Equaliser.....	73
3.7.5	LSMR Equaliser Simulation Results .....	74
3.8	Low Complexity LSMR-based Block Decision Feedback Equaliser (LSMR-BDFE) for DFrFT-OCDM (Nonlinear equaliser). .....	77
3.9	RLS-LSMR Sliding Window Equaliser.....	80
3.10	Conclusion.....	83
4.	Novel Multicarrier System Based on the Discrete Fractional Cosine Transform....	85
4.1	Introduction.....	85
4.2	Fractional Cosine Transform.....	86
4.2.1	Eigenvectors and Eigenvalues of DCT and DST Kernel Matrices.....	86
4.2.2	Properties of DFrCT and DFrST .....	89
4.3	DFrCT-OCDM Bases.....	90
4.4	The DFrCT-OCDM System.....	91
4.5	DFrCT-OCDM System Equalisation and Performance.....	92
4.6	DFrCT-OCDM System Simulation.....	94
4.6.1	DFrCT-OCDM System Performance Using the MMSE Equaliser .....	94

4.6.2	DFrCT-OCDFM System Performance Using the Low complexity $LDL^H$ factorization equaliser .....	96
4.6.3	DFrCT-OCDFM System Performance Using the Low complexity LSMR Equaliser .....	98
4.7	DFrCT-OCDFM PAPR Calculations .....	98
4.7.1	Multicarrier System from the PAPR Point of View .....	99
4.7.2	PAPR Reduction Techniques .....	100
4.7.3	Selection of PAPR Reduction Technique .....	104
4.7.4	PAPR Simulations .....	105
4.8	Multicarrier Systems Based On Different Unitary Transformation Matrices Comparison under Doubly Selective Fading Channel Scenario .....	108
4.9	Conclusion .....	111
5.	MIMO Based DFrCT-OCDFM .....	112
5.1	Introduction .....	112
5.2	MIMO Systems .....	113
5.3	Novel Alamouti MISO STBC System Based on OCDFM Systems .....	114
5.3.1	Low Complexity Banded MMSE Equaliser .....	118
5.4	Space-Time Block Coding (STBC) Scheme Based on OCDFM .....	119
5.5	Proposed Space-Time Decoding .....	121
5.5.1	Open Loop EO-STBC Decoding with Equalisation .....	122
5.6	A Novel MIMO-OCDFM System .....	123
5.6.1	MIMO-OCDFM System Model .....	124
5.6.2	MIMO-OCDFM System Equalisation .....	126
5.6.3	MIMO-OCDFM System with low Complexity Equalisation .....	127
5.7	Simulation and results .....	127
5.7.1	Alamouti MISO OCDFM System Performance .....	127
5.7.2	Multicarrier EO-STBC DFrCT-OCDFM MISO Transceiver System Performance .....	130
5.7.3	MIMO-OCDFM System Performance .....	132
5.8	Conclusion .....	135
6.	Conclusion and Future Work .....	136
6.1	Introduction .....	136
6.2	Conclusion .....	136
	Appendices .....	140
A.	OFDM System Implementation on Real DSP Board .....	140

A.1	Project Overview .....	140
A.2	DSP Implementation.....	150
A.3	System Results .....	157
A.4	Conclusion and Future Work.....	160
Author's Publications.....		162
References.....		164

# List of Figures

---

Fig. 2.1 Received OFDM signal in the frequency domain .....	7
Fig. 2.2 The Multi-Carrier concept .....	12
Fig. 2.3 First setup block diagram for multicarrier transmission.....	14
Fig. 2.4 Second setup block diagram for multicarrier transmission .....	15
Fig. 2.5 OFDM Signal in Time and Frequency Domain.....	17
Fig. 2.6 The cyclic prefix .....	22
Fig. 2.7 Function of the guard period for protecting against ISI and time Offset.....	23
Fig. 2.8 OFDM Block diagram .....	25
Fig. 2.9 The DWT-MCM transceiver model .....	28
Fig. 2.10 DCT-MCM subcarriers.....	31
Fig. 2.11 DHT-MCM Subcarriers.....	32
Fig. 2.12 Signal $xt$ at different transformation angle $\alpha$ .....	34
Fig. 2.13 The DFrFT-OFDM system with a complicated equaliser .....	36
Fig. 2.14 DFrFT-OCDM basis for the 1 <sup>st</sup> and the 20 <sup>th</sup> basis signals.....	37
Fig. 2.15 Spectral Energy Distribution for the 1 <sup>st</sup> and the 20 <sup>th</sup> basis signals .....	37
Fig. 2.16 the Wigner distribution for the 1 <sup>st</sup> basis signal and the 20 <sup>th</sup> basis signal.....	37
Fig. 2.17 The Adaptive bit loading. ....	39
Fig. 2.18 OFDM communication system equipment.....	44
Fig. 2.19 OFDM communication system overview .....	45
Fig. 3.1 Rayleigh and Rician distributions.....	51
Fig. 3.2 Rayleigh fading with a maximum Doppler shift of 10 Hz .....	53
Fig. 3.3 Rayleigh fading with a maximum Doppler shift of 100 Hz. ....	53
Fig. 3.4 General time-domain linear equaliser.....	55
Fig. 3.5 OFDM Block diagram .....	57
Fig. 3.6 DFrFT-OCDM System Block diagram.....	58
Fig. 3.7 DFrFT-OCDM and OFDM Subcarriers .....	61
Fig. 3.8 DFrFT-OCDM and OFDM Multimode System .....	62
Fig. 3.9 Multimode OFDM and DFrFT-OCDM System with $\alpha$ Selection.....	62
Fig. 3.10 OFDM and DFrFT-OCDM BER comparison in time invariant channel environment.....	64
Fig. 3.11 OFDM and DFrFT-OCDM BER comparison in time variant channel environment.....	64
Fig. 3.12 The desired structure for the band matrix $B$ inside the whole matrix $H\alpha$ .....	66
Fig. 3.13 Bit error ratio for MMSE equalisation using block ( $Q = Na = 96$ ) and low- complexity ( $Q = 5$ ) approaches for DFrFT-OCDM ( $\alpha = 0.2\pi 2$ ) and OFDM .....	68
Fig. 3.14 Percentage of power of $H\alpha$ contained in $Bn$ , measured by $Q$ in dependence of the number of off-diagonal elements $Q$ considered by $M$ , comparing OFDM and DFrFT- OCDM ( $\alpha = 0.2\pi 2$ ).....	68

Fig. 3.15 LSMR Algorithm flow chart.....	70
Fig. 3.16 DFrFT-OCDM and DFT-OFDM Uncoded BER Comparison (Q=5) .....	74
Fig. 3.17 Uncoded BER Comparison between LSMR , LSQR ,ZF.....	75
Fig. 3.18 Uncoded BER Comparison between BMMSE, LSQR and LSMR equalisers .	76
Fig. 3.19 BDFE Structure.....	78
Fig. 3.20 DFrFT-OCDM and DFT-OFDM Uncoded BER Comparison (Q = 5) .....	79
Fig. 3.21 RLS-LSMR sliding window equaliser and the Banded MMSE equaliser BER Comparison (Q = 5).....	82
Fig. 3.22 DFrFT-OCDM and OFDM Uncoded BER Comparison using the RLS-LSMR sliding window equaliser.....	83
Fig. 4.1 DFrCT, DFrFT-OCDM with $\alpha = 0.95\pi/2$ and DFT-OFDM Subcarrier 2 .....	90
Fig. 4.2 The DFrCT-OCDM system with a Complicated equaliser .....	92
Fig. 4.3 DFrCT-OCDM System Block diagram .....	93
Fig. 4.4 The BER Comparison between DFrCT, DFrFT-OCDM and OFDM .....	95
Fig. 4.5 The BER Comparison between DFrCT-OCDM and OFDM using the <i>LDLH</i> factorization equaliser .....	95
Fig. 4.6 Percentage of power of $H\alpha$ contained in $B$ , measured by $pQ$ in dependence of the number of off-diagonal elements $Q$ considered by $M$ , comparing OFDM, DFrFT-OCDM and DFrCT-OCDM transmission.....	96
Fig. 4.7 The BER Comparison between DFrCT -OCDM and OFDM using the RLS-LSMR equaliser .....	97
Fig. 4.8 A Block Diagram of The Multicarrier System Transmitter.....	99
Fig. 4.9 A block diagram of the SLM technique.....	102
Fig. 4.10 PTS block diagram.....	104
Fig. 4.11 PAPR performance of DFrCT-OCDM, DFrFT-OCDM and the OFDM system without PAPR reduction with QPSK at sub carriers, $\alpha = 0.25$ , and the number of sub carriers (a) $N = 32$ , (b) $N = 64$ and (c) $N = 128$ .....	106
Fig. 4.12 PAPR performance of DFrCT-OCDM and OFDM systems without PAPR reduction.....	107
Fig. 4.13 PAPR reduction performance of DFrCT-OCDM, DFrFT-OCDM and the OFDM systems with and without SLM - PAPR reduction.....	107
Fig. 4.14 MCM System Block diagram .....	109
Fig. 4.15 The BER performance comparison between OFDM, DCT-MCM, DHT-MCM, DFrFT-OCDM and DFrCT-OCDM; MCM systems using MMSE equalize .....	110
Fig. 5.1 The Alamouti coded OCDM system .....	115
Fig. 5.2 An example of a fractional-domain doubly dispersive channel matrix $N = 35$ .....	117
Fig. 5.3 An example of a fractional-domain doubly dispersive banded channel matrix $B$ with $N = 35$ .....	117
Fig. 5.4 An example of a fractional-domain doubly dispersive banded channel matrix after permutation $B\mathcal{P}$ with $N = 35$ .....	118
Fig. 5.5 EO-STBC in a multicarrier configuration with equivalent multicarrier channel matrices $U_i, n, i = 0 \dots 3$ , and beamsteering by rotations $\phi_n$ and $\theta_n$ which are based	

feedback from the transmitter and can maximize the diversity and array gain of this system.....	120
Fig. 5.6 The MIMO-OCDM system .....	124
Fig. 5.7 Uncoded BER Comparison for the classical Alamouti space-time coded OFDM system with time invariant and time variant channels .....	128
Fig. 5.8 Uncoded BER Comparison for the classical Alamouti space-time coded OFDM system with different Alamouti STBC systems based on OFDM, DFrFT and DFrCT-OCDM using MMSE equaliser under time variant channel .....	129
Fig. 5.9 Uncoded BER Comparison for different Alamouti space-time coded systems based on OFDM, DFrFT and DFrCT-OCDM using low complexity MMSE equaliser.....	130
Fig. 5.10 BER Comparison of the multicarrier EO-STBC system based on OCDM and classical OFDM with block equalisation .....	131
Fig. 5.11 BER Comparison of the multicarrier EO-STBC system based on OCDM and classical OFDM with banded equalisation $Q = 12$ .....	131
Fig. 5.12 The MIMO system performance with 2 transmit antennas and 3 receive antennas using MMSE equaliser.....	133
Fig. 5.13 BER Comparison between the MIMO and SISO DFrCT-OCDM system with 2 transmit antennas and 3 receive antennas using MMSE equaliser .....	133
Fig. 5.14 The MIMO system performance with 2 transmit antennas and 3 receive antennas using banded low complexity MMSE equaliser .....	134
Fig. A.1 OFDM System Implementation.....	140
Fig. A.2 OFDM communication system overview .....	141
Fig. A.3 Signal Constellations Of The Modulation Schemes BPSK, QPSK and 16QAM. ....	142
Fig. A.4 The cyclic prefix .....	143
Fig. A.5 Upsampling and pulse shaping. ....	144
Fig. A.6 Synchronization using correlation between the training sequence and the matched filter output. ....	146
Fig. A.7 The training sequence correlation output.....	147
Fig. A.8 The Constellation points angles changes with time.....	148
Fig. A.9 The Adaptive bit loading.....	149
Fig. A.10 PING/PONG Buffering.....	153
Fig. A.11 Buffer handling at the receiver .....	154
Fig. A.12 Transmitter and Receiver flow chart.....	156
Fig. A.13 Data to send.....	157
Fig. A.14 The root raise cosine filter Impulse response. ....	157
Fig. A.15 The synchronization signal (Sin wave).....	158
Fig. A.16 The Feedback data with sin for synchronization and the bit allocation.....	158
Fig. A.17 Transmitter training sequence.....	158
Fig. A.18 1 <sup>st</sup> data frame from the transmitter.....	159
Fig. A.19 Received data.....	159

# List of Tables

---

Table 3.1 <i>Storage and computational requirements for various LS methods</i> .....	72
--------------------------------------------------------------------------------------	----

# Abbreviations

---

ADSL	Asymmetric Digital Subscriber Lines
AWGN	Additive White Gaussian Noise
BDFE	Block Decision Feedback Equaliser
BER	Bit Error Rate
BMMSE	Banded MMSE
CCDF	Complementary Cumulative Distribution Function
CDMA	Code Division Multiple Access
CG	Conjugate Gradient
CIR	Channel Impulse Response
CLT	Central Limit Theorem
COFDM	Coded OFDM
CP	Cyclic Prefix
CSI	Channel State Information
DAB	Digital Audio Broadcasting
DCT	Discrete Cosine Transform
DF	Decision-Feedback
DFrCT	Discrete Fractional Cosine Transform
DFrCT	Discrete Fractional Cosine Transform
DFrFT	Discrete Fractional Fourier Transform
DFrHT	Discrete Fractional Hartley Transform

DFrST	Discrete Fractional Sine Transform
DFT	Discrete Fourier Transform centre
DHT	Discrete Hartley Transform
DMT	Discrete Multi-Tone
DTTB	Digital Terrestrial Television Broadcasting
DVB	Digital Video Broadcasting
DVB-C	Cable Systems DVB
DVB-H	Digital Video Broadcasting Handheld Devices
DVB-S	Satellite TV DVB
DVB-T	Terrestrial Transmissions DVB
DWT	Discrete Wavelet Transform
EO-STBC	Extended Orthogonal STBC
ETSI	European Telecommunications Standards Institute
FDM	Frequency Division Multiplexing
FEC	Forward Error Correction
FFT	Fast Fourier Transform
FIR	Finite Impulse Response Filter
FLOPS	Floating-Point Operations Per Second
FPGA	Field programmable gate array
FrCT	Fractional Cosine Transform
FrST	Fractional Sine Transform
HDSL	High Bit-Rate Digital Subscriber Line
HIPERMAN	High-Performance Metropolitan Area Networks
HPF	High Path Filter

ICI	Inter-Carrier Interference
IDFrCT	The Inverse Fractional Cosine Transform
IDFT	The Inverse Discrete Fourier Transform
IDWT	The Inverse Discrete Wavelet Transform
IFFT	Inverse FFT
iid	Independent And Identically Distributed
IIR	Infinite Impulse Response Filter
ISI	Inter-Symbol Interference
JML	Joint Maximum-Likelihood
LLS	Linear Least Squares
LOS	Line Of Sight
LPF	Low Path Filter
LS	Least-Squares
LSMR	least-square MINRES iterative algorithm
LTE	Long-Term Evolution, Marketed As 4G LTE
MAC	Media Access Control
Magic WAND	Magic Wireless ATM Network Demonstrator
MC-CDMA	Combination Of OFDM And Code Division Multiple Access
MCM	Multicarrier Modulation
MIMO	Multi Input Multi Output
MISO	Multi Input Single Output
MMSE	Minimum Mean-Square Error
MRC	Maximum-Ratio Combining
MSE	Mean Square Error

NLOS	Non-Line Of Site
OCDM	Orthogonal Chirp Division Multiplexing
OFDM	Orthogonal Frequency Division Multiplexing
OFDMA	Orthogonal Frequency Division Multiple Access
PAPR	Peak-To-Average Power Ratio
pdf	Power Density Function
PLC	Power Line Communications
PTS	Partial Transmit Sequence
QoS	Quality Of Service
RLS	Regularized Least Squares
SFNs	Single-Frequency Networks
SIMO	Single-Input Multi Output
SISO	Single-Input Single-Output
SLM	Selected Mapping Technique
SNR	Signal-To-Noise Ratio
STBCs	Space Time Block Codes
TDM	Time Division Multiplexing
TDMA	Time Division Multiple Access
UWB	Ultra Wide Band
WiMAX	(Worldwide Interoperability For Microwave Access)
ZF	Zero-Forcing

# List of Symbols

---

$T_S$	Symbol duration
$\tau$	Channel delay spread
$N$	Number of sub-channels
$B$	Signal bandwidth
$\varepsilon$	Roll off factor
$\tau_m$	Channel delay spread
$R_b$	Bit rate
$M$	Single carrier modulation scheme index
$f_{d \max}$	Maximum Doppler frequency
$c$	Coherency factor
$K$	Number of parallel sub-streams
$\mathbf{g}(t)$	Baseband transmission pulse
$f_k$	The $k^{th}$ sub-carrier frequency
$\mathbf{s}_{kl}$	The complex modulation symbol
$k$	The frequency index
$l$	The time index
$\mathbf{s}(t)$	The complex baseband signal
$f_0$	DC in the complex baseband
$f_c$	The centre frequency in the passband

$\mathbf{g}_k(t)$	The $k^{th}$ pulse shape
$\mathbf{s}_k(t)$	The $k^{th}$ subcarrier sinusoid waveform
$T$	Time sampling period
$A_n(t)$	The $n^{th}$ subcarrier amplitude
$\omega_n$	Angular frequency of the $n^{th}$ subcarrier
$\phi_n(t)$	Phase shift of the $n^{th}$ subcarrier
$T$	The time sampling period
$T_G$	The length of the guard period in samples
$T_{FFT}$	The OFDM data frame time correspond to the size of the IFFT
$\mathbf{r}_n$	The received sequence
$\mathbf{H}$	The $N \times N$ channel matrix
$\mathbf{F}$	The DFT matrix
$\mathbf{F}^*$	The IDFT matrix
$\mathbf{d}_n$	The transmitted data vector in the $n^{th}$ OFDM symbol
$\mathbf{z}_n$	White Gaussian noise in the time domain
$\tilde{\mathbf{r}}_n$	Received sequence after demodulation with the DFT
$\mathbf{F}_\alpha$	Discrete Fractional Fourier Transform
$\alpha$	The fractional angle
$K_\alpha(t, u)$	The transformation kernel of the continuous FrFT
$p$	Order of the chirp period
$T_p$	Chirp period
$F_p$	Chirp frequency
$\mathbf{F}_\alpha$	The DFrFT transformation matrix

$F_{-\alpha}$	The IDFrFT transformation matrix
$X_n(t), Y_n(t)$	Reflected signals orthogonal components
$Z$	The circularly symmetric complex Gaussian random variable
$\sigma^2$	Variance of the circularly symmetric complex Gaussian random variable
$I_o(\cdot)$	The modified Bessel function of the first kind and zero order
$K$	The Rician $K$ factor
$f_n$	The Doppler shift on ray $n$ in Jakes' model
$f_d$	The Doppler shift
$\Phi_n$	Angles where the scatters signals is uniformly distributed around a circle at it.
$N$	Number of the scatters signals
$R(t, k)$	The Rayleigh fading of the $k^{th}$ waveform over time $t$
$\phi, \beta_n$ and $\theta_{n,k}$	Jakes' model parameters
$\Delta v$	The velocity difference between the transmitter and the receiver
$C$	The speed of light
$f_c$	The signal carrier frequency
$W(t)$	Time-domain equaliser impulse response
$h(t)$	The channel impulse response
$s(t)$	Transmitted signal
$z(t)$	Added noise signal
$r(t)$	Received signal
$\hat{d}(t)$	Estimated data
$E\{ \}$	Expectation

$\varepsilon$	Mean-square error
$\mathbf{d}_n$	The data vector in the $n^{th}$ OFDM symbol
$\mathbf{P}$	Permutation matrix
$N_a$	Active subcarriers
$\mathbf{0}_{L \times M}$	$L \times M$ matrix with zero entries
$\mathbf{s}_n$	Transmitted vector in the $n^{th}$ OFDM symbol
$\mathbf{h}(n, v)$	The doubly dispersive channel impulse response
$\mathbf{H}$	The doubly dispersive channel (time-variant, circular) convolution matrix
$L$	Cyclic prefix
$N_h$	The maximum delay spread
$\mathbf{r}_n$	The received samples for the $n^{th}$ ofdm symbol after discarding the CP
$\mathbf{z}_n$	Samples of white Gaussian noise
$\mathbf{y}$	The received signal after demodulation by the DFT matrix
$\hat{\mathbf{d}}_n$	The estimated data vector
$\tilde{\mathbf{H}}$	Frequency domain channel matrix
$\tilde{\mathbf{z}}$	The noise vector in the frequency domain
$\mathbf{W}_n$	The equaliser matrix
$\mathbf{U}_{n,\alpha}$	The system matrix in the fractional domain
$\tilde{\mathbf{r}}_n$	The demodulated received samples
$\tilde{\mathbf{z}}$	The noise vector in the frequency domain
$\tilde{\mathbf{H}}_\alpha$	The channel matrix in the fractional domain
$\tilde{\mathbf{H}}_\alpha^H$	The channel matrix conjugate transpose in the fractional domain

$\hat{\mathbf{d}}_{ZF}$	Estimated data using ZF equaliser
$\hat{\mathbf{d}}_{MMSE}$	Estimated data using MMSE equaliser
$\mathbf{I}_{N_A}$	The identity $N_a \times N_a$ matrix
$\gamma$	The signal-to-noise ratio (SNR)
$\tilde{\mathbf{H}}_\alpha^+$	The Moore-Penrose pseudo-inverse of the channel matrix in the fractional domain
$\Delta f$	Subcarrier spacing
$\mathbf{M}$	Binary masking matrix
$Q$	The number of the first sub- and super-diagonals
$\mathbf{B}_n$	The masked equaliser matrix
$\mathbf{W}_{n,MMSE}$	The MMSE equaliser
$\rho[Q]$	The ratio between the power components in the original system matrix $\tilde{\mathbf{H}}_\alpha$ and in the reduced matrix $\mathbf{B}_n$ after masking.
$\mathbf{F}_F$	Decision Feedback Equaliser feed-forward filter
$\mathbf{F}_B$	Decision Feedback Equaliser feedback filter
$\mathbf{e}$	The error vector between the estimated and actual data vector
$\mathbf{R}_{ee}$	The autocorrelation matrix of the error vector $\mathbf{e}$
$\sigma^2$	The noise variance
$\mathbf{L}$	The lower triangular matrix with unit diagonal in the $LDL^H$ algorithm
$\mathbf{D}$	The diagonal matrix in the $LDL^H$ algorithm
$\mathbf{B}_{n,k}$	The matrix which is part of the equivalent banded system matrix $\mathbf{B}_n$ with $P \times K$ size
$P$	The width of the sliding window matrix

$\mathbf{C}_\alpha(u)$	The fractional cosine transform (FrCT)
$\mathbf{S}_\alpha(u)$	The fractional sine transform (FrST)
$\mathbf{C}_{N,\alpha}$	The $N$ -point DFrCT kernel
$\mathbf{C}_\alpha$	The unitary $N \times N$ DFrCT matrix
$\mathbf{C}_{-\alpha}$	The unitary $N \times N$ IDFrCT matrix
$\gamma$	PAPR threshold
$\mathbf{C}_l(s)$	The output of the clipping function
$W$	The number of allowed phase factors in the PTS PAPR reduction algorithm
$\mathbf{F}_\alpha$	Can be any unitary transformation matrix
$\mathbf{s}_1, \mathbf{s}_2$	Are any two successive OCDM symbols
$\mathbf{r}_1, \mathbf{r}_2$	The received signals in two successive OCDM symbol periods
$\mathbf{H}_{i,j}$	The time domain channel matrix between transmit antenna $i$ and the receive antenna in symbol time $j$
$\mathbf{B}_{i,j}$	The $(N \times N)$ channel banded matrices
$\mathbf{B}$	A $2 \times 2$ block matrix of $\mathbf{B}_{i,j}$ $(N \times N)$ banded matrices
$\mathcal{P}$	The permutation matrix which is $2N \times 2N$ matrix
$\mathbf{B}_{\mathcal{P}}$	The permuted banded fractional domain channel matrix
$\mathbf{d}_{\mathcal{P}}$	The data from the same subcarriers of different transmit antennas are grouped together
$\mathbf{Y}_{\mathcal{P}}$	Received signals after permutation
$\mathbf{s}_{i,n}, i = 0 \dots 3$	The MCM transmit symbols emitted from the four antennas
$\phi_n, \theta_n$	The phase rotations to subcarriers
$\mathbf{U}_{i,n}$	The equivalent multicarrier channel model

$\underline{\mathbf{d}}$	The all data vectors transmitted from different antennas
$\tilde{\mathbf{H}}$	The combination of all channel matrices between different antennas
$\underline{\mathbf{r}}$	The combination of all received signals between different antennas
$\underline{\mathbf{z}}$	The combination of all added noise signals between different antennas
$\mathbf{C}_{\mathbf{O}_{zz}}$	MIMO noise covariance
$\mathcal{P}_{(M,N)}$	The permutation matrix
$\mathcal{R}$	The permuted received vector in MIMO
$\mathcal{H}$	The permuted fractional MIMO channel matrix
$\mathbf{d}$	The permuted data vector in MIMO.
$\mathbf{z}$	The permuted noise vector in MIMO
$\mathbf{I}_{M_R \times M_T}$	The Identity matrix with $M_R \times M_T$ elements
$\mathcal{M}$	The MIMO masking matrix
$\mathcal{B}_{(Q)}$	The banded version of the fractional MIMO channel matrix
$\mathcal{W}_{n,MMSE}$	The MIMO MMSE equaliser matrix

# 1. Introduction

---

## 1.1 Preface

Digital Video Broadcasting (DVB) is a European multimedia communication broadcasting standard. The system is based on a transmission of audio/video stream from the MPEG-2 family, using orthogonal frequency deviation multiplexing (OFDM) modulation which is a multicarrier modulation system (MCM) system. OFDM is a well-known modulation scheme for wideband digital communications which in the last few decades has become the most adopted modulation scheme of modern digital communications scenarios such as wireless networking and broadband Internet access. Since the first OFDM-based standard in 1995, ETSI Digital Audio Broadcasting standard Eureka by ETSI, the number of systems adopting OFDM has rapidly increased due to the system ability to cope with severe multipath fading channels and the presence of severe interference caused by Single-Frequency Networks (SFNs). Furthermore OFDM has excellent demodulation performance, spectral efficiency, low complexity and simple channel equalisation. Although the benefits of OFDM were known from 1960s, OFDM popularity these days come from the low-cost digital signal processing components that efficiently calculate the Discrete Fourier Transform (DFT). Consequently the OFDM is affected by different types of interference and communication channel scenarios that may cause system performance degradation.

## 1.2 Motivation of Research

The aim of this thesis is to explore new signal processing techniques which can be used to improve the MCM systems performance and reduce the system complexity under doubly dispersive fading channels.

The objectives of the research presented in this thesis are twofold. The first objective is to develop new low complexity equalisers for the MCM systems to solve the

problem of inter carrier interference under doubly dispersive fading channel scenario due to subcarriers losing orthogonality. The second objective is to investigate the MCM systems bases under doubly dispersive fading channels and searching for new bases that can improve the overall system performance

The thesis will address the enhancements, modifications, and inventions required to improve the MCM systems performance using new signal processing techniques while avoiding as much as possible any additional complexity or increase in the computational cost.

### **1.3 Summary of Original Contributions**

The research detailed in this thesis includes original contributions to the field of multimedia communication and MCM systems under high speed movement of the transmitter and/or the receiver which forms doubly dispersive channels. These contributions are as follows:

- 1- A new multimode system based on the classical OFDM and the discrete fractional Fourier transform orthogonal chirp division multiplexing (DFrFT-OCDFM) is implemented which can switch between both of them to improve the system performance under time invariant and time variant channels. The performance enhancements using the multimode system are presented and the enhancement in the probability of error at different SNR's are also described.
- 2- A low complexity equaliser is proposed for the use with the DFrFT-OCDFM system which reduces the system complexity and preserves good performance with respect to the OFDM system.
- 3- A new low complexity equaliser based on the LSMR iterative algorithm is developed that handle the MCM systems equalisation complexity resulting from the need for large channel matrix inversion that arises in doubly dispersive channel scenarios. The technique is based on the use of the LSMR iterative algorithm to solve the matrix inversion iteratively. The relative performance of the new low complexity equaliser method over traditional

based methods is assessed using simulation for a range of environments. The proposed equaliser configuration succeeds in reducing the equalisation system complexity without degrading the overall system performance. Different low complexity equaliser schemes based on the LSMR algorithm are proposed and investigated.

4- A new basis for the MCM systems is proposed that is adopted from the DFrCT transformation for the modulation and demodulation process. The new DFrCT-OCDM system offers a solution to the inter-carrier interference problem resulting from the fading channel frequency variation due to the Doppler effect as the new chirp bases can cope with the channel frequency variation to reduce its effect. The DFrCT-OCDM system performance is assessed using simulation for a doubly dispersive channel scenario and the probability of error with multi signal to noise ratios is shown. The proposed system improves the overall system performance without increasing the system complexity.

5- A new Alamouti space time block codes (STBC), a new extended orthogonal STBC (EO-STBC) and a new MIMO system based on both new equalisers and chirp bases is developed that offers a solution to the classical versions of the previously presented MIMO techniques against the doubly dispersive channel scenarios. The proposed system configuration is shown to reduce the channel effect over the MIMO systems. The new system is shown to improve the MIMO systems performance without increasing the MIMO system complexity.

## **1.4 Thesis Organization**

The remainder of this thesis is divided into five chapters (excluding this chapter), as follows:

Chapter 2 provides an overview of OFDM systems in order to introduce the classical MCM system which will be used throughout the thesis. It starts with the OFDM

history and the concept of multicarrier transmission is then presented. Later on in this chapter, the mathematical model for the basic OFDM system is investigated. There after the Cyclic prefix (CP) which is important part in the OFDM system is reviewed, followed by OFDM equalisation. MCM systems that are based on transformations other than the Fourier transform are investigated next. Later on The OFDM system advantage, disadvantage and applications are listed, and finally last part of this chapter presents the OFDM system implementation on a DSP board.

Chapter 3 presents the equalisation problem for the MCM systems under doubly dispersive fading channels. A review of the doubly dispersive channels is presented, followed by a review on communication channel equalisation. OFDM and DFrFT-OCDFM equalisation techniques under doubly dispersive fading channel algorithms and formulation are also discussed. A novel multimode transmission method using OFDM and DFrFT-OCDFM is presented and a set of simulation results are presented for different channel scenarios. Low complexity band  $LDL^H$  factorization equaliser is presented for the DFrFT-OCDFM and a novel low complexity set of equalisers based on the LSMR algorithm is proposed with their formulation and simulation results.

Chapter 4 introduces new bases for the MCM systems based on the DFrCT transform with the aim of overcoming the MCM systems inter-carrier interference (ICI) problem under doubly dispersive fading channel problem. Section 4.2 reviews the fractional cosine transform and its properties. Section 4.3, 4.4 and 4.5 propose the novel DFrCT-OCDFM system bases, structure and equalisation respectively. Section 4.6 proposes a set of simulation results that present the DFrCT-OCDFM system performance with different equalisers. Section 4.7 presents the peak to average power ratio (PAPR) problem and its effect on the MCM systems with set of simulation to investigate the PAPR for both DFrFT and DFrCT-OCDFM systems. Finally in section 4.8 a simulation is carried to investigate the different MCM systems performance under doubly dispersive channel scenario. Section 4.9 concludes the chapter.

Chapter 5 presents an extension for the DFrCT-OCDFM systems to the MIMO systems including Alamouti STBC, EO-STBC and the classical MIMO systems. Section 5.2 introduces the historical background for the MIMO systems. In section 5.3 a novel

Alamouti STBC system based on OCDM systems and low complexity equaliser are presented. Section 5.4, 5.5 presents collaborative work on open loop EO-STBC with OCDM systems and low complexity equalisers. In section 5.6 a novel MIMO-OCDM system based on OCDM systems is proposed. A simulation set for the Alamouti STBC, EO-STBC and the MIMO systems is presented in section 5.7. Finally the chapter conclusion is stated in section 5.8.

Chapter 6 presents the conclusions of this thesis, along with a discussion for suggestion of potential areas and further future work.

The appendices contain some detailed theoretical material and calculations which would impede the flow of the thesis. A list of the author's publications resulting from the research undertaken in this thesis is also provided.

# 2. OFDM Fundamentals

---

## 2.1 Introduction

Wireless channels can limit the communication system capacity and performance due to the multipath propagation problem in them which will result in frequency selective fading. The fundamental problem of these wireless channels is how to share the common transmission medium with many mobile and stationary users (multiple access) in order to accommodate as many users as possible with good quality of service (QoS). This is not an easy task because the frequency spectrum allocation is limited. As wireless communications have experienced great success and are widely used, the demands for good quality and variety of services have increased. To fulfil these desires, development for high speed wireless communication systems has been investigated. Using single carrier systems cannot achieve high-data-rate transmission over delay-dispersive channels. One successful approach to achieve reliable and efficient high speed data transmission is the OFDM.

OFDM is a multicarrier modulation scheme that has been widely adopted in wireless communication especially for a very high-data-rate transmission over delay-dispersive channels. It allows digital data to be efficiently and reliably transmitted over a radio channel even in multipath environments. If only a single frequency band (single carrier) is used, then the symbol duration ( $T_S$ ) has to be very small in order to achieve the required data rate, when symbol duration  $T_S$  is not larger than the channel delay spread ( $\tau$ ), inter-symbol interference (ISI) occurs and the communication systems will not be able to achieve good system performance. Moreover, a very small symbol duration has a very long bandwidth, thus requires a complicated equaliser (mathematically expensive) with a large number of taps at the receiver and increases the computational effort [1, 2].

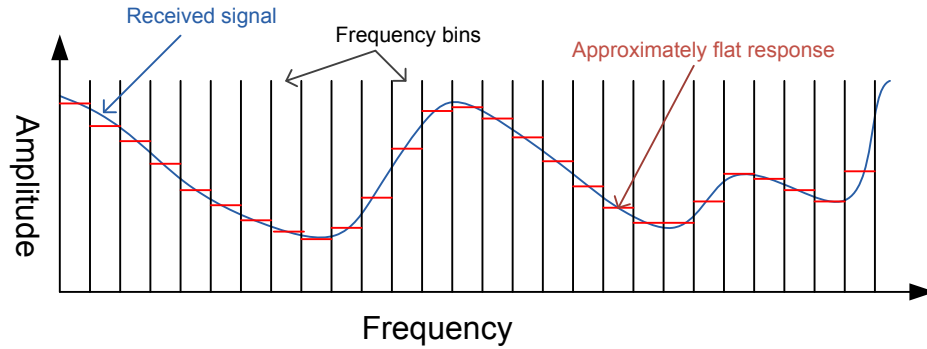


Fig. 2.1 Received OFDM signal in the frequency domain

OFDM converts the high data rate stream into a number of low- data-rate streams (sub-channels)  $N$  and modulates each one of the low-data-rate streams over one of the sub-channels. These are then transmitted at the same time keeping the total desired data rate constant, with the property that each of the sub-channels has  $T_S \gg \tau$  and hence effectively ISI-free channels and the multipath fading channel can be seen as flat fading channel for each subcarrier (sub-channels experience relatively flat fading) as shown in Fig. 2.1. The sub-channels are orthogonal under ideal propagation condition. Moreover ISI can be completely eliminated through the use of a cyclic prefix.

This chapter provides an overview of OFDM, an introduction to OFDM history in 2.2, the basic principles of multicarrier transmission in 2.3, the mathematical basics of the OFDM signal and how it can be generated and received in 2.4, 2.5, 2.6, OFDM equalisation is considered in 2.7, a survey of other multicarrier systems based on different transformation-bases are listed in 2.8, advantages, disadvantage and applications of OFDM transmission are discussed in 2.9, 2.10, 2.11. OFDM system implementation on a DSP board in 2.12. Finally the chapter conclusion in 2.13.

## 2.2 OFDM History

OFDM can be viewed as a collection of single carrier transmission techniques combined together and transmitted in the same time. When this technique is applied in a wireless environment, it is referred to as OFDM. In the wired environment, such as asymmetric digital subscriber lines (ADSL), it is referred to as discrete multi-tone

(DMT). In OFDM, each carrier is orthogonal to all other carriers, a condition that is not always maintained in DMT. OFDM is an optimal version of MCM transmission schemes.

The origins of OFDM development may be traced back to the 1950's [1] with the introduction of Frequency Division Multiplexing (FDM) for data communications in early telephone lines. FDM divides the channel bandwidth into sub-channels and transmits multiple relatively low rate signals by carrying each signal on a separate carrier frequency. Guard-bands are left between the different sub-channels to ensure elimination of the ISI and separation between sub-channels, which led to bandwidth inefficiency. In 1966 Chang patented the structure of OFDM [3] and published the concept of using orthogonal overlapping multi-tone signals for data communications. The concept of using parallel data transmission was illustrated by Salzberg in 1967 [4]. In 1970 and 1971, Darlington [5] and Weinstein [6] introduced the idea of using a DFT concept in the generation and reception of OFDM signals, and eliminating the requirement for banks of analogue sub-carrier oscillators. This presented an opportunity for a more achievable implementation of OFDM, especially with the use of Fast Fourier Transform (FFT), which is an efficient implementation of the DFT. This suggested that the easiest implementation of OFDM is with the use of an Field programmable gate array (FPGA) or a Digital Signal Processor (DSP), which can implement FFT algorithms. It is only recently that the advances in integrated circuit technology have made the implementation of OFDM cost effective. In the 1980s, the OFDM technique was developed for high-speed modems, digital mobile communications, and high density recording.

Peled and Ruiz in 1980 introduced Cyclic Prefix (CP) that solves the orthogonality issue [7]. They filled the guard space with a cyclic extension of the OFDM symbol with the assumption that the CP is longer than the delay spread of the channel. In 1985, Cimini described the use of OFDM for mobile communications [8]. It was not until the late 1980's that work began on the development of OFDM for commercial use, with the introduction of the Digital Audio Broadcasting (DAB) system, which was the first commercial use of OFDM technology [9]. In 1987 Alard & Lasalle introduced

Coded OFDM (COFDM) for digital broadcasting [10]. COFDM is OFDM that makes use of interleaving and forward error correction (FEC) coding for protection of data against errors. Generally, convolutional coding was used for error correction. Development of DAB started in 1987 and services began in U.K and Sweden in 1995. DAB is a replacement for FM audio broadcasting, by providing high quality digital audio and information services. OFDM was used for DAB due to its multipath tolerance. Multipath is a major problem as it causes extensive ghosting of the transmitted signal. This ghosting causes ISI blurring the time domain signal.

For single carrier transmissions, the effects of ISI can be mitigated using adaptive equalisation. This process uses adaptive filtering to approximate the impulse response of the radio channel. An inverse channel response filter is then used to recombine the blurred copies of the symbol bits. This process is however complicated and slow due to the time needed by the adaptive equaliser to reach it's optimum values. Additionally it becomes difficult to equalize signals that suffer ISI of more than a couple of symbol periods.

OFDM overcomes the effects of multipath by breaking the signal into many narrow bandwidth carriers as shown in Fig. 2.1 with long symbol time which the amount of ISI. In addition to this, a guard period is added to the start of each symbol, removing the effects of ISI for multipath signals delayed less than the guard period (which will be discussed in details in section 2.5). The high tolerance to multipath makes OFDM more suited to high data transmissions in terrestrial environments than single carrier transmissions.

Doppler spread is a phenomenon caused by rapid changes in the channel response due to movement of the transmitter/receiver through a multipath environment which is also known as a doubly selective channel response. It results in random frequency modulation of the OFDM sub-carriers, leading to system performance degradation. The amount of Doppler spread is proportional to the transmission frequency and the velocity of movement. The closer the sub-carriers are spaced together, the more susceptible the OFDM signal is to Doppler spread, thus a trade-off exists between the amount of multipath protection (length of the guard period) which is

bandwidth inefficient and the Doppler spread tolerance which is needed to reduce the Doppler spread effect.

For traditional FM broadcasting, neighbouring cities must use different RF frequencies even for the same radio station, to prevent multipath causes by re-broadcasting at the same frequency. However, with DAB it is possible for the same signal to be broadcast from every area requiring coverage, eliminating the need for different frequencies to be used in neighbouring areas [11, 12]. The development of the Digital Video Broadcasting (DVB) standards started in 1993 [11, 13]. DVB is a transmission scheme of high quality compressed digital audio and video. It is an enhanced replacement of the analogue television broadcast standard, as DVB provides a flexible transmission medium for the delivery of video, audio and data services [11, 14]. The DVB standards specify the delivery mechanism for a wide range of applications, including satellite TV (DVB-S), cable systems (DVB-C) and terrestrial transmissions (DVB-T) [15]. The physical layer of each of these standards is optimized according to the transmission channel.

In 1999, the IEEE 802.11 committee on wireless LANs released the 802.11a standard for OFDM operation in the 5GHz ISM band. In 2002, the IEEE 802.16 committee released an OFDM-based standard for wireless broadband access for metropolitan area networks under revision 802.16a. The IEEE 802.11 committee in 2003 released the 802.11g standard for operation in the 2.4GHz band. The multiband OFDM standard for ultra wideband was developed, showing OFDM's usefulness in low-SNR systems.

In 1997, searching for new multicarrier modulation basis started to overcome some of the OFDM multicarrier system disadvantages. Alan R. Lindsey proposed the Wavelet packet modulation for orthogonally multiplexed communication [16], and in the same year, Chatonda J. Mtika and Ramakrishna Nunna proposed the Wavelet transform as the basis for a multicarrier modulation scheme [17] to overcome the ISI problem. In 1998, S. Attallah and J.E.M. Nilsson proposed the Discrete Cosine Transform (DCT) transformation as a novel basis for multicarrier modulation [18] to improve the system frequency bandwidth. In 2000, Chin-Liang Wangt proposed the Discrete Hartley

transform as a new basis for multicarrier modulation [19] to reduce system complexity. In 2001, Martone proposed the Fractional Fourier transform (FrFT) as a new basis for a multicarrier system [20] to increase the system resistance to doubly dispersive fading channels as the new FrFt basis can cope with the fading channel frequency variations .

In the same period around 2000, other research started to improve the OFDM performance under different channel conditions. In 1999, Jean Armstrong [21] studied the methods of reducing inter-carrier interference due to carrier frequency offset in OFDM. Won Gi Jeon proposed a new equaliser for time-variant multipath channels [22]. In 2004, Schniter [23] proposed a low complexity equaliser for doubly selective channels.

From 2004 to 2007, further revisions to 802.16a were made and completed in 2004. This revised standard, IEEE 802.16-2004, replaces 802.16, 802.16a, and 802.16c with a single standard, which has also been adopted as the basis for high-performance metropolitan area networks (HIPERMAN) by the European Telecommunications Standards Institute (ETSI). In 2003, the 802.16 group began work on enhancements to the specifications to allow vehicular mobility applications. That revision, 802.16e, was completed in December 2005 and was published formally as IEEE 802.16e-2005. It specifies scalable OFDM for the physical layer and makes further modifications to the media access control (MAC) layer to accommodate high-speed mobility [15, 24].

### **2.3 The Concept of Multicarrier Transmission**

Most multi-access techniques like time division multiple access (TDMA) and code division multiple access (CDMA) become problematic at very high data rates due to the use of a single frequency band (single carrier frequency) which lead to a very small symbol duration  $T_S$  and the system bandwidth becomes very large [2].

Consider a digital transmission scheme with linear carrier modulation (e.g. MPSK or M-QAM) and a symbol duration denoted by  $T_S$ . Let  $B$  be the occupied bandwidth. Typically,  $B$  is of the order of  $T_S^{-1}$ , for example,  $B = (1 + \varepsilon)T_S^{-1}$  for raised-cosine pulses with a roll off factor  $\varepsilon$ . For a transmission channel with a delay spread  $\tau$ , a reception free of ISI is only possible if the condition:

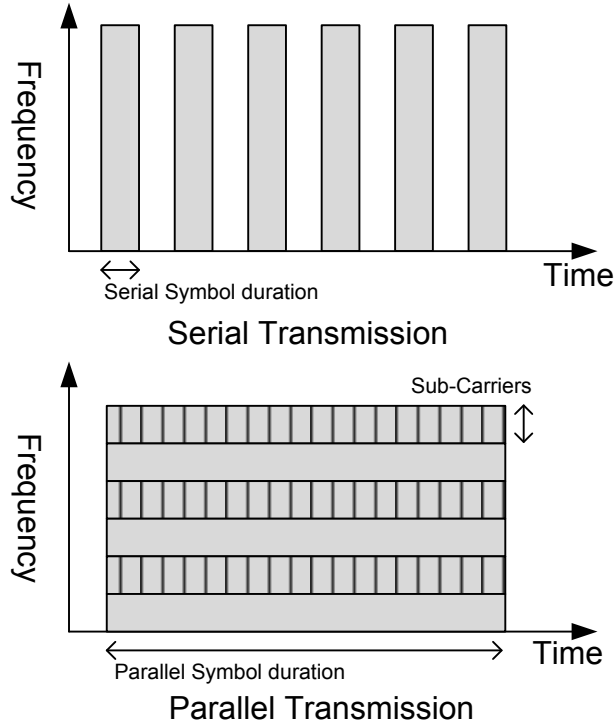


Fig. 2.2 The Multi-Carrier concept

$$\tau \ll T_S \quad (2.1)$$

is fulfilled. As a consequence, the possible bit rate is given by:

$$R_b = \log_2 (M) T_S^{-1} \quad (2.2)$$

for a given single carrier modulation scheme which is limited by the delay spread of the channel where  $M$  is the single carrier modulation index. The simple idea of multicarrier transmission to overcome this limitation is to split the data stream into  $N$  substreams of lower data rate and transmit these data substreams on adjacent subcarriers.

In Fig. 2.2, for  $N = 6$ , it can be regarded as a parallel transmission in the frequency domain, and it does not affect the total bandwidth that is needed. Each subcarrier has a bandwidth  $B/N$ , while the symbol duration  $T_S$  is increased by a factor of  $N$ , which allows for  $N$  times higher data rate for a given delay spread. The factor  $N$ , however, cannot be increased arbitrarily, because too long symbol durations make the

transmission too sensitive against the time incoherence of the channel that is related to the maximum Doppler frequency  $f_{d\max}$ [25], where it is stated that the condition:

$$f_{d\max} T_S \ll 1 \quad (2.3)$$

must be fulfilled. Both conditions in (2.1) and (2.3) can only be valid simultaneously if the coherency factor  $c = f_{d\max} \tau$  fulfils the condition  $c \ll 1$  for a given and sufficiently small factor  $c$ . There exists a symbol duration  $T_S$  that satisfies both requirements together to give the best possible transmission conditions for that channel. This optimal symbol duration may be chosen to match the channel and parallelize the given data stream in an appropriate way.

There are two possible setups to look at and implement this idea of multicarrier transmission. Both are equivalent with respect to their transmission properties. Even though mathematically closely related, they differ slightly from the conceptual point of view. The first setup emphasizes the multicarrier concept by having  $N$  individual carriers that are modulated independently [25]. The second setup, on the other hand, is based on a filter bank of  $N$  adjacent bandpass filters that are excited by a parallel data stream, leading to a transmission parallel in frequency. This concept is usually implemented in practical systems. The first concept keeps the sub-carrier frequency fixed and considers the modulation in the time direction for each sub-carrier. The second one keeps a time slot of length  $T_S$  fixed and considers modulation in the frequency direction for each time slot.

In the first setup, the data stream is split up into  $N$  parallel substreams, and each one is modulated on its own sub-carrier at frequency  $f_n$  in the complex baseband, described by the complex harmonic wave  $e^{j2\pi f_n t}$ . The complex (e.g. M-PSK or M-QAM) modulation symbol is denoted by  $d_{n,k}$ , where  $n$  is the frequency index and  $k$  is the time index. With a baseband transmission pulse  $g(t)$ , this setup can be visualized in Fig. 2.3. The parallel data stream excites replicas of the same pulse-shaping filter  $g(t)$ , and the filtered signals are modulated on the different carriers and summed up before transmission. The complex baseband signal is then given by the expression:

$$s(t) = \sum_n e^{j2\pi f_n t} \sum_k d_{n,k} g(t - kT_S) \quad (2.4)$$

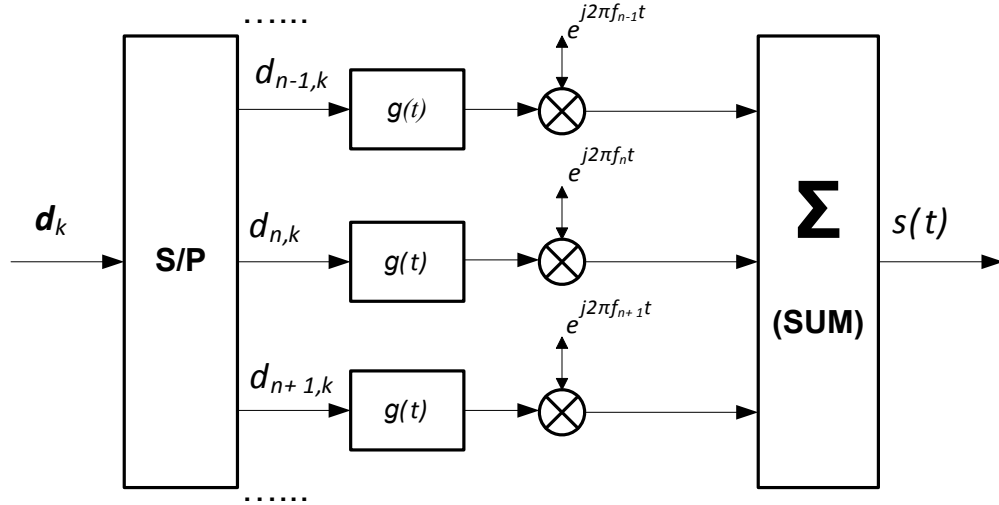


Fig. 2.3 First setup block diagram for multicarrier transmission

where  $T_S$  is the parallel symbol duration. To keep the notation flexible, the domain of the summation indices is not specified. If it is convenient, the time index  $k$  may run from zero or minus infinity to infinity. Since every real transmission starts and stops at some time instant, it is more realistic to let  $k$  run from 0 to  $K - 1$ , where  $K$  is an integer. The frequency index may only run over a limited domain of  $N$  different frequencies. From the mathematical point of view,  $n = 0, 1, \dots, N - 1$ . However, it would be preferred to have  $f_0$  in the middle, corresponding to DC in the complex baseband and to the centre frequency  $f_c$  in the passband, with negative  $n$  for the lower sideband and positive  $n$  for the upper sideband. For reasons of symmetry, the number of carriers will be chosen to be  $N + 1$ , where  $N$  is an even integer, and let  $n = 0, \pm 1, \pm 2, \dots, \pm N/2$ .

For implementation reasons, in practical systems, the DC component will sometimes be left empty, that is, only the subcarriers at  $n = \pm 1, \pm 2, \dots, \pm N/2$  are used. In the second setup, a base transmit pulse  $g(t)$  will be used. The frequency-shifted replicas of this pulse will be:

$$g_n(t) = g(t)e^{j2\pi f_n t} \quad (2.5)$$

that is, if  $g(t) = g_0(t)$  is located at the frequency  $f = 0$ , then  $g_n(t)$  is located at  $f = f_n$ . In contrast to the first setup, for each time instant  $k$ , the set of  $N$  (or  $N + 1$ )

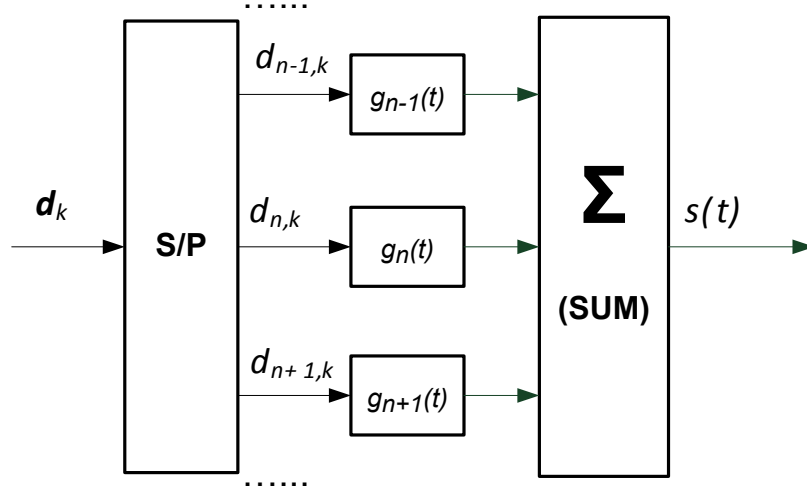


Fig. 2.4 Second setup block diagram for multicarrier transmission

modulation symbols is transmitted by using different pulse shapes  $g_n(t)$ , the parallel data stream excites a filter bank of  $N$  (or  $N + 1$ ) different bandpass filters. The filter outputs are then summed up before transmission. This setup is depicted in Fig. 2.4. The transmitted signal in the complex baseband representation is given by:

$$s(t) = \sum_k \sum_n d_{n,k} g_n(t - kT_S) \quad (2.6)$$

For the domain of the summation indices  $n$  and  $k$ , the same remarks apply as for the discussion of the first setup. By defining:

$$g_{n,k}(t) = g_n(t - kT_S) = e^{j2\pi f_n(t - kT_S)} g(t - kT_S) \quad (2.7)$$

to get the compact expression:

$$s(t) = \sum_{n,k} d_{n,k} g_{n,k}(t) \quad (2.8)$$

It is obvious that if the modulation symbol  $d_{n,k}$  is replaced by  $d_{n,k} e^{-j2\pi f_n(kT_S)}$  in (2.4), this leads to the first setup. Such a time-frequency-dependent phase rotation does not change the performance, so both methods can be regarded as equivalent. However, the second (the filter bank) point of view is closer to implementation, especially for the case of OFDM, where the filter bank is just an FFT.

## 2.4 Signal Orthogonality

Signals are orthogonal if they are mutually independent of each other. Orthogonality is a property that allows multiple information signals to be transmitted perfectly over a common channel and detected without interference. Loss of orthogonality results in blurring between these information signals and degradation in communications [1]. Many common multiplexing schemes are inherently orthogonal.

Time division multiplexing (TDM) allows transmission of multiple information signals over a single channel by assigning unique time slots to each separate information signal. During each time slot, only the signal from a single source is transmitted preventing any interference between the multiple information sources. Because of this, TDM is orthogonal in nature. In the frequency domain, most FDM systems are orthogonal as each of the separate transmission signals are well spaced out in frequency preventing interference.

Although these methods are orthogonal, the term OFDM has been reserved for a special form of FDM. The subcarriers in an OFDM signal are spaced as close as is theoretically possible, while maintaining orthogonality between them [26].

One of the basic fundamentals to understand OFDM is the orthogonality of different sinusoids. Sine and Cosine waves form one of the most basic orthogonal pairs. Mathematically speaking, an orthogonal signal is in 90 degree phase shift to the other signal. However, in communication, two periodic signals are orthogonal when the integral of their product, over one period, is equal to zero. This is true of certain sinusoids for the continuous time and discrete time, respectively, as illustrated in (2.9) and (2.10):

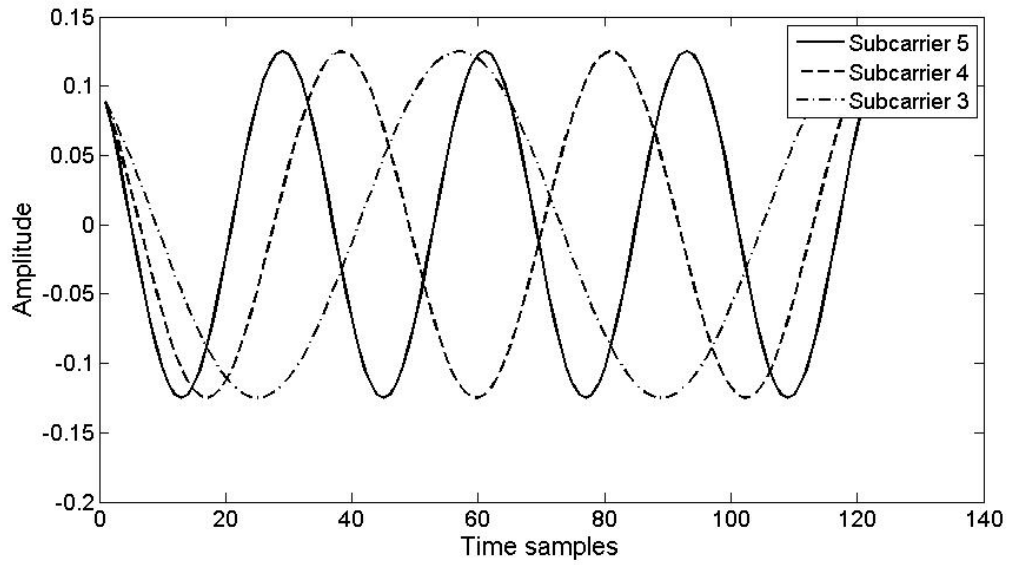
*Continuous Time*

$$\int_0^T \cos(2\pi n\Delta ft) \cos(2\pi m\Delta ft) dt = 0 \quad (n \neq m) \quad (2.9)$$

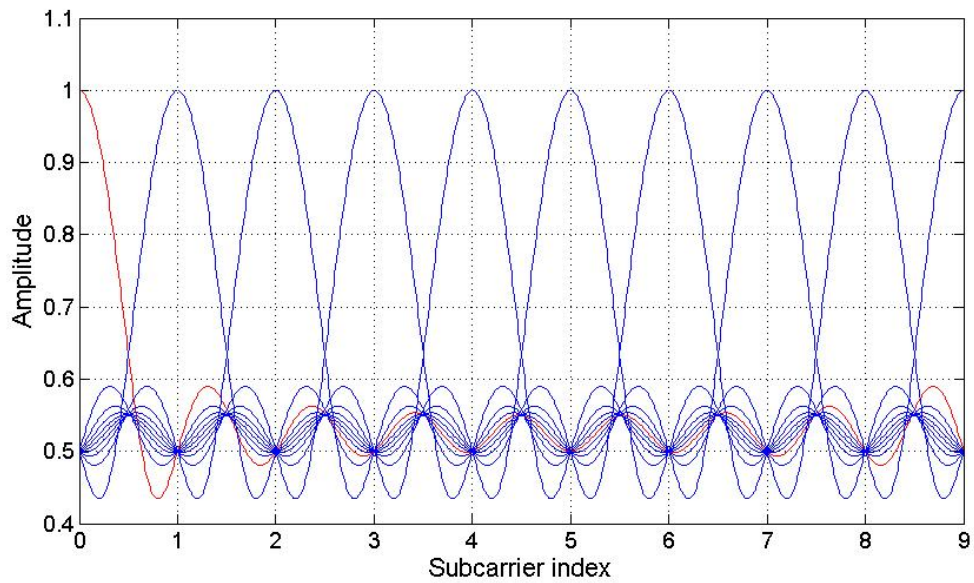
*Discrete Time*

$$\sum_0^{N-1} \cos\left(\frac{2\pi kn}{N}\right) \cos\left(\frac{2\pi km}{N}\right) = 0 \quad (n \neq m) \quad (2.10)$$

where  $k, m$  and  $n$  are integers.



(a)



(b)

Fig. 2.5 OFDM Signal in Time and Frequency Domain

If information signals are loaded into two orthogonal, carriers they do not interfere with each other. To maintain orthogonality between the two carriers, it is necessary to ensure that the symbol time contains one or multiple cycles of each sinusoidal tone waveform [27]. The carriers of an OFDM system are sinusoids that meet

this requirement because each one is a multiple of a fundamental frequency. Each one has an integer number of cycles in the fundamental period, as shown in Fig. 2.5.

OFDM achieves orthogonality in the frequency domain by allocating each of the separate information signals onto different subcarriers. Due to this, the spectrum of each carrier has a null at the centre frequency of each of the other carriers in the system, as shown in Fig. 2.5(a) and Fig. 2.5(b). This results in no interference between the carriers, allowing them to be spaced as close as theoretically possible. OFDM signals are made up from a sum of sinusoids, each corresponding to a subcarrier.

The baseband frequency of each subcarrier is chosen to be an integer multiple of the inverse of the symbol time, resulting in all subcarriers having an integer number of cycles per symbol.

$$s_n(t) = \begin{cases} \sin(2\pi n \Delta f t) & 0 \leq t \leq T_S, \\ 0 & \text{otherwise} \end{cases} \quad n = 1, 2, \dots, N \quad (2.11)$$

where  $\Delta f$  is the carrier spacing,  $T_S$  is the symbol period and  $s_n(t)$  is the  $n^{\text{th}}$  subcarrier sinusoid waveform. In (2.11),  $\sum_1^N s_n(t)$  is a set of orthogonal sinusoids which represent the subcarriers for an un-modulated real OFDM signal. Since the highest frequency component is  $N \Delta f$  the transmission bandwidth is also  $N \Delta f$ .

### 2.4.1 Preliminary Concepts

When the DFT of a time signal is taken, the frequency domain results are a function of the time sampling period  $T$  and the number of samples  $N$ . The fundamental frequency of the DFT is equal to  $1/NT$  (1/total sample time). Each frequency represented in the DFT is an integer multiple of the fundamental frequency. The maximum frequency that can be represented by a time signal sampled at rate  $1/T$  is  $f_{max} = 1/2T$  as given by the *Nyquist sampling theorem*. This frequency is located in the centre of the DFT points. All frequencies beyond that point are images of the representative frequencies. The maximum frequency bin of the DFT is equal to  $(1/T - 1/NT)$  [2].

The inverse discrete Fourier transform (IDFT) performs the opposite operation to the DFT. It takes a signal defined by frequency components and converts them to a time

signal. The parameter mapping is the same as for the DFT. The time duration of the IDFT time signal is equal to the number of DFT bins  $N$  times the sampling period  $T$ .

It is perfectly valid to generate a signal in the frequency domain, and convert it to a time domain equivalent for practical use. This is how modulation is applied in OFDM. In practice FFT and inverse FFT (IFFT) are used in place of the DFT and IDFT.

#### 2.4.2 Definition of Sub-Carriers

The maximum number of sub-carriers used by OFDM is limited by the size of the IFFT. This is determined as follows:

$$N_{Carriers} \leq \frac{IFFT_{size}}{2} - 2 \quad (\text{real - valued time signal}) \quad (2.12)$$

$$N_{Carriers} \leq \frac{IFFT_{size}}{2} - 1 \quad (\text{complex - valued time signal}) \quad (2.13)$$

In order to generate a real-valued time signal, OFDM (frequency) sub-carriers must be defined in complex conjugate pairs, which are symmetric about the Nyquist frequency ( $f_{max}$ ). This makes the number of potential carriers equal to the  $IFFT_{size}/2$ . The Nyquist frequency is the symmetry point, so it cannot be part of a complex conjugate pair. The DC component also has no complex conjugate. These two points cannot be used as carriers so they are subtracted from the total available.

If the carriers are not defined in conjugate pairs, then the IFFT results in a time domain signal that has imaginary components. This must be a viable option as there are OFDM systems defined with carrier counts that exceed the limit for real-valued time signals given in (2.8). Further processing requires quadrature technique. The complex time waveform in (2.8) has all IFFT bins available as carriers except the DC bin.

Both IFFT size and assignment (selection) of carriers can be dynamic. The transmitter and receiver have to use the same parameters. This is one of the advantages of OFDM over banked filters. OFDM bandwidth usage (and bit rate) is varied according to varying user requirements. A simple control message from a base station can change a mobile unit's IFFT size and carrier selection to match the channel variation and improving the system performance.

### 2.4.3 Mathematical Description of OFDM

OFDM transmits a large number of narrowband subcarriers closely spaced in the frequency domain. In order to avoid a large number of modulators and filters at the transmitter and complementary filters and demodulators at the receiver, DSP techniques, such as FFT are used.

Mathematically, each OFDM symbol can be described as a complex wave[26]:

$$s(t) = \frac{1}{N} \sum_{n=0}^{N-1} A_n(t) e^{j[\omega_n t + \phi_n(t)]} \quad (2.14)$$

where,  $\omega_n = \omega_0 + n\Delta\omega$  and  $\omega_0 = 2\pi f_0$ . If the waveform of each component is considered over one symbol period, then the variables  $A_n(t)$  and  $\phi_n(t)$  take on fixed values, which depend on the frequency of that particular carrier, and so  $A_n(t)$  and  $\phi_n(t)$  can be rewritten:

$$\begin{aligned} A_n(t) &\rightarrow A_n \\ \phi_n(t) &\rightarrow \phi_n \end{aligned} \quad (2.15)$$

If the signal is sampled using a sampling frequency of  $1/\Delta T$ , then the resulting signal is represented by:

$$s(k\Delta T) = \frac{1}{N} \sum_{n=0}^{N-1} A_n e^{j[(\omega_0 + n\Delta\omega)kT + \phi_n]} \quad (2.16)$$

At this point, we have restricted the time over which we analyse the signal to  $N$  samples. It is convenient to sample over the period of one data symbol. Thus, the time sampling period  $T$  is calculated from (2.14):

$$T = N\Delta T \quad (2.17)$$

without a loss of generality by letting  $\omega_0 = 0$ , then the signal becomes:

$$s(k\Delta T) = \frac{1}{N} \sum_{n=0}^{N-1} A_n e^{j\phi_n} e^{j(n\Delta\omega)kT} \quad (2.18)$$

Now, (2.16) is compared with the general form of the IFFT:

$$g(kT) = \frac{1}{N} \sum_{n=0}^{N-1} G\left(\frac{n}{N\Delta T}\right) e^{j2\pi nk/N} \quad (2.19)$$

where  $G(\frac{n}{N\Delta T})$  is the frequency domain representation of the time domain  $g(kT)$  signal. In (2.16), the function  $A_n e^{j\theta_n}$  is no more than a definition of the signal in the sampled frequency domain, and  $s(k\Delta T)$  is the time domain representation. Equations (2.16) and (2.18) are equivalent if:

$$\Delta f = \frac{\Delta\omega}{2\pi} = \frac{1}{N\Delta T} = \frac{1}{T} \quad (2.20)$$

This is the same condition that was required for orthogonality, thus one consequence of maintaining orthogonality is that the OFDM signal can be defined by using Fourier transform procedures.

## 2.5 Cyclic Prefix

The symbol rate for an OFDM signal is much lower than a single carrier transmission scheme using the same system bandwidth. For example for a single carrier BPSK modulation, the symbol rate corresponds to the bit rate of the transmission. However for OFDM the system bandwidth is broken up into  $N$  sub-carriers, where  $N$  is the number of sub-carriers in the system, resulting in a symbol rate that is  $N$  times lower than the single carrier transmission. This low symbol rate makes OFDM naturally resistant to effects of ISI caused by multipath propagation [7].

Multipath propagation is caused by the radio transmission signal reflecting off objects in the propagation environment, (such as walls, buildings, mountains... etc.). These multiple signals arrive at the receiver at different times due to the transmission distances being different. This spreads the symbol boundaries causing energy leakage between them. The effect of ISI on an OFDM signal can be further reduced by the addition of a guard period to the start of each symbol. This guard period is a cyclic copy that extends the length of the symbol waveform. Let's consider one subcarrier without a CP which is equal to the length of the IFFT size used to generate the signal, which contains an integer number of cycles. This way of encapsulating the CP results in a continuous signal, with no discontinuities at the joints. Thus by copying the end of a symbol and appending this to the start results in a longer symbol time. Fig. 2.6 shows the insertion of a guard period.

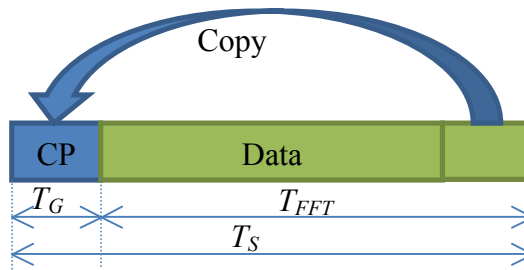


Fig. 2.6 The cyclic prefix

The total length of the symbol is  $T_S = T_G + T_{FFT}$ , where  $T_S$  is the total length of the symbol in samples,  $T_G$  is the length of the guard period in samples, and  $T_{FFT}$  is the time of the data frame which correspond to the size of the IFFT used to generate the OFDM signal. In addition to protecting the OFDM from ISI, the guard period also provides protection against time-offset errors in the receiver.

### 2.5.1 CP Protection against Time Offset

To decode the OFDM signal, the receiver has to take the FFT of each received symbol and work out the phase and amplitude of the sub-carriers. For an OFDM system that has the same sample rate for both the transmitter and receiver, it must use the same FFT size at both receiver and transmitter in order to maintain sub-carrier orthogonality. Each received symbol occupies a time interval equal to  $T_G + T_{FFT}$  due to the added guard period as shown in Fig. 2.6. The receiver only needs the samples received during the  $T_{FFT}$  period of the received symbol to decode the signal. The remaining samples during the time  $T_G$  are redundant. For an ideal channel with no delay spread, the receiver can pick any time offset up to the length of the guard period and still get the correct number of samples without crossing a symbol boundary [12]. Because of the cyclic nature of the guard period, changing the time offset simply results in a phase rotation of all the sub-carriers in the signal. The amount of this phase rotation is proportional to the sub-carrier frequency, with a subcarrier at the Nyquist frequency changing by  $180^\circ$  for each sample time offset. Provided the time offset is held constant from symbol to symbol, the phase rotation due to a time offset can be removed as part of the channel equalisation.

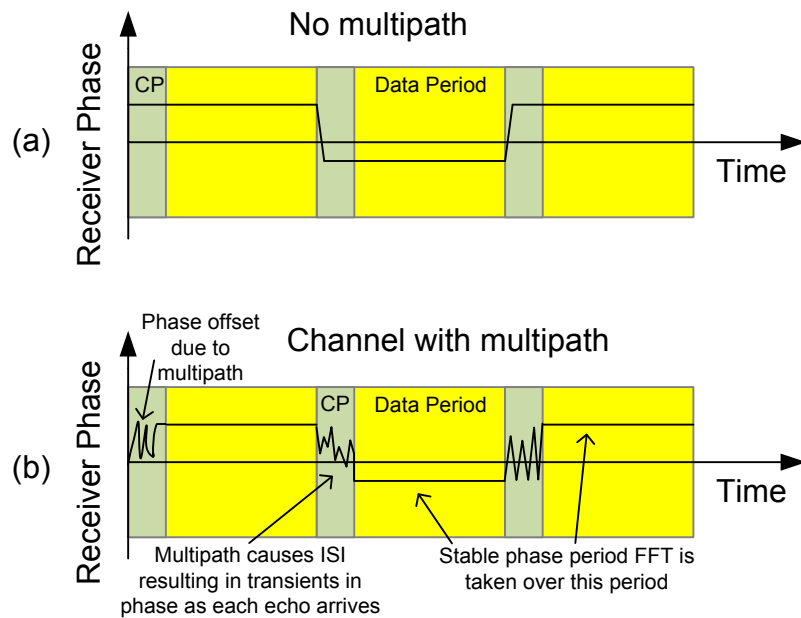


Fig. 2.7 Function of the guard period for protecting against ISI and time Offset

### 2.5.2 CP Protection against ISI

In an OFDM signal, the amplitude and phase of the sub-carrier must remain constant over the period of the symbol in order for the sub-carriers to maintain orthogonality. If they are not constant, it means that the spectral shape of the subcarriers will not have the correct sinc shape, and thus the nulls will not be at the correct frequencies, resulting in inter-carrier interference (ICI). At the symbol boundary, the amplitude and phase change to the new value required for the next data symbol. In multipath environments, ISI causes spreading of the energy between the symbols, resulting in transient changes in the amplitude and phase of the sub-carrier at the start of the symbol. The length of these transient effects corresponds to the delay spread of the radio channel. The transient signal is a result of each multipath component arriving at slightly different times, changing the received sub-carrier vector. Fig. 2.7 shows this effect. Adding a guard period allows time for the transient part of the signal to decay, so that the FFT is taken from a steady state portion of the symbol. This eliminates the effect of ISI provided that the guard period is longer than the delay spread of the radio channel.

The remaining effects caused by multipath, such as amplitude scaling and phase rotation are corrected by channel equalisation.

As shown in Fig. 2.7, the guard period protects against transient effects due to multipath and removes the effects of ISI as long as it is longer than the channel delay spread. This example shows the instantaneous phase of a single carrier for 3 symbols. The addition of a guard period removes most of the effects of ISI. However, in practice, multipath components tend to decay slowly with time, resulting in some ISI even when a relatively long guard period is used.

### **2.5.3 CP effect in equalisation**

The CP has a great effect in OFDM system equalisation. Choosing the CP to be the last part of the OFDM symbol and inserting it in the first part makes it feasible to transfer the multipath frequency fading channel matrix into a circulant matrix that can be diagonalized by an FFT at the receiver side. The diagonalized channel matrix can be compensated using a single tap equaliser which can be considered as a simple multiplication with gain and phase components. This will be elaborated more in section 2.7.

## **2.6 Traditional OFDM Block Diagram**

The block diagram of the OFDM system is shown in Fig. 2.8. The binary stream is modulated to symbols in the modulator functional block. The data is separated into streams that equal the amount of subcarrier channels. This is the serial to parallel functional. Each sub-carrier is assigned some data to transmit. The required amplitude and phase of the carrier is then calculated based on the modulation or mapping scheme (typically BPSK, QPSK, or QAM). It then transforms this spectral representation of the data into the time domain using the IFFT block. The separate parallel data streams are placed back into a serial data stream. The cyclic extension function block adds a cyclic extension, which is a copy of a number of subcarriers at the end of the OFDM symbol. This copy is placed at the start of the symbol. The signal is converted to an analogue signal using D/A block and up-converted to the required frequency for transmission.

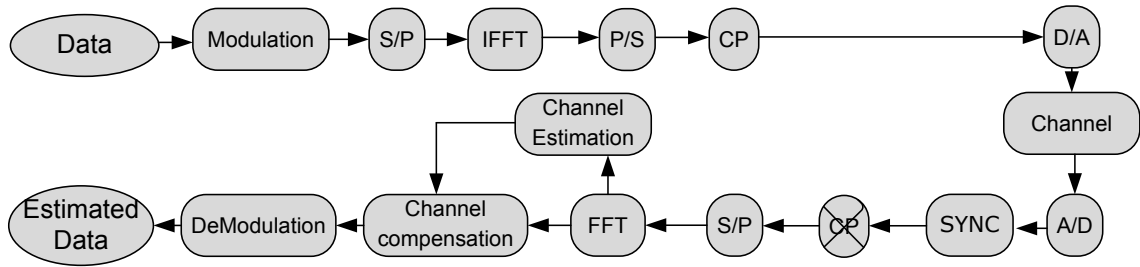


Fig. 2.8 OFDM Block diagram

The signal becomes corrupted after the channel and the purpose of the receiver is to extract the useful information from it. At the other side of the radio channel, the receiver processes the received signal, and converts it back to its original form.

The receiver needs to adjust these imperfections prior to signal demodulation using the synchronization function block. Together with the synchronized signal and the timing signals, the CP is removed. Following the CP removal function block, the serial data stream is split into parallel data streams. The number is equal to the number of subcarrier channels as in the transmitter. The data streams are demodulated from OFDM symbols using the FFT function block. The resultant symbols are converted back into a serial signal stream where the channel estimation starts. Using the estimated channel the equalisation process starts. The signal is converted to a binary stream in the demodulation function block so the resultant estimated data is now back to its original form.

## 2.7 OFDM Equalisation

Single carrier communication systems suffer from time-invariant frequency selective multipath channels, thus the need for a complicated equaliser arises to preserve QoS with an accepted probability of error. On the other hand, OFDM with CP can compensate the time invariant multipath channel effect using a single tap equaliser.

Let's consider the communication system in Fig. 2.8, with a block by block processing over a linear time-invariant frequency selective noisy channel. The received symbols are given by

$$\mathbf{r}_n = \mathbf{H} \mathbf{F}^* \mathbf{d}_n + \mathbf{z}_n \quad (2.21)$$

where  $\mathbf{r}_n$  is the received sequence and  $\mathbf{H}$  is the  $N \times N$  channel matrix,  $N$  is the number of subcarriers,  $\mathbf{F}$  is the DFT matrix and  $\mathbf{F}^*$  is the IDFT matrix,  $\mathbf{d}_n$  is the transmitted data vector in the  $n^{\text{th}}$  OFDM symbol and  $\mathbf{z}_n$  is a white Gaussian noise in the time domain. After demodulation, using DFT the received vector is given by:

$$\tilde{\mathbf{r}}_n = \mathbf{F}\mathbf{H}\mathbf{F}^*\mathbf{d}_n + \mathbf{F}\mathbf{z}_n \quad (2.22)$$

as  $\mathbf{H}$  is circulant matrix (because of the cyclic prefix),  $\mathbf{F}\mathbf{H}\mathbf{F}^*$  becomes a diagonal matrix [28] and we can equalize the received signal by simple adjustment of the phase and amplitude for the received sequence [29].

This property is one of the main advantage of OFDM as it simplifies the equalisation process in a multipath fading channel, which is a harsh environment and needs a very complicated equalisers [30]. However, this property is valid only in time-invariant frequency selective multipath channels [31].

When there is a frequency offset in the receiver [32], or the channel is doubly selective, that is, time-frequency-selective [33-36], this traditional methodology fails because the DFT cannot diagonalise the channel matrix anymore and inter-carrier interference (ICI) appears. In this situation, OFDM needs a complicated equaliser [22, 30]. More details about OFDM equalisation in Chapter 3.

## 2.8 Multicarrier Systems based on different Transformations

MCM techniques based on the Discrete Fourier Transform (DFT) have proven to be effective for the optimization of the transmission performance over channels with moderate or severe ISI and ICI [31, 35, 37]. Such techniques have received great attention in communication systems design as the modulation/demodulation scheme in several digital communications standards. These include wire-line standards such as ADSL, which offer several megabits of data transmission per second on ordinary phone lines, and wireless standards such as DAB/DVB, IEEE 802.11a/g/n, and IEEE802.16a/e.

Due to different applications, channel scenarios and system complexity capabilities, many researchers tried to find another basis for MCM systems. Recently, the Wavelet transform was proposed as a basis for MCM systems [38-40] due to its flexibility and good bandwidth efficiency resulting from higher suppression of the side

lobes. The DCT transform has also been proposed as a basis for MCM systems [18, 41, 42]. The DCT bases have a very good energy concentration and spectral compaction, which eliminates ICI. DCT uses real arithmetic, which reduces the computational complexity and the DSP circuit's power consumption. Discrete Hartley transform (DHT) was proposed in [19, 43, 44] to benefit from real-valued computation of the DHT, which reduces the computational complexity over the DFT.

The DFT based MCM system cannot deal with doubly selective channels, which are common in mobile communications. Martone and others were motivated by this scenario [20, 45], to introduce the Discrete Fractional Fourier Transform (DFrFT) as a basis for MCM systems in doubly selective channel scenarios. Investigation of all the stated bases will be provided in the next subsections.

### **2.8.1 Wavelet Transform**

Wavelet transforms can be considered as forms of time-frequency representation of analogue signals[46]. Discrete wavelet transforms depend on discrete-time filterbanks, which may be containing either finite impulse response (FIR) or infinite impulse response (IIR) filters. These filter banks are called the wavelet and scaling coefficients in wavelets nomenclature. It is understood that Fourier analysis works by breaking up a signal into sine waves of various frequencies. Similarly, wavelet analysis breaks up a signal into shifted and scaled versions of the original (or *mother*) wavelet.

The Discrete Wavelet Transform (DWT) was proposed as a basis for MCM systems first in [17] and now it is used in communication applications. Wavelet-MCM used as the core modulation scheme in HD-PLC, a power line communications (PLC) technology developed by Panasonic.

DWT-MCM is a wavelet transform basis type that uses low and high pass filters to operate as quadrature mirror filters satisfying reconstruction and orthogonal basis properties. The DWT-MCM transceiver model is shown in Fig. 2.9.

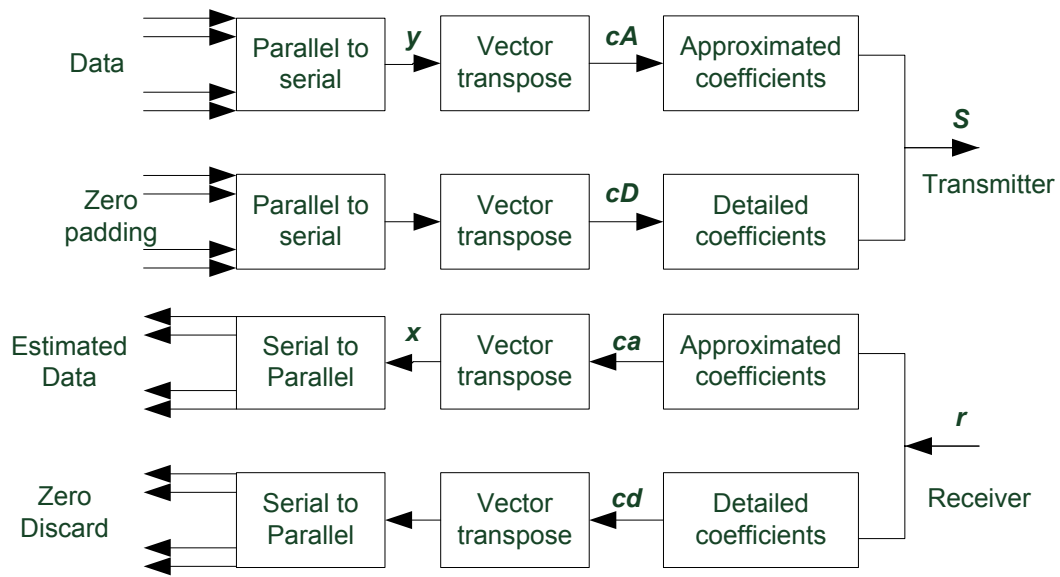


Fig. 2.9 The DWT-MCM transceiver model

The DWT-MCM transmitter shown in the top part of Fig. 2.9 first uses a digital modulator (i.e 16 – QAM) which maps the serial bits into symbols within N parallel data stream. The transmitter task is to perform the DWT modulation by constructing orthonormal wavelets. Each data symbol is converted to serial representation having a vector  $y$  which will next be transposed into  $cA$  which means that  $cA$  have their imaginary parts inverting signs and its form is changed to a parallel matrix. Then, the signal is up-sampled and filtered by the LPF coefficients or namely as approximated coefficients. Since the aim is to have low frequency signals, the modulated signals  $cA$  perform circular convolution with LPF filter whereas the HPF filter also performs the convolution with zeroes padding signals  $cD$  respectively. Note that the HPF filter contains detailed coefficients or wavelet coefficients. Different wavelet families have different filter length and values of approximated and detailed coefficients. Both of these filters have to satisfy orthonormal bases in order to operate as wavelet transform. Both filters are also assumed to have perfect reconstruction property. This means that the input and output of the two filters are expected to be the same. On receiver side, the reverse process is needed. The  $ca$  signal will be processed to the QAM demodulator for

data recovery. However, the *cd* signal is discarded because it does not contain any useful information.

Constructing the orthogonal Wavelet bases for the DWT-MCM in the transmitter is done using the Inverse discrete Wavelet transform (IDWT) by up-sampling and filtering (circular convolution) the data signal by the low path filter (LPF) and the same for the zero padded signals by the high path filter (HPF) coefficients. The LPF filter contains the approximated coefficients and the HPF contains the detailed coefficients. Different wavelet families like rbior3.3, bior3.3 and bior5.5 have different filter lengths and values of approximated and detailed coefficients[47]. LPF and HPF filters have to be orthogonal and normal to each other to satisfy orthonormal bases in order to operate as wavelet transform. As in OFDM, the opposite process is done in the receiver using DWT. But the basic algorithm for the DWT is not limited to a dyadic length and is based on a simple scheme that uses convolution and down-sampling. As usual, when a convolution is performed on finite-length signals, border distortions arise. To deal with border distortions, the border should be treated differently from the other parts of the signal. One method is by zero padding to the signal borders in the transmitter before using the IDWT[48]. This will ensure perfect reconstruction of the transmitted signal.

Wavelet-MCM does not require a Guard Interval, which is an overhead in OFDM systems bit rate. This makes it superior to OFDM systems because DFT only gives frequency resolution but no time resolution whereas the wavelet transform gives both the frequency and time resolution. It is important to say DWT- MCM systems require more complicated equalisers compared to the OFDM in the doubly selective channel scenario. DWT- MCM schemes use block lengths longer than the DFT length, typically four times longer, as shown in [49].

In MCM systems, spectral efficiency increases if DWT- MCM is used instead of OFDM because OFDM uses a rectangular pulse shape of sinusoidal carriers which have high side lobes that also increase sensitivity to ICI. On the other hand Wavelets have better spectral shaping and much lower side lobes in transmitted signals, which results in higher immunity against narrow band interference (NBI) and good performance in power line communications.

### 2.8.2 Discrete Cosine transform (DCT)

DCT is a Fourier-related transform similar to the DFT, but using only real numbers. DCT expresses signals in terms of a sum of cosine functions oscillating at different frequencies. There are eight types of DCT [50], the most common one is the type-II DCT. It is the most popular in practice and used in JPEG, MPEG, and H.261 standards. The size- $N$  type-II DCT is defined by the real orthogonal matrix whose  $(m, n)$  entry is given by:

$$F(m, n) = \begin{cases} \sqrt{\frac{2}{N}} \cos\left(\frac{(n-1)(2m-1)\pi}{2N}\right), & 1 \leq n, m \leq N, n \neq 1 \\ \sqrt{\frac{1}{N}}, & n = 1 \end{cases} \quad (2.23)$$

It is straight forward to check that  $F^T F = F F^T = I_N$ , where  $t$  is the matrix transpose. DCT-MCM system architecture is the same as the OFDM system in Fig. 2.8 except using the IDCT instead of the IDFT at the transmitter and the DCT instead of the DFT at the receiver. Typical DCT-MCM subcarriers are shown in Fig. 2.10. The number of DCT-MCM subcarrier samples is half that of OFDM subcarrier samples in Fig. 2.5.

The DCT-MCM system has numerous advantages including:

- 1- DCT basis have superb spectral compaction and energy concentration properties.
- 2- More robust against frequency offset, as it has less ICI power leakage to adjacent subcarriers than in OFDM.
- 3- The DCT uses only real arithmetic, which reduces the signal-processing complexity/power consumption almost twice over DFT.

The main disadvantage of DCT-MCM with respect to OFDM is the need for a pre-filter at the receiver to make the channel impulse response (CIR) symmetric in order for it to be diagonalizable by the DCT using symmetric guard sequence and pre-filter designs [42, 51]. The DCT-MCM cannot deal with the complex signals due to its real arithmetic nature without more complexity in the system [51] which is another disadvantage.

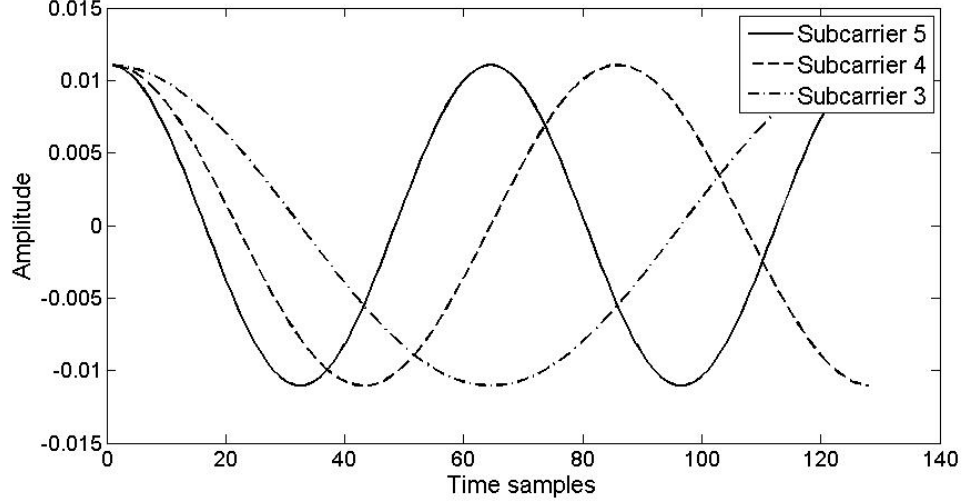


Fig. 2.10 DCT-MCM subcarriers

The main difference between DWT-MCM and DCT-MCM is that DCT-MCM can achieve perfect diagonalisation in fading channels; i.e. a simple one-tap equaliser per subchannel can be used. This is unlike DWT-MCM schemes, where there is still residual ICI and ISI and hence more complex equalisation is needed.

### 2.8.3 Discrete Hartley transform (DHT)

The Hartley transform is an integral transform closely related to Fourier [19], which transforms real-valued functions to real-valued functions (as opposed to requiring complex numbers). The Hartley transform of a function  $f(t)$  is defined by:

$$\mathbf{H}(\omega) = \{\mathcal{H}f\}(\omega) = \frac{1}{\sqrt{2\pi}} \int_0^{T_s} f(t) \text{cas}(\omega t) dt \quad (2.24)$$

where  $\text{cas}(t) = \cos(t) + \sin(t) = \sqrt{2} \cos\left(t - \frac{\pi}{4}\right) = \sqrt{2} \sin\left(t + \frac{\pi}{4}\right)$  and  $\omega$  is the angular frequency. The Hartley transform has the convenient property of being its own inverse: DHT and its inverse IDHT have the same transform definition where the DHT of a real sequence  $\mathbf{d} = [d_0 \ d_1 \ \dots \ d_{N-1}]^T$  and its inverse are given by

$$\begin{aligned} x_n &= \sum_{k=0}^{N-1} d_k \text{cas}\left(\frac{2\pi kn}{N}\right), \quad 0 \leq n \leq N-1 \\ \mathbf{d}_k &= \sum_{n=0}^{N-1} x_n \text{cas}\left(\frac{2\pi kn}{N}\right), \quad 0 \leq k \leq N-1 \end{aligned} \quad (2.25)$$

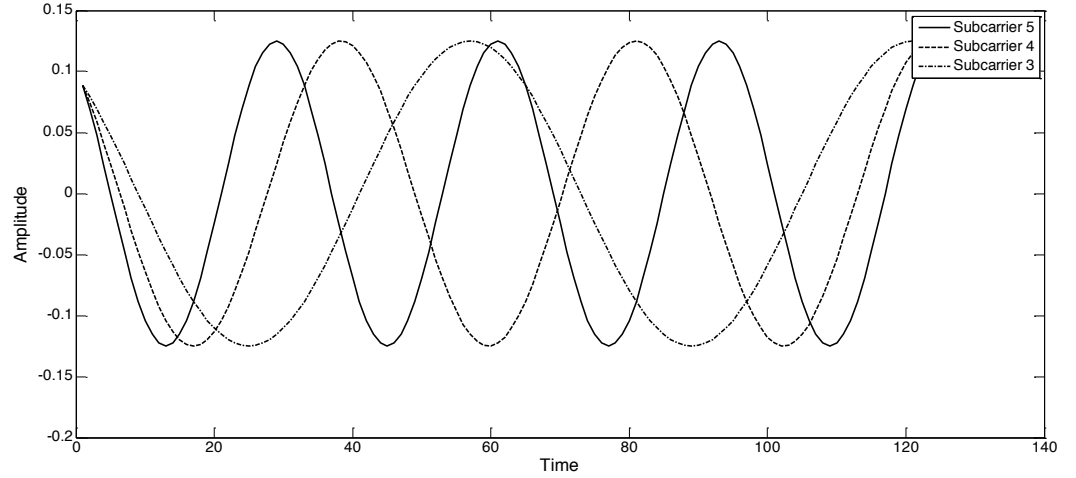


Fig. 2.11 DHT-MCM Subcarriers

The DHT real orthogonal matrix is given using cosine and sine matrix representation [43]. Let us define the  $(n, m)$  entries of  $N \times N$  matrices  $\mathbf{C}$  and  $\mathbf{S}$  as follows:

$$\begin{aligned} \mathbf{C}(m, n) &= \cos\left(\frac{2\pi nm}{2N}\right) \\ \mathbf{S}(m, n) &= \sin\left(\frac{2\pi nm}{2N}\right) \end{aligned} \quad 0 \leq n, m \leq N - 1 \quad (2.26)$$

Thus the DHT matrix can be given by:

$$\mathbf{H} = \frac{1}{\sqrt{N}}(\mathbf{C} + \mathbf{S}) \quad (2.27)$$

It is straight forward to show that  $\mathbf{H}\mathbf{H} = \mathbf{I}_N$ .

Following the same steps as the DCT-MCM, the DHT-MCM system architecture is the same as the OFDM system [43] in Fig. 2.8 except using the DHT instead of the IDFT at the transmitter and the DHT instead of the DFT at the receiver, which is one of the advantages of using the DHT as a basis for the MCM system, i.e. The same DHT hardware can be used in the transmitter and the receiver.

DHT-MCM subcarriers are shown in Fig. 2.11, the DHT-MCM subcarriers are identical to the OFDM subcarriers in Fig. 2.5, except that they do not contain imaginary parts as they are pure real signals.

Although the DHT is an attractive transformation that can be used as an alternative to the DFT in the MCM systems, because DHT has less computational complexity than DFT and the DHT and its inverse IDHT are identical, there are two main problems for DHT-based MCM to apply to wireless communications. First, since DHT is a real-valued transformation, only one-dimensional (1D) modulation schemes such as PAM and binary phase-shift keying (BPSK) are considered. Second, DHT-MCM cannot directly diagonalise the multipath channel impulse response (CIR) due to the inherent property of DHT. The authors in [44] proposed a DHT-MCM system that diagonalises the fading channel equivalent matrix and applies 2-D modulation formats like QPSK but with a more complicated system. A complicated equaliser is also needed as the OFDM in doubly selective fading channel scenarios.

#### **2.8.4 Discrete Fractional Fourier Transform (DFrFT)**

The fractional Fourier transform (FrFT) was introduced as an idea in 1929 [52], as a generalization of the Fourier transform, Namias re introduced FrFT in mathematics for applications in quantum mechanics in 1980 [53]. The Discrete Fractional Fourier Transform (DFrFT) transformation appeared after many groups of researchers reinvented it [54-57]. Later, low complexity representations, computational cost and applications for the DFrFT were investigated in [52, 58-61]. Now DFrFT is used in various applications:

- 1- ***Optics***: quantum optics, optical diffraction theory, and optical beam propagation including lasers [55, 58, 62].
- 2- ***Image processing***: image recovery, compression, and restoration, enhancement [63-65]
- 3- ***Signal processing***: signal recovery, detectors, encryption and compression, correlation, convolution, pattern recognition, beam forming speech processing , digital watermarking, multiplexing, tomography, blind source separation and energy localization problems, high resolution trigonometric interpolation, and securing information in digital holography [66-70]

One of the FrFT definitions is that:

“A Fractional Fourier transform is a rotation operation on the time frequency distribution by angle  $\alpha$ ”[54].

For  $\alpha = 0$ , there will be no change after applying DFrFT, and for  $\alpha = \pi/2$ , DFrFT becomes a Fourier transform, which rotates the time frequency distribution with  $\pi/2$ . For other values of  $\alpha$ , the DFrFT rotates the time frequency distribution according to  $\alpha$ . Fig. 2.12 illustrates the relationships between the time, and frequency outputs from the DFrFT ( $F_\alpha$ ) when the fractional angle  $\alpha$  changes:

$$\mathbf{F}_\alpha = \begin{cases} \mathbf{F}_0[x(t)] = x(t) & \text{for } \alpha = 0 \xrightarrow{\text{yields}} \text{Time domain} \\ \mathbf{F}_{\pi/2}[x(t)] = X(f) & \text{for } \alpha = \pi/2 \xrightarrow{\text{yields}} \text{Frequency domain} \\ \mathbf{F}_\pi[x(t)] = x(-t) & \text{for } \alpha = \pi \xrightarrow{\text{yields}} \text{Inverse time domain} \\ \mathbf{F}_{3\pi/2}[x(t)] = X(-f) & \text{for } \alpha = 3\pi/2 \xrightarrow{\text{yields}} \text{Inverse frequency domain} \end{cases} \quad (2.28)$$

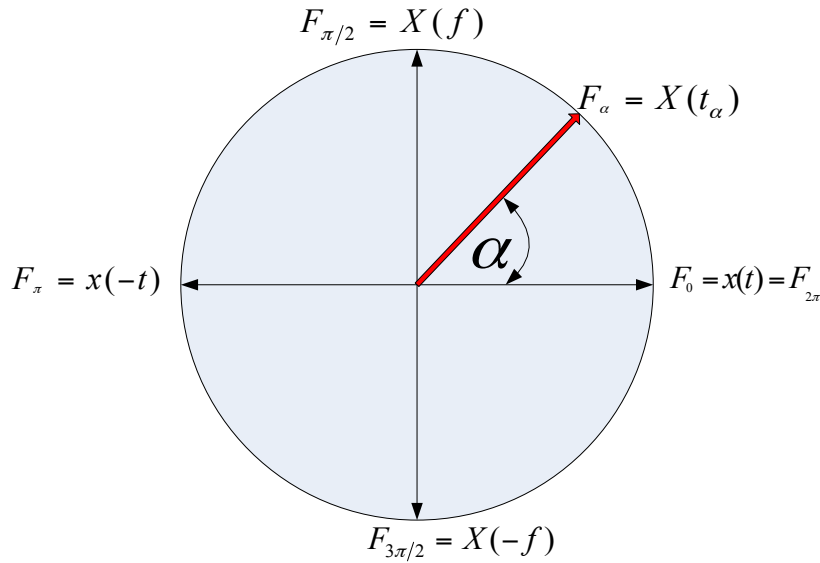


Fig. 2.12 Signal  $x(t)$  at different transformation angle  $\alpha$

It can also be seen from Fig. 2.12 that  $\mathbf{F}_{2\pi}[x(t)] = \mathbf{F}_0[x(t)] = x(t)$ . The transformation kernel of the continuous FrFT is defined as[71]:

$$K_\alpha(t, u) = A_\alpha e^{j\pi(t^2+u^2) \cot \alpha - j2\pi tu \csc \alpha} \quad (2.29)$$

where  $\alpha$  is the rotation angle for transformation process and

$$A_\alpha = \frac{e^{\{-j\pi \text{sign}[\sin \alpha]/4 + j\alpha/2\}}}{\sqrt{|\sin \alpha|}} \quad (2.30)$$

The forward FRFT is defined as:

$$f_\alpha\{x(t)\}(u) = X_\alpha(u) = \int_{-\infty}^{\infty} x(t) K_\alpha(t, u) dt \quad (2.31)$$

$$x(t) = \int_{-\infty}^{\infty} X_\alpha(u) K_{-\alpha}(t, u) du \quad (2.32)$$

The domains of the signal for  $0 < |\alpha| < \pi$  are defining the fractional Fourier domains. Substituting with  $\alpha = \pi/2$  in (2.31) and (2.32) gives the well-known Fourier transform. There are a number of DFrFT algorithms with different properties and accuracies. In our work the DFrFT proposed in [72] is chosen because its transformation kernel and its inverse transform are orthogonal and reversible.

Assume that the input function  $f(t)$  and the output function  $\mathbf{F}_\alpha(u)$  of the DFrFT have the chirp period of order  $p$  with the period  $T_p = N \Delta t$  and  $\mathbf{F}_p = M \Delta u$ , and sampled signals are with the interval  $\Delta t$  and  $\Delta u$  as:

$$x(n) = f(n \Delta t), X_\alpha(m) = \mathbf{F}_\alpha(m \Delta u) \quad (2.33)$$

where  $n = 0, 1 \dots N - 1$  and  $m = 0, 1 \dots M - 1$ . When  $\alpha \neq D \cdot \pi$  ( $D$  is an integer), (2.31) can be converted to:

$$X_\alpha(m) = A_\alpha \Delta t e^{\frac{j}{2} \cot \alpha \cdot m^2 \Delta u^2} \sum_{n=0}^{N-1} e^{\frac{j}{2} \cot \alpha \cdot n^2 \Delta t^2} e^{j \csc \alpha \cdot n \cdot m \cdot \Delta t \cdot \Delta u} x(n) \quad (2.34)$$

The transformation is reversible when  $M = N$ , with the condition:

$$\Delta t \Delta u = 2\pi \sin \alpha / M \quad (2.35)$$

Equation (2.34) can also be written in matrix vector multiplication form,

$$\mathbf{X} = \mathbf{F}_\alpha \mathbf{x} \quad (2.36)$$

where  $\mathbf{X} = [X_\alpha(0), X_\alpha(1), \dots, X_\alpha(N - 1)]^T$ ,  $\mathbf{x} = [x(0), x(1), \dots, x(N - 1)]^T$  and  $\mathbf{F}_\alpha$  is an  $N * N$  matrix in a similar manner, the IDFrFT can be written as:

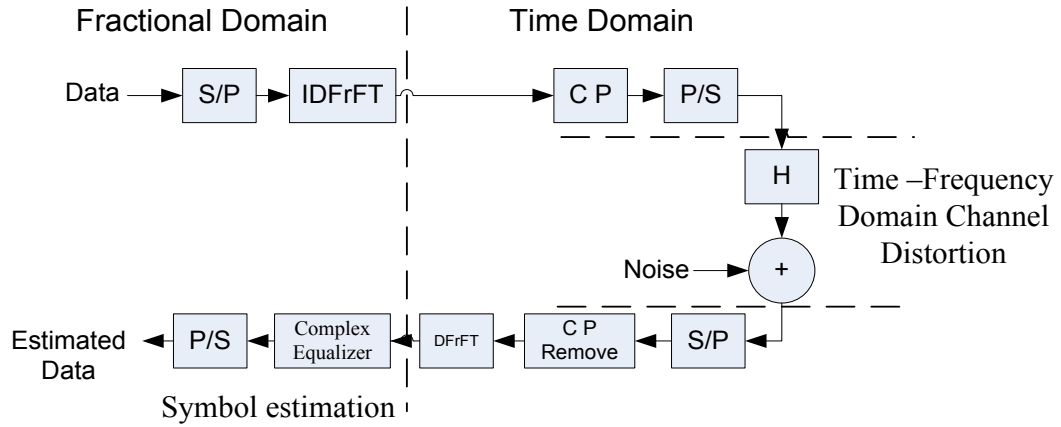


Fig. 2.13 The DFrFT-OFDM system with a complicated equaliser

$$\mathbf{x} = \mathbf{F}_{-\alpha} \mathbf{X} \quad (2.37)$$

where  $\mathbf{F}_{-\alpha} = \mathbf{F}_{\alpha}^H$ .

OFDM is sensitive to frequency offset and Doppler frequency spread [32] when the channel is doubly selective like Digital Video Broadcasting Handheld (DVB-H) channels [33-35, 73], as ICI increases the system performance is degrade. Many efforts have been spent in the equalisation field to deal with this problem. Using the DFrFT to replace the FFT in multicarrier systems was introduced in [20, 45, 74] to reduce the effects of Doppler frequency spreads. DFrFT-MCM system architecture is shown in Fig. 2.13.

The DFrFT-MCM system is a block transfer system and the subcarriers are chirp signals which are orthogonal to each other, so we can call it DFrFT- Orthogonal Chirp Division Multiplexing DFrFT-OCDM. Two bases for the DFrFT-OCDM system are shown in Fig. 2.14 and the spectral energy distribution for the two bases is shown in Fig. 2.15.

The Wigner distribution in time and frequency domain for the 1<sup>st</sup> basis signal and the 20<sup>th</sup> basis signal with  $\alpha = 0.7$  are shown in Fig. 2.16. The figure shows that the DFrFT bases are frequency varying with time which is a property for the DFrFT transformation.

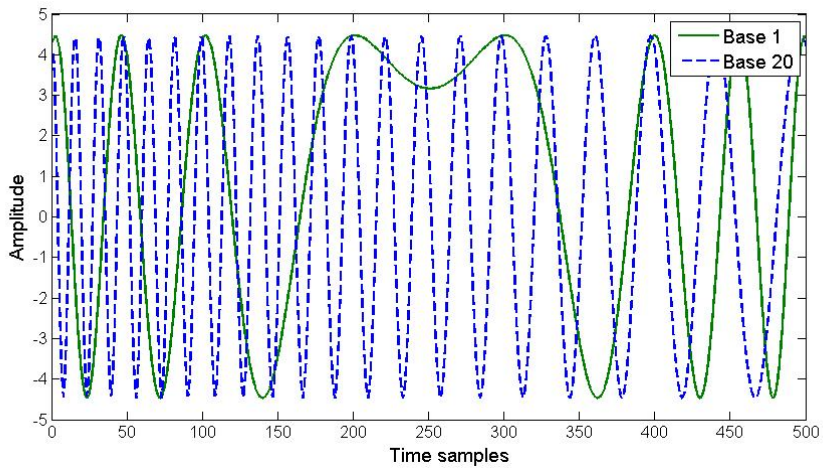


Fig. 2.14 DFrFT-OCDM basis for the 1<sup>st</sup> and the 20<sup>th</sup> basis signals

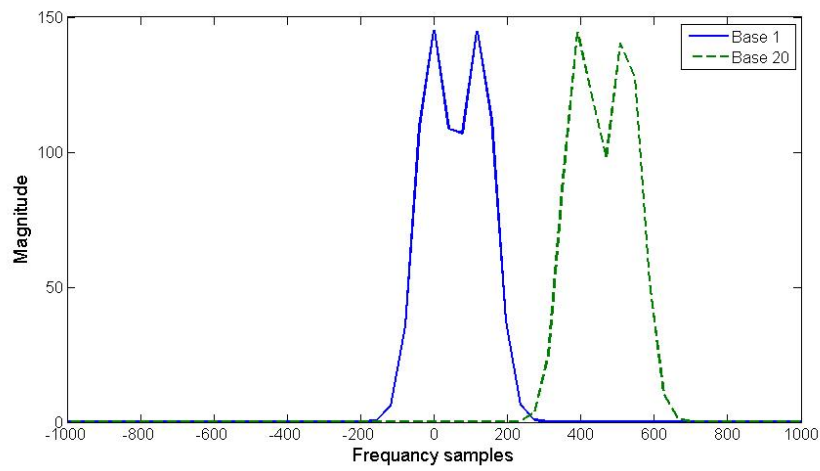


Fig. 2.15 Spectral Energy Distribution for the 1<sup>st</sup> and the 20<sup>th</sup> basis signals

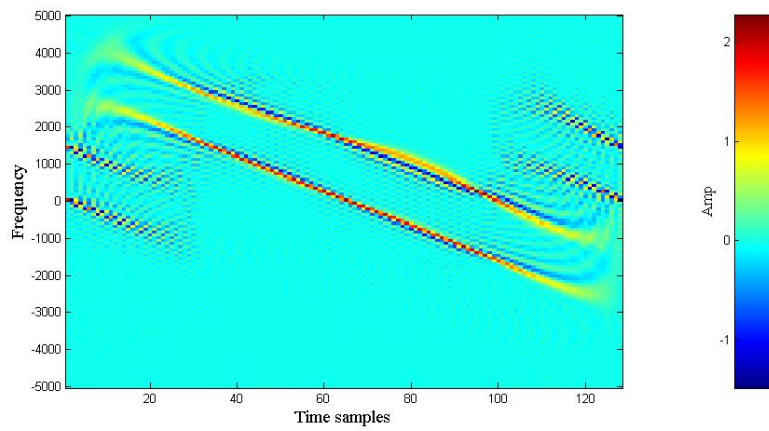


Fig. 2.16 the Wigner distribution for the 1<sup>st</sup> basis signal and the 20<sup>th</sup> basis signal

The transmitted DFrFT-OCDM signal is a combination of many blocks, each starting with a cyclic prefix (CP) to eliminate inter-symbol interference. However, the need for fast mobile communications with large data rates and long symbols introduces larger ICI which forces the use of complicated equalisers such as the minimum mean square error (MMSE) equaliser. Such equalisers require excessive matrix inversion processes, especially for a large number of subcarriers which is the case in multimedia communication systems [23]. Detailed representation for the equalisation problem will be introduced in the next chapter.

The complexity of the DFrFT-OFDM system is approximately the same as the traditional OFDM system [20], and both systems exhibit almost the same performance when the channel is time invariant. However both of them cannot diagonalize the time variant channel matrix but the DFrFT-OCDM can compress it much more effectively, which is the main advantage of the DFrFT-OCDM system as it gives better performance than OFDM and gives the opportunity to use low complexity equalisers while preserving the better performance. More details about the DFrFT-OCDM will be given in chapter 3.

## **2.9 OFDM advantages**

OFDM possesses some inherent advantages for wireless communications.

### **2.9.1 Multipath Delay Spread Tolerance**

The increase in the symbol time of the OFDM symbol by  $N$  times,  $N$  being the number of subcarriers, leads to a corresponding increase in the effectiveness of OFDM against the ISI caused due to multi-path delay spread. Furthermore, using the cyclic extension process and proper design, ISI and ICI were completely eliminated from the system.

### **2.9.2 Effectiveness against Channel Distortion**

In addition to delay variations in the channel, the lack of amplitude flatness in the frequency response of the channel also causes ISI in digital communication systems. In systems that use single-carrier transmission, an equaliser might be required to mitigate

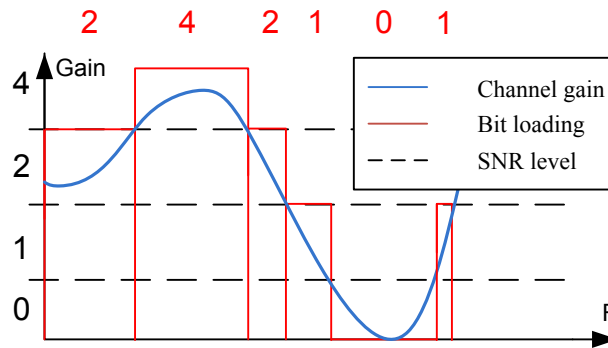


Fig. 2.17 The Adaptive bit loading.

the effect of channel distortion. The complexity of the equaliser depends upon the severity of the channel distortion and there are usually issues such as equaliser non-linearity and error propagation that cause additional trouble.

In OFDM systems, since the bandwidth of each sub-carrier is very small, the amplitude response over this narrow bandwidth is basically flat. Even in the case of extreme amplitude distortion, a single tap equaliser of very simple structure is enough to correct the distortion in each subcarrier. CP converts the channel matrix to a circulant form, which can be diagonalised using the DFT.

### 2.9.3 Throughput maximization

The use of sub-carrier modulation improves the flexibility of OFDM to channel fading and distortion makes it possible for the system to transmit at maximum possible capacity using a technique called channel loading or adaptive bit loading. Suppose the transmission channel has a fading notch in a certain frequency range corresponding to a certain sub-carrier. If the presence of this notch can be detected by using channel estimation schemes and assuming that the notch does not vary fast enough compared to

the symbol duration of the OFDM symbol. It is possible to change (scale down/up) the modulation and coding schemes for this particular sub-carrier, i.e., increase their robustness against noise, or just upload it with null data Fig. 2.17, so that capacity as a whole is maximized over all the sub-carriers. Numbers shown in Fig. 2.17 correspond to the number of bits in every modulation scheme such that 1 means BPSK and 2 means

QPSK and 4 means 16 QAM. However, this requires the data from channel estimation algorithms to be fed-back to the transmitter, which increases the system complexity. In the case of single carrier systems, nothing can be done against such fading notches.

In relatively slow time-varying channels, it is possible to significantly enhance the capacity by adapting the data rate per subcarrier according to the signal to noise ratio (SNR) of that particular subcarrier.

#### **2.9.4 Computational Efficiency**

Use of FFT structure at the receiver reduces the computation complexity of the Fourier transform to  $N \log_2 N$  Floating-Point Operations Per Second (COMPLEX OPERATIONS) [2] instead of using multiple local oscillators to implement the subcarriers (local oscillator for each subcarrier). As the number of carriers grows, higher efficiency is achieved as the computational complexity increases for each subcarrier with  $\log_2 N$  [1].

#### **2.9.5 Frequency Diversity**

OFDM is the best place to employ frequency diversity as each symbol contains multiple frequency components. Moreover, in a combination of OFDM and Code Division Multiple Access called the MC-CDMA transmission technique; frequency diversity is inherently present in the system (i.e., it is available for free).

#### **2.9.6 Robustness against Narrowband Interference**

OFDM is robust against narrowband interference, because such interference affects only a small percentage of the sub-carriers.

#### **2.10 OFDM disadvantage**

Even though, OFDM provides numerous advantages for wireless transmission, it has a few serious disadvantages that must be overcome for this technology. The following sub-sections discuss two serious problems associated with OFDM transmission.

### 2.10.1 Peak to Average Power Ratio (PAPR)

OFDM signals exhibit high peak to average power ratio (PAPR), which is a serious disadvantage of OFDM. As a result of PAPR, the D/A converters and amplifiers need to have a large dynamic range, which leads to inefficiency in power and cost [27, 29]. The PAPR of OFDM increases exponentially with the number of subcarriers. If the power amplifiers are not operated with large power back-offs, it is impossible to keep the out-of-band power below the specified limits. This situation leads to very inefficient amplification and expensive transmitters. So it is highly desirable to reduce PAPR.

Theoretically, the difference of PAPR between any MCM and single-carrier is a function of the subcarrier number  $N$  i.e.  $\Delta (dB) = 10\log_{10}N$ . When  $N = 1000$ , the difference can be as large as 30dB. However, this theoretical value rarely occurs. Well scrambled input data lowers the chances of reaching this maximum limit, especially, when the constellation size is large [30].

Different techniques were proposed for reducing the PAPR problem like clipping [75, 76], coding[77-79], and multiple signal representation techniques such as partial transmit sequence (PTS) [80] and selected mapping (SLM) [81]. These techniques reduce the PAPR with one or more overheads of transmitted signal power increase, computational complexity increase, data rate loss and bit error rate (BER) increase. PAPR problem will be investigated in details in chapter 4.

### 2.10.2 Frequency offset

Carrier frequency errors result in a shift of the received signal's spectrum in the frequency domain. If the frequency error is an integer multiple ( $C$ ) of the sub-carrier spacing  $\Delta f$ , then the received frequency domain subcarriers are shifted by  $(C * \Delta f)$ . The subcarriers are still mutually orthogonal, but the received data symbols, which were mapped to the OFDM spectrum, are in the wrong position in the demodulated spectrum, resulting in bit error rate increasing.

If the carrier frequency error is not an integer multiple of the subcarrier spacing, then energy is spilling over between the subcarriers resulting in loss of their mutual

orthogonality. In other words, interference is observed between the subcarriers, which deteriorate the bit error rate of the system.

### **2.10.3 Sensitive to Doppler Shift.**

OFDM has recently been considered in fast mobile communication scenarios with rapid time and Frequency fading channel variations (doubly selective channel), i.e. large Doppler frequency shifts [33-36]. Examples include Flash-OFDM, mobile reception of DVB-T and base station cooperation in LTE. In these channel scenarios, the DFT cannot diagonalise the channel matrix anymore and ICI appears.

The substantial ICI resulting from large Doppler shifts can be reduced via pulse shaping [82]. To mitigate the remaining ICI, various frequency-domain complex equalisation methods have been proposed, including zero-forcing (ZF) and minimum mean-square error (MMSE) schemes [22, 30]. Complicated equalisers use the inverse of the estimated channel matrix to mitigate the channel effect which is a very computationally expensive process and is related directly to the number of subcarriers. Multimedia services that adapt OFDM as a physical layer for its communication systems always use a huge number of subcarriers. For example, DVB-T subcarriers can reach up to 8000 subcarrier and DVB-T2 can reach up to 32000 subcarriers. Hence, there is a great demand for low complexity equalisers. In all schemes, equaliser complexity can be reduced by exploiting the (approximate) band structure of the frequency-domain [83-86] channel matrix which will be investigated in chapter 3. The band approximation can be improved by pulse shaping or time-domain windowing [21].

## **2.11 Examples of OFDM applications**

OFDM has been adopted as the new European DAB standard, DVB-T [14, 87-91] and the mobile communication 4<sup>th</sup> generation.

In fixed-wire applications, OFDM is employed in ADSL and high bit-rate digital subscriber line (HDSL) systems. It has been proposed for power line communication systems as well due to its resilience to dispersive channels and narrow band interference.

Here is a brief discussion on five applications that have incorporated the OFDM technique.

### **2.11.1 Digital Audio Broadcasting (DAB-T)**

DAB is the first standard to use OFDM. The DAB network is efficient in handling multipath delay spread. As a result, new data services and higher spectrum efficiency can be achieved.

### **2.11.2 Terrestrial Digital Video Broadcasting (DVB-T)**

DVB was created by a pan-broadcasting-industry group in 1993. DVB defined a set of specifications for delivery of digital television over cable, DSL, and satellite. In 1997, Digital Terrestrial Television Broadcasting (DTTB) was standardized. It utilizes an OFDM system in the 2000 and 8000 sub carrier modes [14, 91].

### **2.11.3 Magic WAND**

Magic Wireless ATM Network Demonstrator (WAND) is a wireless OFDM based ATM network. This system operates in the 5GHz band and is gaining acceptance for OFDM in high-rate wireless communications. It also acts as a basis for HIPERLAN2.

### **2.11.4 IEEE802.11a/HIPERLAN2 and MMAC Wireless LAN**

All the above systems operate in the 5GHz band. 802.11a is selected by IEEE to be used in the US, targeting a range of data rates up to 54 Mbps. ETSI BRAN in Europe is working on three extensions for OFDM in the HiperLAN standard:

- 1- HiperLAN2, a wireless indoor LAN with a QoS provision.
- 2- HiperLink, a wireless indoor backbone.
- 3- HiperAccess, an outdoor fixed wireless network providing access to a wired infrastructure.

### **2.11.5 WiMAX (Worldwide interoperability for Microwave Access)**

Despite the marketing hype and the broad industry support for the development of WiMAX, its success is not a foregone conclusion. The WiMAX physical layer (PHY)

is based on OFDM, as it offers good resistance to multipath, and allows WiMAX to operate in non-line of site (NLOS) conditions. OFDM had established itself as a method of choice for dealing with multipath for broadband and was already part of the revised IEEE 802.11 standards. Besides the OFDM physical layers, 802.16a also specified additional MAC-layer options, including support for orthogonal frequency division multiple access (OFDMA). Further revisions to 802.16a were made and completed in 2004. This revised standard, IEEE 802.16-2004, replaced 802.16, 802.16a, and 802.16c with a single standard, which has also been adopted as the basis for HIPERMAN by ETSI. In 2003, the 802.16 group began work on enhancements to the specifications to allow vehicular mobility applications.

### 2.12 OFDM System Implementation on Real DSP Board

The key building blocks of an OFDM Modem have been designed and implemented. The functionality of the modem is verified with the real system using the TI C6713 DSK board.

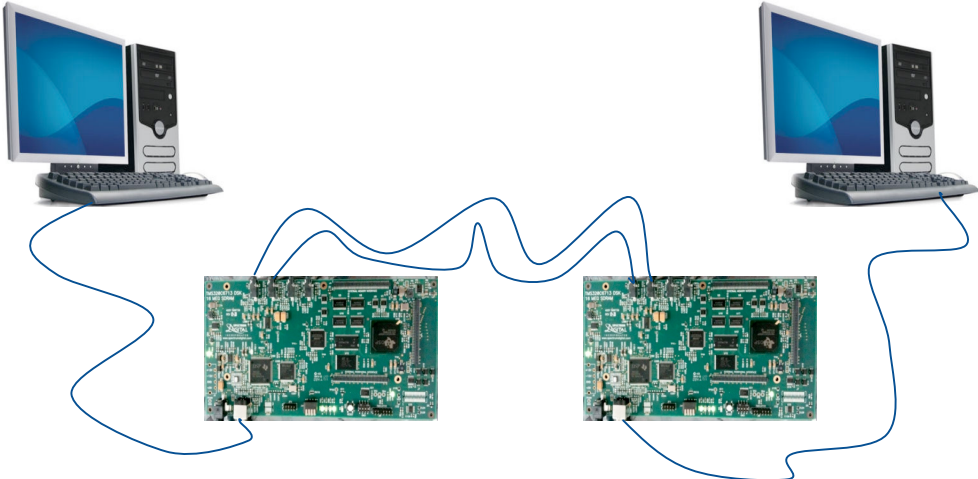


Fig. 2.18 OFDM communication system equipment

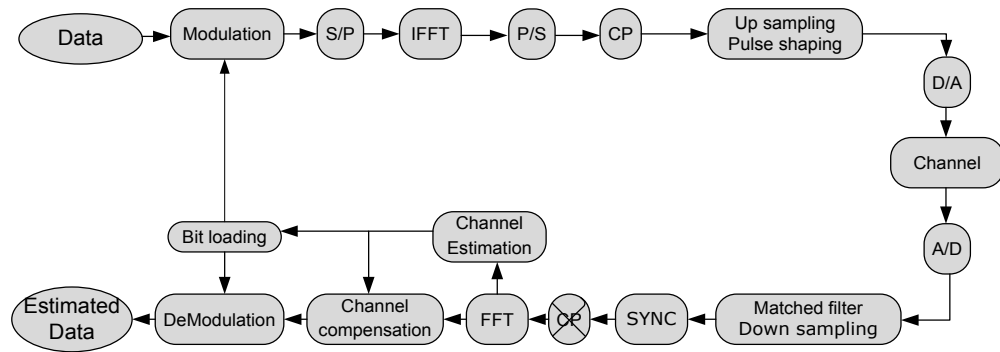


Fig. 2.19 OFDM communication system overview

### 2.12.1 Equipment

The following equipment was used to complete the project Fig. 2.18:

1- Hardware

- two PCs.
- Two Texas Instruments C6713 DSP boards.

2- Software:

- MATLAB R2007a.
- Code Composer Studio 6713 DSK V3.1.

### 2.12.2 Project Overview

The aim of this project is to implement a digital OFDM communication system with bit loading using the channel information from a feedback link. Two sets of PCs were used, each equipped with a DSP card, where one set acts as a transmitter and the other acts as a receiver, i.e. a simplex communication system. The system block diagram is shown in Fig. 2.19. All the system design and simulations details are listed in appendix A.

## 2.13 Conclusion

This chapter has introduced the basic idea of OFDM as multicarrier modulation technique, illustrated that OFDM provides superior frequency spectrum management rather than single frequency technique like (TDMA, CDMA) which become problematic at very high data rate. OFDM achieves orthogonality in the frequency domain by allocating each of the separate information signals onto different subcarriers. FFT provide an ease, low complexity and efficient implementation for OFDM.

Modern communication systems that adapt OFDM for the core of its physical layer use a huge number of subcarriers with the excessive need for high speed mobile communication; both complicated the ICI problem due to the large Doppler frequency shifts and the need for complicated equalisers arises.

One effective solution for this problem is using different subcarrier basis (new transformation) that can match the channel variations like DFrFT accompanied with a low complexity equaliser which will be discussed in the next chapter.

# 3. Novel MCM Equalisers for Doubly Dispersive Channels

---

## 3.1 Introduction

The popularity of orthogonal frequency division multiplexing (OFDM) systems is based on the DFT ability to diagonalise the circulant matrices as discussed in chapter 2. This can be fully exploited under stationary communication channel conditions, but in the presence of carrier frequency offset or Doppler spread (doubly dispersive channel) [31, 32, 36, 73] which is the case in communication channel for digital video broadcasting handheld devices (DVB-H) the circulant property of the effective channel matrix is not valid and therefore the optimality of OFDM against ICI are lost.

Doubly dispersive channel will be investigated through this chapter with its effect on OFDM and DFrFT-OCDM systems. The equalisation problem will be stated and a comparison between known complicated equalisers will be provided then novel equalisation methods will be introduced. Also a new cognitive communication system based on Hybrid DFrFT and DFT based MCM system will be developed.

## 3.2 Doubly Dispersive channel

For mobile-radio applications, the channel is time-variant because of motion between the transmitter and receiver results in propagation path changes. The rate of change of these propagation conditions accounts for the fading rapidity (rate of change of the fading environments).

In the environment of multimedia mobile communications like DVB-H, multiple copies of the transmitted signal arrive at the receiver with different delays and phases creating the phenomenon of multipath. Furthermore, due to the mobile unit motion, the

signal experiences a random frequency modulation on each of the multipath components due to the Doppler shifts. Hence, the resultant received signal can suffer harsh attenuation and interference which can lead to errors in the receiver and system performance degradation.

The multipath effects are based on many different factors like the existence of reflecting objects in the propagation environment which forms a constantly varying channel. The energy of some waves are dissipated due to reflections and scattering, while sometimes a line of sight (LOS) component exists, that arrives at the receiver straight without any obstacles. Also, the distances travelled by each of the multipath components. Consequently, multipath components with random phases and amplitudes results in variations in the received signal strength.

It is found to be impossible to define the channel impulse response deterministically, due to complicated transmitter or receiver motion combined with great number of multipath components. These multipath component delays and path gains are also complicated but assuming they are random then central limit theorem (CLT) can be applied. In this case the channel response and its frequency response both follow a complex Gaussian distribution with envelope process equivalent to Rayleigh or Rician fading process.

When the received signal is made up of several reflective rays plus a significant line-of-sight (nonfaded) component, the envelope amplitude due to small-scale fading has a Rician power density, and is referred to as Rician fading which is the case in highways and small villages. The nonfaded component is called the specular component. As the amplitude of the specular component approaches zero, the Rician power density function (pdf) approaches a Rayleigh pdf [92]. Rayleigh model can be used in heavily built-up city centres and may be used in tropospheric and ionospheric signal propagation as the many particles in the atmospheric layers act as scatterers. In other words, the small-scale fading statistics with the line of sight path is being blocked are said to be Rayleigh and Rician otherwise.

In order to design, simulate and benchmark wireless communication systems, it is important to develop channel models that follow real channels variation in time,

frequency and space. Models are classified as either statistical or empirical. Statistical models are simpler and are useful for analysis and simulations. Empirical models are more complicated but usually represent a specific type of channel more accurately.

### 3.2.1 Rayleigh fading channel model

In a multipath environment, reflected signals can be described in terms of orthogonal components  $X_n(t)$  and  $Y_n(t)$ . If the number of such stochastic components is large and all are nearly equivalent, then at a certain time, the variables  $X_r(t)$  and  $Y_r(t)$ , resulting from their addition, will have a Gaussian pdf [2].

The Central Limit Theorem can be applied with large numbers of paths; each path can be represented as circularly symmetric complex Gaussian random variable with time. This model is called Rayleigh fading channel model. The circularly symmetric complex Gaussian random variable can be expressed by:

$$Z = X_r + jY_r \quad (3.1)$$

where real and imaginary parts are zero mean independent and identically distributed (iid) Gaussian random variables. The expectation for a circularly symmetric complex random variable  $Z$  is given by:

$$E[Z] = E[e^{j\theta} Z] = e^{j\theta} E[Z] \quad (3.2)$$

where  $Z$  distribution is rotationally invariant and  $\theta$  is the rotation angle. The circularly symmetric complex Gaussian random variable statistics are fully identified by the variance:

$$\sigma^2 = E[Z^2] \quad (3.3)$$

The magnitude of  $|Z|$  has a probability density function given by [2]:

$$P(z) = \begin{cases} \frac{z}{\sigma^2} e^{\left(\frac{-z^2}{2\sigma^2}\right)}, & z \geq 0 \\ 0 & \textit{otherwise} \end{cases} \quad (3.4)$$

and called a Rayleigh random variable.

This model, called Rayleigh fading channel model, is reasonable environment model for many reflectors without line-of-sight component.

### 3.2.2 Rician fading channel

When the received signal is a combination of multiple reflected rays plus a dominant line-of-sight (non-faded) component, the received envelope amplitude has a Rician pdf as shown below in (3.5) and the fading is referred to as Rician fading[93]:

$$P(z) = \begin{cases} I_0 \left( \frac{Az}{\sigma^2} \right) \frac{z}{\sigma^2} e^{-\left(\frac{z^2+A^2}{2\sigma^2}\right)}, & z \geq 0, A \geq 0 \\ 0 & \text{otherwise} \end{cases} \quad (3.5)$$

where,  $\sigma^2$  is the pre-detection mean power of the multipath signal.  $A$  is the peak magnitude of the non-faded signal component (called the specular component) and  $I_0(\cdot)$  is the modified Bessel function of the first kind and zero order which is defined as[92]:

$$I_0(x) = \frac{1}{2\pi} \int_0^{2\pi} e^{x \cos \theta} d\theta \quad (3.6)$$

Although  $Z(t)$  varies dynamically with motion (time), at any *fixed time* it is a random variable, whose value stems from the ensemble of real positive numbers. Hence, in describing probability density functions, it is appropriate to drop the function dependence on time.

The Rician distribution is often described in terms of a parameter  $K$ , which is called the Rician  $K$  factor and defined as “the ratio of the power in the specular component to the power in the multipath signal”. It is given by:

$$K = \frac{A^2}{2\sigma^2} \quad (3.7)$$

As the magnitude of the specular component approaches zero or as  $K \xrightarrow{\text{yields}} -\infty$  (dB), the Rician pdf approaches a Rayleigh pdf, expressed in (3.4). Fig. 3.1 shows Rayleigh and Rician pdf distributions where several different kinds of Rician pdfs are labelled using the Rician  $K$  factor.

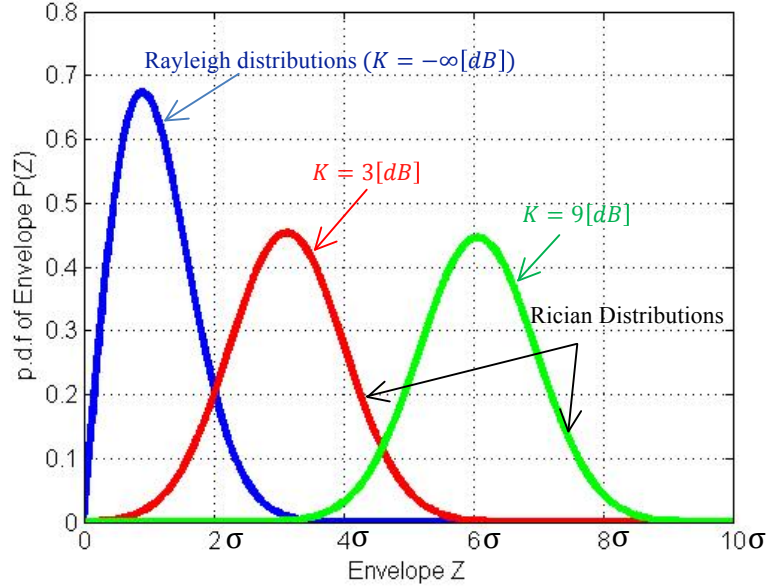


Fig. 3.1 Rayleigh and Rician distributions.

### 3.2.3 Jakes' Model

Rayleigh and Rician fading channels can be modelled by generating the real and imaginary parts of a complex number according to independent normal Gaussian variables. Jakes popularised a model for Rayleigh and Rician fading [94] based on summing sinusoids. Assuming the scatters signals is uniformly distributed around a circle at angles  $\phi_n$  with  $k$  rays emerging from each scattered signal. The Doppler shift on ray  $n$  is given by:

$$f_n = f_d \cos \phi_n \quad (3.8)$$

with  $N$  such scatterers, the Rayleigh fading of the  $k^{th}$  waveform over time  $t$  can be modelled as:

$$R(t, k) = 2\sqrt{2} \left[ \sum_{n=1}^N (\cos \beta_n + j \sin \beta_n) \cos(2\pi f_n t + \theta_{n,k}) + \frac{1}{\sqrt{2}} (\cos \phi + j \sin \phi) \cos(2\pi f_n t) \right] \quad (3.9)$$

where  $\phi$ ,  $\beta_n$  and  $\theta_{n,k}$  are model parameters with  $\phi$  usually set to zero,  $\beta_n$  chosen so that there is no cross-correlation between the real and imaginary parts of  $R(t)$ :

$$\beta_n = \frac{\pi n}{N + 1} \quad (3.10)$$

and  $\theta_{n,k}$  used to generate multiple waveforms. If a single-path channel is being modelled, so that there is only one waveform then  $\theta_n$  can be zero. If a multipath, frequency-selective channel is being modelled so that multiple waveforms are needed, Jakes suggests that uncorrelated waveforms are given by:

$$\theta_{n,k} = \beta_n + \frac{2\pi(k - 1)}{N + 1} \quad (3.11)$$

A modified Jakes' model [95] selects a different arrangement for the scattered signals and scales their waveforms using Walsh-Hadamard sequences to ensure zero cross-correlation as there was a cross-correlation between the waveforms:

$$\phi_n = \frac{\pi(n - 0.5)}{2N}, \quad \beta_n = \frac{\pi n}{N} \quad (3.12)$$

results in the following model, usually termed the Dent or the modified Jakes model:

$$R(t, k) = \sqrt{\frac{2}{M}} \sum_{n=1}^N A_k(n) (\cos \beta_n + j \sin \beta_n) \cos(2 \pi f_n t + \theta_n) \quad (3.13)$$

where  $A_k(n)$  is the weighting functions which are the  $k^{th}$  Walsh-Hadamard sequence in  $n$ . Since these scattered signals have zero cross-correlation by design, this model results in uncorrelated waveforms. The phases  $\theta_n$  can be initialised randomly and have no effect on the correlation properties. The Jakes' model also popularised the Doppler spectrum associated with Rayleigh fading, and as a result, this Doppler spectrum is often termed Jakes' spectrum.

### 3.2.4 Fading Channels with Doppler Effect

The variation in channel fading depends also on the moving speed of the receiver and/or transmitter where motion causes Doppler shift in the received signal components. When there is a variation in the fading channel frequency response with time due to Doppler shift the fading channel called doubly dispersive fading channel. Doppler shift calculations are given by:

$$f_d = (\Delta v/C)f_c \quad (3.14)$$

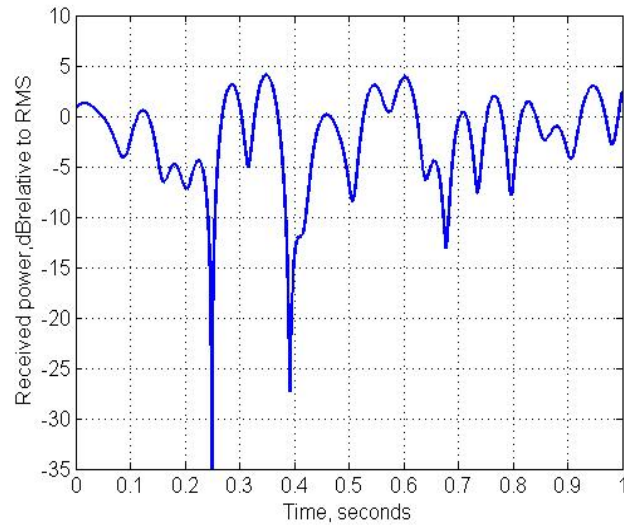


Fig. 3.2 Rayleigh fading with a maximum Doppler shift of 10 Hz

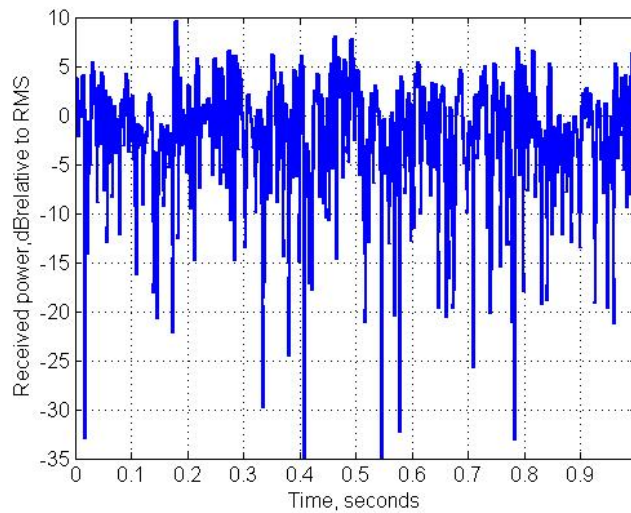


Fig. 3.3 Rayleigh fading with a maximum Doppler shift of 100 Hz.

where  $f_d$  is the Doppler shift,  $\Delta v$  is the velocity difference between the transmitter and the receiver,  $C$  is the speed of light and  $f_c$  is the signal carrier frequency.

Fig. 3.2 and Fig. 3.3 show the common shape of Rayleigh fading channel with a maximum Doppler shift of 10 Hz and 100 Hz respectively. These Doppler shifts correspond to velocities of 6 km/h (4 mph) and 60 km/h (40 mph) respectively at 1800

MHz, one of the operating frequencies for GSM mobile phones. In some 'deep fades' the signal strength can drop by a factor of several thousand or 30-40 dB.

### 3.3 Communication Channel Equalisation

In single carrier modulation systems, estimating the transmitted signal with the minimum number of errors is the receiver's responsibility which has to be done effectively and with the minimum computation cost. The main source for errors in the receiver side is the channel distortion and the most effective method to compensate channel distortion is equalisation Fig. 3.4.

The aim of equalisation is to compensate the channel effect and restore the original signal shape [93, 96]. The most basic equalisation approach is to select the receiver filter to fully compensate the radio channel frequency selectivity. This can be achieved by selecting the receiver filter impulse response to fulfil the relation:

$$\mathbf{W} \otimes h = 1 \quad (3.15)$$

where  $\mathbf{W}$  is the equaliser impulse response,  $h$  is the channel impulse response and “ $\otimes$ ” denotes linear convolution. This is known as Zero-Forcing (ZF) equalisation [2, 93, 96], and is able to provide full compensation for any radio channel frequency selectivity and thus full suppression of any related signal corruption. However, ZF equalisation may lead to very large increase in the noise level (noise amplification) after filtering which degrade the system performance.

A better alternative is to select a filter setting that provides a trade-off between signal corruption due to radio-channel frequency selectivity, and noise/interference. This can, for example, be done by selecting the filter to minimize the mean-square error ( $\varepsilon$ ) between the equaliser output and the transmitted signal:

$$\varepsilon = E \left\{ |\hat{d}(t) - d(t)|^2 \right\} \quad (3.16)$$

where  $\hat{d}(t)$  is the estimated signal and  $d(t)$  is the actual transmitted signal. This is also referred to as a Minimum Mean-Square Error (MMSE) equaliser.

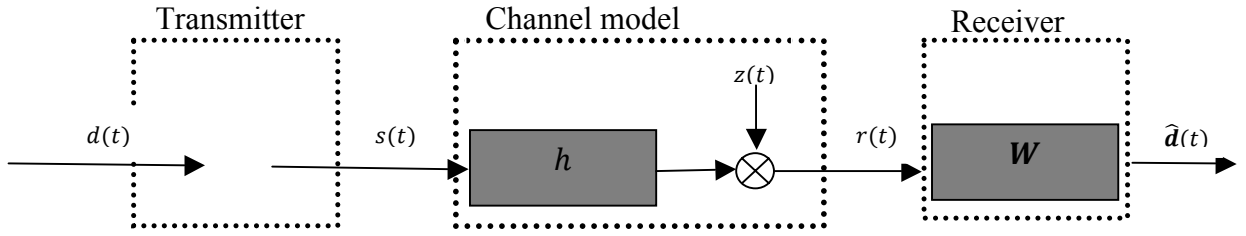


Fig. 3.4 General time-domain linear equaliser.

It is obvious that using single carrier modulation system in frequency fading channel will be inefficient due to the time equalisation complexity. On the other hand the OFDM systems give an instant solution to this problem using a single tap equaliser in the frequency domain which was considered earlier in Section 2.7. As OFDM cannot deal with doubly dispersive channels there is a motivation to search for other bases that can match the channel frequency variation with time like DFrFT. Although it was found that OFDM and DFrFT-OCDM require complicated equalisers to compensate the effects of the channel, the DFrFT-OCDM always provided superior results.

### 3.4 OFDM and DFrFT-OCDM Equalisation Techniques under Doubly Dispersive Fading Channel

In an OFDM and DFrFT-OCDM systems, loss of subcarrier orthogonality happens with the mobility of the receiver due to Doppler frequency and time variation in the frequency fading channel over an MCM block period producing ICI which degrade the OFDM and the DFrFT-OCDM system performance. ICI increases significantly with the increase of the MCM block size, carrier frequency and velocity.

A lot of work have been done in this area to calculate the effects of time selective multipath fading on OFDM systems for broadband mobile applications many of them give bounds for the ICI errors [31, 33, 35] and for the DFrFT-OCDM in [97]. Recently, various techniques have been proposed to counteract such ICI effects in OFDM system [23, 30, 85, 86, 98-102] and in DFrFT-OCDM system [45, 74, 83].

It has been shown that nonlinear equalisers based on ICI cancellation generally outperform linear approaches [22, 98]. At least, linear schemes still preserve their importance for the following reasons:

- 1- Linear equalisers are usually simpler, and therefore less complex.
- 2- Nonlinear schemes usually use a linear equaliser to get the temporary decisions that they use to cancel out the ICI.

### 3.4.1 OFDM and DFrFT-OCDM systems under Doubly Dispersive Fading Channel

Consider the OFDM system in Fig. 3.5. The transmitted data vector in the  $n^{th}$  OFDM symbol is given by  $\mathbf{d}_n = [d_0, d_1, \dots, d_{N_a-1}]^T$  its samples in the frequency domain, permuted by the binary matrix  $\mathbf{P} \in \mathbb{Z}^{N \times N_a}$  which assigns a data vector  $\mathbf{d}_n \in \mathbb{C}^{N_a}$  to  $N$  subcarriers, of which only  $N_a$  are active according to:

$$\mathbf{P} = \begin{bmatrix} \mathbf{0}_{N_a \times (N-N_a)/2} & \mathbf{I}_{N_a} & \mathbf{0}_{N_a \times (N-N_a)/2} \end{bmatrix} \quad (3.17)$$

where  $\mathbf{0}_{X \times Y}$  is an  $X \times Y$  matrix with zero entries, and  $\mathbf{I}_X$  is an  $X \times X$  identity matrix. The vector  $\mathbf{s}_n = [s_0, s_1, \dots, s_N]^T$  is calculated from:

$$\mathbf{s}_n = \mathbf{F}^* \mathbf{P} \mathbf{d}_n \quad (3.18)$$

where  $\mathbf{F}^*$  is used to denote the  $N$ -point unitary IDFT matrix.

The doubly dispersive channel can be modelled by the time variant discrete impulse response  $h(n, v)$ , where  $n$  is the time instant and  $v$  is the time delay. Model justification can be found in more details in [33, 35, 36] and it can be expressed in the form of (time-variant, circular) convolution matrix by:

$$[H]_{n,v} := h(n, \langle n - v \rangle_N) \quad (3.19)$$

Assuming causal channel and the cyclic prefix  $L$  is longer than the maximum delay spread  $N_h \leq L$ , the received samples for the  $n^{th}$  OFDM symbol after discarding the CP can be given by:

$$\mathbf{r}_n = \mathbf{H}_n \mathbf{d}_n + \mathbf{z}_n \quad (3.20)$$

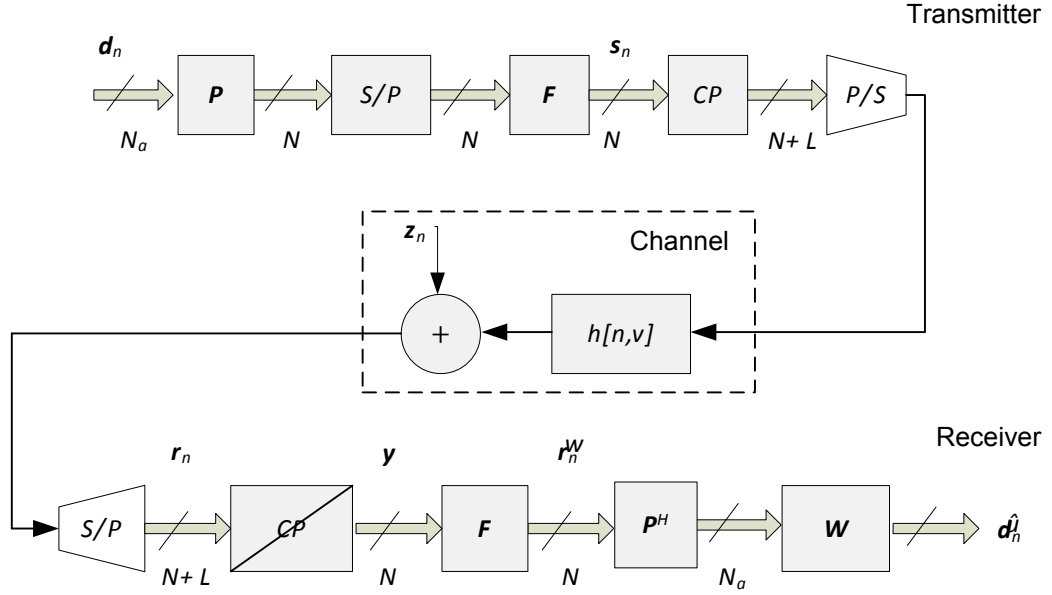


Fig. 3.5 OFDM Block diagram

where  $\mathbf{z}_n$  are samples of white Gaussian noise (AWGN) with variance  $\sigma^2$ . In stationary conditions,  $\mathbf{H}_n$  is circulant, and can be decoupled by the DFT matrix. Received subcarriers are demodulated using the DFT

$$\mathbf{y} = \mathbf{F} \mathbf{r}_n \quad (3.21)$$

where  $\mathbf{F}$  is the DFT matrix and  $\mathbf{y}$  is the received signal after demodulation by the DFT matrix. The equaliser matrix  $\mathbf{W}_n \in \mathbb{C}^{N_a \times N_a}$  operates on the input:

$$\tilde{\mathbf{r}}_n = \mathbf{P}^H \mathbf{F} \mathbf{H}_n \mathbf{F}^* \mathbf{P} \mathbf{d}_n + \mathbf{P}^H \mathbf{F} \mathbf{z} = \mathbf{U}_n \mathbf{d}_n + \tilde{\mathbf{z}}_n \quad (3.22)$$

with a system matrix  $\mathbf{U}_n \in \mathbb{C}^{N_a \times N_a}$ , where  $\mathbf{U}_n = \mathbf{P}^H \mathbf{F} \mathbf{H}_n \mathbf{F}^* \mathbf{P}$ . The purpose of the binary matrix  $\mathbf{P}$  is not only to act as a frequency guard band and help lower out-of-band emissions, but also to eliminate components that would appear in the upper right and lower left corners in  $\mathbf{U}_n$  [23]. The estimated data vector is given by:

$$\hat{\mathbf{d}}_n = \mathbf{W} \tilde{\mathbf{r}}_n \quad (3.23)$$

where  $\mathbf{W}$  is the equaliser matrix. The equivalent  $N_a \times N_a$  subcarrier coupling matrix (frequency domain channel matrix) and the noise vector in the frequency domain are given by  $\tilde{\mathbf{H}} = \mathbf{F} \mathbf{H} \mathbf{F}^*$  and  $\tilde{\mathbf{z}} = \mathbf{F} \mathbf{z}$  respectively. It is straight forward to show that  $[\tilde{\mathbf{H}}]_{m,k} = \tilde{h}(m-k, k)$ , where

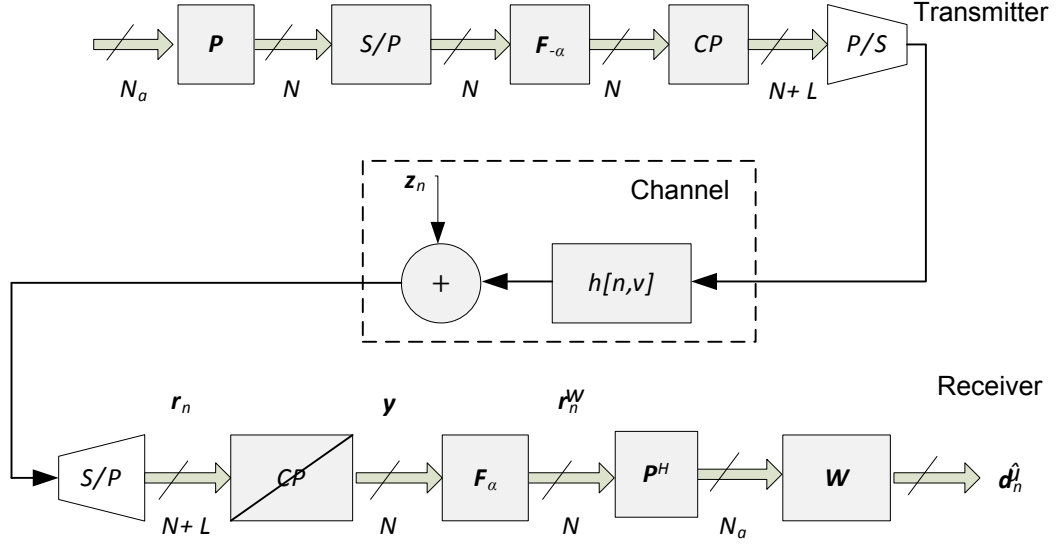


Fig. 3.6 DFrFT-OCDM System Block diagram

$$\tilde{h}(m, k) = \frac{1}{N} \sum_{n=0}^{N-1} \sum_{v=0}^{N-1} h(n, v) e^{-j2\pi(vk+mn)/N} \quad (3.24)$$

From (3.24) it can be shown that  $\{\tilde{h}(0, :)\}$  appears on the main diagonal of  $[\tilde{H}]_{m,k}$ ,  $\{\tilde{h}(-1, :)\}$  on the first super-diagonal,  $\{\tilde{h}(1, :)\}$  on the first sub-diagonal and so on. This means that  $\tilde{h}(m, k)$  can be considered as the frequency-domain response, at subcarrier  $k + m$ , to a frequency-domain impulse centred at subcarrier  $k$ . In  $\tilde{h}(m, k)$ ,  $m$  can be understood as Doppler index and  $k$  as the frequency index. In  $h(n, v)$ ,  $n$  can be interpreted as the time index and  $v$  as the lag index.

Now consider the DFrFT-OCDM system in Fig. 3.6, it is almost the same as the OFDM system except the modulation and demodulation blocks are replaced by the inverse fractional Fourier transform IDFrFT and the fractional Fourier transform DFrFT respectively. Applying the same procedure for the data to be transmitted in the transmitter and the receiver so it is straight forward to show that the equaliser matrix  $\mathbf{W}_n \in \mathbb{C}^{N_a \times N_a}$  operates on the input:

$$\tilde{\mathbf{r}}_n = \mathbf{P}^H \mathbf{F}_\alpha \mathbf{H}_n \mathbf{F}_{-\alpha} \mathbf{P} \mathbf{d}_n + \mathbf{P}^H \mathbf{F}_\alpha \mathbf{z} = \mathbf{U}_{n,\alpha} \mathbf{d}_n + \tilde{\mathbf{z}}_n \quad (3.25)$$

where  $\mathbf{F}_\alpha$  is the DFrFT,  $\mathbf{F}_{-\alpha}$  is the IDFrFT,  $\alpha$  is the fractional angle in the fractional domain and  $\mathbf{U}_{n,\alpha}$  is the system matrix with  $\mathbf{U}_{n,\alpha} \in \mathbb{C}^{N_\alpha \times N_\alpha}$ . The equivalent  $N_\alpha \times N_\alpha$  channel matrix and the noise vector in the fractional domain are given by  $\tilde{\mathbf{H}}_\alpha = \mathbf{F}_\alpha \mathbf{H} \mathbf{F}_{-\alpha}$  and  $\tilde{\mathbf{z}} = \mathbf{F}_\alpha \mathbf{z}$  respectively.

$\tilde{\mathbf{H}}$  and  $\tilde{\mathbf{H}}_\alpha$  are nondiagonal subcarrier channel matrices introduce ICI, which is the case when the dispersive channel comprises a multipath doubly dispersive channel. This will make the symbol estimation task particularly complicated due to the need for complicated equaliser.

### 3.4.2 Zero Forcing and MMSE Block Equalisers

The linear ZF and MMSE estimates [23] can be found by minimizing  $E\{\|\mathbf{d}_n - \mathbf{W}\tilde{\mathbf{r}}_n\|\}$ , yielding:

$$\hat{\mathbf{d}}_{ZF} = \tilde{\mathbf{H}}_\alpha^+ \tilde{\mathbf{r}}_n = \tilde{\mathbf{H}}_\alpha^H (\tilde{\mathbf{H}}_\alpha \tilde{\mathbf{H}}_\alpha^H)^{-1} \tilde{\mathbf{r}}_n \quad (3.26)$$

$$\hat{\mathbf{d}}_{MMSE} = \tilde{\mathbf{H}}_\alpha^H (\tilde{\mathbf{H}}_\alpha \tilde{\mathbf{H}}_\alpha^H + \gamma^{-1} \mathbf{I}_{N_\alpha})^{-1} \tilde{\mathbf{r}}_n \quad (3.27)$$

where  $\tilde{\mathbf{H}}_\alpha$  can be reduced to  $\tilde{\mathbf{H}}$  when  $\alpha = \pi/2$  and the fractional domain will reduce to the frequency domain,  $\hat{\mathbf{d}}_{ZF}$  and  $\hat{\mathbf{d}}_{MMSE}$  are the estimated data after ZF and MMSE equalisation respectively,  $\tilde{\mathbf{H}}_\alpha^H$  is the channel matrix conjugate transpose in the fractional domain,  $\mathbf{I}_{N_\alpha}$  is the identity matrix with  $N_\alpha \times N_\alpha$  elements,  $\gamma$  is the signal-to-noise ratio (SNR) and  $\tilde{\mathbf{H}}_\alpha^+$  is the Moore-Penrose pseudo-inverse of the channel matrix in the fractional domain[103]. In (3.26) and (3.27) perfect knowledge of the channel matrix  $\mathbf{H}_\alpha$  is assumed and the equaliser does not use guard subcarriers. Furthermore it is assumed that:  $E\{\mathbf{d}_n\} = E\{\tilde{\mathbf{z}}_n\} = 0, E\{\mathbf{d}_n \mathbf{d}_n^H\} = \mathbf{I}, E\{\mathbf{d}_n \tilde{\mathbf{z}}_n^H\} = 0, E\{\tilde{\mathbf{z}}_n \tilde{\mathbf{z}}_n^H\} = \sigma^2 \mathbf{I}$

ZF equaliser performance is poor due to noise enhancement. On the other hand the MMSE equaliser gives the best performance in all linear equalisers [98] but it is very complex due to channel matrix inversion which needs  $\mathcal{O}(N_\alpha^3)$  complex operations [104] which is not practical for high values of  $N_\alpha$  which is the case in DVB-T and DVB-H and WiMAX.

### 3.4.3 Low Complexity Equalisers

Although MMSE equaliser outperform all other linear equalisers, the MMSE complexity makes it not practical in long symbols such as for broadcasting applications case due to matrix inversion in (3.27). Many equalisers are proposed for reducing the MMSE equalisers complexity [23, 30, 85, 86, 99, 100, 102]. In [23] a serial MMSE equaliser is proposed and in [85] banded equalisers were proposed. All these low complexity equalisers give almost the same or near performance as block MMSE while reducing the complexity of calculations.

As stated in [23] doubly dispersive channels produce a nearly banded channel matrix in frequency domain and fractional domain, from this criteria more complexity reduction can be done using  $LDL^H$  factorization[28, 85] instead of direct matrix inversion. All the low complexity equalisers are stated for OFDM not for DFrFT-OCDM system. In the following sections low complexity equalisers will be examined with DFrFT-OCDM.

## 3.5 A Novel Multimode Transmission Method Using OFDM and DFrFT-OCDM

The proposed multimode transmission method adaptively changes some system components such as transmission rate or modulation, corresponding to the status of the transmitter, the receiver, data, or the transmission environment. It facilitates an increase of transmission throughput and quality. Since the transmission environment change frequently and significantly in wireless communications, the multimode transmission is effective for wideband communications by means of the efficient use of resources such as signal power and spectrum bandwidth.

As shown in Fig. 3.7, DFrFT-OCDM and OFDM have different subcarriers where OFDM subcarriers are orthogonal Frequencies with constant frequency per subcarrier and the DFrFT-OCDM are orthogonal chirp signals with different frequencies per subcarrier. This difference appears as the difference of transmission performance in time invariant fading channels and time variant channels. That is, the degradation of

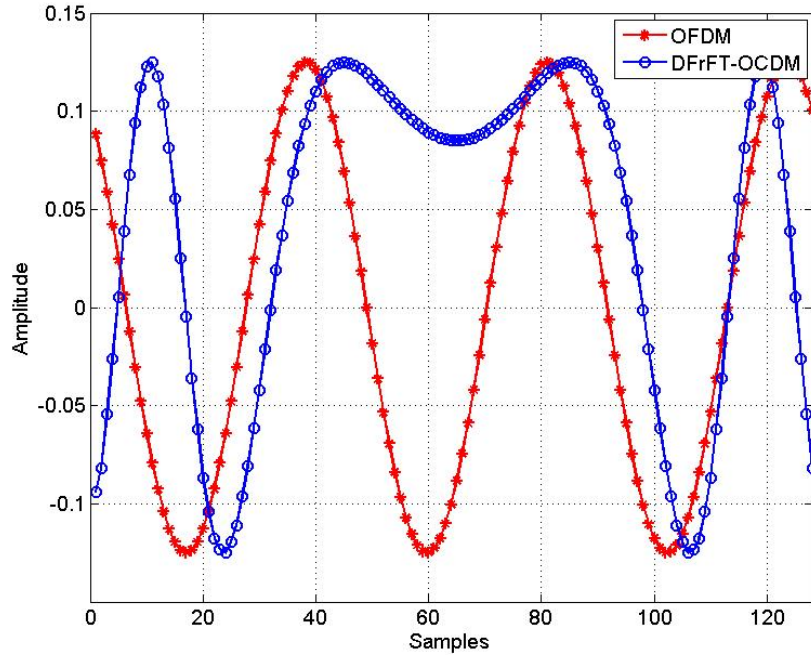


Fig. 3.7 DFrFT-OCDM and OFDM Subcarriers

Transmission in time-variant fading channels environment can be reduced by use of DFrFT-OCDM, and in the case of time invariant multipath fading environments can be suppressed by use of OFDM. Therefore, we propose a multimode system with DFrFT-OCDM and OFDM, wherein the advantages of both will be obtained. For example, in the case of indoor wireless transmission the radio waves suffer from time invariant multipath fading. In addition, deep time variant multipath fading occurs when the mobile terminal is moving especially with high speeds. In such case, the multimode transmission that switches between DFrFT-OCDM and OFDM corresponding to the transmission environments is effective, and the degradation can be suppressed.

The block diagram of multimode transmission with DFrFT-OCDM and OFDM is shown Fig. 3.8. In the transmitter, some modes including OFDM and different DFrFT-OCDM where each mode has a different  $\alpha$  with different chirp signal are prepared, and data are transmitted in one mode corresponding to the transmission environment. In the receiver, the transmitter mode is known and the data are decoded, the channel configuration can be determined through channel estimation and proper transmission

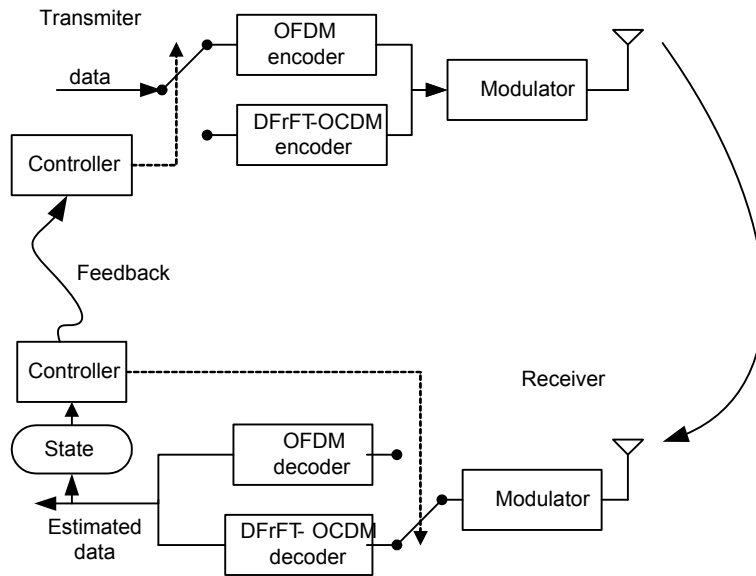


Fig. 3.8 DFrFT-OCDM and OFDM Multimode System

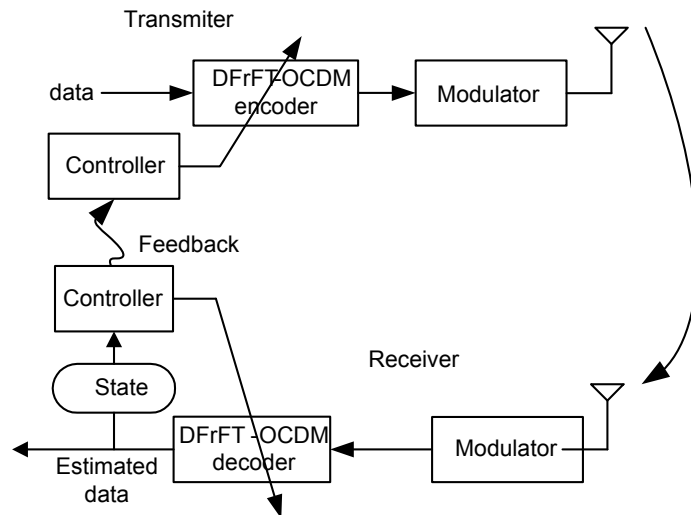


Fig. 3.9 Multimode OFDM and DFrFT-OCDM System with  $\alpha$  Selection

mode must be selected and transmitted back to receiver. As a result, an increase in system performance will be expected in those severe environments. On the other hand there will be a slightly increase in the system complexity due to the need for calculating the optimum fractional order  $\alpha$  needed and the existence of two modulation blocks for

OFDM and DFrFT-OCDFM there is also losses in the system baud rate due to the feedback process.

It is important to note that there is no need for separate DFrFT-OCDFM and OFDM blocks in both the transmitter and the receiver as shown in Fig. 3.9. This is due to the fact that one of the properties of the fractional Fourier transform that it can have any fractional angle ( $0 \leq \alpha \leq \pi/2$ ) where  $\alpha = \pi/2$  is the Fourier transforms itself.

### 3.5.1 Performance Analysis

The uncoded bit error rate (BER) performance of the traditional OFDM and the DFrFT-OCDFM systems are investigated in both channel environments:

- 1- Time invariant channel.
- 2- Time variant channel.

An OFDM system with  $N = 128, N_a = 96, L = 8$ , and QPSK modulation is assumed. Rayleigh fading channels are simulated with an exponential power delay profile and root-mean-square delay spread of 3. The carrier frequency is  $f_c = 10 \text{ GHz}$  and the subcarrier spacing is  $\Delta f = 20 \text{ kHz}$ . Simulation is carried over  $10^5$  continuous channels and different OFDM symbols which mean  $10^5 * 96 * 4$  data bits.

#### 3.5.1.1 Time invariant channel:

In the time invariant channel environment the Doppler frequency  $f_d = 0$ . The OFDM system uses the single tap equaliser and the DFrFT-OCDFM system use the MMSE equaliser. Fig. 3.10 shows the BER performance for the both systems. The OFDM system performance is compared to the work carried in [86] and it was found to be matched.

From Fig. 3.10 although the DFrFT-OCDFM system has superior performance, the OFDM system with the single tap equaliser has very good performance with much less complexity. As a result it is better to use the OFDM mode in time invariant fading channel scenarios.

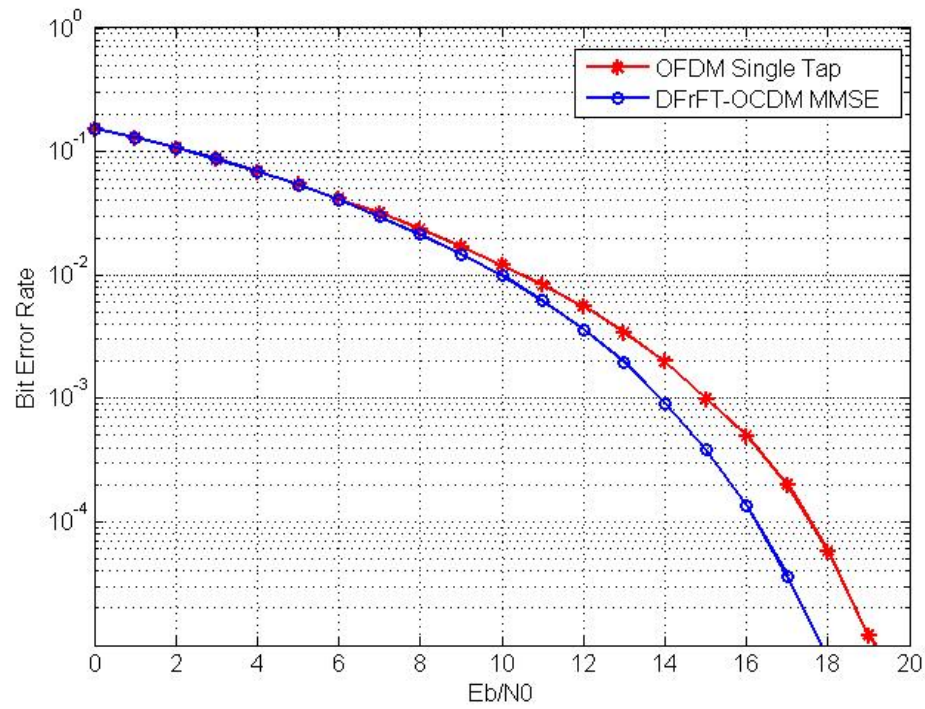


Fig. 3.10 OFDM and DFrFT-OCDM BER comparison in time invariant channel environment

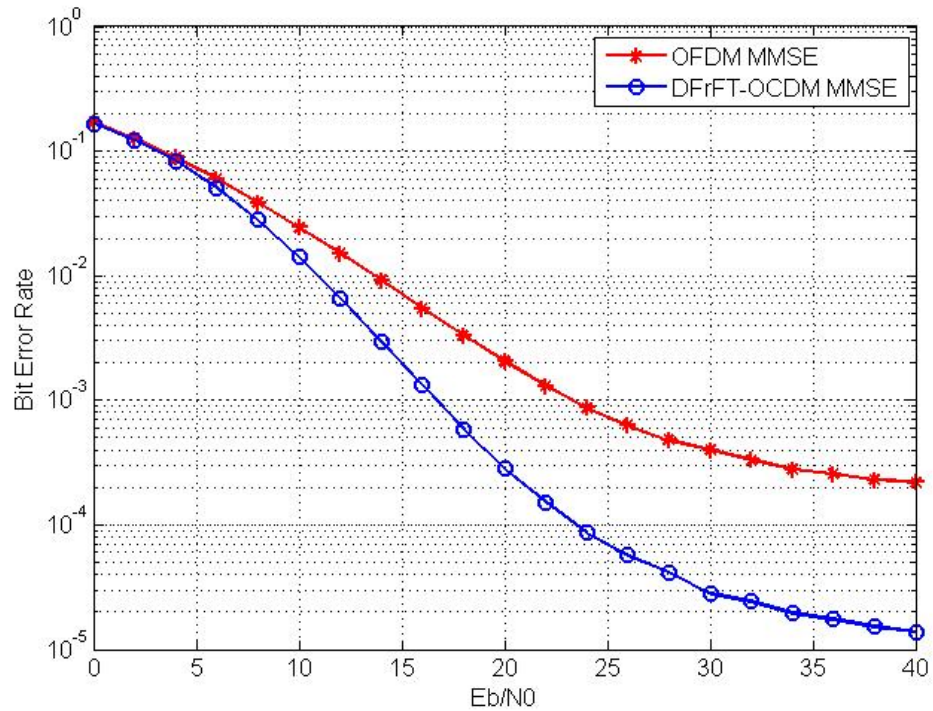


Fig. 3.11 OFDM and DFrFT-OCDM BER comparison in time variant channel environment

### 3.5.1.2 Time variant channel

In the time variant channel environment we consider the maximum Doppler frequency  $f_d = 0.15\Delta f$ . The MMSE equaliser was used for both the OFDM system and the DFrFT-OCDFM system. Fig. 3.11 shows the BER performance for the both systems with the same block MMSE equaliser.

From Fig. 3.11 the DFrFT-OCDFM system has superior performance over the OFDM system with the same MMSE equaliser with the same complexity. As a result it is better to use the DFrFT-OCDFM mode in time variant fading channel scenarios.

### 3.5.2 Multimode Scheme Conclusion

In this section a multimode transmission method using the DFrFT-OCDFM and OFDM is presented which can be applied to multiple transmission environments. Using the different transmission characteristics between DFrFT-OCDFM and OFDM in multipath fading and doubly dispersive multipath fading environments, good performance was obtained in both environments using the lowest complexity. The BERs of DFrFT-OCDFM and OFDM in fading environments were also calculated. The results demonstrated the relations between fading types and performances. Using the proposed multimode system will ensure the best transmission quality with the lowest complexity.

## 3.6 Low Complexity Band $LDL^H$ Factorization Equaliser for DFrFT-OCDFM. (Linear equaliser)

$LDL^H$  factorization equaliser was proposed in [86] as a low complexity equaliser for the OFDM systems benefitting from the banded properties of the frequency domain channel matrix  $\tilde{\mathbf{H}}$ . In the same manner the  $LDL^H$  factorization equaliser can be used with DFrFT-OCDFM systems as system matrix in the fractional domain is approximately banded [20].

The calculation of the equaliser matrix  $\mathbf{W}_n$  is restricted to the first  $Q$  sub- and super-diagonals of  $\tilde{\mathbf{H}}_\alpha$  by means of a binary masking matrix  $\mathbf{M}$  with elements:

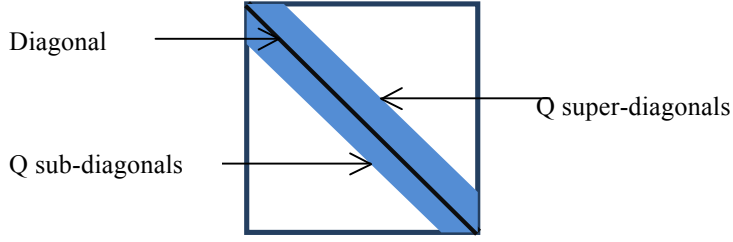


Fig. 3.12 The desired structure for the band matrix  $B$  inside the whole matrix  $\tilde{H}_\alpha$

$$\mathbf{M}(m, n) = \begin{cases} 1 & 0 \leq |m - n| \leq Q \\ 0 & Q < |m - n| < N_a \end{cases} \quad (3.28)$$

The shape of this matrix is imprinted on the masked matrix:

$$\mathbf{B}_n = \mathbf{M} \odot \tilde{\mathbf{H}}_\alpha \quad (3.29)$$

as illustrated in Fig. 3.12 where  $\odot$  represents element-wise multiplication. Based on the masked matrix, analogously to [86] the MMSE equaliser can be defined as:

$$\mathbf{W}_{n,MMSE} = \mathbf{B}_n^H (\mathbf{B}_n \mathbf{B}_n^H + \gamma^{-1} \mathbf{I}_{N_a})^{-1} \quad (3.30)$$

The band structure of  $\mathbf{B}_n$  with  $Q$  off-diagonal terms below and above the main diagonal leads to a band structure for  $(\mathbf{B}_n \mathbf{B}_n^H)$ , where only the first  $2Q$  off-diagonal terms above and below the diagonal contain finite elements. This can simplify the calculation of the MMSE equaliser in (3.30). However, since (3.30) is time-dependent,  $\hat{\mathbf{d}}_n = \mathbf{W}_{n,MMSE} \tilde{\mathbf{r}}_n$  will be calculated without explicitly determining  $\mathbf{W}_{n,MMSE}$ .

The  $LDL^H$  factorisation of the Hermitian band matrix  $\mathbf{B}_n \mathbf{B}_n^H + \gamma^{-1} \mathbf{I}_{N_a} = \mathbf{LDL}^H$  is numerically straightforward[104], and leads to:

$$\hat{\mathbf{d}}_n = \mathbf{B}_n^H (\mathbf{LDL}^H)^{-1} \tilde{\mathbf{r}}_n = \mathbf{B}_n^H \mathbf{x}_n \quad (3.31)$$

Instead of calculating the inverse in (3.31), the system:

$$(\mathbf{LDL}^H)^{-1} \tilde{\mathbf{r}}_n = \mathbf{x}_n \quad (3.32)$$

$$\tilde{\mathbf{r}}_n = (\mathbf{LDL}^H) \mathbf{x}_n \quad (3.33)$$

$$\tilde{\mathbf{r}}_n = \mathbf{L} \mathbf{D} \overbrace{\mathbf{L}^H \mathbf{x}_n}^{x_{1,n}} \quad (3.34)$$

$x_{2,n}$

is solved by forward substitution to obtain  $\mathbf{x}_{2,n}$  via the lower left triangular matrix  $\mathbf{L}$  and a rescaling by the diagonal matrix  $\mathbf{D}^{-1}$  to calculate  $\mathbf{x}_{1,n}$ . Finally back substitution with the upper right triangular  $\mathbf{L}^H$  yields  $\mathbf{x}_n$ , which can be inserted into (3.31) in order to determine  $\hat{\mathbf{d}}_n$ .

The overall complexity for obtaining  $\hat{\mathbf{d}}_n$  is  $(8Q^2 + 22Q + 4)N_a$  complex operations [86]. The parameter  $Q$  choice is a trading off between performance and complexity. This implies that by choosing larger  $Q$  yields a smaller approximation error and therefore a performance improvement. However the resulting complexity increases due to the higher bandwidth of  $\mathbf{B}$ , and vice versa.

To assess the performance of the proposed system, an OFDM transmission with  $N = 128$  subcarriers of which  $N_a = 96$  are active, a cyclic prefix of length  $L = 8$ , and QPSK modulation. Simulations are performed over an ensemble of  $10^5$  Rayleigh fading channels defined by an exponential power delay profile with an RMS delay spread of three sampling periods. This channel model uses the same statistics as in [85], including a maximum Doppler spread  $f_d$  equal to 15% of the carrier spacing.

Comparison between the block MMSE equaliser and the  $LDL^H$  low complexity equaliser (Banded MMSE) is shown in Fig. 3.13 for both the OFDM system and the DFrFT-OCDFM system ( $\alpha = 0.2\pi/2$ ), The low complexity equaliser is operated with  $Q = \{5, 96\}$ , whereby the second setting is equivalent to a standard block MMSE equaliser. Performance results in terms of bit error rate are shown in Fig. 3.13. The OFDM curves match those reported in [86]. The proposed DFrFT-OCDFM system with  $Q = 5$  shows a degradation over the full scheme at high SNR, but only requires 3.4% [86] of the computational cost in terms of complex operations and still outperforms OFDM even with a full block MMSE equaliser with a computation cost of  $\mathcal{O}(N_a^3)$  complex operations.

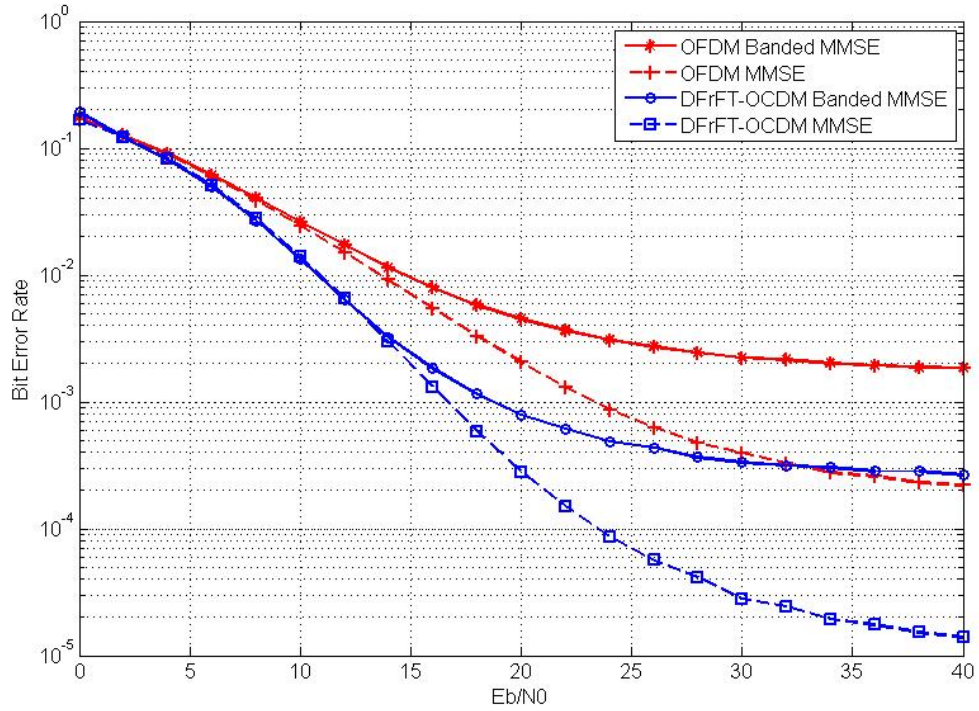


Fig. 3.13 Bit error ratio for MMSE equalisation using block ( $Q = N_a = 96$ ) and low-complexity ( $Q = 5$ ) approaches for DFrFT-OCDM ( $\alpha = 0.2\pi/2$ ) and OFDM

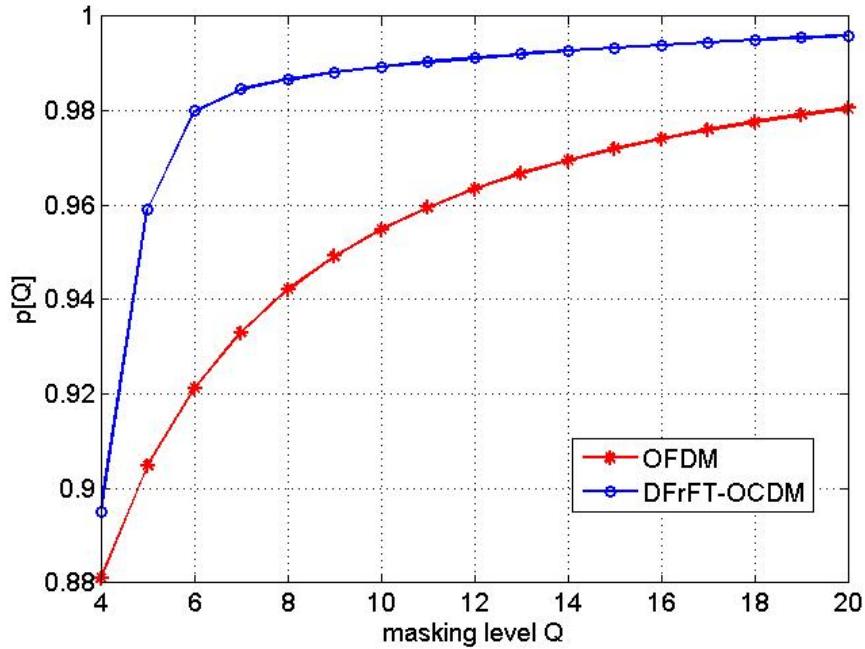


Fig. 3.14 Percentage of power of  $\tilde{\mathbf{H}}_\alpha$  contained in  $\mathbf{B}_n$ , measured by  $[Q]$  in dependence of the number of off-diagonal elements  $Q$  considered by  $\mathbf{M}$ , comparing OFDM and DFrFT-OCDM ( $\alpha = 0.2\pi/2$ )

To assess the impact of the masking level  $Q$ , a comparison between the power components in the original system matrix  $\tilde{\mathbf{H}}_\alpha$  and in the reduced matrix  $\mathbf{B}_n$  after masking by  $M$  is needed. Averaged over the ensemble and using the trace operator  $tr\{\cdot\}$ , this power ratio is defined as:

$$\rho[Q] = \varepsilon \frac{\left\{ tr\{\mathbf{B}_n \mathbf{B}_n^H\} \right\}}{\left\{ tr\{\tilde{\mathbf{H}}_\alpha \tilde{\mathbf{H}}_\alpha^H\} \right\}}, \quad 0 \leq \rho[Q] \leq 1 \quad (3.35)$$

Results shown in Fig. 3.14 clearly indicate that OFDM experiences a spread of energy away from the main diagonal due to Doppler fading which is not limited to nearby off-diagonals, hence requiring a high value for  $Q$  to capture most of the power contained in  $\tilde{\mathbf{H}}$ . DFrFT-OCDFM does not manage to diagonalise  $\tilde{\mathbf{H}}_\alpha$ , but in contrast to OFDM, the leaked power is contained in neighboring off-diagonal element, and a much lower value of  $Q$  suffices to capture most of the components of  $\tilde{\mathbf{H}}_\alpha$  in  $\mathbf{B}_n$ .

### 3.7 Low-Complexity LSMR Equalisation (Linear equaliser).

MMSE equaliser complexity comes from the matrix inversion in (3.27), solving this matrix inversion iteratively is one of the clever ideas to reduce the MMSE equaliser complexity. In [84, 105-107] authors use the iterative LSQR algorithm [108], which has superb performance in solving the channel matrix inversion problem (typically ill-conditioned matrix) by early termination of the iterations at low complexity as the complexity order per iteration is  $\mathcal{O}(N_a N_h)$  operations, where  $N_h$  is the maximum delay of the channel. Thus, the method is mostly smart when the channel's maximum delay is not too large. Recently a new iterative algorithm called LSMR was proposed in [109].

LSMR is an iterative algorithm for solving linear systems  $\mathbf{Ax} = \mathbf{b}$ , least-squares (LS) problems  $min\|\mathbf{Ax} - \mathbf{b}\|_2$  and regularized least squares (RLS)  $min \left\| \begin{pmatrix} \mathbf{A} \\ \lambda \mathbf{I} \end{pmatrix} \mathbf{x} - \begin{pmatrix} \mathbf{b} \\ 0 \end{pmatrix} \right\|_2$  with  $A$  being sparse or a fast linear operator [109]. LSMR is based on the Golub-Kahan bidiagonalisation process and it is analytically equivalent to the MINRES [110] applied to the normal equation  $\mathbf{A}^T \mathbf{Ax} = \mathbf{A}^T \mathbf{b}$ . LSMR is similar in style to the well-known method LSQR in being based on the Golub-Kahan bidiagonalisation of  $\mathbf{A}$ . LSQR is equivalent to the conjugate gradient (CG) method applied to the normal equation:

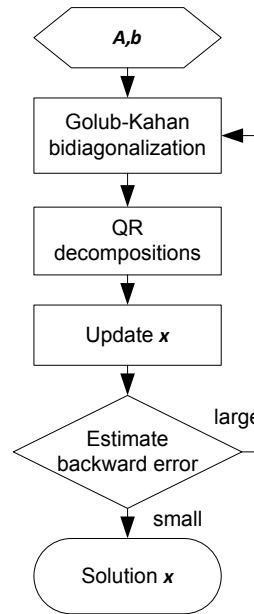


Fig. 3.15 LSMR Algorithm flow chart

$(\mathbf{A}^T \mathbf{A} + \lambda^2 \mathbf{I})\mathbf{x} = \mathbf{A}^T \mathbf{b}$ . It has the property of reducing  $\|\mathbf{r}_k\|$  monotonically, where  $\mathbf{r}_k = \mathbf{b} - \mathbf{A}\mathbf{x}_k$  is the residual for the approximate solution  $\mathbf{x}_k$ . On the other hand, LSMR has the property of reducing both  $\|\mathbf{r}_k\|$  and  $\|\mathbf{A}^T \mathbf{r}_k\|$  monotonically. Although LSQR and LSMR ultimately converge to similar points but LSMR converges faster with fewer iterations. LSMR can solve the inversion matrix problem in MMSE equaliser more effectively with less computational cost due to its faster conversion to the solution.

### 3.7.1 LSMR Algorithm:

LSMR algorithm aims to approximately solve the linear equation given by:

$$\mathbf{A}^T \mathbf{A} \mathbf{x} = \mathbf{A}^T \mathbf{b} \quad (3.36)$$

$$\min \|\mathbf{A}\mathbf{x} - \mathbf{b}\|_2 \quad (3.37)$$

and the regularized least squares given by:

$$(\mathbf{A}^T \mathbf{A} + \lambda^2 \mathbf{I})\mathbf{x} = \mathbf{A}^T \mathbf{b} \quad (3.38)$$

$$\min \left\| \begin{pmatrix} \mathbf{A} \\ \lambda \end{pmatrix} \mathbf{x} - \begin{pmatrix} \mathbf{b} \\ 0 \end{pmatrix} \right\|_2 \quad (3.39)$$

with  $\mathbf{A}$  being sparse or a fast linear operator. Flow chart for the LSMR algorithm is shown in Fig. 3.15.

For simplicity consider (3.36) given  $\mathbf{A}$  and  $\mathbf{b}$  starting from Golub-Kahan bidiagonalisation [111], the direct bi-diagonalisation is given by:

$$\mathbf{U}^T (\mathbf{b} \quad \mathbf{A}) \begin{pmatrix} \mathbf{1} \\ \mathbf{v} \end{pmatrix} = \begin{pmatrix} \times & \times & 0 & 0 \\ 0 & \times & \times & 0 \\ 0 & 0 & \times & \times \\ 0 & 0 & 0 & \times \end{pmatrix} \Rightarrow (\mathbf{b} \quad \mathbf{A}\mathbf{v}) = \mathbf{U}(\boldsymbol{\beta}_1 \mathbf{e}_1 \quad \mathbf{B}) \quad (3.40)$$

using iterative bidiagonalisation Bidiag  $(\mathbf{A}, \mathbf{b})$ :

$$\mathbf{b} = \mathbf{U}_{k+1}(\boldsymbol{\beta}_1 \mathbf{e}_1) \quad (3.41)$$

$$\mathbf{A}\mathbf{V}_k = \mathbf{U}_{k+1}\mathbf{B}_k \quad (3.42)$$

$$\mathbf{A}^T \mathbf{U}_k = \mathbf{V}_k \mathbf{B}_k^T \begin{pmatrix} \mathbf{I}_k \\ 0 \end{pmatrix} \quad (3.43)$$

where

$$\mathbf{B}_k = \begin{pmatrix} \alpha_1 & 0 & 0 & 0 \\ \beta_1 & \alpha_2 & 0 & 0 \\ 0 & \ddots & \ddots & 0 \\ 0 & 0 & \beta_k & \alpha_k \\ 0 & 0 & 0 & \beta_{k+1} \end{pmatrix} \quad \text{and} \quad \begin{matrix} \mathbf{U}_k = (\mathbf{u}_1 & \dots & \mathbf{u}_k) \\ \mathbf{V}_k = (\mathbf{v}_1 & \dots & \mathbf{v}_k) \end{matrix} \quad (3.44)$$

$\mathbf{V}_k$  spans the Krylov subspace:

$$\text{span}\{\mathbf{v}_1, \dots, \mathbf{v}_k\} = \text{span}\{\mathbf{A}^T \mathbf{b}, (\mathbf{A}^T \mathbf{A}) \mathbf{A}^T \mathbf{b}, \dots, (\mathbf{A}^T \mathbf{A})^{k-1} \mathbf{A}^T \mathbf{b}\} \quad (3.45)$$

Define  $\mathbf{x}_k = \mathbf{V}_k \mathbf{y}_k$ , sub-problem to solve:

$$\min_{\mathbf{y}_k} \|\mathbf{A}^T \mathbf{r}_k\| = \min_{\mathbf{y}_k} \left\| \bar{\boldsymbol{\beta}}_1 \mathbf{e}_1 - \begin{pmatrix} \mathbf{B}_k^T \mathbf{B}_k \\ \bar{\boldsymbol{\beta}}_{k+1} \mathbf{e}_k^T \end{pmatrix} \right\| \quad (3.46)$$

where  $\mathbf{r}_k = \mathbf{b} - \mathbf{A}\mathbf{x}_k$ ,  $\bar{\boldsymbol{\beta}}_k = \boldsymbol{\alpha}_k \boldsymbol{\beta}_k$

### 3.7.2 LSMR Complexity:

The storage requirement and computational complexity can be compared for LSMR and LSQR on  $\mathbf{A}\mathbf{x} \approx \mathbf{b}$  and MINRES on the normal equation  $\mathbf{A}^T \mathbf{A}\mathbf{x} = \mathbf{A}^T \mathbf{b}$ . The vector storage (excluding storage for  $\mathbf{A}$  and  $\mathbf{b}$ ) was listed in Table 4.1, Recall that  $\mathbf{A}$  is  $(m \times n)$  and for LS systems  $m$  may be considerably larger than  $n$ .  $\mathbf{A}\mathbf{v}$  denotes the working storage for matrix-vector products, and  $\mathbf{h}_k, \bar{\mathbf{h}}_k$  are scalar multiples of  $\mathbf{w}_k, \bar{\mathbf{w}}_k$ . Work represents the number of floating-point multiplications required for each iteration.

Table 3.1 *Storage and computational requirements for various LS methods*

	Storage		Work	
	$m$	$n$	$m$	$n$
LSMR	$\mathbf{A}\mathbf{v}, \mathbf{u}$	$\mathbf{x}, \mathbf{v}, \mathbf{h}, \bar{\mathbf{h}}$	3	6
LSQR	$\mathbf{A}\mathbf{v}, \mathbf{u}$	$\mathbf{x}, \mathbf{v}, \mathbf{w}$	3	5
MINRES on $\mathbf{A}^T \mathbf{A} \mathbf{x} = \mathbf{A}^T \mathbf{b}$	$\mathbf{A}\mathbf{v}$	$\mathbf{x}, \mathbf{v}_1, \mathbf{v}_2, \mathbf{w}_1, \mathbf{w}_2, \mathbf{w}_3$		8

From Table 3.1 it can be shown that the complexity of the LSMR is slightly more than the LSQR.

### 3.7.3 Linear Least Squares LSMR Equaliser

The doubly dispersive channel matrix is characterized by large maximum delay and Doppler shifts, so the system matrix (Fractional domain channel matrix)  $\tilde{\mathbf{H}}_\alpha$  may have a very high condition number, linear least squares (LLS)-LSMR can be used for equalisation with “implicit regularization”. Using the LLS-LSMR equaliser directly on  $\tilde{\mathbf{H}}_\alpha$  will be complex, so recalling the banded properties of  $\tilde{\mathbf{H}}_\alpha$  and using (3.29) to apply LLS-LSMR on  $\mathbf{B}_n$  produces a major complexity drop. The normal equation for LLS-LSMR equaliser is given by:

$$\mathbf{B}_n^H \mathbf{B}_n \hat{\mathbf{d}}_{ZF} = \mathbf{B}_n^H \tilde{\mathbf{r}}_n \quad (3.47)$$

This normal equation is obtained from (3.25) by ignoring the noise  $\tilde{\mathbf{z}}_n$ , substituting  $\tilde{\mathbf{H}}_\alpha$  with  $\mathbf{B}_n$ , and left-multiplying by  $\mathbf{B}_n^H$ . One can show that in the  $i^{\text{th}}$  LSMR iteration, an approximate solution for the linear least squares problem is obtained by  $\min \|\mathbf{B}_n \hat{\mathbf{d}}_{ZF} - \tilde{\mathbf{r}}_n\|$ .

In zero forcing equaliser, ignoring the noise effect results in noise and modelling errors amplification which degrades the system performance. The same can be considered for LLS-LSMR equaliser as there is no account for noise effect. However, LSMR depends on the number of iterations as a regularization parameter, accordingly, an efficient way of avoiding the amplification of errors and noise can be ensured by early termination of iterations. Using the optimal number of iterations in LSMR can reduce the system errors to a comparable limit with the MMSE equalisation. In practice,

LSMR inputs are known approximately and using the maximum number of iterations clearly amplifies the noise and modelling errors.

### 3.7.4 Regularized Least Squares LSMR Equaliser

The estimated data  $\tilde{\mathbf{d}}_{MMSE}$  from (3.27) in the MMSE sense is given by:

$$\hat{\mathbf{d}}_{MMSE} = \tilde{\mathbf{H}}_{\alpha}^H (\tilde{\mathbf{H}}_{\alpha} \tilde{\mathbf{H}}_{\alpha}^H + \gamma^{-1} \mathbf{I}_{N_a})^{-1} \tilde{\mathbf{r}}_n \quad (3.48)$$

which is equivalent to:

$$\hat{\mathbf{d}}_{MMSE} = (\tilde{\mathbf{H}}_{\alpha}^H \tilde{\mathbf{H}}_{\alpha} + \gamma^{-1} \mathbf{I}_{N_a})^{-1} \tilde{\mathbf{H}}_{\alpha}^H \tilde{\mathbf{r}}_n \quad (3.49)$$

by left multiplying with  $(\tilde{\mathbf{H}}_{\alpha}^H \tilde{\mathbf{H}}_{\alpha} + \gamma^{-1} \mathbf{I}_{N_a})$

$$(\tilde{\mathbf{H}}_{\alpha}^H \tilde{\mathbf{H}}_{\alpha} + \gamma^{-1} \mathbf{I}_{N_a}) \hat{\mathbf{d}}_{MMSE} = \tilde{\mathbf{H}}_{\alpha}^H \tilde{\mathbf{r}}_n \quad (3.50)$$

which is equivalent to the regularized least squares problem  $(\mathbf{A}^T \mathbf{A} + \lambda^2 \mathbf{I}) \mathbf{x} = \mathbf{A}^T \mathbf{b}$  to minimize  $\min \left\| \begin{pmatrix} \mathbf{A} \\ \lambda \end{pmatrix} \mathbf{x} - \begin{pmatrix} \mathbf{b} \\ 0 \end{pmatrix} \right\|_2$ , RLS-LSMR equaliser.

Again it is complex to work with the entire  $\tilde{\mathbf{H}}_{\alpha}$  matrix so using the banded properties of  $\tilde{\mathbf{H}}_{\alpha}$  which leads to the  $\mathbf{B}_n$  matrix using (3.29), the MMSE equaliser problem will be given by:

$$(\mathbf{B}_n \mathbf{B}_n^H + \gamma^{-1} \mathbf{I}_{N_a}) \hat{\mathbf{d}}_{MMSE} = \mathbf{B}_n^H \tilde{\mathbf{r}}_n \quad (3.51)$$

It can be shown that an approximate solution of the regularized least squares equation can be reached using the LSMR.

In this method RLS-LSMR has two regularization parameters: the number of iterations and the signal to noise ratio ( $\gamma$ ) parameter which limits the noise and modelling errors amplification and improves the system performance.

The optimal number of LSMR iterations depends on:

- 1- The noise level.
- 2- The maximum Doppler spread and the maximum delay spread as they affect the distribution of the singular values of the channel matrix.

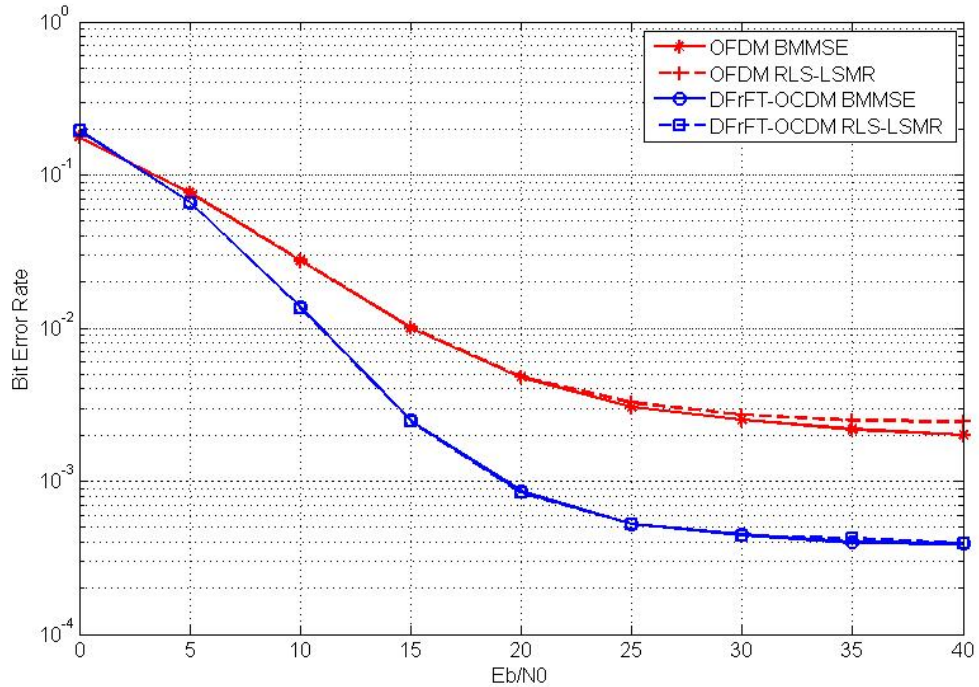


Fig. 3.16 DFrFT-OCDFM and DFT-OFDM Uncoded BER Comparison (Q=5)

However, the number of iterations does not really depend on the number of subcarriers, which appears clearly in simulation.

LSMR is particularly attractive due to its numerical stability, inherent potential for regularization, and low computational complexity of  $\mathcal{O}(N_a(Q+1)i)$  complex operations in total [109] where  $i$  denotes the number of iterations used. Thus, the complexity is just linear in the number of subcarriers  $N$ , the matrix bandwidth  $Q$ , and the number of iterations  $i$ .

### 3.7.5 LSMR Equaliser Simulation Results

The uncoded BER performance of the DFrFT-OCDFM with the RLS-LSMR equaliser is investigated by means of simulation over  $10^5$  multicarrier blocks. An DFrFT-OCDFM system with  $N=128$ ,  $N_A=96$ ,  $L=8$ , and QPSK modulation is assumed.

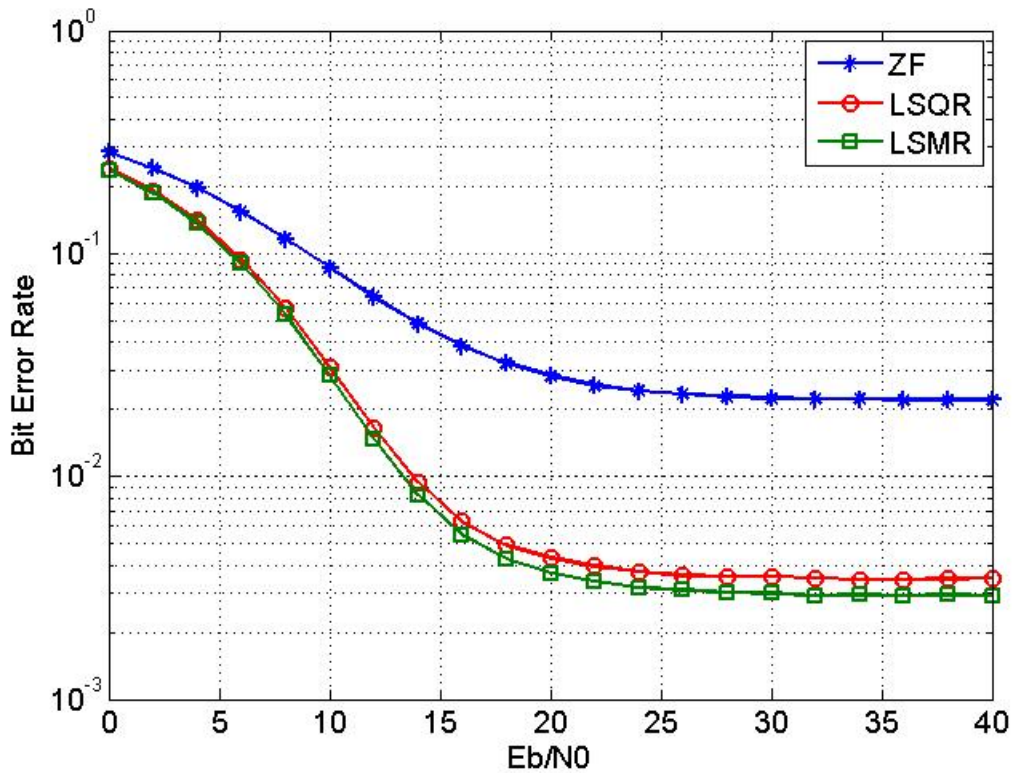


Fig. 3.17 Uncoded BER Comparison between LSMR , LSQR ,ZF

The channel simulation parameters are the same as the Rayleigh fading channel in section 3.6. Fig. 3.16, show a comparison between the DFrFT-OCDM and the OFDM using  $\mu = 5$ , Banded MMSE(BMMSE) and RLS-LSMR equalisers. From Fig. 3.16 it can be seen that the DFrFT-OCDM outperforms the OFDM system with both the LSMR and the MMSE equalisers. However the complexity of the DFrFT-OCDM system is almost the same as the OFDM system.

In Fig. 3.17 we compare the performance of the DFrFT-OCDM system using different equalisers (ZF, LSMR and LSQR). LSMR and LSQR algorithms will solve the linear system  $\mathbf{Ax} = \mathbf{b}$  with limited number of iterations for both LSMR and LSQR.

From Fig. 3.17 it can be seen that the LSMR equaliser provides the best performance and the LSQR equaliser almost give the same performance in low SNR and slightly less than LSMR in higher SNR that because the LSMR algorithm is more stable

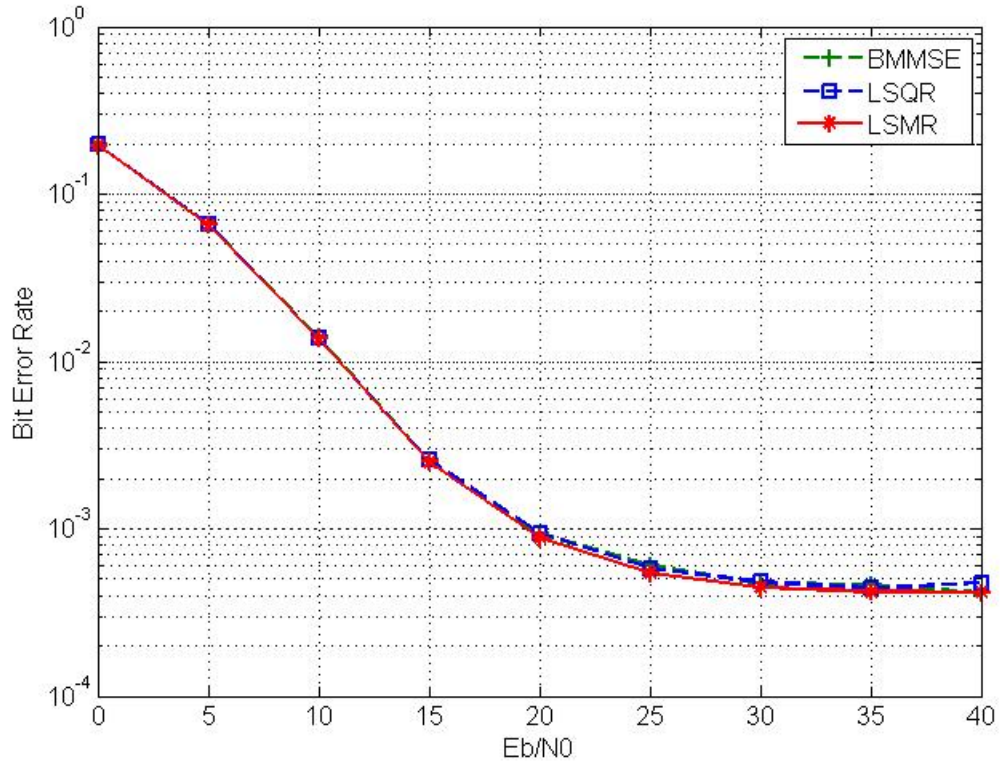


Fig. 3.18 Uncoded BER Comparison between BMMSE, LSQR and LSMR equalisers

than LSQR algorithm when dealing with sparse, possibly ill-conditioned least-squares problems also the LSMR converge faster with less iterations. While the ZF equaliser give the worst performance due to the matrix inversion of the sparse matrix  $\mathbf{B}$ . LSMR and LSQR equalisers give almost the same performance with much less complexity then the ZF equaliser. LSQR can give the same performance as LSMR but with more iterations.

Fig. 3.18 show a comparison between the performance of the DFrFT-OCDM using different equalisers (LSMR - LSQR - BMMSE) where LSMR and LSQR will solve the regularized least squares problem (3.51).

From Fig. 3.18 it is clear that all equalisers give almost the same performance but the complexity of the LSMR and LSQR equalisers is much less than the complexity of the MMSE. Comparing the LSMR and the LSQR, we found that both algorithm

converge to nearly the same point (LSMR is better than LSQR) but the LSMR converge faster with less iterations.

From the numerical simulations shown in Fig. 3.17 and Fig. 3.18 it is clear that the minimum achievable BERs for the LLS-LSMR (3.47) and the RLS-LSMR (3.51) are close to each other even if the noise limits are identified precisely at the receiver. However, a key advantage of RLS-LSMR is that semi-convergence is much minor; that the BER grows gradually with the number of iterations increase after reaching the minimum.

### **3.8 Low Complexity LSMR-based Block Decision Feedback Equaliser (LSMR-BDFE) for DFrFT-OCDM (Nonlinear equaliser).**

Block decision feedback equaliser (BDFE) was proposed in [112] to improve the MMSE equaliser performance by detecting the data recursively (one-by-one) instead of detecting all the data concurrently, as in the earlier showed methods. Hence, the consecutive detection technique was used which is extensively adopted in DS-CDMA systems for the multi-user detection.

An equaliser based on the LSMR and the MMSE-BDFE was designed to reduce the MMSE-BDFE equaliser complexity and improve the performance. The proposed equaliser uses LSMR algorithm to reduce the band approximation error and uses band  $LDL^H$  factorization method with DFE to obtain better performance without increasing the complexity. The MMSE methodology in [112] was adopted to design the feedforwarded ( $F_F$ ) and feedback ( $F_B$ ) filters as shown in Fig. 3.19. This methodology minimizes the error  $\mathbf{e} = \tilde{\mathbf{d}}_n - \mathbf{d}_n$ . Considering that  $F_B$  is strictly upper triangular so the feedback process can be done by successive cancelation.

Using the standard assumption of correct past decisions, that is  $\hat{\mathbf{d}}_n = \mathbf{d}_n$ , the error vector can be expressed by:

$$\mathbf{e} = \mathbf{F}_F \tilde{\mathbf{r}}_n - (\mathbf{F}_B + \mathbf{I}_{N_d}) \mathbf{d}_n \quad (3.52)$$

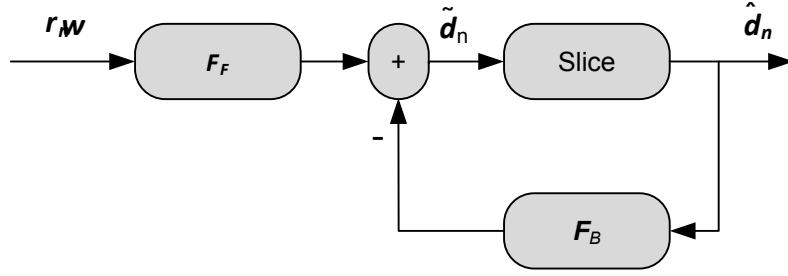


Fig. 3.19 BDFE Structure

which leads to the relation between  $\mathbf{F}_F$  and  $\mathbf{F}_B$  according to the mean square error (MSE) minimization criterion in [112] :

$$\mathbf{F}_F = (\mathbf{F}_B + \mathbf{I}_{N_a}) (\tilde{\mathbf{H}}_\alpha^H \tilde{\mathbf{H}}_\alpha + \gamma^{-1} \mathbf{I}_{N_a})^{-1} \tilde{\mathbf{H}}_\alpha^H = (\mathbf{F}_B + \mathbf{I}_{N_a}) \mathbf{W}_{MMSE} \quad (3.53)$$

by applying the band approximation  $\tilde{\mathbf{H}}_\alpha = \mathbf{B}_n$

$$\mathbf{F}_F = (\mathbf{F}_B + \mathbf{I}_{N_a}) (\mathbf{B}_n \mathbf{B}_n^H + \gamma^{-1} \mathbf{I}_{N_a})^{-1} \mathbf{B}_n^H \quad (3.54)$$

It is obvious that the feedforwarded filter is the cascade of the low-complexity MMSE equaliser and an upper triangular matrix  $\mathbf{F}_B + \mathbf{I}_{N_a}$  with unit diagonal. Designing the feedforwarded and the feedback filters were carried out in details in [112] where the autocorrelation matrix of the error vector  $\mathbf{e}$  is given by:

$$\mathbf{R}_{ee} = \sigma^2 (\mathbf{F}_B + \mathbf{I}_{N_a}) (\mathbf{B}_n \mathbf{B}_n^H + \gamma^{-1} \mathbf{I}_{N_a})^{-1} (\mathbf{F}_B + \mathbf{I}_{N_a})^H \quad (3.55)$$

where  $\sigma^2$  is the noise variance. Using the  $\mathbf{LDL}^H$ :

$$\mathbf{M} = \mathbf{B}_n \mathbf{B}_n^H + \gamma^{-1} \mathbf{I}_{N_a} = \mathbf{LDL}^H \quad (3.56)$$

where  $\mathbf{L}$  is the lower triangular with unit diagonal and  $\mathbf{D}$  is the diagonal matrix. It is straight forward now to minimize the error expectation  $E\{\mathbf{e}^2\}$  by setting:

$$\mathbf{F}_B = \mathbf{L}^H - \mathbf{I}_{N_a} \quad (3.57)$$

which reduces  $\mathbf{R}_{ee}$  diagonal. Using (3.54), (3.57)  $\mathbf{F}_F$  can be expressed by:

$$\mathbf{F}_F = \mathbf{L}^H \mathbf{W}_{MMSE} = \mathbf{L}^H \mathbf{M}^{-1} \mathbf{B}_n^H = \mathbf{D}^{-1} \mathbf{L}^{-1} \mathbf{B}_n^H \quad (3.58)$$

Although (3.58) and (3.57) looks complicated but using the LSMR algorithm with the fact that  $\mathbf{D}$  is diagonal,  $\mathbf{B}$  is banded and  $\mathbf{L}$  is lower triangular and banded, it turns out

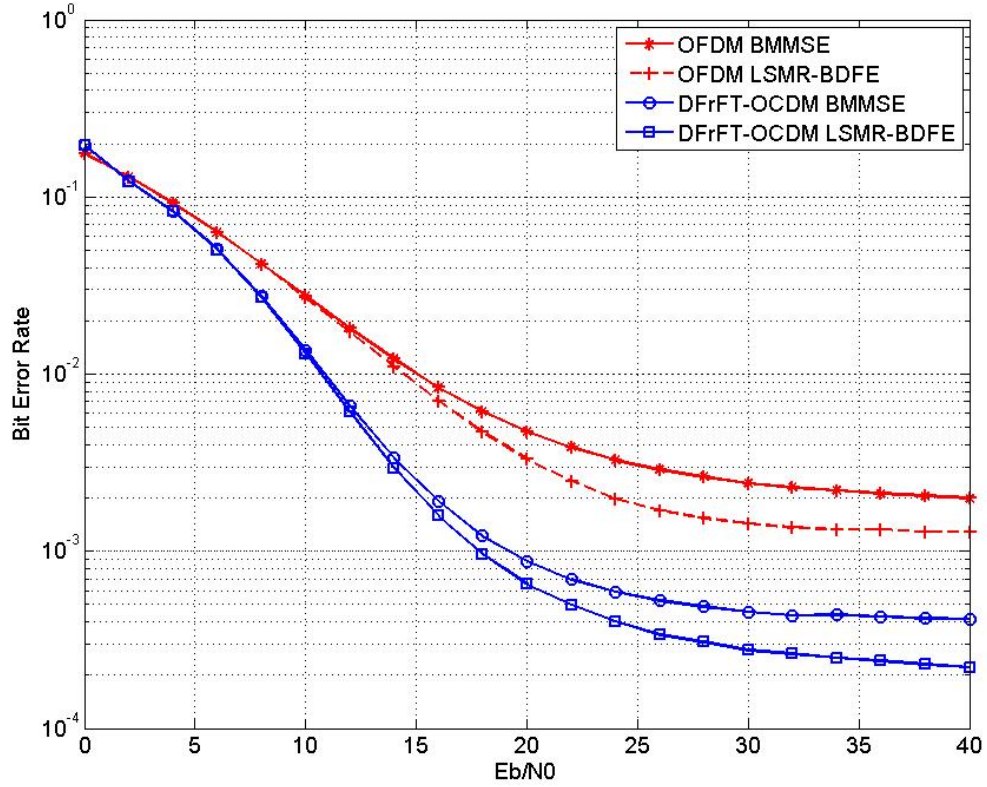


Fig. 3.20 DFrFT-OCDM and DFT-OFDM Uncoded BER Comparison ( $Q = 5$ )

that the banded LSMR-BDFE is characterized by a very low complexity. For the feedforwarded filter:

$$\mathbf{d}_n = \mathbf{F}_F \tilde{\mathbf{r}}_n \quad (3.59)$$

$$\tilde{\mathbf{r}}_n = \mathbf{F}_F^{-1} \mathbf{d}_n = \mathbf{B}^{-H} \mathbf{D} \mathbf{L} \mathbf{d}_n \quad (3.60)$$

from (3.56) it can be shown that:

$$\mathbf{D} \mathbf{L} = (\mathbf{B}_n \mathbf{B}_n^H + \gamma^{-1} \mathbf{I}_{N_a}) \mathbf{L}^{-H} \quad (3.61)$$

$$\tilde{\mathbf{r}}_n = \mathbf{B}_n^{-H} (\mathbf{B}_n \mathbf{B}_n^H + \gamma^{-1} \mathbf{I}_{N_a}) \mathbf{L}^{-H} \mathbf{d}_n = (\mathbf{B}_n + \mathbf{B}_n^{-H} \gamma^{-1}) \mathbf{L}^{-H} \mathbf{d}_n \quad (3.62)$$

which can be solved efficiently using the LSMR algorithm.

The complexity of the proposed LSMR-BDFE equaliser is almost the same as the RLS-LSMR equaliser with a total of  $\mathcal{O}(N(Q+1)i)$  complex operations.

The uncoded BER performance of the DFrFT-OCDM with the LSMR-BDFE equaliser is investigated by means of simulation over 100000 multicarrier blocks. An

DFT-OCDFM system with  $N=128$ ,  $N_A=96$ ,  $L=8$ , and QPSK modulation is assumed. The channel simulation parameters are the same as the Rayleigh fading channel in section 3.6.

Fig. 3.20, show a comparison between the DFT-OCDFM and the OFDM using  $Q = 5$ , LSMR-BDFE and BMMSE equalisers. From Fig. 3.20 it can be seen that the LSMR-BDFE equaliser gives the best performance and the BMMSE equaliser almost give the same performance in low SNR. Again it can be seen that the DFT-OCDFM outperforms the OFDM system with both the BMMSE and the LSMR-BDFE equalisers. However the complexity of the DFT-OCDFM system is almost the same as the OFDM system.

### 3.9 RLS-LSMR Sliding Window Equaliser

Sliding window equaliser was proposed in [113] to reduce the complexity of the MMSE equaliser by dividing the large matrix inversion to a multiple of smaller matrix inversions, for example the complexity of inverting  $N \times N$  matrix equal  $\mathcal{O}(N^3)$ , let  $N = 96$  which will give a complexity equal 884736 complex operations but if the inversion was subdivided to calculate the 96 symbols using a window of 9 so the total complexity will equal  $9^3 \times 96 = 69984$  which is less complicated.

The main idea is to consider a small window from the entire banded system matrix  $\mathbf{B}_n$  to estimate a symbol transmitted on a certain subcarrier in which all the energy corresponding to the symbol of interest are concentrated in this window, while ignoring the rest. This method is then repeated by sliding the window over all the subcarriers of the received multicarrier symbol. Using this technique reduces the dimension of the system under consideration which reduces the complexity considerably without reducing the system performance significantly and it is obvious that the complexity can be reduced more by simply using the LSMR algorithm in solving the reduced dimension system.

Consider the case where the data symbol  $d_{k,n}$  has to be detected; almost all the  $d_{k,n}$  symbol energy is located on the subcarrier  $k$  and its neighbours.  $d_{k,n}$  can be estimated using:

$$\hat{d}_{k,n} = \mathbf{W}_{MMSE,k} \tilde{\mathbf{r}}_k \quad (3.63)$$

where the vector  $\tilde{\mathbf{r}}_k = [\tilde{r}_{k-D} \cdots \tilde{r}_{k+D}]^T$  is part of the received vector  $\tilde{\mathbf{r}}$  which is related to the symbol  $d_{k,n}$  and its neighbors,  $P = 2D + 1$  is the number of the related symbols that equal to the size of the sliding window matrix ( $P \times K$ ),  $\mathbf{K} = (2Q + 1)$ ,  $Q$  is the number of sub- and super-diagonals that define the banded matrix limits and  $\mathbf{W}_{MMSE,k}$  is the MMSE equaliser for the  $k$  symbol window:

$$\mathbf{W}_{MMSE,k} = (\mathbf{B}_{n,k} \mathbf{B}_{n,k}^H + \gamma^{-1} \mathbf{I}_k)^{-1} \mathbf{B}_{n,k}^H \quad (3.64)$$

where  $\mathbf{B}_{n,k}$  matrix is part of the equivalent banded system matrix  $\mathbf{B}_n$  with  $P \times K$  size and can be defined by:

$$\mathbf{B}_{n,k} = \begin{bmatrix} B_{k-D,k-Q} & B_{k-D,k-Q+1} & \cdots & B_{k-D,k+Q} \\ B_{k-D+1,k-Q} & B_{k-D+1,k-Q+1} & \cdots & B_{k-D+1,k+Q} \\ \vdots & \vdots & \vdots & \vdots \\ B_{k+D,k-Q} & B_{k+D,k-Q+1} & \cdots & B_{k+D,k+Q} \end{bmatrix}$$

Using this approach turns the complexity of inverting the  $N_a \times N_a$  matrix into  $N$  inversions of  $P \times K$  matrices which will be reduced more using the LSMR algorithm to solve the regularized least squares problem:

$$(\mathbf{B}_{n,k} \mathbf{B}_{n,k}^H + \gamma^{-1} \mathbf{I}_k) \hat{\mathbf{d}}_k = \mathbf{B}_{n,k}^H \tilde{\mathbf{r}}_k \quad (3.65)$$

Reduction in system complexity depends on the width of the sliding window matrix  $P$ , and using a very small  $P$  does not affect the system performance significantly. Another hidden benefit from this algorithm is the reduction of the effort for perfect channel matrix estimation as it is no longer needed where only a limited number of the channel elements are needed. The complexity of the sliding window equaliser is given by  $\mathcal{O}(N_a P(Q + 1) i_{P \times K})$ . This from the first look appears to exceed the complexity of the other LSMR low complexity equalisers but the number of iterations  $i_{P \times K}$  needed to solve the smaller matrix  $P \times K$  is much less than the number of iterations  $i$  needed to solve the matrix  $N_a \times N_a$ .

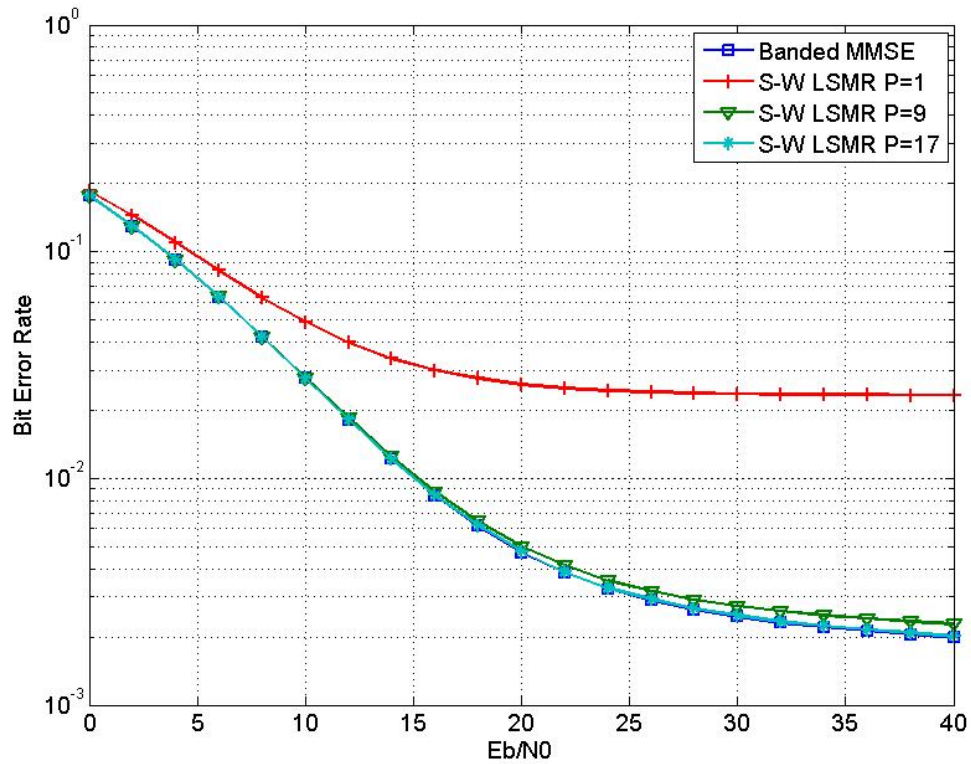


Fig. 3.21 RLS-LSMR sliding window equaliser and the Banded MMSE equaliser BER Comparison ( $Q = 5$ )

The uncoded BER performance of the OFDM with the RLS-LSMR sliding window equaliser is investigated by means of simulation over 100000 multicarrier blocks. An OFDM system with  $N=128$ ,  $N_A=96$ ,  $L=8$ , and QPSK modulation is assumed. The channel simulation parameters are the same as the Rayleigh fading channel in section 3.6.

Fig. 3.21, shows a comparison between the proposed RLS-LSMR sliding window equaliser and the banded MMSE equaliser using  $Q = 5$ , it can be shown that the banded MMSE equaliser gives the best performance and the RLS-LSMR sliding window equaliser almost give the same performance in low SNR. In high signal to noise ratio the performance of the RLS-LSMR sliding window equaliser is slightly degraded but with the benefit of complexity reduction. The performance degradation depends on the window matrix dimension.

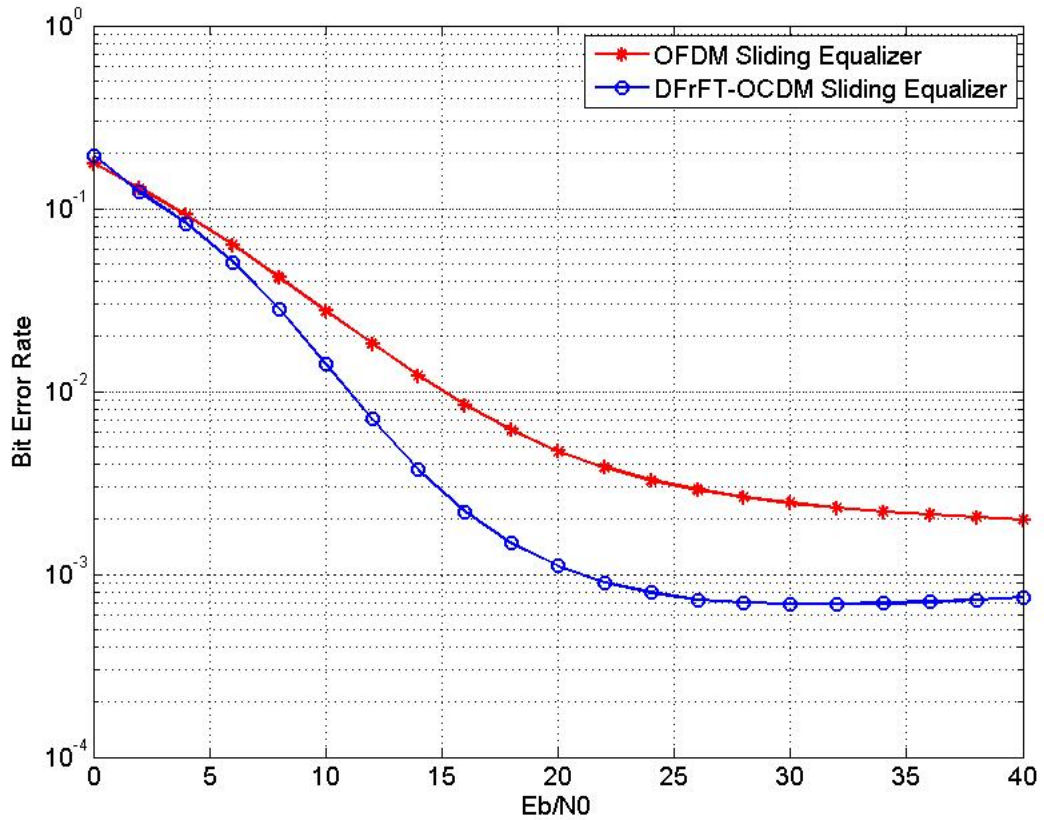


Fig. 3.22 DFrFT-OCDFM and OFDM Uncoded BER Comparison using the RLS-LSMR sliding window equaliser

Fig. 3.22 shows a comparison between the DFrFT-OCDFM and the OFDM systems using the proposed RLS-LSMR sliding window equaliser with  $Q = 5$  and  $P = 9$  it can be seen that the DFrFT-OCDFM outperforms the OFDM system.

### 3.10 Conclusion

In this chapter the doubly dispersive channel and its effect on OFDM system performance were investigated. DFrFT-OCDFM MCM system was investigated as an alternative MCM system that can improve the overall system performance. A novel multimode transmission method was proposed that uses both OFDM and DFrFT-OCDFM

systems as MCM basis depending on the channel statistics. The system uses both OFDM and DFrFT-OCDM in two modes of operation:

- 1- The first mode while the system is facing a time invariant frequency fading channel where the OFDM system gives a good performance with low complexity depending on its single tap equaliser.
- 2- The second mode while the system is facing a doubly dispersive fading channel where the DFrFT-OCDM system gives a better performance than the OFDM system with almost the same system and equaliser complexity.

It was shown that the new multimode system improves the system performance without increasing the complexity.

Low complexity equalisers were proposed with DFrFT-OCDM system and it was shown that this new combination give better performance than using the same low complexity equalisers with OFDM.

Novel low complexity equalisers were proposed using the new LSMR algorithm which gives the same performance with lower complexity comparing to the LSQR and the  $LDL^H$  factorization algorithms.

DFrFT-OCDM found to be a good alternative for OFDM in doubly dispersive channel environment depending on changing the normal OFDM basis with chirp basis using the DFrFT which can cope with the channel variations. In the next chapter a novel basis for the MCM systems will be proposed that can improve the system performance more.

# 4. Novel Multicarrier System Based on the Discrete Fractional Cosine Transform

---

## 4.1 Introduction

Various transformations used as an alternative for the FFT transformation to generate the MCM basis were investigated in section 2.8. The DCT-MCM was shown to give better performance than OFDM as DCT was shown to have better spectral compaction and energy concentration properties [51] with lower complexity. In the same manner the DFrFT-OCM was shown to have a better performance over OFDM under doubly dispersive fading channel due to its ability to cope with the channel frequency variation.

In this chapter a novel OCM MCM system will be proposed that uses the Discrete Fractional Cosine Transform (DFrCT) as a modulator instead of the DFT to improve the MCM system performance in the doubly dispersive channel scenario.

DFrCT will be investigated through this chapter. The DFrCT-OCM system model will be presented and a description of the key aspects of the transceiver will be provided. The DFrCT-OCM system equalisation problem will be stated and a comparison between complicated equalisers and low complexity equalisers will be provided. Also an investigation about the PAPR problem will be provided with the effect of using the DFrCT-OCM and the DFrFT-OCM systems instead of the OFDM. Finally a comparison between MCM systems that are based on unitary matrices under the doubly dispersive channel will be presented.

## 4.2 Fractional Cosine Transform

The computations of DFrFT for even or odd signals can be placed into the half-size DFrCT and Discrete Fractional Sine Transform (DFrST) calculations. This will reduce the computational load of the DFrFT by about one half [50, 114].

Fractional Fourier transform is a generalization of the Fourier transform which can be viewed as the fractional power of the Fourier transform operator. In the time-frequency plane, the original signal in the time domain represented by  $f(t)$  and  $F_\alpha(u)$  is the counterpart in the  $\alpha^{th}$  angle fractional domain. Using the same routine the  $\alpha^{th}$  angle fractional cosine transform (FrCT)  $C_\alpha(u)$  and  $\alpha^{th}$  angle fractional sine transform (FrST)  $S_\alpha(u)$  may be defined as [50, 114]:

$$C_\alpha(u) = A_\alpha e^{j\left(\frac{u^2}{2}\right)\cot\alpha} \int_{-\infty}^{\infty} \cos(\csc\alpha \cdot ut) e^{j\left(\frac{t^2}{2}\right)\cot\alpha} f(t) dt \quad (4.1)$$

$$S_\alpha(u) = A_\alpha e^{j(\alpha-\pi/2)} e^{j(u^2/2)\cot\alpha} \int_{-\infty}^{\infty} \sin(\csc\alpha \cdot ut) e^{j(t^2/2)\cot\alpha} f(t) dt \quad (4.2)$$

where the angle between fractional order axis  $u$  and time axis  $t$  is  $\alpha = -\frac{\pi}{2} \text{ to } \frac{\pi}{2}$ , and

$$A_\alpha = \sqrt{\frac{1-j\cot\alpha}{2\pi}}.$$

In digital signal processing the discrete representation of the transformation is the most important so the discrete fractional cosine transform will be investigated in detail. The description of DFrCT and DFrST are based on the eigen decomposition of DCT and DST kernels. This is the same idea as that of DFrFT [50].

### 4.2.1 Eigenvectors and Eigenvalues of DCT and DST Kernel Matrices

The DFT kernel matrix, eigenvectors and eigenvalues are well studied in [17]–[19], and they were used to develop the DFrFT. The eigenvectors and eigenvalues of DCT and DST kernel matrices were presented in [50] in the development of the DFrCT and DFrST. The DCT and DST eigenvectors can be obtained from the DFT eigenvectors.

- 1) If  $\mathbf{Q} = [q_0, q_1, \dots, q_{N-2}, q_{N-1}, q_{N-2}, \dots, q_1]^T$  is an even eigenvector of the  $(2N - 2)$  point DFT kernel matrix  $\mathbf{F}_{2N-2}\mathbf{Q} = \lambda\mathbf{Q}$ , ( $\lambda = 1, -1$ ). Then

$$\widehat{\mathbf{Q}} = [q_0, \sqrt{2}q_1, \dots, \sqrt{2}q_{N-2}, q_{N-1}]^T \quad (4.3)$$

will be an eigenvector of the  $N$ -point DCT kernel matrix, where  $\lambda$  is the corresponding eigenvalue:

$$\mathbf{C}_N\widehat{\mathbf{Q}} = \lambda\widehat{\mathbf{Q}} \quad (4.4)$$

- 2) If  $\mathbf{Q} = [0, q_1, q_2, \dots, q_N, 0, -q_N, -q_{N-1}, \dots, -q_1]^T$  is an odd eigenvector of the  $2(N + 1)$  point DFT kernel matrix.  $\mathbf{F}_{2N+2}\mathbf{Q} = \lambda\mathbf{Q}$ , ( $\lambda = j, -j$ ). Then

$$\widetilde{\mathbf{Q}} = \sqrt{2}[q_1, q_2, \dots, q_N]^T \quad (4.5)$$

will be an eigenvector of the  $N$ -point DST kernel matrix, where  $j\lambda$  is the corresponding value:

$$\mathbf{S}_N\widetilde{\mathbf{Q}} = j\lambda\widetilde{\mathbf{Q}} \quad (4.6)$$

For the odd DFT eigenvectors, because  $\lambda$  is equal to  $-j$  or  $j$ , the DST eigenvalue will be equal to 1 or  $-1$ . It was clearly stated that the only eigenvalues for the DCT and DST kernel matrices are 1 and  $-1$ .

The orthogonality in DCT and DST eigenvectors can be inferred from that in DFT eigenvectors.

- 1) If  $\mathbf{Q}_m$  and  $\mathbf{Q}_n$  ( $m \neq n$ ) are both the even and orthogonal DFT eigenvectors, the DCT eigenvectors  $\widehat{\mathbf{Q}}_m$  and  $\widehat{\mathbf{Q}}_n$  will also be orthogonal.
- 2) If  $\mathbf{Q}_m$  and  $\mathbf{Q}_n$  ( $m \neq n$ ) are both the odd and orthogonal DFT eigenvectors, the DST eigenvectors  $\widetilde{\mathbf{Q}}_m$  and  $\widetilde{\mathbf{Q}}_n$  will also be orthogonal.

From the previous discussion the DFT orthogonal eigenvectors can be used to generate the DCT and DST orthogonal eigenvectors.

It is known that the DFT, DCT, and DST transform kernels have infinite eigenvectors. In [9], [10], and [18], a novel matrix  $S$  was introduced to compute a complete set of DFT eigenvectors. This particular set of eigenvectors constitutes the discrete analogs of the

continuous Hermite–Gaussian functions called the DFT Hermite eigenvectors [9], [10], [18]. Defining the DFrFT with these DFT Hermite eigenvectors produce similar output as continuous DFrFT from the unitarity, additivity, and reversibility properties point of view. Using the same procedures the DFT Hermite eigenvectors can be used in developing DFrCT and DFrST. The eigenvector  $\widehat{\mathbf{Q}}_k$  will have the eigenvalue  $e^{-jk\alpha}$  ( $k$  is even) for the DFrCT kernel matrix. For  $\alpha = \pi/2$  this transfer rule will result in a DCT kernel. Similar to the DFrFT, the  $N$ -point DFrCT kernel can be defined as:

$$\mathbf{C}_{N,\alpha} = \widehat{\mathbf{Q}}_N \widehat{\mathbf{D}}_N^{2\alpha/\pi} \widehat{\mathbf{Q}}_N^T \quad (4.7)$$

$$\mathbf{C}_{N,\alpha} = \widehat{\mathbf{Q}}_N \begin{bmatrix} 1 & \dots & 0 \\ e^{-j2\alpha} & & \\ \vdots & \ddots & \vdots \\ 0 & \dots & e^{-j2(N-1)\alpha} \end{bmatrix} \widehat{\mathbf{Q}}_N^T \quad (4.8)$$

where  $\widehat{\mathbf{Q}}_N = [\widehat{q}_0 | \widehat{q}_2 | \widehat{q}_4 | \dots | \widehat{q}_{2N-2}]$ ,  $\widehat{q}_k$  is the DCT eigenvectors obtained from the  $k^{\text{th}}$ -order DFT Hermite eigenvector using (4.3) and  $\widehat{\mathbf{D}}_N^{2\alpha/\pi}$  is a diagonal matrix whose diagonal elements =  $e^{-j2(N-1)\alpha}$  where  $\alpha$  indicates the rotation angle of transform in the time-frequency plane. The DFrCT will become the conventional DCT when  $\alpha = \pi/2$ , and it will be an identity matrix when  $\alpha = 0$ . Similar to the DFrCT case, the development of DFrST is also based on the DFrFT.

The vector notation for the DFrCT is given by:

$$\mathbf{X} = \begin{bmatrix} X_\alpha(0) \\ X_\alpha(1) \\ \vdots \\ X_\alpha(N-1) \end{bmatrix} = \mathbf{C}_\alpha \begin{bmatrix} x(0) \\ x(1) \\ \vdots \\ x(N-1) \end{bmatrix} = \mathbf{C}_\alpha \cdot \mathbf{x} \quad (4.9)$$

where  $\mathbf{C}_\alpha$  is the unitary  $N \times N$  DFrCT matrix and  $N$  is the number of samples. Similarly the Inverse DFrCT (IDFrCT) can be written as:

$$\mathbf{x} = \mathbf{C}_{-\alpha} \cdot \mathbf{X} \quad (4.10)$$

where  $\mathbf{C}_{-\alpha} = \mathbf{C}_\alpha^H$  and  $(\cdot)^H$  denotes complex conjugate transpose.

The complexity of calculating the DFrCT and the DFrST is equal to  $\mathcal{O}(N \log N)$  using the approximate fast algorithm proposed in [50]. The DFrCT and DFrST are

established with a method similar to the DFrFT so their properties are inherited from the DFrFT.

#### 4.2.2 Properties of DFrCT and DFrST

The DFrCT and DFrST are complex kernel matrices not like the conventional DCT and DST. They have a simple inverse transforms, conserve the angle additivity property, they are periodic and symmetric.

1- Unitarity:

The DFrCT and DFrST are unitary matrices:

$$\mathbf{C}_{N,\alpha}^* = \mathbf{C}_{N,\alpha}^{-1} = \mathbf{C}_{N,-\alpha} \quad (4.11)$$

$$\mathbf{S}_{N,\alpha}^* = \mathbf{S}_{N,\alpha}^{-1} = \mathbf{S}_{N,-\alpha} \quad (4.12)$$

2- Angle additivity:

DFrCT and DFrST can preserve the angle additive property

$$\mathbf{C}_{N,\alpha} \mathbf{C}_{N,\beta} = \mathbf{C}_{N,\alpha+\beta} \quad (4.13)$$

$$\mathbf{S}_{N,\alpha} \mathbf{S}_{N,\beta} = \mathbf{S}_{N,\alpha+\beta} \quad (4.14)$$

3- Periodicity:

The DFrCT and the DFrST are periodic with period  $\pi$  which is half the period of the DFrFT which is  $2\pi$ .

$$\mathbf{C}_{N,\alpha+\pi} = \mathbf{C}_{N,\alpha} \quad (4.15)$$

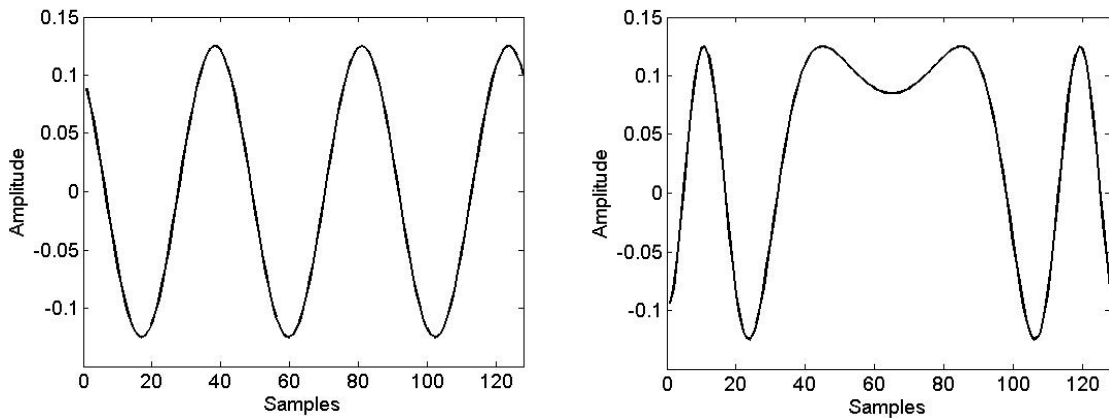
$$\mathbf{S}_{N,\alpha+\pi} = \mathbf{S}_{N,\alpha} \quad (4.16)$$

4- Symmetric:

Both the DFrCT and DFrST kernel matrices are symmetric

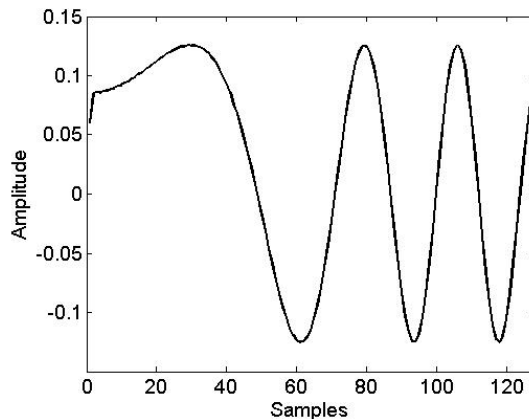
$$\mathbf{C}_{N,\alpha}(a, b) = \mathbf{C}_{N,\alpha}(b, a) \quad (4.17)$$

$$\mathbf{S}_{N,\alpha}(a, b) = \mathbf{S}_{N,\alpha}(b, a) \quad (4.18)$$



(a) DFT-OFDM Subcarriers

(b) DFrFT-OCDM Subcarriers



(c) DFrCT-OCDM Subcarriers

Fig. 4.1 DFrCT, DFrFT-OCDM with  $\alpha = 0.95 \frac{\pi}{2}$  and DFT-OFDM Subcarrier 2

(a) DFT-OFDM, (b) DFrFT-OCDM and (c) DFrCT-OCDM

### 4.3 DFrCT-OCDM Bases

Consider the baseband representation of a multicarrier system:

$$\begin{aligned}
 s(t) &= \sum_{k=-\infty}^{\infty} \sum_{n=0}^{N-1} d_{n,k} g_{n,k}(t) \\
 &= \sum_{k=-\infty}^{\infty} \sum_{n=0}^{N-1} d_{n,k} \phi_n(t - kT_S)
 \end{aligned} \tag{4.19}$$

where  $T_S$  is the symbol period,  $d_{n,k}$  is the information bearing symbol, and  $g_{n,k}(t) = \phi_n(t - kT)$ ,  $n = 0, 1, \dots, N - 1$  are the fundamental basis waveforms. Now considering the use of a signal basis that does not operate a rectangular tiling of the time–frequency plane (Fourier transform), for example [50]

$$g_{n,k}(t) = \Phi_n(t - kT) = g_n(t - kT)C_{-\alpha,n}(t - kT) \quad (4.20)$$

where  $C_{\alpha,n}(t)$  is given in (4.1). The choice of this function is inspired by the fact that an impulse in the Fourier domain is a sinusoidal basis in the time domain using the Fourier transform, the basis  $C_{\alpha,n}(t)$  corresponds (up to a constant factor) in the Fractional Cosine domain to an impulse. The basis  $C_{\alpha,n}(t)$  is orthonormal to each other.

$$\int_{-\infty}^{\infty} C_{\alpha,m}(t)C_{\alpha,n}^*(t)dt = \begin{cases} 1 & \text{for } m = n \\ 0 & \text{for } m \neq n \end{cases} \quad (4.21)$$

A comparison between the DFrCT, DFrFT-OCDM and OFDM real part of Subcarrier 2 are shown in Fig. 4.1 where  $\alpha = 0.95\frac{\pi}{2}$  has been used. It is well known that the OFDM subcarriers are constant frequency signals. the DFrCT-OCDM subcarrier are chirp like signal as shown in Fig. 4.1 with twice the frequency variations in the DFrFT-OCDM chirp signal which give more frequency diversity and thus potentially more robustness against doubly dispersive channels.

The transmission system in (4.19) and (4.20) is equivalent to a new modulation method where the generic basis signal is a chirp signal. The condition in (4.21) shows that the transmitted symbols (without the channel distortions) can be recovered by performing the following matched filtering operation:

$$d_{n,k} = \int_{-\infty}^{\infty} s(t)g_{n,k}^*(t)dt = \int_{-\infty}^{\infty} s(t)g^*(t - kT)C_{\alpha,n}^*(t - kT)dt \quad (4.22)$$

#### 4.4 The DFrCT-OCDM System

Recalling the traditional OFDM system in Fig. 2.8 where an IDFT matrix is used to modulate the data vector, using the same method an IDFrCT matrix is used to modulate the data vector to produce the novel DFrCT based OCDM system, the DFT matrix is replaced by a DFrCT matrix  $\mathbf{C}$  as shown in Fig. 4.2. The subcarriers for the DFrCT-OCDM system are chirp signals as shown in Fig. 4.1(c). CP is added to improve the system immunity against block and symbol interference which is removed after receiving the channel distorted signal. The received signal is distorted by the channel  $\mathbf{H}$  and the additive noise  $\mathbf{z}$ . The DFrCT matrix is used to demodulate the received signal where a complicated equaliser is needed to restore the data vector.

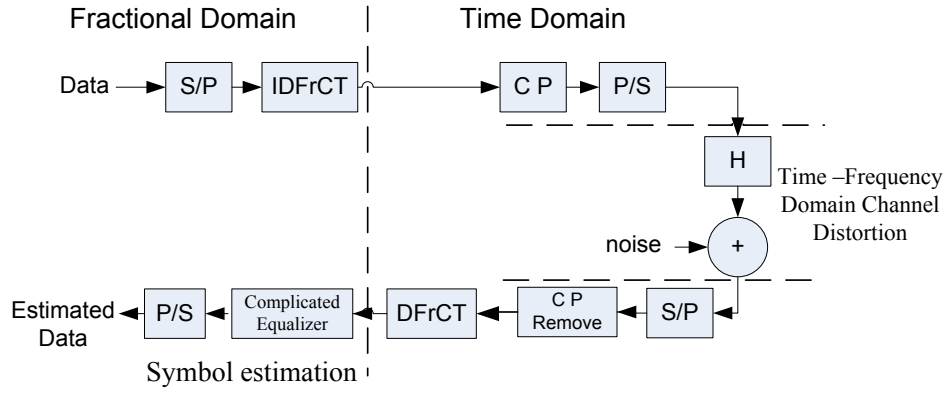


Fig. 4.2 The DFrCT-OCDM system with a Complicated equaliser

The DFrCT-OCDM system needs a complicated equaliser to deal with the distorted received signal even if the channel is a frequency fading channel which can be equalized using a single tap equaliser in the OFDM case. On the other hand the performance of the DFrCT-OCDM system is better than the OFDM system in the doubly dispersive channel scenario and in some cases when the frequency fading channel suffer from deep notches in the channel frequency response, in next section the system equalisation will be investigated.

#### 4.5 DFrCT-OCDM System Equalisation and Performance

Consider the DFrCT-OCDM system in Fig. 4.3, applying the same procedure in section 3.4 for the data  $\mathbf{d}_n$  to be transmitted through a dispersive Channel in the so it is straight forward to show that the equaliser matrix  $\mathbf{W}_n \in \mathbb{C}^{N_a \times N_a}$  operates on the input:

$$\tilde{\mathbf{r}}_n = \mathbf{P}^H \mathbf{C}_\alpha \mathbf{H}_n \mathbf{C}_{-\alpha} \mathbf{P} \mathbf{d}_n + \mathbf{P}^H \mathbf{C}_\alpha \mathbf{z} = \mathbf{U}_{n,\alpha} \mathbf{d}_n + \tilde{\mathbf{z}}_n \quad (4.23)$$

where  $\mathbf{C}_\alpha$  is the DFrCT,  $\mathbf{C}_{-\alpha}$  is the IDFrCT,  $\alpha$  is the fractional order in the fractional Cosine domain and  $\mathbf{U}_{n,\alpha}$  is the system matrix with  $\mathbf{U}_{n,\alpha} \in \mathbb{C}^{N_a \times N_a}$

The equivalent  $N_a \times N_a$  channel matrix and the noise vector in the fractional Cosine domain are given by  $\tilde{\mathbf{H}}_\alpha = \mathbf{C}_\alpha \mathbf{H} \mathbf{C}_{-\alpha}$  and  $\tilde{\mathbf{z}} = \mathbf{C}_\alpha \mathbf{z}$  respectively.

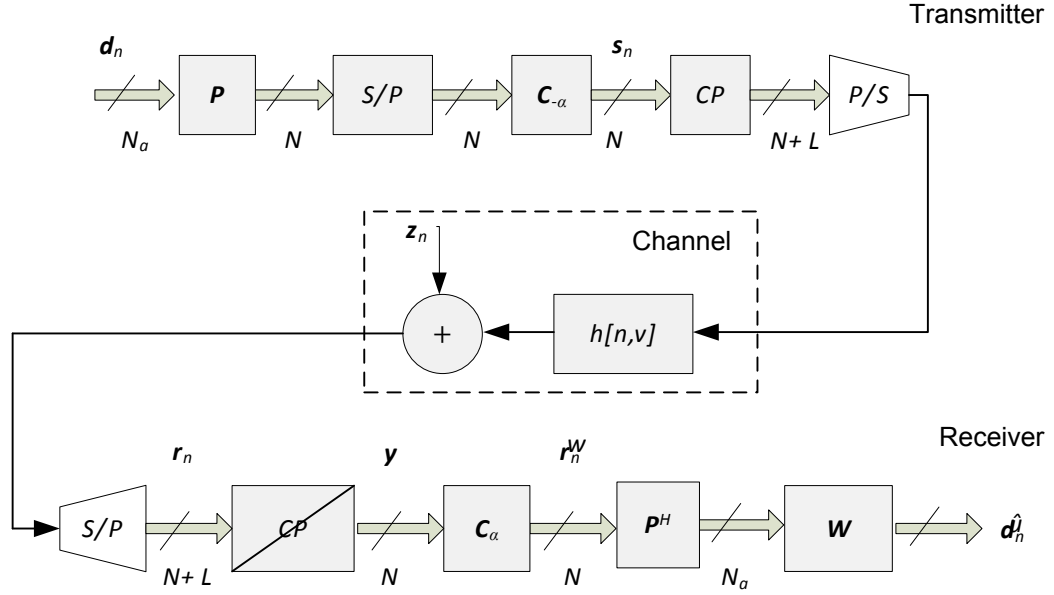


Fig. 4.3 DFrCT-OCDM System Block diagram

$\tilde{\mathbf{H}}_\alpha$  is a nondiagonal channel matrix which introduce ICI due to losing subcarriers orthogonality, which is the case when the dispersive channel comprises a multipath doubly dispersive channel. This will make the symbol estimation task particularly complicated due to the need for complicated equaliser.

The DFrCT-OCDM System can use the same equalisers as the OFDM and the DFrFT-OCDM systems as they are members in the MCM family. The DFrCT-OCDM System can adopt the ZF equaliser which is given by:

$$\hat{\mathbf{d}}_{ZF} = \tilde{\mathbf{H}}_\alpha^+ \tilde{\mathbf{r}}_n \quad (4.24)$$

and the MMSE equaliser:

$$\hat{\mathbf{d}}_{MMSE} = \tilde{\mathbf{H}}_\alpha^H (\tilde{\mathbf{H}}_\alpha \tilde{\mathbf{H}}_\alpha^H + \gamma^{-1} \mathbf{I}_{N_\alpha})^{-1} \tilde{\mathbf{r}}_n \quad (4.25)$$

where  $\hat{\mathbf{d}}_{ZF}$  and  $\hat{\mathbf{d}}_{MMSE}$  are the estimated data after ZF and MMSE equalisation respectively,  $\tilde{\mathbf{H}}_\alpha^H$  is the channel matrix conjugate transpose in the fractional Cosine domain,  $\mathbf{I}_{N_\alpha}$  is the identity matrix with  $N_\alpha \times N_\alpha$  elements,  $\gamma$  is the signal-to-noise ratio (SNR) and  $\tilde{\mathbf{H}}_\alpha^+$  is the Moore-Penrose pseudo-inverse of the channel matrix in the fractional domain[103]. In (4.24) and (4.25) perfect knowledge of the channel matrix  $\tilde{\mathbf{H}}_\alpha$

is assumed and the equaliser does not use guard subcarriers. Furthermore it is assumed that:  $E\{\mathbf{d}_n\} = E\{\tilde{\mathbf{z}}_n\} = 0, E\{\mathbf{d}_n \mathbf{d}_n^H\} = \mathbf{I}, E\{\mathbf{d}_n \tilde{\mathbf{z}}_n^H\} = 0, E\{\tilde{\mathbf{z}}_n \tilde{\mathbf{z}}_n^H\} = \sigma^2 \mathbf{I}$

It is mentioned before that the ZF equaliser performance is poor due to noise enhancement and the MMSE equaliser give the best performance in all linear equalisers [98] but it is very complex due to channel matrix inversion which needs  $\mathcal{O}(N_a^3)$  complex operations [104] which is not practical for high values of  $N_a$  which is the case in DVB-T and DVB-H.

Low complexity equalisers which proposed in Chapter 3 like  $LDL^H$  factorization, RLS-LSMR, LSMR-BDFE and RLS-LSMR sliding window equalisers can be used with the DFrCT-OCDM System without any modification as they can be applied directly to the MCM systems. The DFrCT-OCDM System equalisation performance and comparison with both the OFDM and DFrFT-OCDM systems will be introduced in the simulation results section.

## 4.6 DFrCT-OCDM System Simulation

The uncoded BER performance of the DFrCT-OCDM is investigated by means of simulation over 100000 multicarrier blocks. An FrCT-OCDM system with  $N=128$ ,  $N_A=96$ ,  $L=8$ , and QPSK modulation is assumed. The channel simulation parameters are the same as the Rayleigh fading channel in section 3.6.

### 4.6.1 DFrCT-OCDM System Performance Using the MMSE Equaliser

Fig. 4.4 shows the comparison between the DFrCT-OCDM system, the OFDM and DFrFT-OCDM systems performance using the MMSE equaliser, from which it can be seen that there is an improvement in the performance of the DFrCT-OCDM system compared to both the OFDM and DFrFT-OCDM systems. From Fig. 4.4 it is observed that the proposed DFrCT at 25 dB SNR provides approximately 2 dB better performance compared to the traditional OFDM and about 0.5 dB better than the DFrFT-OFDM system.

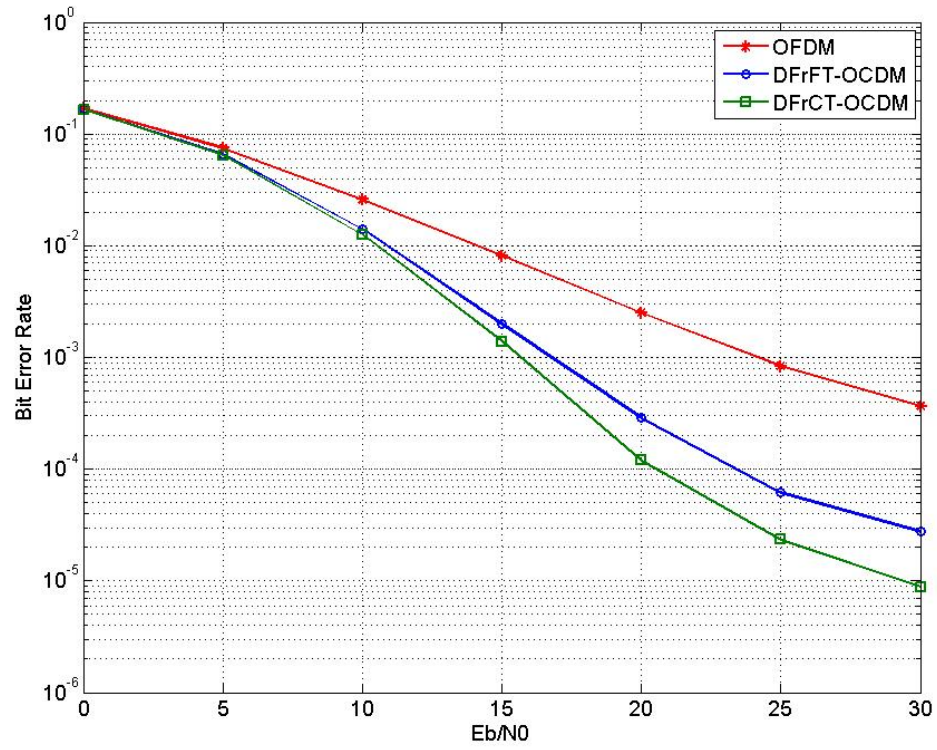


Fig. 4.4 The BER Comparison between DFrCT, DFrFT-OCDM and OFDM

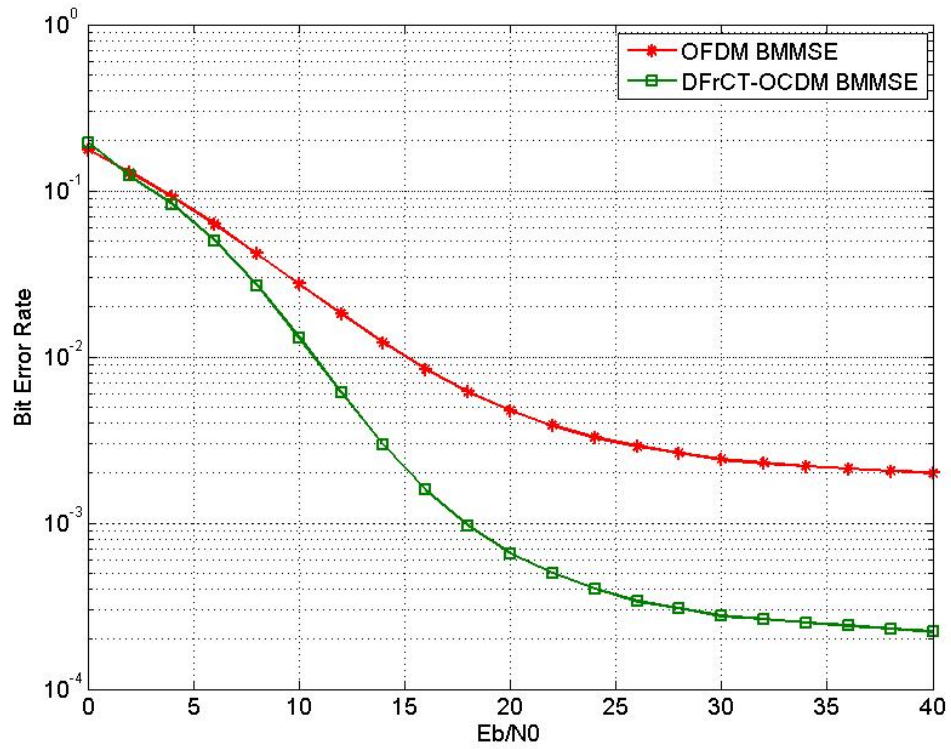


Fig. 4.5 The BER Comparison between DFrCT-OCDM and OFDM using the  $LDL^H$  factorization equaliser

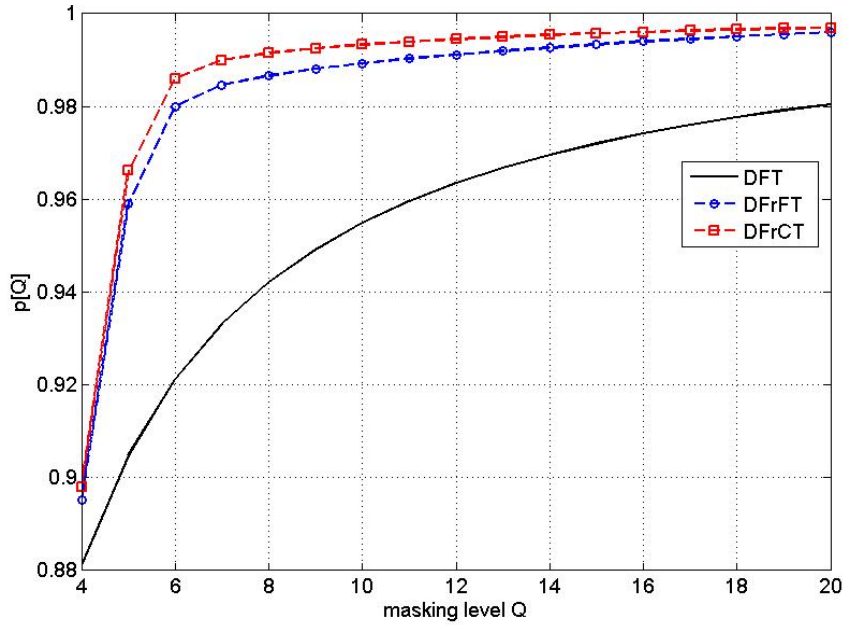


Fig. 4.6 Percentage of power of  $\tilde{\mathbf{H}}_\alpha$  contained in  $\mathbf{B}$ , measured by  $p[Q]$  in dependence of the number of off-diagonal elements  $Q$  considered by  $\mathbf{M}$ , comparing OFDM, DFrFT-OCDM and DFrCT-OCDM transmission

#### 4.6.2 DFrCT-OCDM System Performance Using the Low complexity $LDL^H$ factorization equaliser

The low complexity  $LDL^H$  factorization equaliser was shown to give a good performance with the DFrFT-OCDM system in the chapter 3. The  $LDL^H$  factorization equaliser can be used with the DFrCT-OCDM system using the same technique. The uncoded BER performance of the DFrCT-OCDM compared to the OFDM system is investigated by means of simulation over 100000 multicarrier blocks. An FrCT-OCDM system with  $N=128$ ,  $N_A=96$ ,  $L=8$ , and QPSK modulation is assumed. The channel simulation parameters are the same as the Rayleigh fading channel in section 3.6.

From Fig. 4.5 it is obvious that the DFrCT-OCDM system performance is superior to the conventional OFDM system with the same low complexity equaliser.

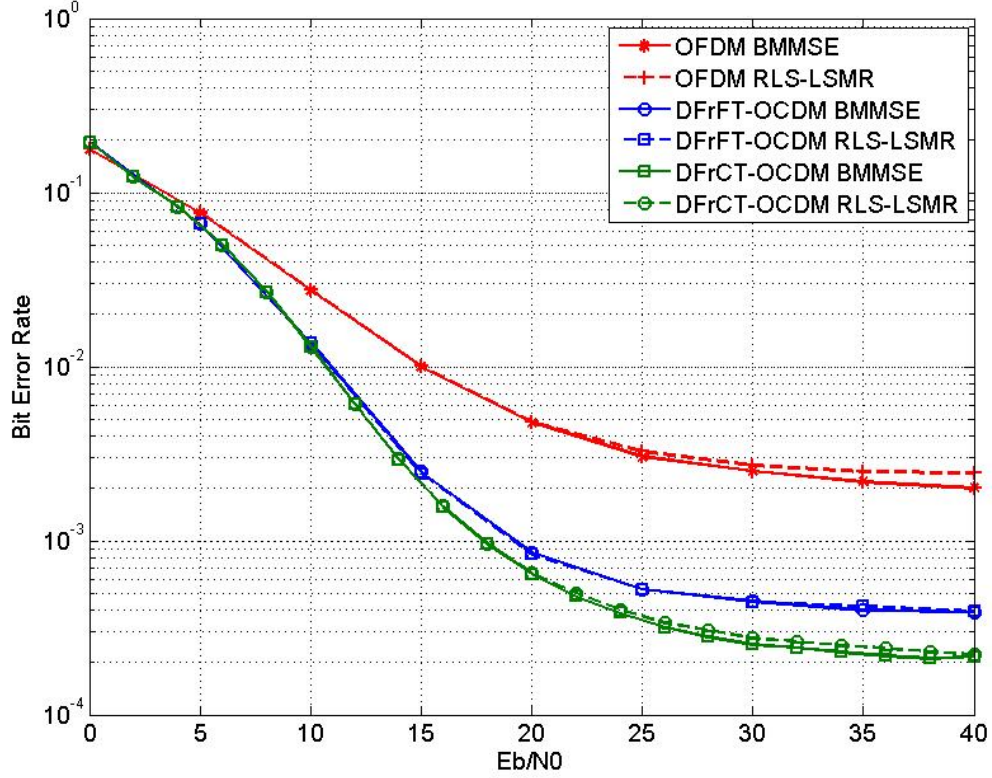


Fig. 4.7 The BER Comparison between DFrCT -OCODM and OFDM using the RLS-LSMR equaliser

It is important to investigate the effect of the masking level  $Q$  from (3.28) and (3.29) in the system performance, a comparison between the power components in the original system matrix  $\tilde{\mathbf{H}}_\alpha$  and in the reduced matrix  $\mathbf{B}_n$  after masking by  $\mathbf{M}$  is needed. Averaged over the ensemble and using the trace operator  $tr\{\cdot\}$ , this power ratio is defined in (3.35).

Results in Fig. 4.6 indicate that OFDM experiences a spread of energy away from the main diagonal due to Doppler fading which is not limited to nearby off-diagonals, hence requiring a high value for  $Q$  to capture most of the power contained in  $\tilde{\mathbf{H}}$ . DFrFT-OCODM and DFrCT-OCODM transmission does not manage to diagonalize the channel matrix  $\mathbf{H}$  but in contrast to OFDM, the leaked power is contained in neighbouring matrix elements close to the diagonal, and hence the better performance. Moreover, DFrCT-OCODM concentrates the power more efficient than DFrFT-OCODM.

### 4.6.3 DFrCT-OCDM System Performance Using the Low complexity LSMR Equaliser

The novel low complexity LSMR equaliser was proposed in chapter 3. LSMR was shown to give almost the same performance as the LSQR equaliser and the  $LDL^H$  factorization equaliser but with lower complexity. LSMR equaliser can be used with the DFrCT-OCDM following the same technique that was followed with the DFrFT-OCDM.

Fig. 4.7 indicates that the DFrCT-OCDM system performance is better than both the conventional OFDM system and the DFrFT-OCDM system with the same low complexity equaliser.

The different equaliser techniques that are based on the LSMR method can be used all with the DFrCT-OCDM system and it is predicted that the DFrCT-OCDM system will be better than the DFrFT-OCDM system and the OFDM systems.

## 4.7 DFrCT-OCDM PAPR Calculations

All multicarrier systems suffer from high PAPR problem, which is caused due to the addition of large number of independently modulated signals. Hence, to avoid nonlinear distortion and spectral spreading of the eliminated transmitted signal, highly linear amplifiers operating with a large back-off have to be used which is less efficient. This may have a deleterious effect on battery lifetime in mobile applications [115] like WiMAX and DVB-H.

The hard limiting of the transmitted signal may be considered as another source for noise as the in-band distortion will increase the errors and the out of band distortion will reduce the spectral efficiency[116]. Therefore, reducing the PAPR is always been an important factor for practical system design and implementation. Recently, there have been some works to evaluate the PAPR for the case of the OFDM system [77, 117-119]and for the DFrFT-OCDM based system [120, 121]. It is obvious that there is a need to extend the PAPR study to the case of the DFrCT-OCDM based system.

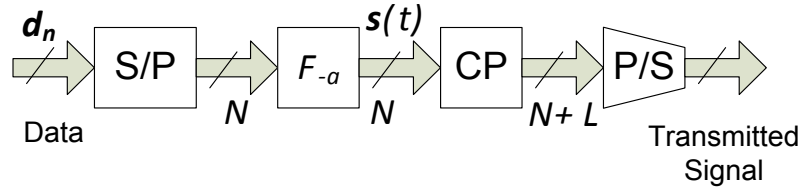


Fig. 4.8 A Block Diagram of The Multicarrier System Transmitter

#### 4.7.1 Multicarrier System from the PAPR Point of View

A multicarrier signal is the sum of a great number of independently modulated signals onto sub-channels of equal bandwidth. In continuous-time and discrete time versions, the transmitter of a multicarrier system can be presented as shown in Fig. 4.8.

One particular drawback of all multicarrier systems is its peak-to-average power ratio (PAPR) (large fluctuations in the transmitted signal envelop), which is higher than that of single-carrier UWB systems and pulsed-based UWB approaches. Large PAPR needs an expensive power amplifier with large linear region and introduces increased complexity of the analogue-to-digital and digital to-analogue converters. Therefore, it is important to investigate the PAPR performance of the multicarrier systems.

The PAPR of the discrete transmit signal is given by [115, 120, 121]:

$$PAPR = \frac{\max_{0 \leq t \leq NT} |s(t)|^2}{1/NT \int_0^{NT} |s(t)|^2 dt} = \frac{\max_{0 \leq n \leq N-1} |s_n|^2}{E[|s_n|^2]} \quad (4.26)$$

where the numerator denotes the maximum instantaneous power and the denominator denotes the average power of the signal. The PAPR performance of a multicarrier system is evaluated in terms of the complementary cumulative distribution function (CCDF) of PAPR which denotes the probability that the PAPR of a data block exceeds a given threshold  $\gamma$ , i.e.,  $P_r(PAPR > \gamma)$ .

In [1] a simple approximate expression is derived for the CCDF of the PAPR of a multicarrier signal with Nyquist rate sampling. From the central limit theorem, the real and imaginary parts of the time domain signal samples follow Gaussian distributions, each with a mean of zero and a variance of  $0.5$  for a multicarrier signal with a large number of subcarriers. Hence, the amplitude of a multicarrier signal has a Rayleigh

distribution, while the power distribution becomes a central chi-square distribution with two degrees of freedom with a cumulative distribution given by:

$$F(\gamma) = 1 - \exp(-\gamma) \quad (4.27)$$

To derive the CCDF for the peak power per OFDM symbol, assuming the samples are mutually uncorrelated which is true for non over sampling, the probability that the PAPR is below some threshold level  $\gamma$  can be written as:

$$P(PAPR > \gamma) = 1 - P(PAPR \leq \gamma) \quad (4.28)$$

$$P(PAPR > \gamma) = 1 - F(\gamma)^N \quad (4.29)$$

substituting (4.28) in (4.29):

$$P(PAPR > \gamma) = 1 - (1 - \exp(-\gamma))^N \quad (4.30)$$

The above expression is independent of the DFrFT and DFrCT transform order  $\alpha$  only under the Gaussian assumption.

## 4.7.2 PAPR Reduction Techniques

Different techniques were proposed for the PAPR reduction problem like clipping [75, 76], coding[77-79], and multiple signal representation techniques such as partial transmit sequence (PTS) [80] and selected mapping (SLM) [81]. These techniques reduce the PAPR with one or more overheads of transmit signal power increase, computational complexity increase, data rate loss or bit error rate (BER) increase.

### 4.7.2.1 Clipping

Amplitude clipping is the simplest technique for PAPR reduction as it limits the peak envelope of the input signal to a predetermined value as follows:

$$\mathbf{C}_l(s) = \begin{cases} s & \text{if } |s| \leq A \\ A & \text{if } |s| > A \end{cases} \quad (4.31)$$

where  $\mathbf{C}_l(s)$  is the output of the clipping function and  $A$  is the clipping amplitude.

Clipping may be considered as a source of in-band and out of-band distortion. Filtering after clipping is proposed in [76] where the out of-band distortion can be reduced while the in-band distortion effect can be reduced in the receiver by iteratively reconstruct the signal before clipping [116].

#### 4.7.2.2 Coding

Reducing the PAPR may be possible by avoiding the transmission of certain sequences which are known to have large PAPR. However, this technique suffers from complexity limitations, as searching for the best codes and the storage of large lookup tables for encoding and decoding, especially for a large number of subcarriers. A more complex approach proposed in [79] attempted to benefit from different code-words by using its error correcting properties and to reduce the PAPR of the resulting coded signals. This approach is simple to implement, but it requires extensive calculations to find good codes. Golay complementary sequences with their attractive PAPR control properties and the classical first-order Reed-Muller code with all of the encoding, decoding, and error correcting capability were proposed in [78].

These coding techniques effectiveness are limited for practical multicarrier systems PAPR reduction due to the exhaustive search needed for finding a good code and it's limitation to multicarrier systems with a small number of subcarriers.

#### 4.7.2.3 The Selected Mapping Technique

In the selected mapping technique (SLM) [81], the transmitter generates a number of different candidate data blocks which are equivalent to the original data block, and selects the one with the lowest PAPR for transmission. A block diagram for the SLM technique is shown in Fig. 4.9. Each data block is multiplied by  $U$  different phase sequences, each of length equal to the data block length.

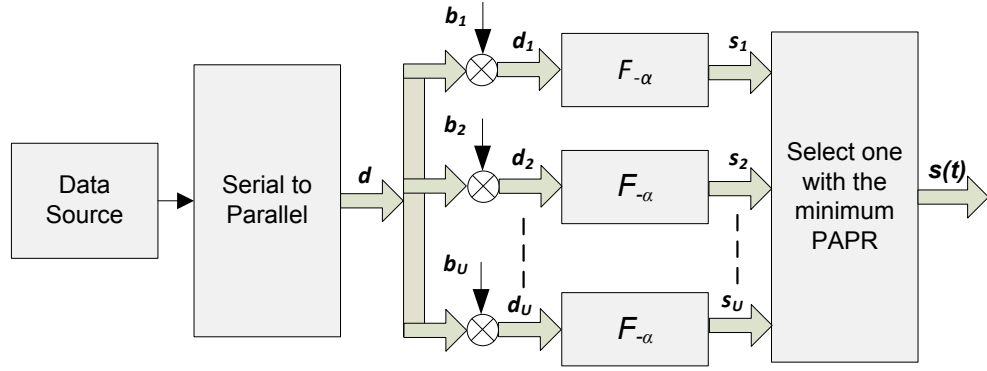


Fig. 4.9 A block diagram of the SLM technique

$$\mathbf{B}_u = [\mathbf{b}_{u,0}, \mathbf{b}_{u,1}, \dots, \mathbf{b}_{u,N-1}]^T, u = 1, 2, \dots, U \quad (4.32)$$

resulting in  $U$  adapted data blocks.  $\mathbf{b}_l$  is set to be all one vector to include the original data block in our search. The  $u^{th}$  candidate vector that is generated by the multiplication of data block with the phase vector is denoted as  $\mathbf{d}_u$ , so we can write the equation to get the  $k^{th}$  element of  $u^{th}$  candidate vector as:

$$\mathbf{d}_{u,k} = d_k \mathbf{B}_{u,k}, u = 1, 2, \dots, U \quad (4.33)$$

The adapted data block for the  $u^{th}$  phase sequence will be:

$$\mathbf{d}_u = [d_0 \mathbf{b}_{u,0}, d_1 \mathbf{b}_{u,1}, \dots, d_{N-1} \mathbf{b}_{u,N-1}]^T, u = 1, 2, \dots, U \quad (4.34)$$

after applying SLM to  $\mathbf{d}$ , the multicarrier signal is given by:

$$\mathbf{s}_u = \mathbf{F}_{-\alpha} \cdot \mathbf{d}_u \quad (4.35)$$

The minimum PAPR is selected from the adapted data blocks to be transmitted. The receiver needs Information about the selected independent vectors to ensure the correct recovery of the transmitted signals. These sequences should be transmitted to the receiver as side information. For implementation, the SLM technique needs  $U - 1$  extra transformation operations, and the number of required side information bits is  $(\log_2 U)$  for each data block. This approach is applicable with all types of modulation and any number of subcarriers.

Selecting the frame with the lowest PAPR for transmission from  $U$  statistically independent OFDM frames that represent the same information, the probability that  $PAPR_{min}$  exceeds  $\gamma$  using (4.30) is given by:

$$P(PAPR_{min} > \gamma) = (P(PAPR > \gamma))^U \quad (4.36)$$

$$P(PAPR_{min} > \gamma) = (1 - (1 - \exp(-\gamma))^N)^U \quad (4.37)$$

From (4.37) the amount of PAPR reduction for SLM depends on the number of phase sequences  $U$  and the design of the phase sequences. PAPR reduction is possible for all data blocks but its efficiency may vary from one to one.

#### 4.7.2.4 The Partial Transmit Sequence Technique

In the partial transmit sequence (PTS) approach [80] the input data block is partitioned into multi disjoint sub-blocks or clusters. The subcarriers in each sub-block are weighted by carefully chosen phase factor for that sub-block in such a way that minimizes the PAPR of the combined signal. Generally, three methods of partition have been provided: adjacent partition, pseudo-random partition and interleaved partition.

The block diagram of the PTS technique is shown in Fig. 4.10. The input data block  $\mathbf{d}$  is partitioned into  $K$  disjoint sub-blocks where  $K$  is an integer number; each block contains  $N/K$  nonzero elements and  $N - (N/K)$  zeros (each one is completed by zero padding), so the  $k^{th}$  sub-block is given by:

$$\mathbf{d}_k = [0, \dots, 0, \mathbf{d}_{(k-1)(N/K)}, \dots, \mathbf{d}_{k(N/K)-1}, 0, \dots, 0]^T$$

where  $\mathbf{d}_k$  is  $N$  element vector and  $\mathbf{d} = \sum_{k=1}^K \mathbf{d}_k$ ,  $k = 1, 2, \dots, K$ , the time domain signal  $\mathbf{s}_k$  is obtained after the transformation of each one of the portioned signals  $\mathbf{d}_k$ , these time domain signals are called the partial transmit sequences. These PTSs are combined with different complex phase factors from the set denoted by  $\mathbf{b} = [\mathbf{b}_1, \mathbf{b}_2, \dots, \mathbf{b}_K]^T$ .

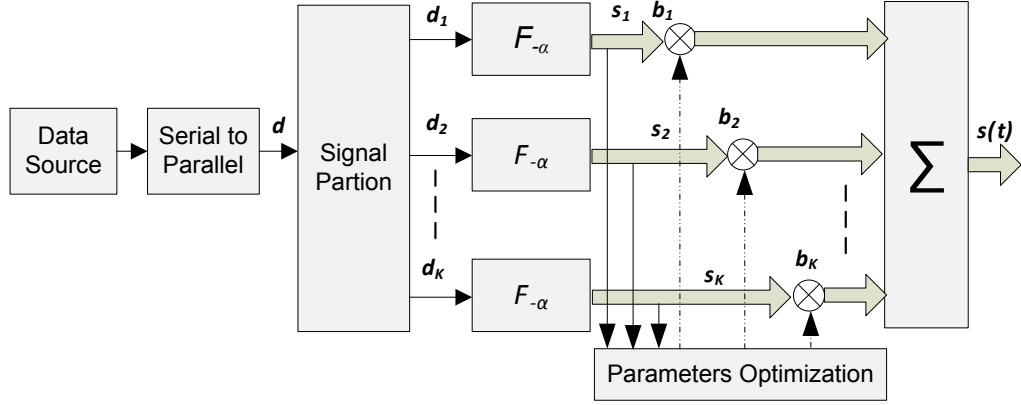


Fig. 4.10 PTS block diagram

The main task is to find the set of phase factors that minimizes the PAPR. To reduce the search complexity for the best phase factors, a limited finite number of elements are defined by:

$$\mathbf{P} = e^{j2\pi l/\omega}, l = 0, 1, \dots, \omega - 1 \quad (4.38)$$

where  $\omega$  is the number of allowed phase factors. It is clear that the search complexity increases exponentially with the number of sub-blocks  $K$ .

It is obvious, that the receiver must have knowledge about the generation process of the transmitted signal and the phase factors used so that the subcarriers can be rotated back appropriately. The number of bits required to represent this side information is the amount of redundancy introduced by the PAPR reduction scheme with PTS. Note that the number of the redundancy bits for the PTS technique is less than that needed for the SLM technique.

The amount of PAPR reduction depends on the number of sub-blocks  $K$  and the number of allowed phase factors  $\omega$ . Another factor that may affect the PAPR reduction performance in PTS is the sub-block partitioning method. The PTS technique works with an arbitrary number of subcarriers and any modulation scheme.

### 4.7.3 Selection of PAPR Reduction Technique

Choosing one of the previously discussed PAPR techniques is limited to many factors and there are some costs must be paid for PAPR reduction. These factors and

costs include computational complexity increase, PAPR reduction capability, power increase in transmit signal, BER increase at the receiver and losses in data rate.

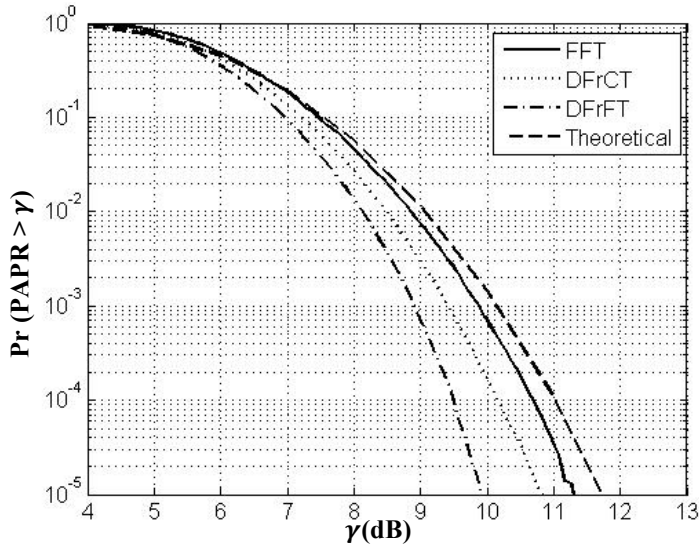
Due to these factors the choice for the best PAPR candidate technique depends on the multicarrier system application.

#### 4.7.4 PAPR Simulations

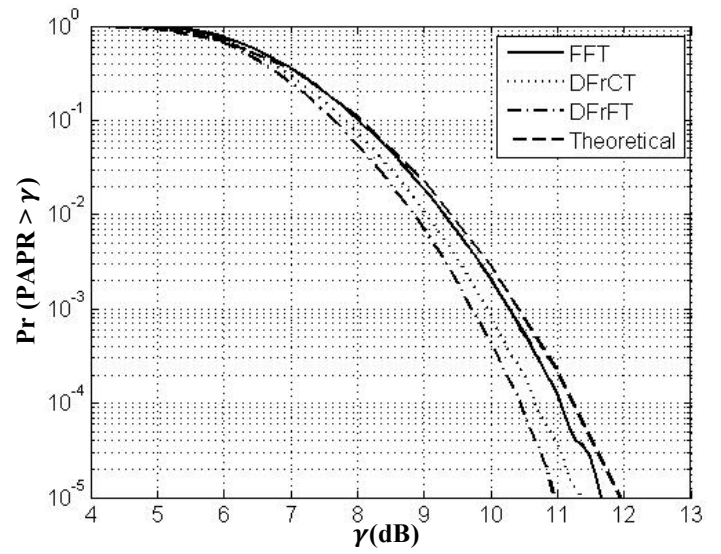
Computer simulations are now used to investigate the performance of the algorithms described above. DFrCT-OCDFM PAPR performance is measured without using any PAPR reduction methods using QPSK and 32, 64 and 128 subcarriers modulation and fractional order  $\alpha = 0.25$  with  $10^6$  blocks of data generated.

In Fig. 4.11 it is seen that using DFrCT or DFrFT as a bases for the multicarrier system reduces the PAPR. The simulation results are in a good agreement with the analytical approximation given by (4.30). Increasing the number of subcarriers limits the PAPR reduction gained by the DFrFT and the DFrCT. DFrFT-OCDFM system can reduce the PAPR more efficiently than the DFrCT-OCDFM system as shown in Fig. 4.11 (a). Different values of fractional order  $\alpha$  can change the PAPR of the multicarrier system which is shown in Fig. 4.12. Very small values of  $\alpha$  can convert the system from a multicarrier system to a single carrier one which has a very small PAPR compared to multicarrier systems.

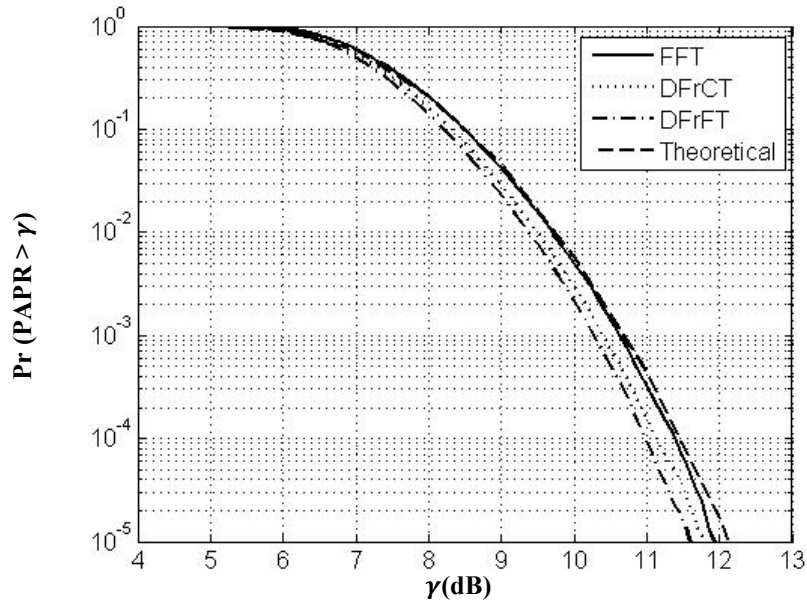
SLM can be considered as one of the best PAPR reduction techniques as it is an efficient and low complexity technique. The PAPR performance of the DFrCT-OCDFM system using the SLM reduction technique is shown in Fig. 4.13.



(a)  $N = 32, \alpha = 0.25$



(b)  $N = 64, \alpha = 0.25$



(c)  $N = 128, \alpha = 0.25$

Fig. 4.11 PAPR performance of DFrCT-OCDM, DFrFT-OCDM and the OFDM system without PAPR reduction with QPSK at sub carriers,  $\alpha = 0.25$ , and the number of sub carriers (a)  $N = 32$ , (b)  $N = 64$  and (c)  $N = 128$

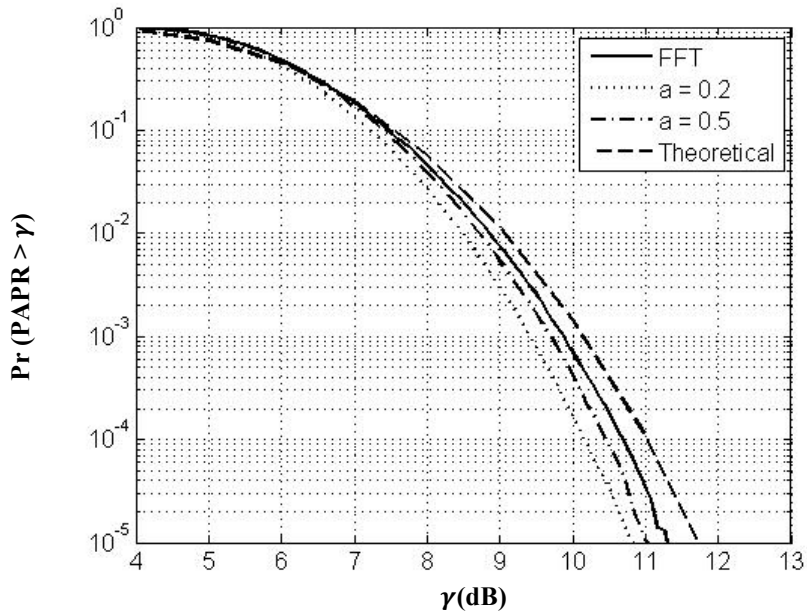


Fig. 4.12 PAPR performance of DFrCT-OCDM and OFDM systems without PAPR reduction with  $\alpha = 0.2, 0.5$ , and  $N = 32$

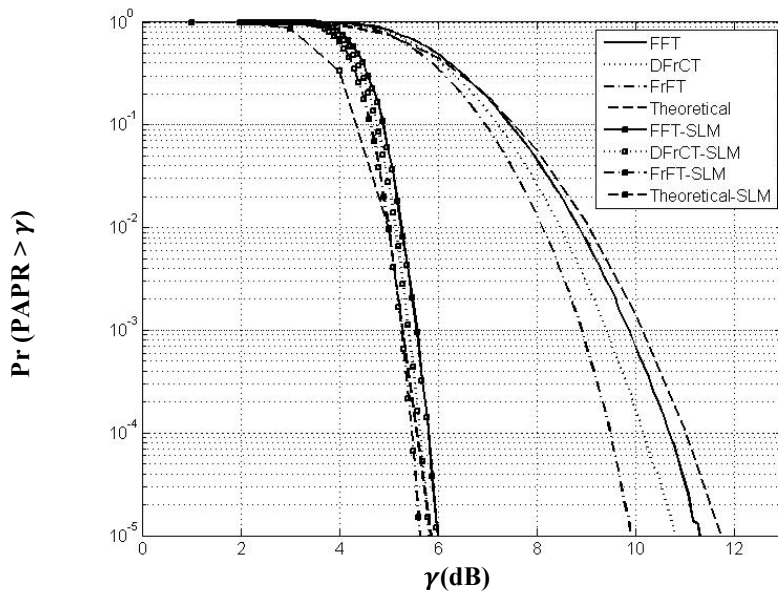


Fig. 4.13 PAPR reduction performance of DFrCT-OCDM, DFrFT-OCDM and the OFDM systems with and without SLM - PAPR reduction

From Fig. 4.13 SLM PAPR reduction technique reduce the PAPR for the DFrCT-OCDM, DFrFT-OCDM and the OFDM systems almost with the same ratio which

indicate that the PAPR reduction methods can work efficiently with the DFrCT-OCDM. It is clear that the simulations results are in agreement with the theoretical ones from (4.37). The PAPR performance of the MCM system based on the DFrCT was studied. Theoretical as well as simulations results suggest that the DFrCT-OCDM system outperforms OFDM system. However, for a large value of sub carriers, both systems become equivalent. Furthermore, the conventional methods of PAPR reduction were introduced into the fractional Cosine domain and it is presented that it is possible to extend techniques developed for OFDM system (such as SLM and PTS technique) to DFrCT-OCDM system.

#### **4.8 Multicarrier Systems Based On Different Unitary Transformation Matrices Comparison under Doubly Selective Fading Channel Scenario**

MCM systems popularity started after the use of Fourier transformation as the modulation/demodulation technique in many wired and wireless communication standards. The idea is to adopt a unitary transformation basis as the basis for the MCM system which reduces the modulation and demodulation complexity. It was shown in the literature review chapter that not only the Fourier transform is adopted as basis for MCM systems but the DHT, DCT and DFrFT is also used as a basis for MCM systems and DFrCT was proposed in this thesis.

Comparing the performance of the different transformations used as basis for the MCM system under the doubly dispersive channel scenario will give a good vision for the developers of the new techniques under the great demand on mobile data communication and green devices.

Starting from Fig. 3.5 for the OFDM system, Fig. 3.6 for the DFrFT-OCDM system and Fig. 4.3 for the DFrCT-OCDM system and using (3.22), (3.23), (3.25) and (4.23) it is straight forward to identify a general MCM system block diagram and an equation that can specify the estimated data vector in the receiver for all the previously listed transformation based MCM systems.

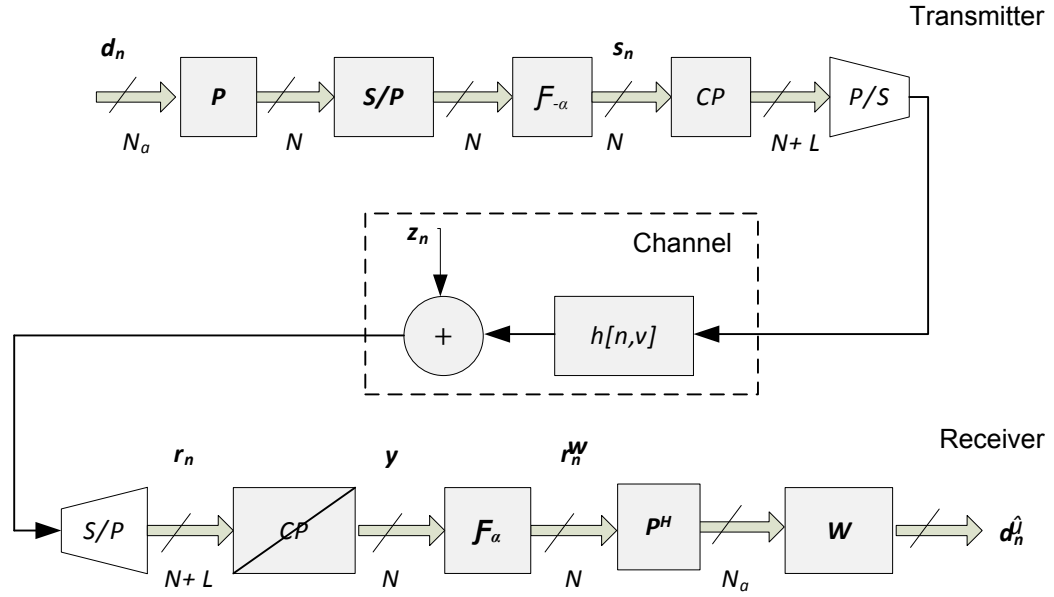


Fig. 4.14 MCM System Block diagram

The general MCM system block diagram shown in Fig. 4.14 differs from the other block diagrams in the transformation used in the MCM system so it can be any one of the previously listed unitary transformations. The general equation for the estimated data vector in the receiver can be given by:

$$\tilde{\mathbf{r}}_n = \mathbf{P}^H \mathbf{F}_\alpha \mathbf{H}_n \mathbf{F}_{-\alpha} \mathbf{P} \mathbf{d}_n + \mathbf{P}^H \mathbf{F}_\alpha \mathbf{z} = \mathbf{U}_{n,\alpha} \mathbf{d}_n + \tilde{\mathbf{z}}_n \quad (4.39)$$

$$\hat{\mathbf{d}}_n = \mathbf{W} \tilde{\mathbf{r}}_n \quad (4.40)$$

where  $\mathbf{F}_\alpha$  can be any unitary transformation matrix and  $\mathbf{W}$  can be any equaliser.

A BER performance comparison between OFDM, DCT-MCM, DHT-MCM, DFrFT-OCDFM and DFrCT-OCDFM MCM systems was done by means of simulation over 100000 multicarrier blocks for each one. A general MCM system with  $N=128$ ,  $N_A=96$ ,  $L=8$ , and QPSK modulation is assumed. The doubly dispersive channel simulation parameters are the same as the Rayleigh fading channel in section 3.6. The MMSE equaliser was used to compensate the doubly dispersive channel distortion.

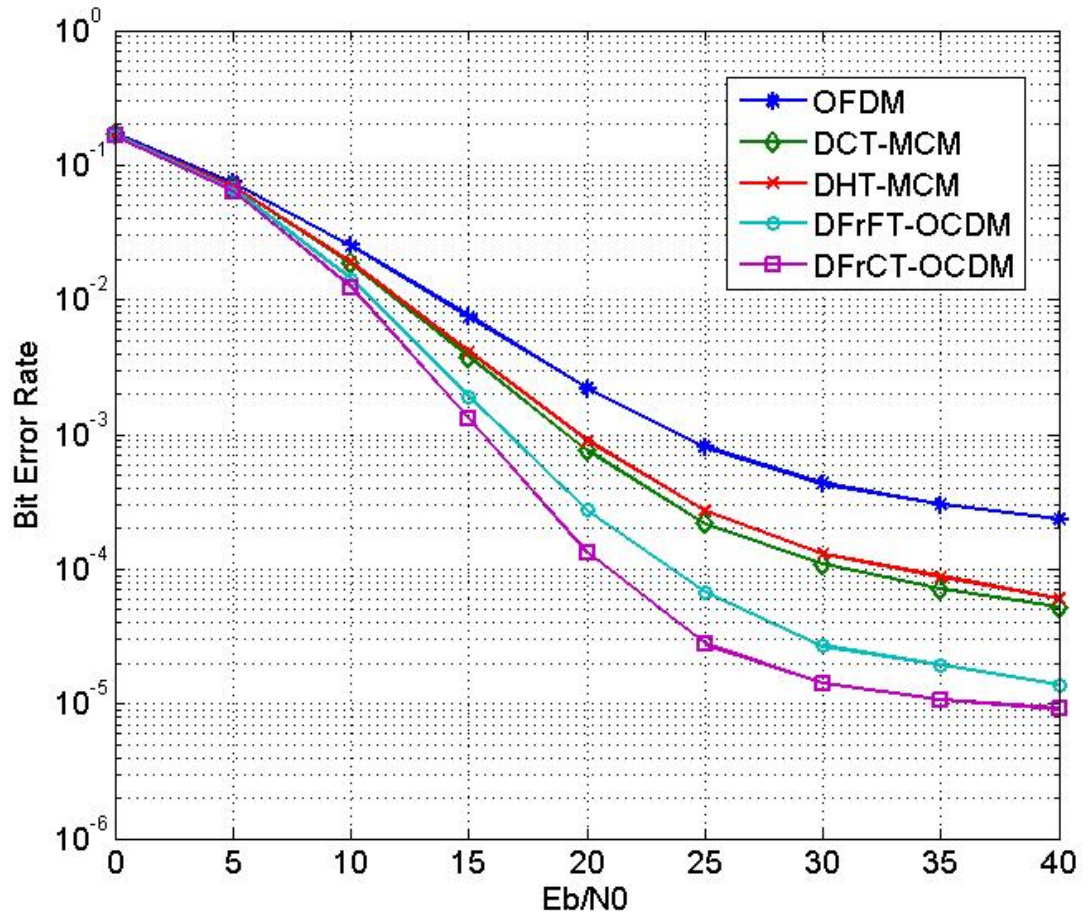


Fig. 4.15 The BER performance comparison between OFDM, DCT-MCM, DHT-MCM, DFrFT-OCODM and DFrCT-OCODM; MCM systems using MMSE equalize

Fig. 4.15 shows the comparison results which indicate that the OFDM system gives the poorest performance. The DHT-MCM and the DCT-MCM systems give a moderate performance and their performances are close to each other. The best performance is given by the novel DFrCT-OCODM which is proposed previously in this chapter and the nearest system performance is the DFrFT-OCODM system.

The fractional based MCM systems can deal with the doubly dispersive channels as its chirp basis can cope with the channel frequency variations. The DFrCT-OCODM system gives the best performance due to its basis frequency components variation which is higher than the frequency variation in the DFrFT-OCODM system.

## 4.9 Conclusion

In this chapter the DFrCT was presented and the new DFrCT-OCDFM MCM system was proposed as an alternative for the OFDM system in the doubly dispersive channel scenario which is a common scenario nowadays due to the huge demand of mobile data communications and the great development in transportation facilities speed which complicated the channel scenario more. The DFrCT-OCDFM system provides a superior performance over the OFDM and the DFrFT-OCDFM system under the doubly dispersive channel conditions without increasing the system complexity.

Equalisation for the novel DFrCT-OCDFM system was investigated and it was shown that the low complexity equalisers can be used efficiently with the novel system.

One of the hardest MCM systems problems which is PAPR and its solutions were investigated with DFrCT-OCDFM system and a comparison with the OFDM system and the DFrCT-OCDFM system was established. The DFrFT-OCDFM system found to be the best system in reducing the PAPR and the DFrCT-OCDFM system found to be better than the OFDM system.

Finally a comparison between the multicarrier systems based on different unitary transformation matrices comparison under doubly selective fading channel scenario was introduced and the DFrCT-OCDFM system found to give the best performance.

The next chapter will present the extension of the DFrCT-OCDFM Single-input single-output (SISO) system to the DFrCT-OCDFM multiple-input and multiple-output (MIMO) systems.

# 5. MIMO Based DFrCT-OCDFM

---

## 5.1 Introduction

In the previous chapters the SISO OFDM and OCDM systems were investigated carefully under the doubly dispersive channel scenario. Currently there is a great demand on higher data throughput with a restricted limited bandwidth that is facilitated using MIMO systems. MIMO is one of several forms of smart antenna technologies which improve the communication performance by using multiple antennas at both the transmitter and receiver. A popular approach in MIMO systems is to combine with multicarrier methods such as OFDM to improve the overall system performance which is known as MIMO-OFDM.

A prime example for the MIMO-OFDM is the MISO Alamouti space-time block code (STBC) and the MISO extended orthogonal space-time block coding (EO-STBC) combined with OFDM system to achieve spatial and multipath diversity gains and reduce the ICI error floor. However, under high mobility, implementing the Alamouti STBC or the EO-STBC over adjacent OFDM symbols is not effective due to the significant channel time variations.

In this chapter a novel Alamouti STBC MISO MCM system, a novel EO-STBC MISO MCM system and a novel MIMO system will be introduced based on the OCDM MCM systems which are shown to improve these systems performance under doubly dispersive channels scenario. MIMO systems will be investigated through this chapter. The Alamouti STBC MISO system, the EO-STBC MISO system and the MIMO system accompanied with the OCDM MCM systems will be presented and a description of the key realization of the transceiver will be provided. The system's equalisation problem will be stated and a comparison between complicated equalisers and low complexity equalisers will be provided.

## 5.2 MIMO Systems

The earliest ideas in MIMO belongs to work by A.R. Kaye and D.A. George (1970), Branderburg and Wyner (1974) [122] and W. van Etten (1975, 1976). MIMO is one of the most important technologies in wireless communications, because it offers an increase in data throughput and link range without extra bandwidth or increased transmission power. It achieves these objectives by dividing the same total transmit power over the antennas to acquire array gain which can improve the spectral efficiency (more bits per second per hertz of bandwidth) and/or to acquire diversity gain which enhance the link reliability as it reduces fading. These properties increased the interest in MIMO and it becomes important part of recent wireless communication standards such as IEEE 802.11n (Wi-Fi), 4G, 3GPP Long Term Evolution, WiMAX and HSPA+.

There are several special cases of MIMO such as SISO/SIMO/MISO where, SISO is a conventional radio system where neither the transmitter nor receiver has multiple antennas, Multiple-input and single-output (MISO) is a special case when the transmitter have multiple antennas and the receiver has a single antenna. (SIMO) is a special case when the transmitter has a single antenna and the receiver have multiple antennas.

In 1998 Siavash M. Alamouti [123] proposed a simple MISO system using two transmit antennas and one receive antenna the algorithm called Space-time block coding (STBC) which can provide a full diversity order. More details about the Alamouti scheme in the next section.

There are advanced diversity schemes such as extended orthogonal (EO) STBC, where rate one and maximum diversity order [124, 125] are achieved simultaneously despite an operation with 4 transmit antennas due to the use of additional beam steering based on feedback of channel state information (CSI).

Alamouti STBC and the EO-STBC algorithms have been developed in the context of narrowband, stationary channels. In frequency selective channel conditions, a popular approach is the combination with multicarrier methods such as OFDM [126] in order to operate narrowband Alamouti STBC and EO-STBC schemes in decoupled

subcarriers which are free of inter-symbol (ISI) and inter-carrier interference (ICI). In the case of narrowband time-varying systems, the algorithm degradation is minimal as long as the channel variation over one Alamouti STBC or EO-STBC symbol can be considered very small. However, if a time-varying channel exhibits additional delay spread, then the classical use of multicarrier methods leads to considerably longer symbol periods, which will require the introduction of various equalisation approaches in the frequency domain such as ZF and MMSE schemes or other receivers are to be applied for the individual subcarriers, including the zero-forcing (ZF), decision-feedback (DF), and joint maximum-likelihood (JML) detectors[127, 128], however, the neglected ICI introduces an error floor on the BER performance as loss of orthogonality is increased.

In Sections 2.7, 2.10 & 3.4 the loss of orthogonality of OFDM in doubly-dispersive channels was studied and multicarrier schemes based on the DFrFT and DFrCT were developed. Both the DFrFT and the DFrCT-OCDM systems give better performance in the doubly dispersive channel scenario. Therefore, a novel combination between DFrFT and the DFrCT-OCDM systems with Alamouti and EO-STBC will be proposed in the next sections. Combination with equalisation and low cost equalisation approaches will be also investigated.

### 5.3 Novel Alamouti MISO STBC System Based on OCDM Systems

In this work we will consider point to point OCDM multicarrier system based on Alamouti's scheme[123] with [108], two transmit antennas and one receive antenna as shown in Fig. 5.1. It is assumed that the same transmission system as the SISO-OCDM system is used except that every two consecutive OCDM symbols are considered as an Alamouti code word. Assume  $\mathbf{s}_1, \mathbf{s}_2$  are the two successive OCDM symbols, where  $\mathbf{s}_i$  is given by:

$$\mathbf{s}_i = \mathbf{F}_{-\alpha} \mathbf{P} \mathbf{d}_i \quad (5.1)$$

where  $\mathbf{F}_{-\alpha}$  can be IDFrFT or IDFrCT transformation matrix and  $\mathbf{P}, \mathbf{s}_i$  were defined before in (3.17) and (3.18) respectively.

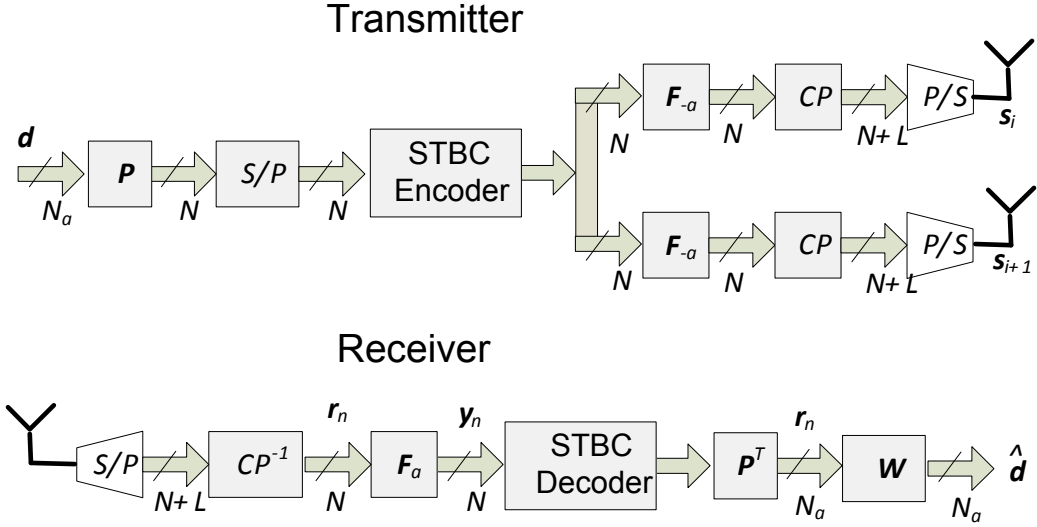


Fig. 5.1 The Alamouti coded OCDM system

During the first OCDM symbol period  $\mathbf{s}_1$  and  $\mathbf{s}_2$  are sent, then during the second OCDM symbol period  $-\mathbf{s}_2^*$  and  $\mathbf{s}_1^*$  are sent from antenna 1 and 2 respectively. After removing the CP at the receiver side, the received signals in two successive OCDM symbol periods can be written as:

$$\mathbf{r}_1 = \mathbf{H}_{1,1} \mathbf{s}_1 + \mathbf{H}_{2,1} \mathbf{s}_2 + \mathbf{z}_1 \quad (5.2)$$

$$\mathbf{r}_2 = -\mathbf{H}_{1,2} \mathbf{s}_2^* + \mathbf{H}_{2,2} \mathbf{s}_1^* + \mathbf{z}_2 \quad (5.3)$$

where  $\mathbf{r}_i$  is the received  $N$  vector in the  $i$ th symbol period,  $\mathbf{H}_{i,j}$  is the time domain channel matrix between transmit antenna  $i$  and the receive antenna in symbol time  $j$  and  $\mathbf{z}$  is the zero mean complex Gaussian random noise.

The DFrCT demodulates the received signal, the two successive demodulated received signals are given by:

$$\mathbf{y}_1 = \mathbf{F}_\alpha \mathbf{r}_1 \quad (5.4)$$

$$\mathbf{y}_2 = \mathbf{F}_\alpha \mathbf{r}_2 \quad (5.5)$$

Combining  $\mathbf{y}_1$  and  $\mathbf{y}_2^*$  in one equation:

$$\begin{bmatrix} \mathbf{y}_1 \\ \mathbf{y}_2^* \end{bmatrix} = \begin{bmatrix} \tilde{\mathbf{H}}_{1,1} & \tilde{\mathbf{H}}_{2,1} \\ \tilde{\mathbf{H}}_{2,2}^* & -\tilde{\mathbf{H}}_{1,2}^* \end{bmatrix} \begin{bmatrix} \mathbf{P} \cdot \mathbf{d}_1 \\ \mathbf{P} \cdot \mathbf{d}_2 \end{bmatrix} + \begin{bmatrix} \tilde{\mathbf{z}}_1 \\ \tilde{\mathbf{z}}_2^* \end{bmatrix} \quad (5.6)$$

where  $\tilde{\mathbf{z}}_i = \mathbf{F}_\alpha \mathbf{z}_i$  is the noise vector in the frequency domain and  $\tilde{\mathbf{H}}_{i,j} = \mathbf{F}_\alpha \mathbf{H}_{i,j} \mathbf{F}_\alpha^H$  is the system matrix, when the channel is time variant  $\tilde{\mathbf{H}}_{i,j}$  is a nearly banded matrix with the most important elements around the main diagonal as shown in Fig. 5.2 which allows the use for low complexity equalisers as proposed in [85, 86, 100, 129]. The fractional domain channel matrix  $\tilde{\mathbf{H}}_{i,j}$  can be approximated by its banded version using the banded matrix which was illustrated in Fig. 3.1 in Section 3.6 and may be written as:

$$\mathbf{B}_{i,j} = \mathbf{M} \odot \tilde{\mathbf{H}}_{i,j} \quad (5.7)$$

where  $\mathbf{M}(m, n)$  is a Toeplitz binary matrix given by:

$$\mathbf{M}(m, n) = \begin{cases} 1 & 0 \leq |m - n| \leq Q \\ 0 & Q < |m - n| < N_a \end{cases} \quad (5.8)$$

In (5.8)  $Q$  is used to control how many sub- and super-diagonals of  $\tilde{\mathbf{H}}_{i,j}$  elements should be included to give a good approximation of the banded fractional-domain channel matrix. This  $Q$  modification allows for a trade-off between equaliser complexity and performance. As a result (5.6) can be written as:

$$\mathbf{Y} = \mathbf{B} \mathbf{d} + \mathbf{z} \quad (5.9)$$

where  $\mathbf{B}$  is a  $2 \times 2$  block matrix of  $\mathbf{B}_{i,j}$  ( $N \times N$ ) banded matrices as shown in Fig. 5.3.  $\mathbf{B}$  can be converted into a  $2N \times 2N$  banded matrix using permutation matrix  $\mathcal{P}$  which is  $2N \times 2N$  matrix with one's at the positions  $\{(i + 1, (i)_{div2} + 1 + N(i)_{mod2})\}_{i=0}^{2N-1}$  and zero's elsewhere[129]. Multiplying (5.9) by  $\mathcal{P}$ :

$$\begin{aligned} \mathbf{Y}_{\mathcal{P}} &= \mathcal{P} \mathbf{Y} = \mathcal{P} \mathbf{B} \mathcal{P}^T \mathcal{P} \mathbf{d} + \mathcal{P} \mathbf{z} \\ &= \mathbf{B}_{\mathcal{P}} \mathbf{d}_{\mathcal{P}} + \mathbf{z}_{\mathcal{P}} \end{aligned} \quad (5.10)$$

where  $\mathbf{B}_{\mathcal{P}}$  is the permuted banded fractional domain channel matrix as shown in Fig. 5.4,  $\mathbf{Y}_{\mathcal{P}}$  and  $\mathbf{d}_{\mathcal{P}}$  are the permuted received and transmitted signal. Now the data from the same subcarriers of different transmit antennas are grouped together in  $\mathbf{d}_{\mathcal{P}}$  and the received data from the same subcarriers in two consecutive OCDM symbol periods are grouped together in  $\mathbf{Y}_{\mathcal{P}}$ .

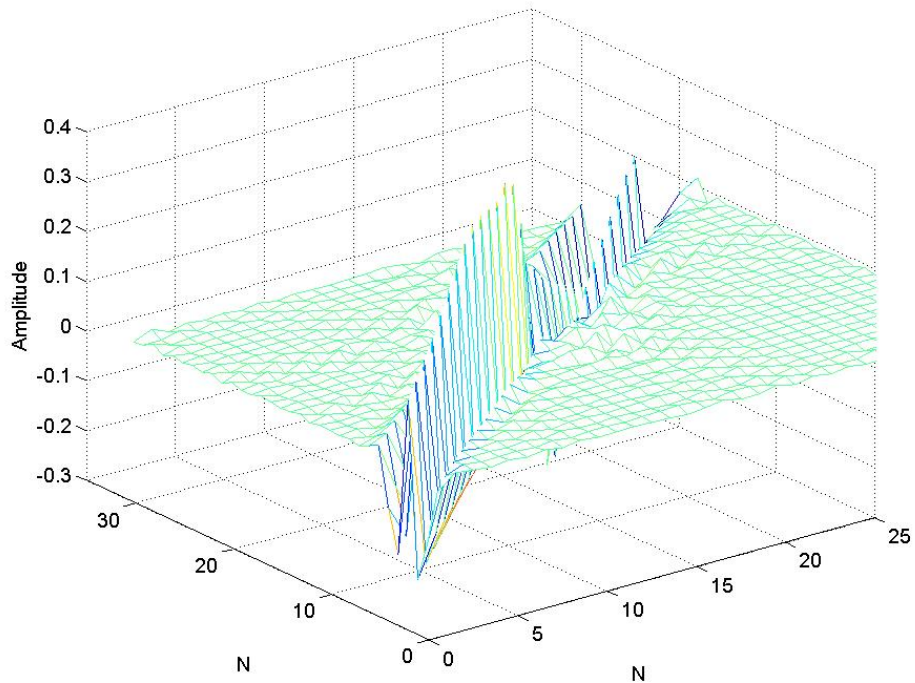


Fig. 5.2 An example of a fractional-domain doubly dispersive channel matrix  $N = 35$

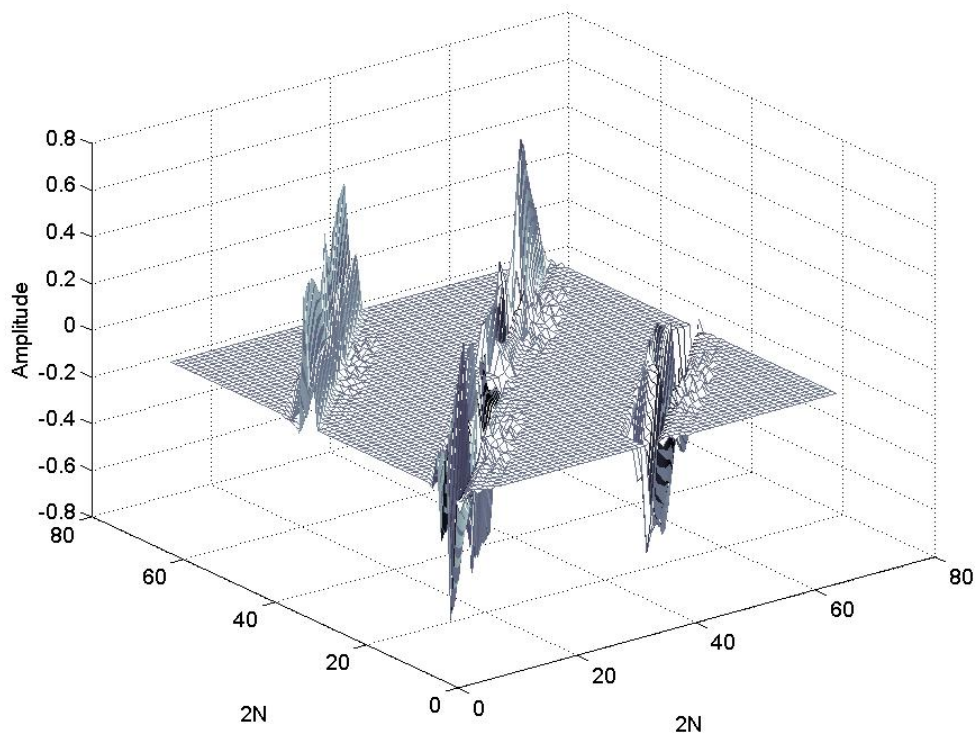


Fig. 5.3 An example of a fractional-domain doubly dispersive banded channel matrix  $B$  with  $N = 35$

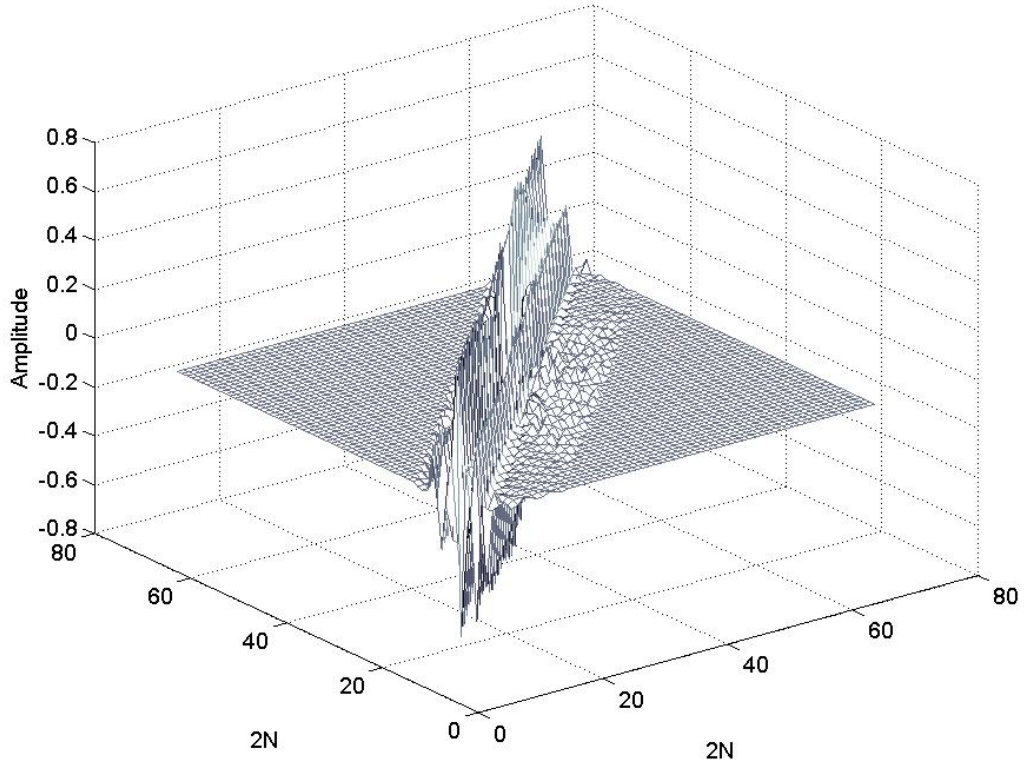


Fig. 5.4 An example of a fractional-domain doubly dispersive banded channel matrix after permutation  $\mathbf{B}_p$  with  $N = 35$

### 5.3.1 Low Complexity Banded MMSE Equaliser

The low-complexity MMSE equalisers designed for SISO-OFDM in Section 3.6 & 3.7 will be extended to the MISO system using the Alamouti coding scheme.

Like the SISO system, perfect knowledge of the channel matrix  $\mathbf{B}_p$  is assumed and the equaliser does not use guard subcarriers. Furthermore it is assumed that:  $E\{\mathbf{d}\} = E\{\mathbf{z}\} = 0, E\{\mathbf{d}\mathbf{d}^H\} = \mathbf{I}, E\{\mathbf{d}\mathbf{z}^H\} = 0, E\{\mathbf{z}\mathbf{z}^H\} = \sigma^2\mathbf{I}$ . Again due to the channel matrix inversion which needs  $\mathcal{O}(N_A^3)$  complex operations MMSE the equaliser is complex especially for high values of  $N_A$ .

The MMSE equaliser  $\mathbf{W}_{MMSE}$  is given by:

$$\mathbf{W}_{MMSE} = (\mathbf{B}_p \mathbf{B}_p^H + \gamma^{-1} \mathbf{I}_{N_A})^{-1} \mathbf{B}_p^H \quad (5.11)$$

The estimated data is given by:

$$\hat{\mathbf{d}}_{MMSE} = \mathbf{W}_{MMSE} \mathbf{Y}_{\mathcal{P}} \quad (5.12)$$

where  $\hat{\mathbf{d}}_{MMSE}$  is the permuted version of  $\hat{\mathbf{d}}$  which can be recovered by:

$$\hat{\mathbf{d}} = \mathcal{P}^T \hat{\mathbf{d}}_{MMSE} \quad (5.13)$$

the complexity for the MMSE banded equaliser is given in Section 3.6 which requires about  $(8Q^2 + 22Q + 4)N_A$  complex operations in total.

Using the same formulation with the iterative MMSE equalisation using the LSMR algorithm will reduce the equaliser complexity to  $\mathcal{O}(N_A(Q + 1)I)$  complex operations in total as in Section 3.7 for the banded matrix case where  $I$  is the number of iterations.

#### 5.4 Space-Time Block Coding (STBC) Scheme Based on OCDM.

EO-STBC is a MISO space-time coder system based on four antennas in the transmitter and one receive antenna. It's a diversity scheme which can achieve both full rate and full diversity gain using an additional feedback link from the receiver to the transmitter that updates the phase rotations applied in the transmitter which ensures both full diversity and array gain [130, 131]. Channel state information (CSI) from the receiver is fed back to the transmitter to optimize these rotations with the assumption that they are delayless and error-free for simplicity. In broadband scenarios, EO-STBC can be easily embedded in MCM schemes [130] such as OFDM or OCDM.

Multicarrier EO-STBC configuration block diagram is shown in Fig. 5.5 where the data vector  $\mathbf{d}_n$  dimension is equivalent to the number of active subcarriers  $N_a$ . The MCM transmit symbols  $\mathbf{s}_{i,n}, i = 0..3$ , emitted from the four antennas are defined over two consecutive symbol periods as:

$$\mathbf{s}_{j,n} = \begin{cases} \mathbf{d}_n, & n \text{ even} \\ \mathbf{d}_n^*, & n \text{ odd} \end{cases} \quad (5.14)$$

$$\mathbf{s}_{(j+2),n} = \begin{cases} \mathbf{d}_{n+1}, & n \text{ even} \\ \mathbf{d}_{n+1}^*, & n \text{ odd} \end{cases} \quad (5.15)$$

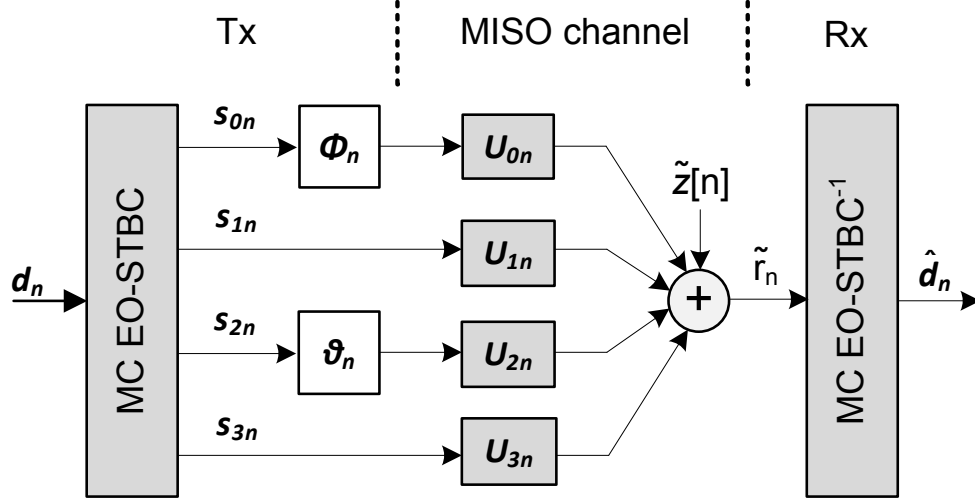


Fig. 5.5 EO-STBC in a multicarrier configuration with equivalent multicarrier channel matrices  $\mathbf{U}_{i,n}, i = 0 \cdots 3$ , and beamsteering by rotations  $\Phi_n$  and  $\theta_n$  which are based feedback from the transmitter and can maximize the diversity and array gain of this system.

where  $j \in \{0, 1\}$ . The first and third antenna signal includes a modification due to the phase rotations as shown in Fig. 5.5, where the phase rotations is given by

$$\Phi_n = \text{diag} \{e^{j\phi_{1,n}} \dots e^{j\phi_{N_a,n}}\} \quad (5.16)$$

$$\theta_n = \text{diag} \{e^{j\vartheta_{1,n}} \dots e^{j\vartheta_{N_a,n}}\} \quad (5.17)$$

which apply a rotation to every subcarrier. Using the equivalent multicarrier channel model  $\mathbf{U}_{i,n} = \mathbf{P}^H \mathbf{F}_\alpha \mathbf{H}_{i,n} \mathbf{F}_{-\alpha} \mathbf{P}$  which was defined in (3.25) in Section 3.4 to describe the four transmit channel paths connecting the transmitter with the receiver, according to Fig. 5.5, the received signal vector  $\tilde{\mathbf{r}}_n$  is given by:

$$\tilde{\mathbf{r}}_n = \mathbf{U}_{0,n} \Phi_n \mathbf{s}_{0n} + \mathbf{U}_{1,n} \mathbf{s}_{1n} + \mathbf{U}_{2,n} \theta_n \mathbf{s}_{2n} + \mathbf{U}_{3,n} \mathbf{s}_{3n} + \tilde{\mathbf{z}}_n \quad (5.18)$$

where  $\tilde{\mathbf{z}}_n = \mathbf{P}^H \mathbf{F}_\alpha \mathbf{z}$  and  $\tilde{\mathbf{z}}_n$  is a circularly symmetric zero mean white complex Gaussian random noise vector with covariance  $E\{\tilde{\mathbf{z}}_n \tilde{\mathbf{z}}_n^H\} = \sigma^2 \mathbf{I}_{N_a}$ , as shown in Fig. 5.5.

Gathering data over two successive OCDM symbol periods, the received signal vector can be written as:

$$\begin{bmatrix} \tilde{\mathbf{r}}_n \\ \tilde{\mathbf{r}}_{n+1}^* \end{bmatrix} = \mathbf{G}_n \begin{bmatrix} \mathbf{d}_n \\ \mathbf{d}_{n+1} \end{bmatrix} + \begin{bmatrix} \tilde{\mathbf{z}}_n \\ \tilde{\mathbf{z}}_{n+1}^* \end{bmatrix} \quad (5.19)$$

where  $\mathbf{G}_n$  is given by:

$$\mathbf{G}_n = \begin{bmatrix} \mathbf{U}_{0,n}\boldsymbol{\phi}_n + \mathbf{U}_{1,n} & \mathbf{U}_{2,n}\boldsymbol{\theta}_n + \mathbf{U}_{3,n} \\ \mathbf{U}_{2,n+1}^*\boldsymbol{\theta}_{n+1} + \mathbf{U}_{3,n+1}^* & -\mathbf{U}_{0,n+1}^*\boldsymbol{\phi}_{n+1} - \mathbf{U}_{1,n+1}^* \end{bmatrix} \quad (5.20)$$

It is worth noting that if the MISO channel is stationary and the DFrFT-OCDM configuration is used with chirp rate  $\alpha = \pm 1$ , the equivalent system channel matrices  $\mathbf{U}_{i,n}$  will be diagonal, ensuring that subcarriers can be EO-STBC decoded individually and ICI can be neglected.

## 5.5 Proposed Space-Time Decoding

In a doubly dispersive channel scenario, Doppler spread destroys the orthogonality between subcarriers and the OFDM system is unable to diagonalise the system matrix in (5.20). Consequently coupling between at least adjacent subcarriers will be introduced leading to degradation in system performance.

Symbols can be detected by ignoring ICI under near-stationary channel scenario which features low Doppler spread, using only the elements on the main diagonal of the channel transfer matrix. Thus the OFDM system can be employed due to it is low complexity. This implies that any off-diagonal components in the equivalent channel matrices  $\mathbf{U}_{i,n}$  will be ignored. The diversity gain can be maximised by ensuring that the angles in  $\boldsymbol{\phi}_n$  and  $\boldsymbol{\theta}_n$  maximise the on-diagonal terms of the reduced system matrix.

The low Doppler Spread EO-STBC receivers can combat crosstalk on each subcarrier separately to enable the feedback diversity gain. In STBC systems, the channels are normally assumed to remain block stationary. In this case, frequency-domain channel sub matrices are orthogonal and the symbols can be simply decoded by the simple maximum-likelihood (SML) algorithm, the complexity of the SML algorithm is linear in the number of subcarriers. However, in time selective fading channels, frequency-domain channel sub matrices are no longer orthogonal, so decoding to decrease effect of cross-talk can be performed by the joint maximum-likelihood (JML) algorithm which have more complexity than algorithms such as zero-forcing (ZF), and decision-feedback (DF) [127, 128].

On the other hand for higher Doppler spread in order to mitigate the impact of high Doppler spread on the EO-STBC decoding performance, equalisation is needed and the feedback of angles to the transmitter is not required. In the next section a novel EO-STBC scheme will be presented.

### 5.5.1 Open Loop EO-STBC Decoding with Equalisation

The EO-STBC system combined with the OCDM performance under higher Doppler spread conditions can be improved using equalisation which will increase the receiver complexity but removes the need for feedback of angles to the transmitter, therefore the beam steering matrices are simply set as  $\boldsymbol{\phi}_n = \boldsymbol{\theta}_n = \mathbf{I}$  where  $\mathbf{I}$  is the identity matrix.

#### 5.5.1.1 OCDM EO-STBC system Low complexity equalisers

Low complexity equalisers can be used with the OCDM EO-STBC system such as banded linear block MMSE, LDL<sup>H</sup> and LSMR equalisers which were described in chapter 3.

Assuming perfect channel state information, a linear block MMSE equaliser is defined based on the system matrix  $\mathbf{G}_n$  in (5.20) which is a  $2 \times 2$  block matrix of  $N \times N$  nearly banded matrices.  $\mathbf{G}_n$  can be transferred to  $2 \times 2$  block matrix of  $N \times N$  banded matrices using the masked matrix  $\mathbf{M}$  which is defined in (5.8) to reduce the equalisation process complexity.

$$\mathbf{B}_n = \begin{bmatrix} \mathbf{M} & \mathbf{M} \\ \mathbf{M} & \mathbf{M} \end{bmatrix} \odot \mathbf{G}_n \quad (5.21)$$

where  $\mathbf{B}_n$  is the banded system matrix version of  $\mathbf{G}_n$ . The received data can be rewritten as:

$$\begin{bmatrix} \tilde{\mathbf{r}}_n \\ \tilde{\mathbf{r}}_{n+1}^* \end{bmatrix} = \mathbf{B}_n \begin{bmatrix} \mathbf{d}_n \\ \mathbf{d}_{n+1} \end{bmatrix} + \begin{bmatrix} \tilde{\mathbf{z}}_n \\ \tilde{\mathbf{z}}_{n+1}^* \end{bmatrix} \quad (5.22)$$

$\mathbf{B}_n$  can be rearranged using the permutation matrix  $\mathcal{P}$   $2N \times 2N$  where the data from the same subcarriers of different transmit antennas are grouped together and the received data from the same subcarriers in two consecutive OCDM symbol periods are grouped together.

$$\mathcal{P} \begin{bmatrix} \tilde{\mathbf{r}}_n \\ \tilde{\mathbf{r}}_{n+1}^* \end{bmatrix} = \mathcal{P} \mathbf{B}_n \mathcal{P}^T \mathcal{P} \begin{bmatrix} \mathbf{d}_n \\ \mathbf{d}_{n+1} \end{bmatrix} + \mathcal{P} \begin{bmatrix} \tilde{\mathbf{z}}_n \\ \tilde{\mathbf{z}}_{n+1}^* \end{bmatrix} \quad (5.23)$$

Similar to (5.11) the MMSE equaliser can be defined as:

$$\mathbf{W}_{n,MMSE} = \mathbf{B}_n^H (\mathbf{B}_n \mathbf{B}_n^H + \gamma^{-1} \mathbf{I}_{N_a})^{-1} \quad (5.24)$$

where  $\gamma$  is the signal to noise ratio (SNR) at the input to the equaliser, assuming corruption by white Gaussian noise. The matrix inversion in (5.24) requires  $\mathcal{O}(8N_a^3)$  complex operations which is not practical for high values of  $2N_a$ . The ZF equaliser  $\mathbf{W}_{n,ZF}$  can be calculated from (5.24) for the special case:

$$\mathbf{W}_{n,ZF} = \mathbf{W}_{n,MMSE}|_{\gamma \rightarrow \infty} = \mathbf{B}_n^H (\mathbf{B}_n \mathbf{B}_n^H)^{-1} \quad (5.25)$$

Similar to (5.24), the matrix inversion in (5.25) is of order  $\mathcal{O}(8N_a^3)$  and it enhances the noise effect thus degrading the system performance. It is obvious that using the low complexity equalisers which were introduced in chapter 3 will decrease the system complexity with almost the same system performance.

#### 5.5.1.2 Low Complexity Equalisers Implementation

The matrix inversion in (5.24) requires a substantial number of  $\mathcal{O}(8N_a^3)$  complex operations, which is excessive for large  $2N_a$ . By applying an  $LDL^H$  factorisation in calculating either MMSE or ZF solutions in (5.24) and (5.25), the number of complex operations compared to standard matrix inversion methods such as Gaussian elimination can be reduced to  $\mathcal{O}(8Q^2 + 22Q + 4)2N_a$  complex operations as in Section 3.6.

The LSMR implementation of either MMSE or ZF solution requires  $\mathcal{O}(2N_a(Q + 1))$  complex operations for each iteration, leading to a total of  $\mathcal{O}(2N_a(Q + 1)i)$  complex operations. LSMR can achieve the same accuracy of inversion with a considerably lower number of complex operations, hence leading to an overall saving in complexity as in Section 3.7.

## 5.6 A Novel MIMO-OCDM System

In the last two sections STBC MISO systems were investigated in detail under the doubly dispersive fading channel and combining the system with the novel OCDM

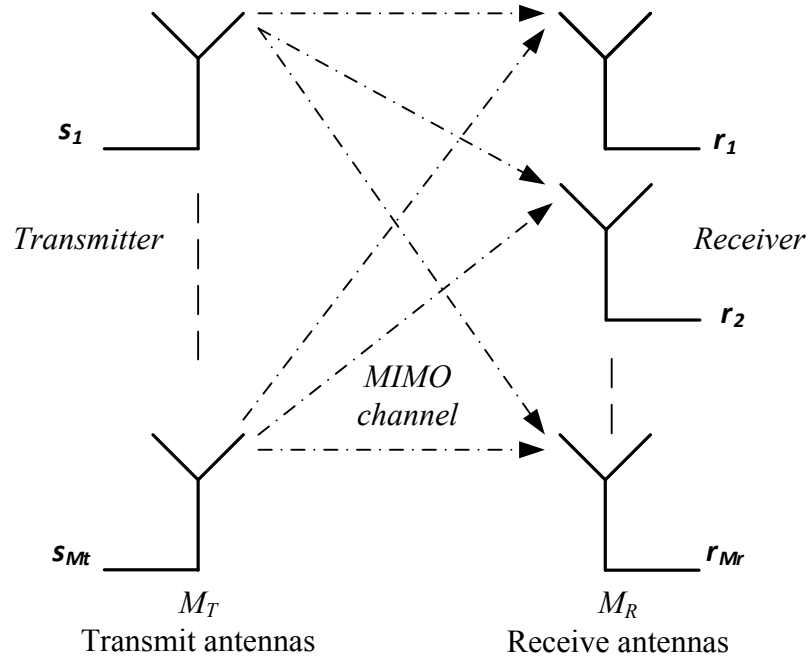


Fig. 5.6 The MIMO-OCDM system

MCM was introduced. In this section combining the MIMO system with the OCDM system will be investigated under the doubly dispersive channel scenario conditions.

The aim of this section is to extend the SISO-OCDM systems to the MIMO-OCDM systems while investigating the capability of using low complexity equalisers which were introduced in chapter 3.

### 5.6.1 MIMO-OCDM System Model

Considering a MIMO-OCDM system with  $N$  subcarriers,  $M_T$  transmit antennas and  $M_R$  receive antennas as shown in Fig. 5.6. The  $M_T M_R$  SISO channels between transmit and receive antennas are considered to be uncorrelated doubly selective and characterized by the same fading statistics, with CP length  $L$  larger than the maximum delay spread. Recalling (3.22) at the  $j$ th receive antenna, the received vector, after inverse transformation (IDFrFT-IDFrCT) and CP removal, can be expressed by:

$$\mathbf{r}_j = \sum_{i=1}^{M_T} \tilde{\mathbf{H}}_{i,j} \mathbf{d}_i + \tilde{\mathbf{z}}_j \quad (5.26)$$

where  $\mathbf{r}_j$  is the  $N \times 1$  received vector,  $\tilde{\mathbf{H}}_{i,j}$  is the  $N \times N$  fractional domain channel matrix between the  $j$ th receive antenna and the  $i$ th transmit antenna,  $\mathbf{d}_i$  is the  $N \times 1$  OCDM fractional domain data block transmitted by the  $i$ th transmit antenna which is independent of the data transmitted from the other antennas, and  $\tilde{\mathbf{z}}_j$  is the  $N \times 1$  noise vector of the  $j$ th receive antenna in the fractional domain  $\tilde{\mathbf{z}}_j = \mathbf{F}_\alpha \mathbf{z}_j$ . Each fractional-domain channel matrix can be expressed by:

$$\tilde{\mathbf{H}}_{i,j} = \mathbf{F}_\alpha \mathbf{H}_{i,j} \mathbf{F}_\alpha^H \quad (5.27)$$

where  $\mathbf{H}_{i,j}$  is the corresponding  $N \times N$  time domain channel matrix between the  $j$ th receive antenna and the  $i$ th transmit antenna, and  $\mathbf{F}_\alpha$  is the  $N \times N$  unitary DFrFT or DFrCT matrix, with the fractional order  $\alpha$ . In time-varying channels both DFrFT and DFrCT cannot diagonalise  $\mathbf{H}_{i,j}$ . As a consequence a certain amount of ICI is present which degrades the system performance.

Following the same steps as in (3.17) the transmitted data vector  $\mathbf{d}_n = [d_0 \ d_1 \ \dots \ d_{N_a-1}]^T$  is permuted by the binary matrix  $\mathbf{P} \in \mathbb{Z}^{N \times N_a}$  which assigns a data vector  $\mathbf{d}_n \in \mathbb{C}^{N_a}$  to  $N$  subcarriers, of which only  $N_a$  are active according to:

$$\mathbf{P} = \begin{bmatrix} 0_{N_a \times (N-N_a)/2} & \mathbf{I}_{N_a} & 0_{N_a \times (N-N_a)/2} \end{bmatrix} \quad (5.28)$$

where  $\mathbf{P}$  is the  $N \times N$  matrix that inserts the  $N - N_a$  frequency guard bands. All the received vectors by the  $M_R$  antennas  $\{\mathbf{r}_j\}_{j=1}^{M_R}$ , can be collected in a single vector:

$$\underline{\mathbf{r}} = \tilde{\mathbf{H}} \underline{\mathbf{d}} + \underline{\mathbf{z}} \quad (5.29)$$

where  $\underline{\mathbf{r}} = [\mathbf{r}_1^T \ \dots \ \mathbf{r}_{M_R}^T]^T$ ,  $\underline{\mathbf{d}} = [\mathbf{d}_1^T \ \dots \ \mathbf{d}_{M_T}^T]^T$ ,  $\tilde{\mathbf{H}}$  is given by:

$$\tilde{\mathbf{H}} = \begin{bmatrix} \tilde{\mathbf{H}}_{1,1} & \dots & \tilde{\mathbf{H}}_{1,M_T} \\ \vdots & \ddots & \vdots \\ \tilde{\mathbf{H}}_{M_R,1} & \dots & \tilde{\mathbf{H}}_{M_R,M_T} \end{bmatrix} \quad (5.30)$$

and  $\underline{\mathbf{z}} = [\mathbf{z}_1^T \ \dots \ \mathbf{z}_{M_R}^T]^T$ , with covariance expressed by  $\mathbf{C}_{\mathbf{z}} = \mathbf{I}_{M_R} \otimes \sigma_z^2$ .

There is a need for a permutation matrix to deal with the MIMO system  $\mathcal{P}_{(M,N)}$  as the  $MN \times MN$  matrix that contains 1's in the positions given by:

$$\{(i + 1, [i/M] + 1 + Ni_{\text{mod}M})\}_{i=0}^{MN-1} \quad (5.31)$$

and 0's elsewhere. Using the permutation matrix  $\mathcal{P}_{(M,N)}$  to permute the received vector in (5.29), will give:

$$\mathcal{R} = \mathcal{P}_{(M_R,N)} \underline{\mathbf{r}} = (\mathcal{P}_{(M_R,N)} \underline{\mathbf{H}} \mathcal{P}_{(M_T,N)}^T) (\mathcal{P}_{(M_T,N)} \underline{\mathbf{d}}) + (\mathcal{P}_{(M_R,N)} \underline{\mathbf{z}}) \quad (5.32)$$

$$\mathcal{R} = \mathcal{H} \mathbf{d} + \mathbf{z} \quad (5.33)$$

where  $\mathcal{R}$  is the permuted received vector,  $\mathcal{H}$  is the permuted fractional MIMO channel matrix,  $\mathbf{d}$  is the permuted data vector and  $\mathbf{z}$  is the permuted noise vector.

It is obvious that the model expressed by (5.29), the permuted model of (5.32), which is equivalent to (3.22), has the property that the data received on the same subcarrier of different antennas are close together. The same property holds for the data transmitted by different antennas. Consequently, also the guard bands relative to data transmitted by different antennas are close together, at the top and at the bottom of  $\underline{\mathbf{d}}$ . It is clear that the estimation of the data vector  $\underline{\mathbf{d}}$  will require complicated equalisers.

### 5.6.2 MIMO-OCDM System Equalisation

The linear zero-forcing (ZF) and MMSE estimates Section 3.4 can be derived by minimizing  $E\{\|\mathbf{d}_n - \mathbf{W}\mathcal{R}\|\}$ , yielding:

$$\hat{\mathbf{d}}_{ZF} = \mathcal{H}^+ \mathcal{R} \quad (5.34)$$

$$\hat{\mathbf{d}}_{MMSE} = \mathcal{H}^H (\mathcal{H}\mathcal{H}^H + \mathbf{C}\mathbf{o}_{zz})^{-1} \mathcal{R} \quad (5.35)$$

where  $\mathbf{C}\mathbf{o}_{zz}$  is the permuted noise covariance vector  $\mathbf{C}\mathbf{o}_{zz} = \mathbf{P}_{(M_R,N_a)} \mathbf{C}\mathbf{o}_{zz} \mathbf{P}_{(M_R,N_a)}$ .  $\hat{\mathbf{d}}_{ZF}$  and  $\hat{\mathbf{d}}_{MMSE}$  are the estimated data after ZF and MMSE equalisation respectively,  $\mathcal{H}^H$  is the fractional MIMO channel matrix conjugate transpose in the fractional domain,  $\mathcal{H}^+$  is the Moore-Penrose pseudo-inverse of the fractional MIMO channel matrix [103].

$\hat{\mathbf{d}}_{MMSE}$  is the permuted version of the estimated data  $\hat{\mathbf{d}}$  which can be recovered by:

$$\hat{\mathbf{d}} = \mathcal{P}^T \hat{\mathbf{d}}_{MMSE} \quad (5.36)$$

ZF equaliser performance is poor due to noise enhancement. On the other hand the MMSE equaliser give the best performance of all linear equalisers [98] but it is very complicated due to MIMO channel matrix inversion.

The permuted MIMO channel matrix  $\mathcal{H}$  is almost banded which means that most of the ICI comes from the nearest subcarriers. As a result, the almost-banded structure of  $\tilde{\mathbf{H}}_{i,j}$  implies that  $\mathcal{H}$  is almost block-banded which indicate the validity of using low complexity equalisers with the MIMO-OCDM system.

### 5.6.3 MIMO-OCDM System with low Complexity Equalisation

The MIMO-OCDM channel matrix  $\mathcal{H}$  can be approximated by its banded version, expressed by:

$$\mathbf{B}_{(Q)} = \mathcal{M} \odot \mathcal{H}, \quad (5.37)$$

where  $\odot$  represents element-wise multiplication and  $\mathcal{M} = \mathbf{M} \otimes \mathbf{I}_{M_R \times M_T}$  and  $\mathbf{M}$  is a binary masking matrix which was given in (5.8) and the parameter  $Q$ , controls the width of the block-band, can be chosen as in SISO-OFDM in Section 3.6. It will be shown that this parameter can be used in the equalisers to trade off performance for complexity.

$\mathbf{B}_{(Q)}$  is the banded version of the fractional MIMO channel matrix  $\mathcal{H}$  which allows the design of low-complexity equalisers called banded equalisers which have been investigated in Section 3.6. Based on the masked channel matrix, the MMSE equaliser can be defined as:

$$\mathbf{w}_{n,MMSE} = \mathbf{B}_n^H (\mathbf{B}_n \mathbf{B}_n^H + \mathbf{C}_{\mathbf{o}_{zz}})^{-1} \quad (5.38)$$

The estimated data vector will be given by:

$$\hat{\mathbf{d}}_{MMSE} = \mathbf{w}_{n,MMSE} \mathcal{R} = \mathbf{B}_n^H (\mathbf{B}_n \mathbf{B}_n^H + \mathbf{C}_{\mathbf{o}_{zz}})^{-1} \mathcal{R} \quad (5.39)$$

The  $LDL^H$  factorization algorithm and all the LSMR algorithm equaliser versions can be used. Simulation for different equalisers will be shown in the next section.

## 5.7 Simulation and results

### 5.7.1 Alamouti MISO OCDM System Performance

The proposed decoding algorithms are now examined and compared by simulation. We consider an Alamouti space-time coded system based on OFDM, DFrFT-OCDM and DFrCT-OFDM with the same specifications as in the SISO scheme.

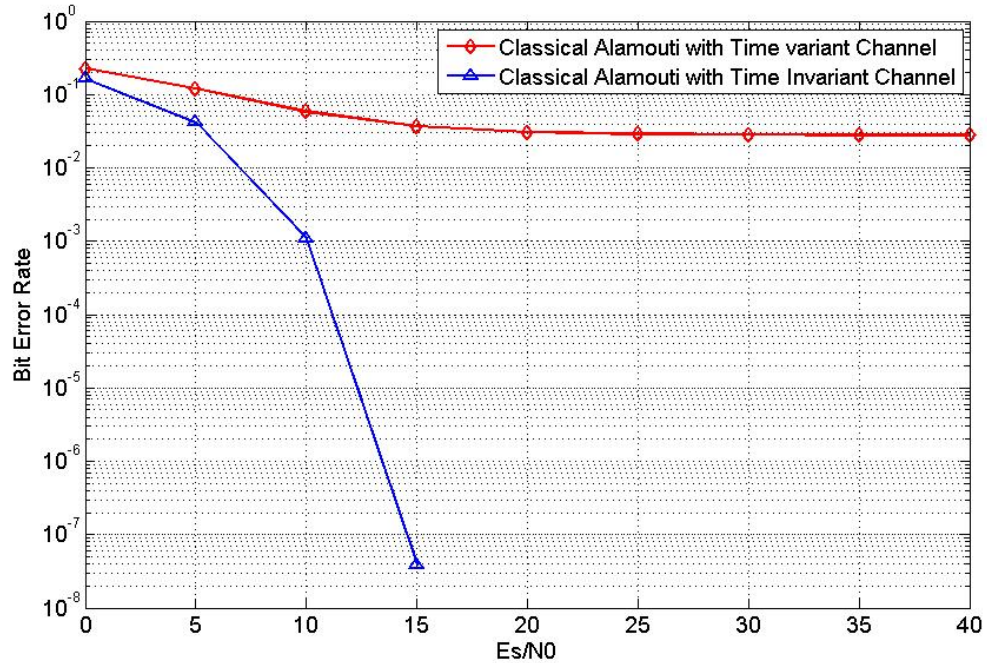


Fig. 5.7 Uncoded BER Comparison for the classical Alamouti space-time coded OFDM system with time invariant and time variant channels

The two SISO channels from the transmit antennas to the receive antenna are assumed to be independent and Rayleigh distributed, the channel simulation parameters are the same as the Rayleigh fading channel in section 3.6.

Fig. 5.7 compares the BER performance of the classical Alamouti space-time coded OFDM system with time invariant and time variant channels. It is obvious that the classical Alamouti decoding fails completely due to time variant channel which destroys the orthogonality between subcarriers.

Fig. 5.8 compares the BER performance of the different Alamouti space-time coded systems based on OFDM, DFrFT and DFCT using MMSE equaliser in decoding with the classical Alamouti decoding system based on OFDM under time variant channel. Using equalisation for the Alamouti system decoding improves the system performance compared to the OFDM case under high mobility conditions (doubly selective channel) however the proposed system using DFrCT-OCDFM give better performance even from the DFrFT-OCDFM system.

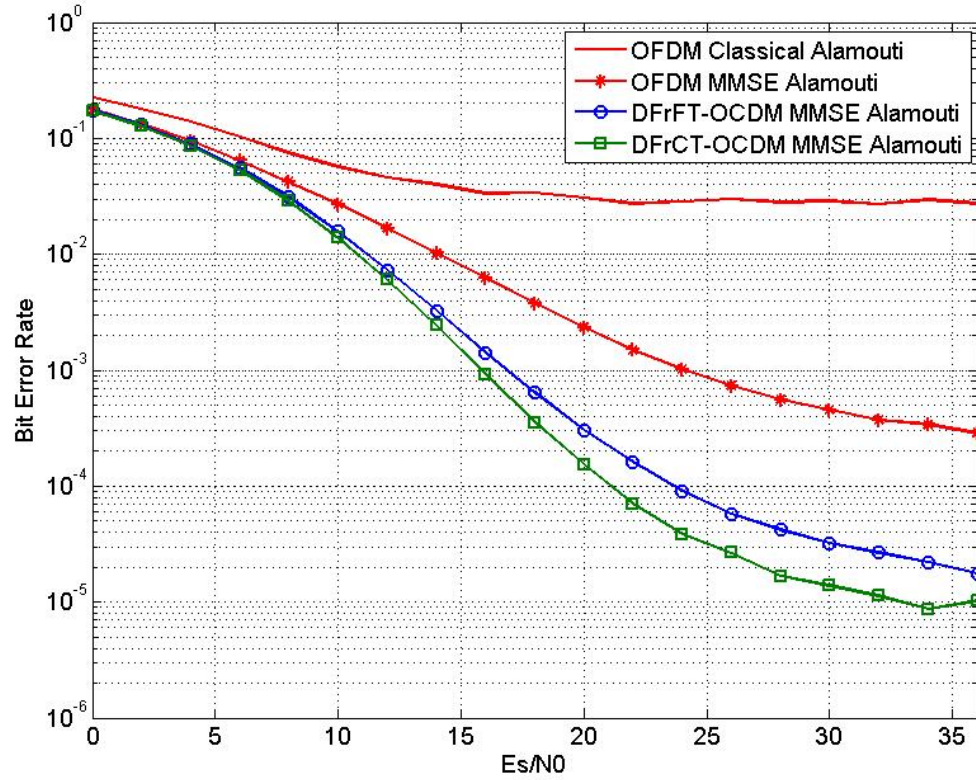


Fig. 5.8 Uncoded BER Comparison for the classical Alamouti space-time coded OFDM system with different Alamouti STBC systems based on OFDM, DFrFT and DFrCT-OCODM using MMSE equaliser under time variant channel

Comparison between the proposed DFrCT-OCODM and the OFDM system using low complexity equalisers for Alamouti coding is shown in Fig. 5.9.

It is clear that using of low complexity equaliser degrades the system performance as banded equalisers have an error floor due to the band approximation error of the channel. The error floor can be reduced by increasing  $Q$  in (5.37).

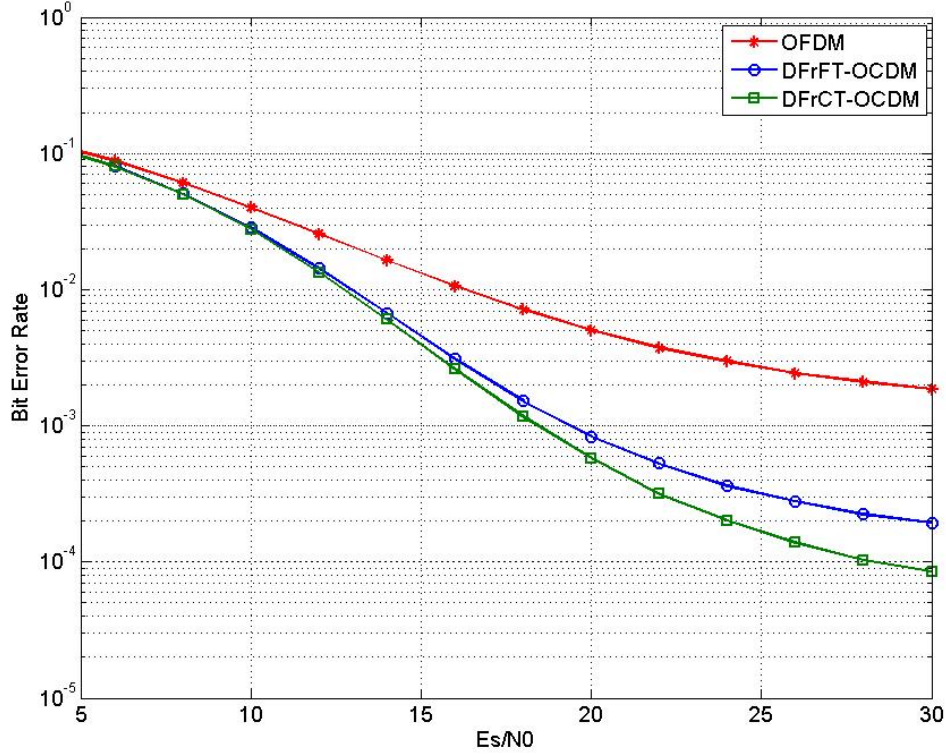


Fig. 5.9 Uncoded BER Comparison for different Alamouti space-time coded systems based on OFDM, DFrFT and DFrCT-OCDM using low complexity MMSE equaliser

### 5.7.2 Multicarrier EO-STBC DFrCT-OCDM MISO Transceiver System Performance

The proposed multicarrier EO-STBC DFrCT-OCDM MISO transceiver will be investigated using simulation under doubly dispersive fading conditions, a comparison between the novel system performance and the EO-STBC OFDM MISO transceiver will be introduced. The channel simulation parameters are the same as the Rayleigh fading channel in section 3.6.

In Fig. 5.10, a comparison between the OCDM and OFDM EO-STBC system performance using block equaliser is provided and in Fig. 5.11 shows the results of using a low complex approach using an equaliser restricted to operating on the  $Q = 12$  sub- and super-diagonals of the permutation system matrix  $G_n$

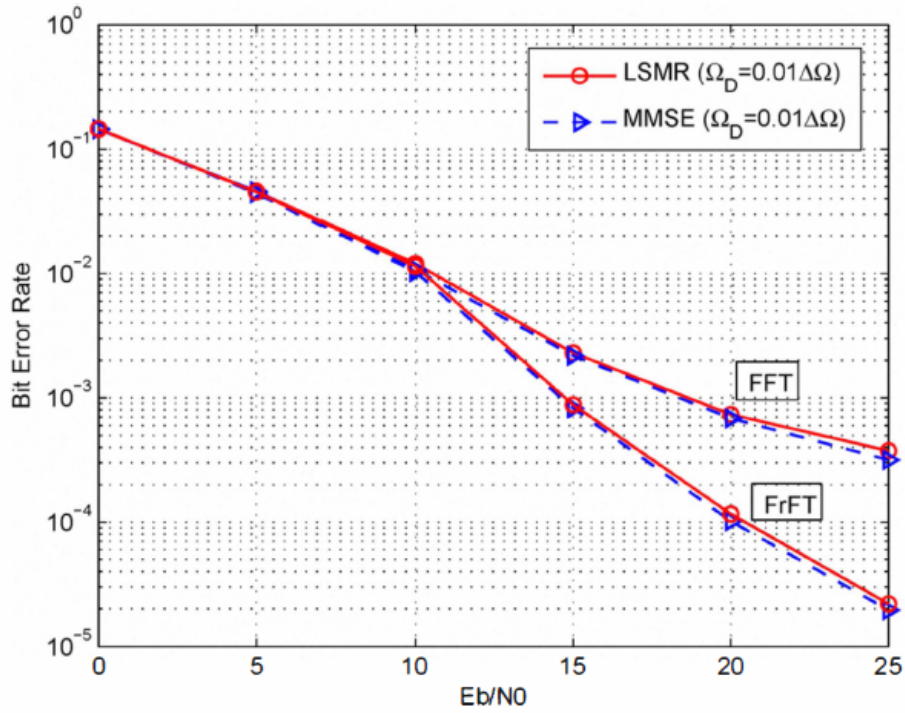


Fig. 5.10 BER Comparison of the multicarrier EO-STBC system based on OCDM and classical OFDM with block equalisation

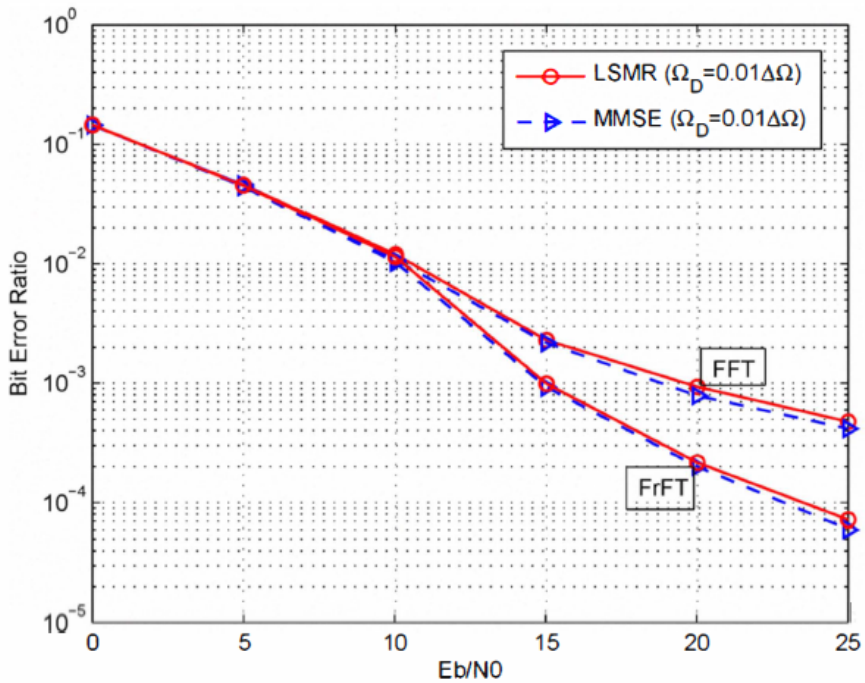


Fig. 5.11 BER Comparison of the multicarrier EO-STBC system based on OCDM and classical OFDM with banded equalisation  $Q = 12$

As seen in Fig 5.10 and 5.11 the BER performance for the OFDM and the DFrFT-OCDM systems is almost the same up to approx. 10dB Eb/N0 due to the AWGN.. At higher EB/N0 the BER performance degrades in the banded equaliser case due to the error in omitting off-diagonals greater than  $Q = 12$ . Since in the OCDM case most of the energy within the channel matrix is concentrated around the main diagonal as in Section 3.6, it can achieve a better performance than OFDM based system despite having very similar complexity. The approach labelled MMSE in Fig 5.11 represents a standard inversion of the approximate channel matrix  $B_n$ , while the LSMR approach implements an MMSE design but with the reduced complexity of the iterative LSMR algorithm in Section 3.6.

### 5.7.3 MIMO-OCDM System Performance

The proposed MIMO-OCDM transceiver will be investigated using simulation under doubly dispersive fading conditions, a comparison between the novel system performance and the MIMO-OFDM transceiver will be introduced. The channel simulation parameters are the same as the Rayleigh fading channel in section 3.6 and the simulation is carried over 100000 different symbols and different channels.

Comparison between the MIMO-OCDM and the MIMO-OFDM systems is carried using 2 transmit antennas and 3 receiving antennas with the block MMSE equaliser is shown in Fig. 5.12. From the figure it is clear that the MIMO-OCDM systems are much better than the MIMO-OFDM system and the MIMO-DFrCT system is better than the MIMO-DFrFT system. The figure shows that the OCDM MIMO systems outperform the OFDM system in the 1% uncoded BER area by 1.3 dB and in the 0.1% uncoded BER area by 2.5 dB. It is clear that the DFrCT-OCDM system outperform the DFrCT-OCDM system in the 0.1% uncoded BER area by 0.5 dB.

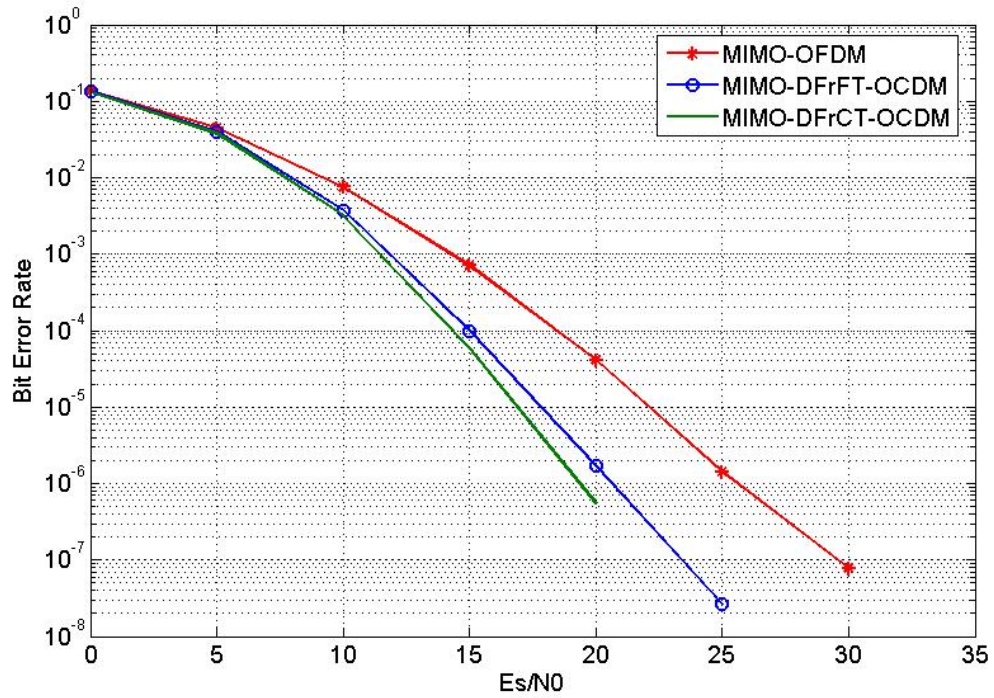


Fig. 5.12 The MIMO system performance with 2 transmit antennas and 3 receive antennas using MMSE equaliser

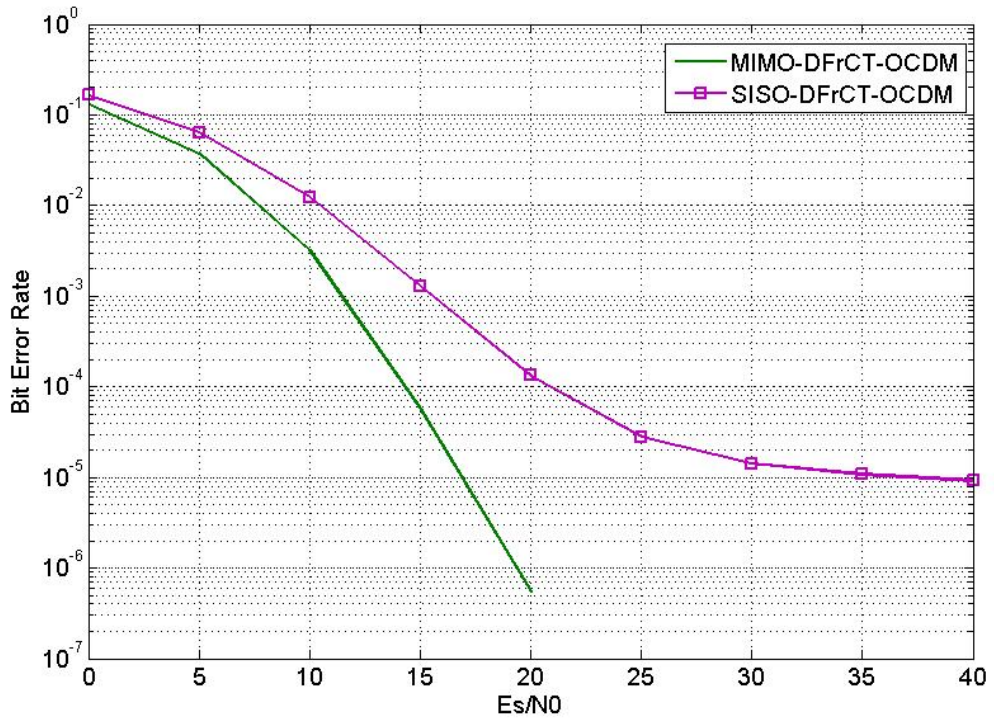


Fig. 5.13 BER Comparison between the MIMO and SISO DFrCT-OCDFM system with 2 transmit antennas and 3 receive antennas using MMSE equaliser

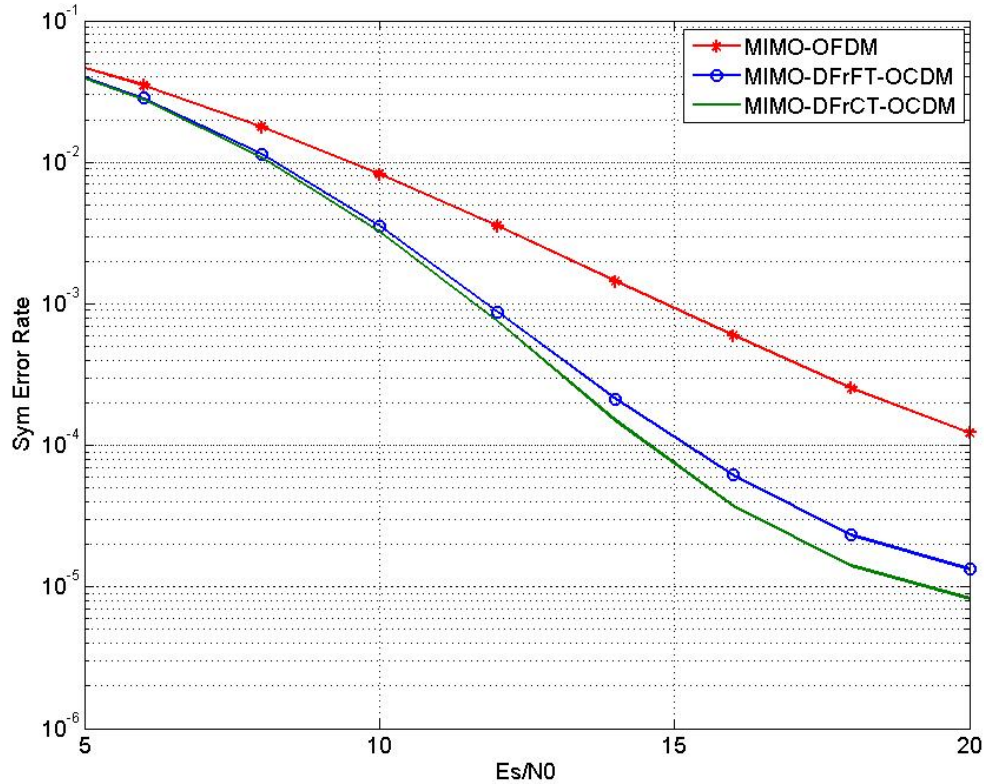


Fig. 5.14 The MIMO system performance with 2 transmit antennas and 3 receive antennas using banded low complexity MMSE equaliser

Comparison between the MIMO-DFrCT and the SISO-DFrCT system is carried using the block MMSE equaliser is shown in Fig. 5.13. It is obvious that the MIMO-DFrCT system is better than the SISO-DFrCT system because of the diversity gain of the MIMO system.

Comparison between the MIMO-OCDM and the MIMO-OFDM systems is carried using 2 transmit antennas and 3 receiving antennas with the low complexity banded MMSE equaliser is shown in Fig. 5.14. From the figure it is clear that the MIMO-OCDM systems are much better than the MIMO-OFDM system and the MIMO-DFrCT system is better than the MIMO-DFrFT system. It is clear also that the banded low complexity MMSE equaliser performance is less than the MMSE equaliser due to banded approximation.

## 5.8 Conclusion

In this chapter novel MIMO-OCDM were investigated. MISO systems based on Alamouti decoding were investigated and a combination with OCDM was proposed that would lead to an improvement in system performance. EO-STBC transmission was studied over a doubly-dispersive channel. To mitigate the temporal dispersion, a multi carrier scheme was deployed. The frequency dispersion due to Doppler spread, however, can lead to significant performance degradation wherein the decoupling of subcarriers is lost. For the case of low Doppler spread and near stationary channel conditions, the proposition is to ignore ICI. In the case of higher Doppler spread, a combined approach of a general multicarrier system based on the OCDM with equalisation was proposed. Compared to classical OFDM, the OCDM tends to retain more channel energy along the main diagonal, which leads to better system performance, or permits equalisation with lower complexity given the same performance than OFDM systems. Finally the MIMO-OCDM systems were proposed to improve the system performance of the MIMO-MCM systems under doubly dispersive channels. The novel MIMO and MISO-OCDM systems were investigated using low complexity equalisers and were shown to provide a better performance than the MIMO and MISO OFDM systems.

In the next chapter conclusions and proposed future work will be given.

# 6. Conclusion and Future Work

---

## 6.1 Introduction

The main purpose of the work described in this thesis was to explore and develop new signal processing techniques which can improve the multicarrier modulation systems performance under doubly dispersive fading channels. The key achievements of the research are twofold. New low complexity equalisers were developed to solve the equalisation complexity problem. The second objective was to develop new bases for the MCM systems that adopt DFrCT transformation for the modulation and demodulation process.

This chapter concludes the research work presented and indicates areas where future work could be directed.

## 6.2 Conclusion

This thesis focused on improving the MCM systems performance under high speed mobility conditions and was based on new non-traditional signal processing tools and methods that provide enhanced system performance, reduced system errors and complexity.

The review of the OFDM system as the basic MCM system and the most important factors that affect its operation and performance with brief introduction to different MCM systems that were based on different transformations, its advantages and limitations were presented in chapter 2.

A discussion on doubly dispersive fading channels and its effect on the OFDM and DFrFT-OCDFM equalisation algorithms with equaliser's complexity analysis introduced in chapter 3.

A novel multimode transmission method that was based on both the DFrFT-OCDM and the OFDM systems was proposed and simulation demonstrated its benefits in reducing the system complexity and improving performance under different channel scenarios by using the OFDM system under time invariant channel scenario and using DFrFT-OCDM under time variant channel scenario in section 3.5.

OFDM has low equalisation complexity under fading channels as a single tap equaliser can be used, while on the other hand the DFrFT-OCDM system needs a complicated equaliser even under fading channel scenario as, unlike the DFT, the DFrFT cannot diagonalise the fading channel matrix.. Changing the transmitter or receiver speed introduces a doubly dispersive fading channel which is a complicated channel for both systems and complicated equalisers are required. It was shown in Section 3.4 that the DFrFT-OCDM system performance under this scenario is superior to that of the OFDM system performance.

A  $LDL^H$  Low complexity equaliser was proposed for the DFrFT-OCDM system to reduce the computational complexity of the MMSE equaliser in section 3.6. The DFrFT-OCDM system performance and the OFDM system performance were compared using the low complexity  $LDL^H$  equaliser and it was shown that the DFrFT-OCDM system outperform the OFDM system even if the OFDM system uses a complicated MMSE equaliser. The DFrFT-OCDM system was found to compensate the power leakage from the main subcarrier to other subcarriers due to Doppler fading more effectively than the OFDM system which explains the performance difference between both systems that was described in Section 3.6.

The idea of low complexity equalisers based on reducing the computational complexity of the channel matrix inversion needed in the MMSE equaliser which is a mathematically expensive operation especially for long MCM symbols. The LSMR algorithm presented in Section 3.7 is a new mathematical algorithm that can solve matrix inversion problem iteratively. New low complexity equalisers based on the LSMR algorithm were proposed in section 3.7. The LSMR algorithm storage and computation requirements were shown to be almost the same as the well-known LSQR algorithm however the LSMR converges faster than the LSQR so the LSMR algorithm

overall complexity is lower than the LSQR algorithm. LLS-LSMR equaliser which may look like the zero forcing equalizer was proposed and the simulation results indicate that the LLS-LSMR give better results than the ZF equaliser due to the fact that the LLS-LSMR terminates the iterations early before the noise components enhancement. The RLS-LSMR equaliser was shown to be equivalent to the MMSE equaliser and simulation results and simulation results presented indicates that the RLS-LSMR equaliser can give the same performance as the low complexity MMSE equalisers (banded MMSE equalisers) with less complexity. The LSMR-BDFE equaliser was proposed in section 3.8 and it was shown to give better performance than other LSMR equalizers due to the feedback process which reduce the subcarriers interference but it is obvious there is increase in complexity. Finally in chapter 3, the RLS-LSMR sliding window equaliser was proposed which is the lowest complexity between all the LSMR equalisers and it was shown to give a good performance compared to the other equalisers.

The works have been done in this chapter can be continued in several directions as follow:

Investigating the optimal fractional order for the DFrFT-OCDM, which is able to compensate the doubly dispersive channel effect and gives the best enhancement for the OCDM system. Investigating new techniques for equalisation like Neural Networks as a sort of low complexity equalisers to mitigate the doubly dispersive channel effect. Time domain windowing is one of the promising methods to improve the equalisation process by combining with the low complexity equalizers proposed in this thesis to improve the BER performance. Investigating the use of Single carrier modulation systems with nonlinear chirp domain equalisation.

The Discrete Fractional Cosine Transform (DFrCT) was investigated as an alternative bases for the MCM systems instead of the DFT transformation in chapter 4. The DFrCT-OCDM system was shown to give better performance than the DFrFT-OCDM and the OFDM systems with almost the same system complexity. It was shown that the DFrCT-OCDM can be used with low complexity equalisers without affecting its performance.. The PAPR problem and its reduction techniques with the DFrCT and

DFrFT-OCDM systems were investigated and it was shown that all the PAPR reduction techniques can be easily used with the new OCDM systems with almost the same results as with the OFDM system. A comparison between all the MCM based on different unitary transformation matrices under doubly dispersive channel scenario was investigated and it was shown that the chirp bases give the best performance over OFDM, DCT-MCM and DHT-MCM. These comparison results showed that the DHT-MCM system gave a superior performance than the OFDM system which indicates that it may be better to use the discrete Hartley fractional transform (DFrHT) as a new basis for the MCM systems.

Proposing new bases for MCM systems include the challenge of channel estimation which complexity depend on the bases nature and it can affect the system performance.

Finally MIMO systems were investigated as an extension to our new bases and equalisers in chapter 5. Classical Alamouti STBC system and EO-STBC system were investigated under doubly dispersive channel and it was shown that both systems fail to give good performance under doubly dispersive channels. Novel Alamouti STBC and EO-STBC systems based on Orthogonal Chirp Division Multiplexing (OCDM) systems with equalisation were proposed and it was shown that the new systems give superior performance under doubly dispersive channel scenarios. A novel MIMO-OCDM system was proposed and simulation showed the superior performance under different channel scenarios.

# Appendices

---

## A.OFDM System Implementation on Real DSP Board

### A.1 Project Overview

This project goal is to implement a digital OFDM communication system with bit loading using the channel information from a feedback link. Two sets of PCs, each equipped with a DSP card one set act as a transmitter and the other act as a receiver i.e. simplex communication is considered.

#### A.1.1 Equipment

The following equipment used to complete the project Fig. A.1:

1- Hardware

- two PCs
- Two Texas Instruments C6713 DSP boards

2- Software

- MATLAB R2007a
- Code Composer Studio 6713 DSK V3.1

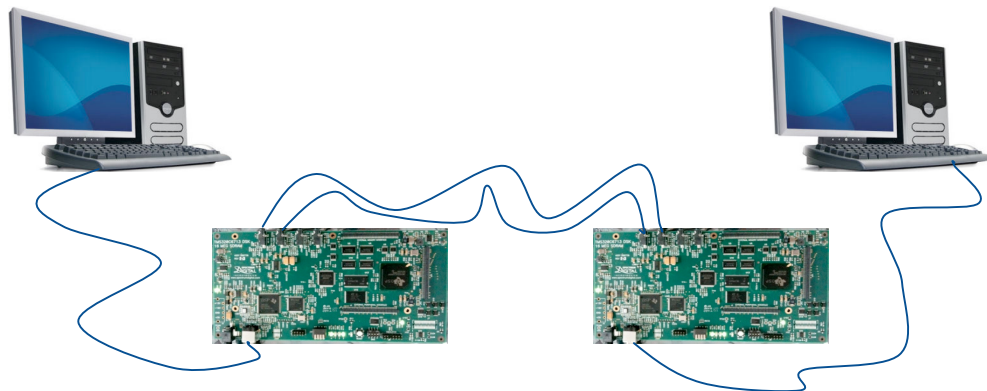


Fig. A.1 OFDM System Implementation

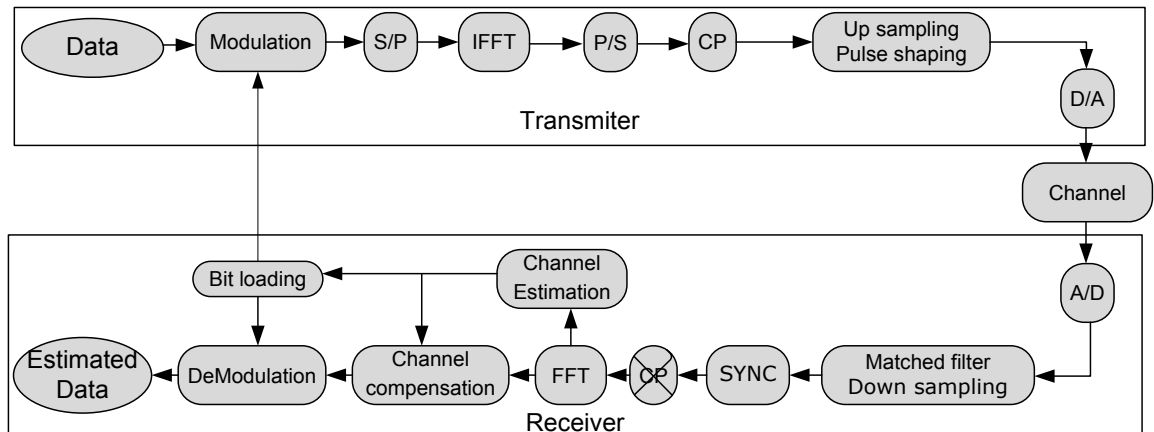


Fig. A.2 OFDM communication system overview

### A.1.2 OFDM Communication System Overview

The OFDM communication system presents two sets of PCs, each connected with a DSP card through the USB cable. A simplex communication system is considered:

One of the PCs with one of the DSP boards work as the transmitter whereas the other set works as the receiver. The receiver estimates the channel on each subcarrier and feeds back channel information to the transmitter through the feedback link.

### A.1.3 OFDM Communication System Model

The system model is divided into transmitter and receiver as shown in Fig. A.2.

### A.1.4 Transmitter

*Modulation* - modulator maps information bits to a set of complex numbers corresponding to a signal constellation. The modulation order depends on the subcarrier. PSK/ QAM symbols are used to modulate the orthogonal carriers where three types of modulation schemes have been used in this block:

- 1- BPSK
- 2- QPSK
- 3- 16-QAM

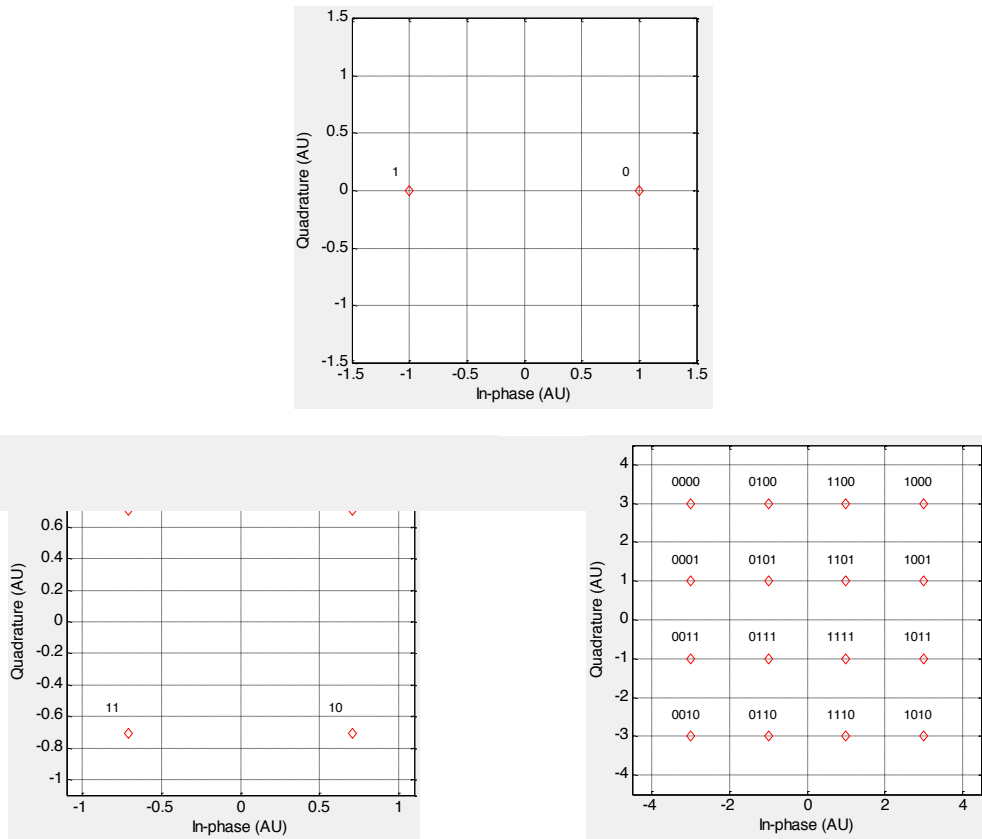


Fig. A.3 Signal Constellations Of The Modulation Schemes BPSK, QPSK and 16QAM.

Grey encoding was implied while making modulation constellation to reduce bit errors. Constellation diagrams of these modulation schemes are shown in Fig. A.3: Modulation and demodulation are done by using simple look-up tables at the transmitter and receiver. The system is made adaptive to maximize the throughput, by adapting different modulation schemes for different subcarriers based on SNR of each sub-channel. The sub-channel with high SNR will be assigned more bits than a sub-channel with low SNR. Modulations implemented here are BPSK, QPSK and 16QAM.

*IFFT* - parallel data are transformed into time-domain using IFFT. The total number of subcarriers translates into the number of points of the IFFT/FFT. A mirror operation is performed before IFFT in order to get real symbols as output.

*Cyclic Prefix (CP)* - To preserve the orthogonality property over the duration of the useful part of signal, a cyclic prefix is then added. Cyclic prefix is just copying the last few samples in OFDM symbols and appending them before the start of symbol as



Fig. A.4 The cyclic prefix

shown in Fig. 2.6. The time duration of cyclic prefix is chosen to be greater than maximum delay spread of the channel to combat inter-symbol interference (ISI). The idea behind this is to convert the channel matrix to a circular matrix so the FFT convert the channel matrix to a diagonal matrix which can be compensated with simple single tap equaliser. Adding the cyclic prefix also makes the receiver less sensitive to timing errors. In the AWGN channel case, the cyclic prefix can also be used for synchronization purpose. However, synchronization based on the cyclic prefix fails completely in multi-path channel.

*D/A* - Converts digital symbols to analogue signals. This operation is done using the AIC codec inside the DSP.

#### A.1.5 Receiver

*A/D* - Convert received analogue signals to digital symbols for processing.

*Synchronization* - Digital communication system including OFDM requires a reliable synchronization at the receiver due to the clock difference between transmitter and receiver.

*Remove cyclic prefix* - This block simply removes the cyclic prefix added in the transmitter.

*Symmetrical FFT* - Data are transformed back to frequency-domain using FFT. Then the complex conjugate mirror added in the transmitter is removed.

*Channel estimation* - The estimation is achieved by pilot frames.

*Channel compensation* - The channel estimation is used to compensate for channel distortion.

*Bit loading* - The receiver computes the bit allocation and send it to the transmitter. It is implemented using the spectrum information of both the channel and

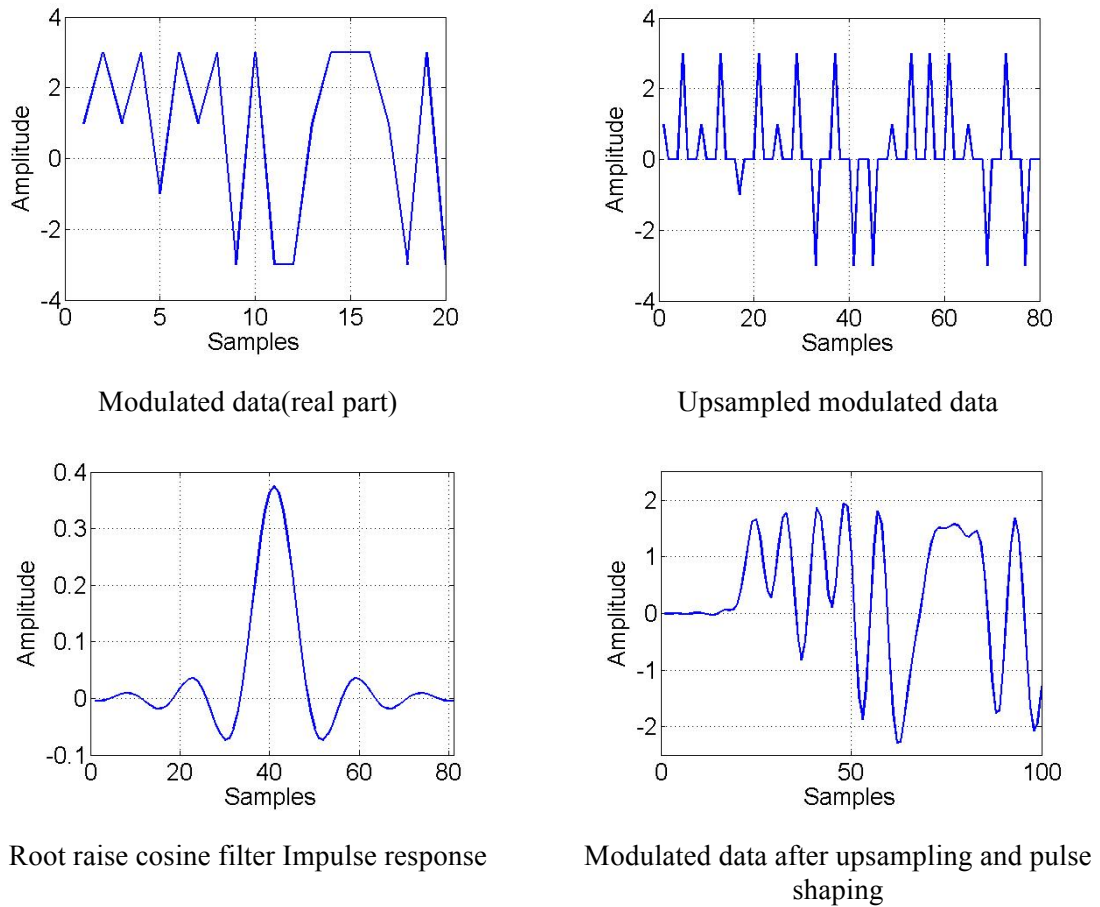


Fig. A.5 Upsampling and pulse shaping.

noise power. The choice of number of allocated bits is only limited to 1 (BPSK), 2 QPSK and 4 (16QAM).

*Demodulation* - Symbols are transformed back to bits. The inverse of the estimated channel response is used to compensate the channel gain. Demodulation scheme is based on information of bits allocation.

#### A.1.6 Pulse Shaping and Matched Filter

In common communication system, pulse shaping and matched filter are implemented for two reasons. Firstly, the system can choose a pulse shape and matched filter to change the spectrum of transmitted signal for fitting into the frequency response of channel more properly as shown in Fig. A.5.

In another words, we can consider that pulse shaping can change properties of the channel so that transmission can perform better. For example, in a band-pass channel, we can apply a root raise cosine pulse shape and root raise matched filter which satisfies Nyquist Criterion, then channel can be regarded as an all pass channel. The other reason is that, pulse shaping and matched filter can be used to increase signal to noise ratio (SNR), which is the property of matched filter.

#### *A.1.7 Synchronization*

OFDM system Synchronization is the most crucial part of the system design. OFDM symbol duration is much longer and there is also a cyclic prefix, which makes the OFDM scheme less sensitive to timing errors as compared to single carrier system where timing errors cause inter-symbol interference (ISI). However, OFDM is more sensitive to frequency errors. Synchronization usually consists of two parts:

1- Frame detection

Frame detection is used to determine roughly the beginning of the pilot sequence.

2- Time offset estimation correction

Due to the small sampling clock difference between the transmitter and receiver, each signal sample is off from its correct sampling time by a small amount which is linearly increasing with the proceeding samples. Frame synchronization has to be done for every frame in wireless systems due to rapid channel variations. In this project synchronization is done periodically every 10 frames as the system channel response is almost stable.

#### *Frame detection*

Since data is transmitted in time domain for OFDM system, the name time synchronization is used. Two methods are available for this kind of synchronization, using cyclic prefix or training sequence (which is also called pilot in OFDM system). Using the cyclic prefix is less efficient due to channel delay and ISI.

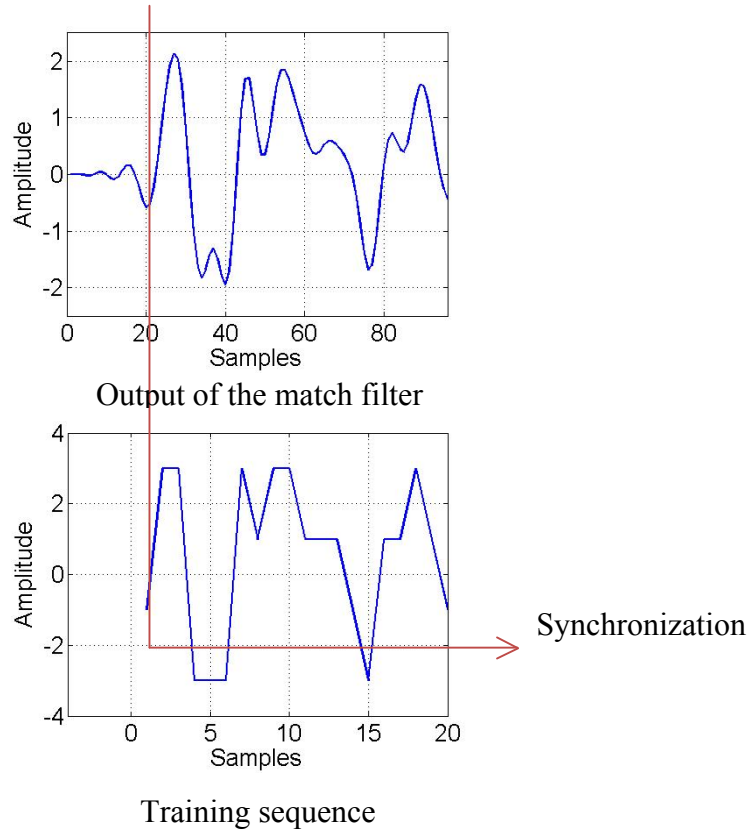


Fig. A.6 Synchronization using correlation between the training sequence and the matched filter output.

Frame synchronization in this project was done using training sequence by taking two same OFDM symbols, namely training sequences to do cross-correlation, just as what is done by 802.11, as shown in Fig. A.6 Maximum Likelihood estimation is applied to estimate the start of the frame. Assume that an interval  $T$  consecutive samples of OFDM signal  $r(k)$  is observed, and these samples contain one entire OFDM symbol. The delay  $\alpha$  is obtained by the Maximum Likelihood estimation as:

$$\hat{\alpha} = \arg \max_{\alpha} \{|\gamma(\alpha)| - \rho\varepsilon(\alpha)\} \quad (\text{A.1})$$

$$\gamma(N) = \frac{1}{2} \sum_{k=N}^{N+L-1} \gamma(k) \gamma^*(k + N) \quad (\text{A.2})$$

$$\rho = \frac{\sigma_s^2}{2} \sum_{k=N}^{N+L-1} \gamma(k) \gamma^*(k + N) \quad (\text{A.3})$$

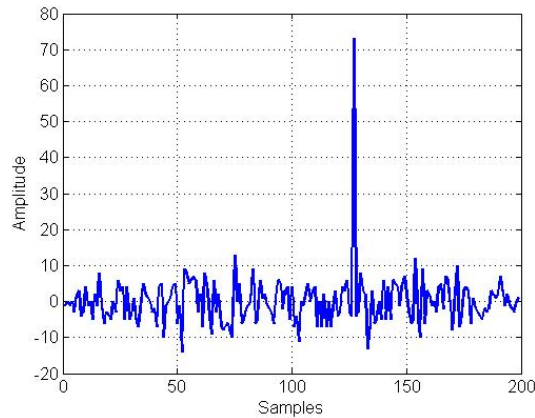


Fig. A.7 The training sequence correlation output.

The correlation properties of the training sequence are important as they affect the estimation accuracy. Ideally, the autocorrelation function for the pilot frame should equal a delta pulse, i.e., zero correlation everywhere except at lag zero. Therefore, the pilots frame should be carefully designed. It is always generated using pseudorandom sequence generators due to its autocorrelation function properties.

An example of what the correlation look like is shown in Fig. A.7 and the maximum of the correlation indicates the beginning of the training frame.

#### *Time offset estimation correction*

Due to a slight difference between the transmitter and the receiver clock frequencies, the system experiences a frequency offset. This phenomenon makes the angles of points in the constellation to change linearly overtime as shown in Fig. A.8. If the variation is too fast, the demodulation becomes unreliable. Then, for large files, we have to compensate the frequency offset. This is done with the channel estimation and compensation.

The frequency response of channel has to be estimated to compensate the channel effect on each subcarrier. The system can benefit from the full knowledge of the channel response and the noise variance as the transmitter and the receiver can determine the subcarrier gain, so that the adaptive bit loading algorithm can proceed to calculate the optimal bit and energy allocation. Since the channel transfer function is not

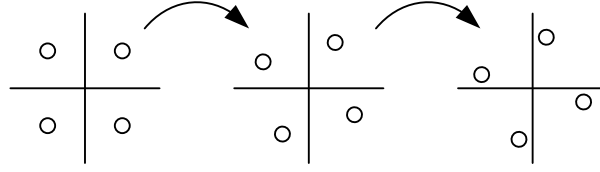


Fig. A.8 The Constellation points angles changes with time.

changing very rapidly, block type channel estimation has been developed, in which the pilot tones are inserted into all of the subcarriers of OFDM symbols

The pilots are inserted to all subcarriers with a specific period and extracted after DFT block. The estimated channel  $\hat{\mathbf{H}}(n)$  is then obtained in channel estimation block. The received signal can be presented as:

$$\mathbf{Y}(n) = \mathbf{X}(n)\mathbf{H}(n) + \mathbf{E}(n) \quad \dots \dots \quad n = 1, 2, \dots, N \quad (\text{A.4})$$

where  $\mathbf{E}(n)$  is zero mean noise. The method we used to implement the channel estimation is based on the forgetting factor technique:

$$\hat{\mathbf{H}}(n) = \frac{\theta(L, n)}{\beta(L, n)} \quad (\text{A.5})$$

$$\theta(L, n) = \gamma \mathbf{X}_p(n, L) \mathbf{Y}_p(n, L) + (1 - \gamma) \theta(n, L - 1) \quad (\text{A.6})$$

$$\beta(L, n) = \gamma \mathbf{X}_p(n, L) \mathbf{X}_p(n, L) + (1 - \gamma) \beta(n, L - 1) \quad (\text{A.7})$$

where  $\mathbf{X}_p(n, L)$  is the transmitted pilot,  $\mathbf{Y}_p(n, L)$  is the received pilot,  $\gamma$  is the forgetting factor,  $L$  is the index of the current pilot frame and  $n$  is the sub-channel index. The forgetting factor will be chosen according to the channel variation speed.

The channel response at the subcarrier estimated from the pilots is then used to find the estimated transmitted signal  $\hat{\mathbf{X}}(n)$ .

$$\hat{\mathbf{X}}(n) = \frac{\mathbf{Y}(n)}{\hat{\mathbf{H}}(n)} \quad (\text{A.8})$$

the empty-pilots used to estimate the channel noise spectrum.

$$\mathbf{E}_e(n) = \mathbf{Y}_0(n) - \hat{\mathbf{H}}(n) \mathbf{X}_0(n) \quad (\text{A.9})$$

here  $\mathbf{X}_0(n) = 0$ , so the variance of  $N$  samples of noise is then calculated as:

$$\sigma_N^2 = \frac{1}{N} \sum_{n=0}^{N-1} \mathbf{Y}_0(n)^2 \quad (\text{A.10})$$

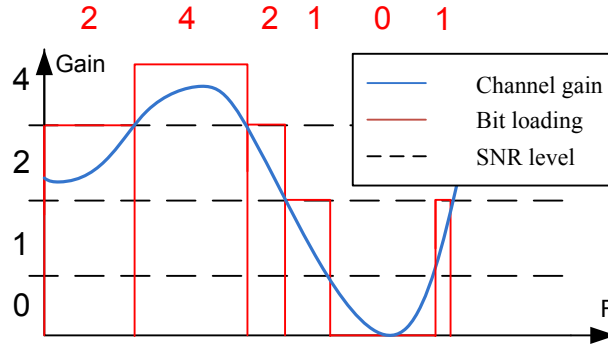


Fig. A.9 The Adaptive bit loading.

#### A.1.8 Adaptive Bit Loading

Power and rate optimization in OFDM system can be achieved efficiently using the adaptive bit loading algorithm based on the knowledge of the sub-channel gains. Sub-channel with higher SNR can deal with more bits (higher modulation order) and energy and vice versa.

Loading algorithms can be divided to two types:

- 1- Maximize data rate at a given fixed performance.
- 2- Maximize performance at a given fixed data rate.

The adaptive technique employed in this system is Rate-Adaptive (RA) which maximizes the number of bits per symbol subject to a fixed energy.

$$\max_{E_n} \mathbf{b}_n = \sum_{n=1}^N \log_2 \left( 1 + \frac{E_n \cdot g_n}{\Gamma} \right) \quad (\text{A.11})$$

Considering that:

$$N \cdot E_x = N \cdot E_n \quad (\text{A.12})$$

where  $b_n$  and  $E_n$  are the bit allocation and the energy for the  $n^{\text{th}}$  sub-channel.  $E_x$  is the average energy per sub-channel.  $\Gamma$  is the gap (parameter of the algorithm). To initialize the bit allocation, the procedure is summarized as follows:

- Compute the sub-channel signal to noise ratios  $g_n$ .
- Sort the sub-channel SNRs to be from largest to smallest. Compute the number of usable sub-channels as

$$N_{use} = N - \text{number of zerogain subchannels} \quad (\text{A.13})$$

Obtain the constant  $K$  and the energy in the worst sub-channel based on the formula:

$$K = \frac{1}{N_{use}} \left( N \cdot E_x + \Gamma \cdot \sum_{n=1}^N \frac{1}{g_n} \right) \quad (\text{A.14})$$

$$E_{n_{min}} = K - \frac{\Gamma}{g_{N_{use}}} \quad (\text{A.15})$$

Solve while  $E_{n_{min}}$  is negative with  $N_{use} \rightarrow N_{use} - 1$  and corresponding  $g_n$  term eliminated.

Determine the bits and energy on usable sub-channels using the formula:

$$E_i = K - \frac{\Gamma}{g_i} \quad i = 0, 1, \dots, N_{use} \quad (\text{A.16})$$

$$b(i) = \frac{1}{2} \cdot \log_2 \left( K \cdot \frac{g_i}{\Gamma} \right) \quad i = 0, 1, \dots, N_{use} \quad (\text{A.17})$$

Return values of bits and energy allocation to original index of unsorted sub-channels and assign 0 bit to zero-gain and eliminated sub-channels. Restrict  $b(i)$  to take value 0, 1, 2, 4 (this corresponds to available modulation orders).

One of the advantages of OFDM is that each sub-channel is relatively narrowband and has flat fading. Although, due to the channel characteristics some sub-channels will face very low gain which result in high BER. Systems which don't use bit loading have to adapt low modulation schemes to keep a relatively low BER, but also low bit rate. Thus, OFDM have to take advantage of high gain sub-channels and adapt it with relatively high modulation schemes to improve the system bit rate. This is the motivation of bit loading and adaptive modulation. The bits and energy allocation is a function of channel property and noise PSD. Therefore, a new adaptation must be implemented each time the channel varies.

## A.2 DSP Implementation

### A.2.1 Overview of the Board

The TI C6713 DSK (DSP Starter Kit) with an approximate size of 5 x 8 in. was equipped with a 225 MHz TMS320C6713 Floating Point DSP and has 265Kbytes of

internal memory. A daughter card expansion is also provided on the DSK board. Two 80-pin connectors provide for external peripheral and external memory interfaces. On board peripherals include two multi-channel buffered serial ports (McBSPs) and an enhanced DMA controller (EDMA). It also has 16 Mbytes of on board SDRAM. With its significant amount of internal memory the whole program was loaded within it, without using any of the SDRAM. The SDRAM was used exclusively for the data to be transmitted. A 32-bit stereo codec TLV320AIC23 (AIC23) for input and output for signal transmission and audio processing uses a sigma–delta technology that provides ADC and DAC. It connects to a 12-MHz system clock. Variable sampling rates from 8 to 96 kHz can be set readily. Codec stands for coder/decoder, the job of the AIC23 is to code analogue input samples into a digital format for the DSP to process, and then decode data coming out of the DSP to generate the processed analogue output. Digital data is sent to and from the codec on McBSP1. both channels of the codec were used for the transmission and feedback. The signal is sampled as 16-bit elements at a rate of 96 kHz and 48 kHz. To speed up the task of copying data between the CPU and audio codec, the EDMA (Enhanced Direct Memory Access) is used to copy one frame between the codec and memory and interrupt the DSP.

The DSK has 4 light emitting diodes (LEDs) and 4 DIP switches that allow users to interact with programs through simple LED displays and user input on the switches.

The 6713 DSK includes a special device called a JTAG emulator on-board that can directly access the register and memory state of the 6713 chip through a standardized JTAG interface port. When a user wants to monitor the progress of his program, Code Composer (the development environment) sends commands to the emulator through its USB host interface to check on any data the user is interested in. We also use this interface together with the GUI to download the file from the host computer to the DSP board for transmission.

The programming was implemented in C and care had to be taken to define precise memory allocation. Fortunately, Code composer Studio compiler does a lot of code optimization.

### A.2.2 Data Transfer

Audio signals are transferred back and forth from the codec via McBSP2, a bi-directional serial port. The EDMA is configured to take every 16-bit signed audio sample arriving on McBSP1 and store it in a buffer in memory to be processed by the DSP. At the same time the EDMA is used to transfer data from memory to the McBSP1 to be sampled and transmitted. The codec is configured and controlled via the McBSP0, a second serial port. The commands are used to configure parameters on the codec (sample rate, gain, audio path).

### A.2.3 Ping Pong Buffering with Linked EDMA transfers

Ping-Pong buffer is used to obtain a better utilization of CPU resource during I/O operations by overlapping the CPU and I/O processing. The timing becomes very tricky when single buffer is used for data transmission between the CODEC, since all the processing must be finished between the instant the current buffer fills up and the next samples arrive. Applying the Ping-Pong buffering technique frees DSP programmers from the real-time scheduling considerations and constrains. The basic idea is to use two logical buffers, namely, Ping and Pong for data transfer on each side instead of a single buffer. The EDMA is configured to fill one buffer, for example the Ping buffer first, then the Pong buffer. In the interval that the Ping buffer is being filled, the DSP is free to process the Pong buffer with the knowledge that the current EDMA transfer won't overwrite it. When the Ping buffer fills up, the configuration is reversed and the role of Ping/Pong buffer is reversed. This Ping-Pong data transfer continues with one buffer always hosting the active data transfer and one remaining stable for the DSP operation. The whole process is illustrated in Fig. A.10:

Separate input and output buffers are used to decouple the receive side from the transmit side while data is being processed. So there are a total of four logical buffers:

- 1- Transmit PING Buffer: gBufferXmtPING
- 2- Transmit PONG Buffer: gBufferXmtPONG
- 3- Receive PING Buffer: gBufferRcvPING
- 4- Receive PONG Buffer: gBufferRcvPONG

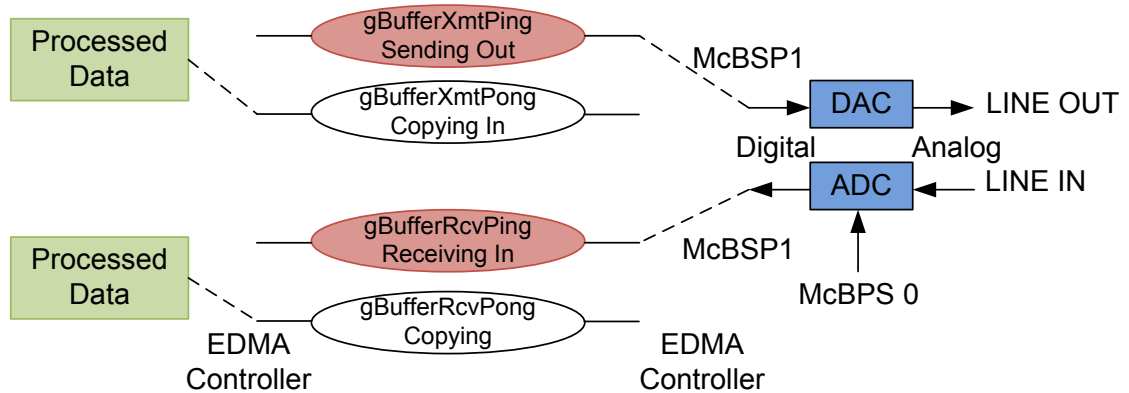


Fig. A.10 PING/PONG Buffering.

For the sake of simplicity, we process the incoming data on a symbol basis which means in every iteration, a bit sequence corresponding to one OFDM symbol is processed and transmitted. In other words, the size of the Ping/Pong buffer is set to be equal to the length of one OFDM symbol.

#### A.2.4 Implementation Issues

##### *Synchronization*

Synchronization done in two steps the 1<sup>st</sup> one in the beginning of the transmission using a sine wave signal which is correlated with its copy in the receiver, the receiver holds the value and the index of the maximum correlation and compares it with a certain threshold. If the value is higher than the threshold then there is a synch and the index is used, if not the frame considered as an empty frame and noise estimation is done. Training sequence start after the sine directly

##### *Assembling frame*

On the receiver side, it's not possible to make the cards work completely synchronously so the frame can start at any point in the buffer. After defining the start of the frame it is saved in temporary buffer and when the next buffer is filled the frame can be completed and processed.

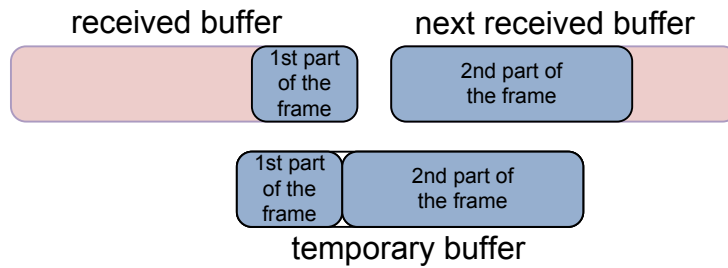


Fig. A.11 Buffer handling at the receiver

### *Memory considerations*

The memory usage in the board is limited especially with many function used to define the OFDM process only very small arrays were possible to declare in the functions. No dynamic memory allocation worked either. The solution was to declare large buffers globally in the beginning and then reuse them. Especially the modulation and demodulation functions caused problems because of the allocation table usage.

### A.2.5 Transmitter Implementation

The functionality of transmitter is defined in Fig. A.12:

- 1- The host load DSP program on transmitter side and download all the data need to be transmitted to the SDRAM of DSP board through the RTDX link.
- 2- DSP initializes all configuration registers of EDMA and Codec.
- 3- A package contains only training sequence is sent to estimate the channel (with a sine wave in the beginning).
- 4- Receiver waits for receiving feedback information of bit allocation to each subcarrier (with a sine wave in the beginning).
- 5- Based on bits allocation information, right amount of data is extracted from original data sequence.
- 6- Extracted data sequence is modulated using bit allocation information and packed before sent to the codec to be transmitted.
- 7- Every 20 frame transmission, the program is automatically set to estimate channel and repeat the steps above again.
- 8- After all data are sent out, the program exists.

#### A.2.6 Receiver Implementation

The functionality of receiver is defined in Fig. A.12.

- 1- The host load DSP program on receiver side.
- 2- DSP initializes all configuration registers of EDMA and Codec.
- 3- System idle. Energy detection.
- 4- Receive two buffers of training sequences.
- 5- Use empty frame to estimate the noise variance in the channel and together with channel estimation got from training sequences, bits allocation information is calculated, sorted and transferred to binary representation.
- 6- BPSK modulation is performed to bits allocation information send out to the transmitter.
- 7- Down sampling and synchronization to find the start point of training sequences.
- 8- Remove cyclic prefix from data frame and do FFT.
- 9- Demodulate based on bits allocation information.
- 10- Every 20 frame, the program is automatically set to estimate channel and repeat the steps above again.
- 11- After all data are received out, the program exists.

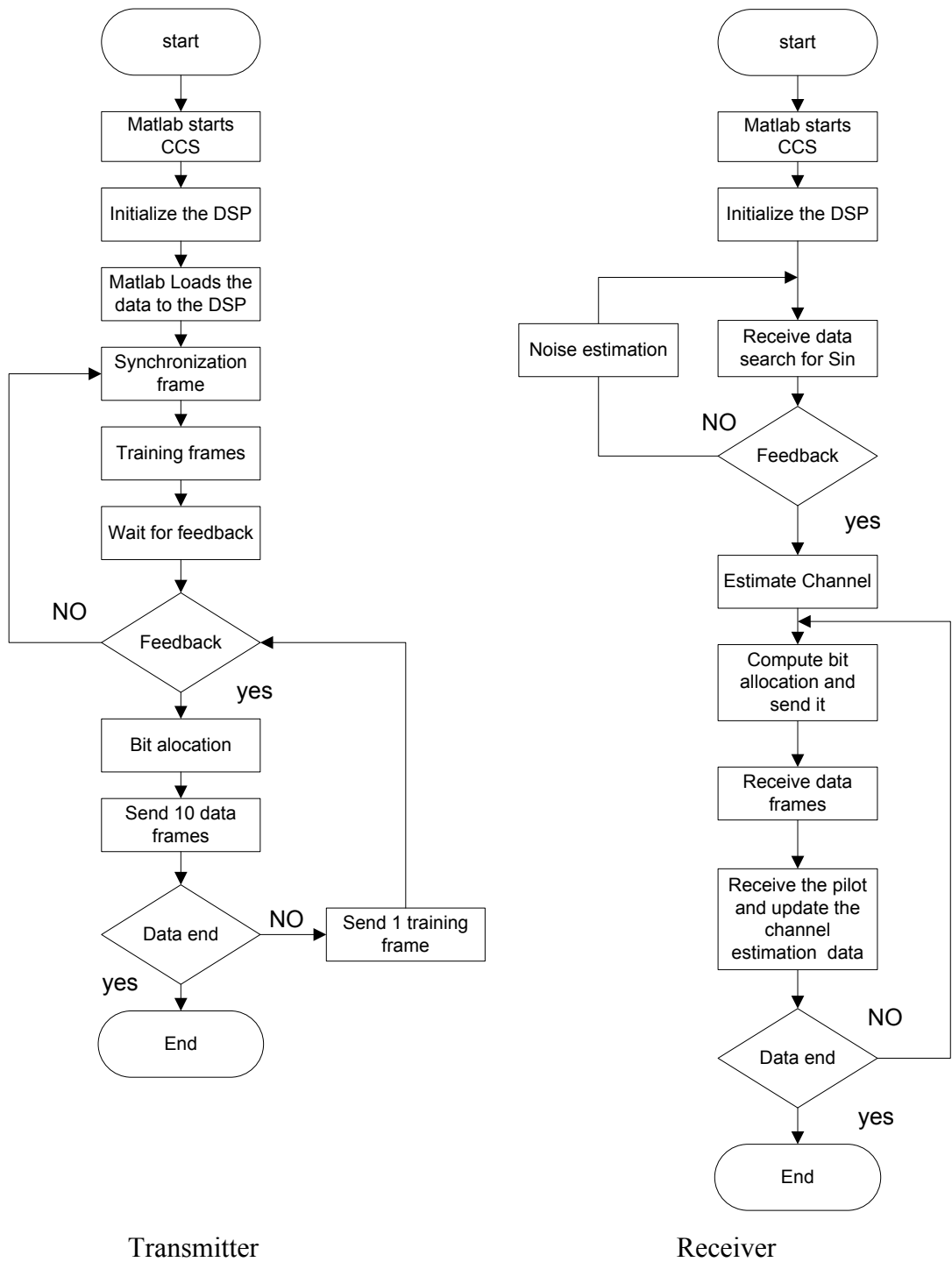


Fig. A.12 Transmitter and Receiver flow chart

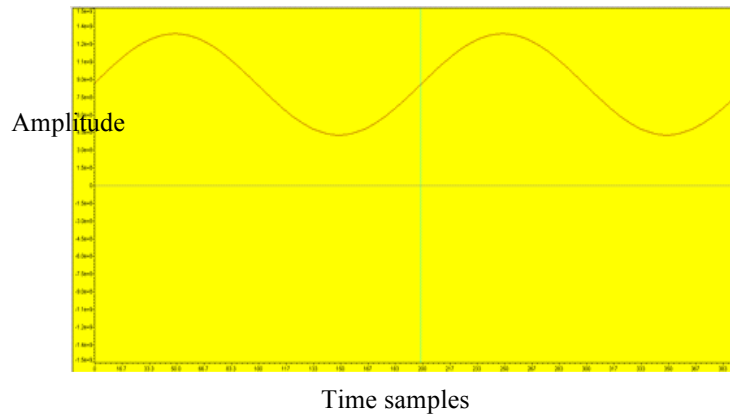


Fig. A.13 Data to send.

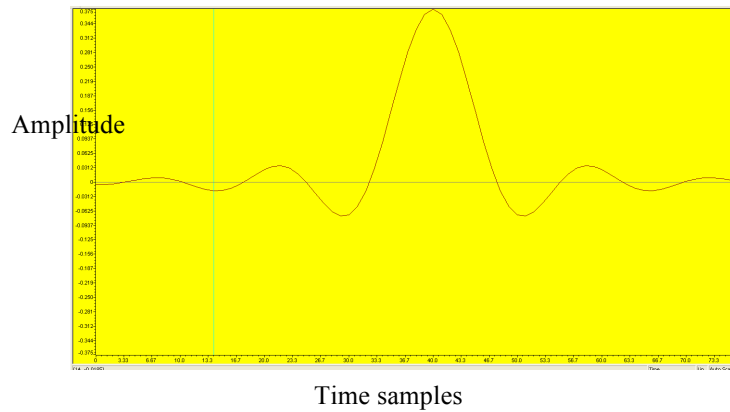


Fig. A.14 The root raise cosine filter Impulse response.

### A.3 System Results

This section discusses the system results which contain the output after each step and how it appears in the real system.

#### A.3.1 Real system outputs

The host program (Matlab) sends the data through the RTDX channel to the DSP Board. DSP start to initialize the transmitter and receiver functions like initialize the root raise cosine filter.

Transmitter sends a synchronization signal to the receiver which is a sine wave.

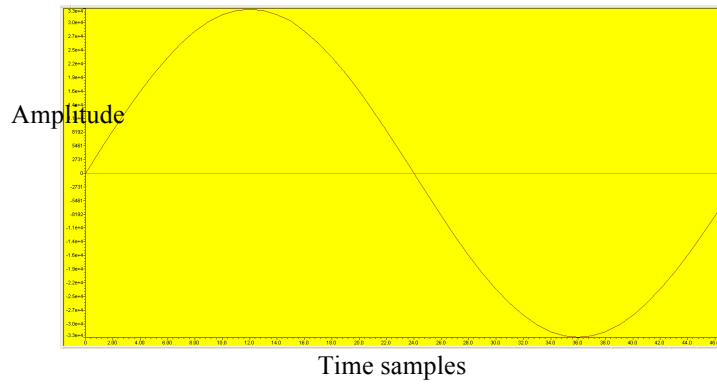


Fig. A.15 The synchronization signal (Sin wave).

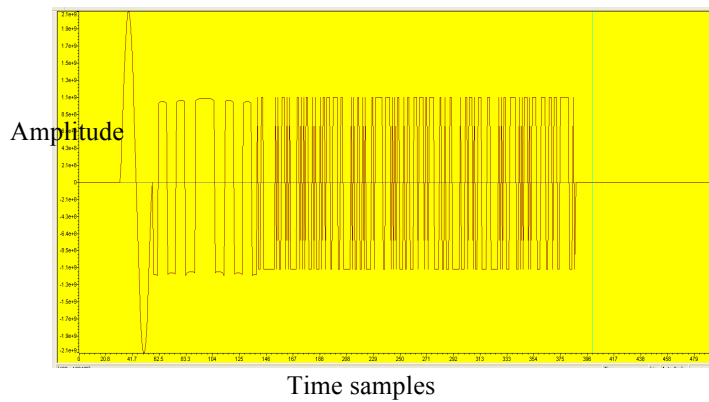


Fig. A.16 The Feedback data with sin for synchronization and the bit allocation.

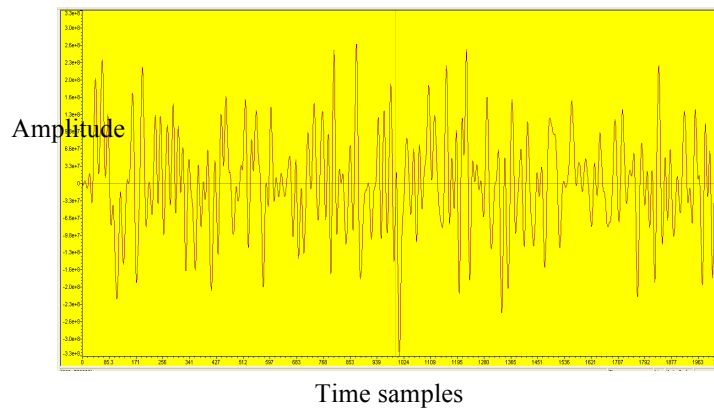


Fig. A.17 Transmitter training sequence.

The receiver starts to calculate the bit allocation depending on the channel estimation after synchronization then transmitting the bit allocation with a

synchronization sin wave through the feedback link. Transmitter sends training sequence to the receiver. After 10 training frames, transmitter send data frames.

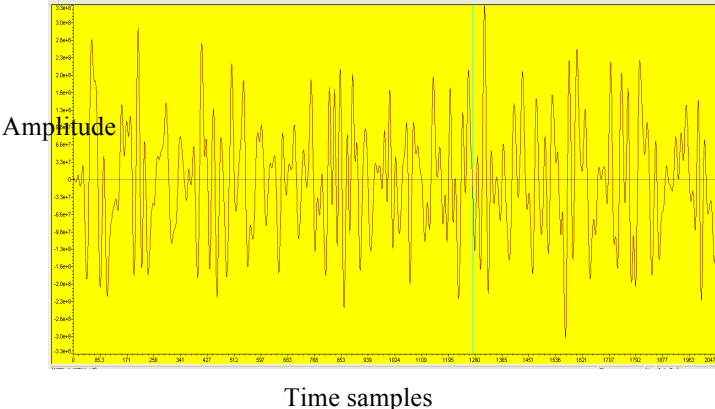


Fig. A.18 1<sup>st</sup> data frame from the transmitter.

Finally the received data collected at the receiver

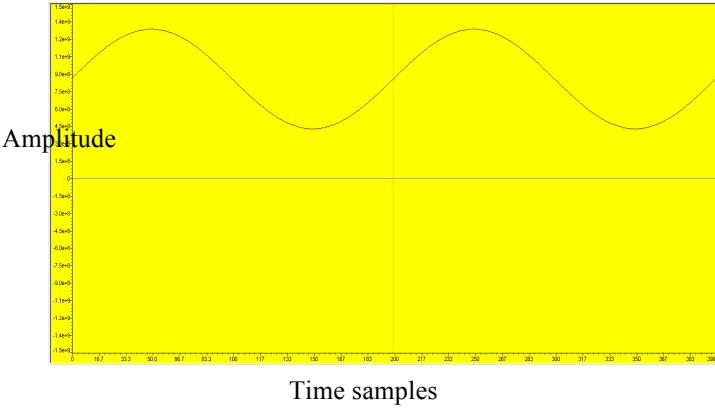


Fig. A.19 Received data.

## **A.4 Conclusion and Future Work**

This section contains brief conclusion and a list of suggested future work.

### *A.4.1 Conclusion*

The key building blocks of an OFDM Modem has been designed and implemented. The functionality of the modem is verified with the real system. Using the TI C6713 DSK board was powerful and successful choice.

The OFDM modem leads to better BER performance than conventional systems. Further, the OFDM system with adaptive algorithm outperforms the OFDM systems having fixed modulation, giving higher bit rate. In conclusion, OFDM is a very promising technology, and practical adaptive rate algorithm serves well to improve performance.

### *A.4.2 Future Work*

#### *Increase the bit rate*

The maximum bit rate for our system is equal to 64,32kbits/s when using sampling rates of 96, 48 kHz respectively, which is low for an OFDM system. This is due to some choices in the system design like up-sampling rate, modulation scheme and cyclic prefix. In order to increase this bit rate, the system designer may reduce the upsampling rate or the size of the cyclic prefix and using higher order modulation scheme.

#### *Peak to average ratio*

One major difficulty about OFDM is its large peak-to-average ratio (PAR). This means that the OFDM signal has a large variation between the average signal power and the maximum signal power. The large dynamic range of the OFDM system can lead to some problems when converting from digital to analogue. A power amplifier has both linear and non-linear regions where the non-linear regions occur for large output powers (i.e., near saturation). To reduce the amount of distortion, the symbols need to be as

much as possible in the linear region. In this way, system has to lower the output power, which leads to inefficiency.

Methods to reduce the PAR can be implemented in an OFDM system. They use some constraints on the modulation sequences and seem quite complex.

*Improving the system*

Some blocks of the system can be improved. Some algorithms like synchronization, bit loading and channel estimation can be improved and optimized to obtain better performance and a faster system. Also, an algorithm to track the frequency offset could have been implemented.

# Author's Publications

---

The following lists the author's publications in reverse chronological order.

## List of Published Papers:

- [6] Solyman, A.A.A., S. Weiss, and J.J. Soraghan., *Analysis Of Peak-To-Average Power Ratio Of Orthogonal Chirp Division Multiplexing Multicarrier System Based on The Discrete Fractional Cosine Transform*. in 3rd International Conference on Wireless Communications and Mobile Computing (MIC-WCMC), 2013 Mosharaka International Conferences, Valencia, Spain, 2013.
  
- [5] Solyman, A.A.A., S. Weiss, and J.J. Soraghan., *A Novel Orthogonal Chirp Division Multiplexing (OCDM) Multicarrier Transceiver Based on the Discrete Fractional Cosine Transform*. in 3rd International Conference on Wireless Communications and Mobile Computing (MIC-WCMC), 2013 Mosharaka International Conferences, Valencia, Spain, 2013.
  
- [4] Solyman, A.A.A., S. Weiss, and J.J. Soraghan.. *CHIRP-BASED MULTICARRIER MODULATION*. in *9th IMA International Conference on Mathematics in Signal Processing (IMA), 2012 Birmingham, United kingdom*. on. 2012.
  
- [3] Hussin, M.N., Solyman, A.A.A., S. Weiss, and J.J. Soraghan.. *DFrFT-based EO-STBC multicarrier system for transmission over doubly-dispersive channels*. in *Wireless Communication Systems (ISWCS), 2012 International Symposium Paris, France*, 2012.

- [2] Solyman, A.A.A., S. Weiss, S. Elgamel and J.J. Soraghan. *Hybrid DFrFT and FFT based Multimode Transmission OFDM System*. In the 8th International Conference on Electrical Engineering (*ICEENG*), 2012 Cairo, Egypt.
- [1] Solyman, A.A.A., S. Weiss, and J.J. Soraghan. *Low-complexity LSMR equalisation of DFrFT-based multicarrier systems in doubly dispersive channels*. in *Signal Processing and Information Technology (ISSPIT), 2011 IEEE International Symposium Bilbao, Spain*, 2011.

### **Papers under Review**

- [1] Solyman, A.A.A., S. Weiss, and J.J. Soraghan., *Low Complexity Equalisation for FrFT-Based Multicarrier Transmission over Doubly-Dispersive Channels*. In *IEEE Communications Letters*.

# References

---

- [1] R. Prasad, *Ofdm for Wireless Communications Systems*: Artech House, 2004.
- [2] A. F. Molisch, ed., *wireless communications*: John Wiley & Sons, Ltd, 2005.
- [3] Robert Chang, "Orthogonal frequency division multiplex data transmission system," filed November 14, 1966, issued Jan. 6, 1970.
- [4] B. Saltzberg, "Performance of an Efficient Parallel Data Transmission System," *Communication Technology, IEEE Transactions on*, vol. 15, pp. 805-811, 1967.
- [5] S. Darlington, "On digital single-sideband modulators," *Circuit Theory, IEEE Transactions on*, vol. 17, pp. 409-414, 1970.
- [6] S. Weinstein and P. Ebert, "Data Transmission by Frequency-Division Multiplexing Using the Discrete Fourier Transform," *Communication Technology, IEEE Transactions on*, vol. 19, pp. 628-634, 1971.
- [7] A. Peled and A. Ruiz, "Frequency domain data transmission using reduced computational complexity algorithms," in *Acoustics, Speech, and Signal Processing, IEEE International Conference on ICASSP '80.*, 1980, pp. 964-967.
- [8] L. Cimini, Jr., "Analysis and Simulation of a Digital Mobile Channel Using Orthogonal Frequency Division Multiplexing," *Communications, IEEE Transactions on*, vol. 33, pp. 665-675, 1985.
- [9] E. Lawrey, "Multiuser OFDM," in *Signal Processing and Its Applications, 1999. ISSPA '99. Proceedings of the Fifth International Symposium on*, 1999, pp. 761-764 vol.2.
- [10] M. Alard and R. Lassalle, "Principles of modulation and channel coding for digital broadcasting for mobile receivers,," vol. EBU Technical Review, no. 224, pp. 3-25, , Aug.1987.
- [11] B. Le Floch, *et al.*, "Digital sound broadcasting to mobile receivers," *Consumer Electronics, IEEE Transactions on*, vol. 35, pp. 493-503, 1989.
- [12] Y. Mostofi and D. C. Cox, "ICI mitigation for pilot-aided OFDM mobile systems," *Wireless Communications, IEEE Transactions on*, vol. 4, pp. 765-774, 2005.
- [13] H. Sari, *et al.*, "Transmission techniques for digital terrestrial TV broadcasting," *Communications Magazine, IEEE*, vol. 33, pp. 100-109, 1995.
- [14] U. Reimers, "Digital video broadcasting," *Communications Magazine, IEEE*, vol. 36, pp. 104-110, 1998.
- [15] U. H. Reimers, "DVB-The Family of International Standards for Digital Video Broadcasting," *Proceedings of the IEEE*, vol. 94, pp. 173-182, 2006.
- [16] A. R. Lindsey, "Wavelet packet modulation for orthogonally multiplexed communication," *Signal Processing, IEEE Transactions on*, vol. 45, pp. 1336-1339, 1997.

- [17] C. J. Mtika and R. Nunna, "A wavelet-based multicarrier modulation scheme," in *Circuits and Systems, 1997. Proceedings of the 40th Midwest Symposium on*, 1997, pp. 869-872 vol.2.
- [18] S. Attallah and J. F. M. Nilsson, "Sequences leading to minimum peak-to-average power ratios for DCT-based multicarrier modulation," *Electronics Letters*, vol. 34, pp. 1469-1470, 1998.
- [19] W. Chin-Liang, *et al.*, "Discrete Hartley transform based multicarrier modulation," in *Acoustics, Speech, and Signal Processing, 2000. ICASSP '00. Proceedings. 2000 IEEE International Conference on*, 2000, pp. 2513-2516 vol.5.
- [20] M. Martone, "A multicarrier system based on the fractional Fourier transform for time-frequency-selective channels," *Communications, IEEE Transactions on*, vol. 49, pp. 1011-1020, 2001.
- [21] J. Armstrong, "Analysis of new and existing methods of reducing intercarrier interference due to carrier frequency offset in OFDM," *Communications, IEEE Transactions on*, vol. 47, pp. 365-369, 1999.
- [22] J. Won Gi, *et al.*, "An equalization technique for orthogonal frequency-division multiplexing systems in time-variant multipath channels," *Communications, IEEE Transactions on*, vol. 47, pp. 27-32, 1999.
- [23] P. Schniter, "Low-complexity equalization of OFDM in doubly selective channels," *Signal Processing, IEEE Transactions on*, vol. 52, pp. 1002-1011, 2004.
- [24] M. Hempel, *et al.*, "A Study of Critical Baseline Performance Characteristics for IEEE 802.16e-2005," in *Wireless Communications and Mobile Computing Conference, 2008. IWCMC '08. International*, 2008, pp. 837-842.
- [25] C. L. u. Henrik Schulze, *Theory and Applications of OFDM and CDMA*: John Wiley & Sons Ltd, 2005.
- [26] R. van Nee and R. Prasad, *OFDM for wireless multimedia communications*: Artech House, 2000.
- [27] S. S. R. Ahamed, "Performance analysis of OFDM," *Journal of Theoretical and Applied Information Technology*, vol. 4, pp. 1-6, 2008.
- [28] G. H. G. a. C. F. V. Loan, *Matrix Computations, 3rd ed*: Johns Hopkins Univ, 1996.
- [29] P. Robertson and S. Kaiser, "The effects of Doppler spreads in OFDM(A) mobile radio systems," in *Vehicular Technology Conference, 1999. VTC 1999 - Fall. IEEE VTS 50th*, 1999, pp. 329-333 vol.1.
- [30] L. Rugini and P. Banelli, "Performance analysis of banded equalizers for OFDM systems in time-varying channels," in *Signal Processing Advances in Wireless Communications, 2007. SPAWC 2007. IEEE 8th Workshop on*, 2007, pp. 1-5.
- [31] W. Burchill and C. Leung, "Matched filter bound for OFDM on Rayleigh fading channels," *Electronics Letters*, vol. 31, pp. 1716-1717, 1995.
- [32] T. Pollet, *et al.*, "BER sensitivity of OFDM systems to carrier frequency offset and Wiener phase noise," *Communications, IEEE Transactions on*, vol. 43, pp. 191-193, 1995.

- [33] L. Ye and L. J. Cimini, Jr., "Bounds on the interchannel interference of OFDM in time-varying impairments," *Communications, IEEE Transactions on*, vol. 49, pp. 401-404, 2001.
- [34] w. Li and a. Hu, "Analyze of the interchannel interference of OFDM in time-varying channel," in *Neural Networks and Signal Processing, 2003. Proceedings of the 2003 International Conference on*, 2003, pp. 845-847 Vol.1.
- [35] C. Xiaodong and G. B. Giannakis, "Bounding performance and suppressing intercarrier interference in wireless mobile OFDM," *Communications, IEEE Transactions on*, vol. 51, pp. 2047-2056, 2003.
- [36] W. Tiejun, *et al.*, "Performance degradation of OFDM systems due to Doppler spreading," *Wireless Communications, IEEE Transactions on*, vol. 5, pp. 1422-1432, 2006.
- [37] M. Russell and G. L. Stuber, "Interchannel interference analysis of OFDM in a mobile environment," in *Vehicular Technology Conference, 1995 IEEE 45th*, 1995, pp. 820-824 vol.2.
- [38] B. G. Negash and H. Nikookar, "Wavelet-based multicarrier transmission over multipath wireless channels," *Electronics Letters*, vol. 36, pp. 1787-1788, 2000.
- [39] B. G. Negash and H. Nikookar, "Wavelet based OFDM for wireless channels," in *Vehicular Technology Conference, 2001. VTC 2001 Spring. IEEE VTS 53rd*, 2001, pp. 688-691 vol.1.
- [40] F. u. D. Farrukh, *et al.*, "MMSE equalization for discrete wavelet packet based OFDM," in *Electrical Engineering, 2009. ICEE '09. Third International Conference on*, 2009, pp. 1-4.
- [41] N. Al-Dhahir and M. Hlaing, "A new multicarrier transceiver based on the discrete cosine transform," in *Wireless Communications and Networking Conference, 2005 IEEE*, 2005, pp. 45-50 Vol. 1.
- [42] S. Satish, *et al.*, "A DCT-Based Broadband Multicarrier Transceiver," in *SoutheastCon, 2006. Proceedings of the IEEE*, 2006, pp. 175-180.
- [43] J. Chin-Kuo, *et al.*, "On the DHT-based multicarrier transceiver over multipath fading channel," in *Personal, Indoor and Mobile Radio Communications, 2009 IEEE 20th International Symposium on*, 2009, pp. 1662-1666.
- [44] J. Chin-Kuo, *et al.*, "DHT-Based OFDM System for Passband Transmission Over Frequency-Selective Channel," *Signal Processing Letters, IEEE*, vol. 17, pp. 699-702, 2010.
- [45] C. Enqing, *et al.*, "The OFDM System Based on the Fractional Fourier Transform," in *Innovative Computing, Information and Control, 2006. ICICIC '06. First International Conference on*, 2006, pp. 14-17.
- [46] A. Jamin, *et al.*, "Wavelet packet modulation for wireless communications: Research Articles," *Wirel. Commun. Mob. Comput.*, vol. 5, pp. 123-137, 2005.
- [47] C. Van Bouwel, *et al.*, "Wavelet packet based multicarrier modulation," in *Communications and Vehicular Technology, 2000. SCVT-200. Symposium on*, 2000, pp. 131-138.
- [48] K. Abdullah, *et al.*, "On the DWT- and WPT-OFDM versus FFT-OFDM," in *GCC Conference & Exhibition, 2009 5th IEEE*, 2009, pp. 1-5.

- [49] C. Kok-Wui and J. M. Cioffi, "Discrete wavelet transforms in multi-carrier modulation," in *Global Telecommunications Conference, 1998. GLOBECOM 98. The Bridge to Global Integration. IEEE*, 1998, pp. 2794-2799 vol.5.
- [50] P. Soo-Chang and Y. Min-Hung, "The discrete fractional cosine and sine transforms," *Signal Processing, IEEE Transactions on*, vol. 49, pp. 1198-1207, 2001.
- [51] N. Al-Dhahir, *et al.*, "Optimum DCT-Based Multicarrier Transceivers for Frequency-Selective Channels," *Communications, IEEE Transactions on*, vol. 54, pp. 760-760, 2006.
- [52] R. Saxena and K. Singh, "Fractional Fourier transform: A novel tool for signal processing," *Journal of Indian Institute of Science*, vol. 58, pp. 11-26 February 2005 2005.
- [53] V. NAMIAS, "The Fractional Order Fourier Transform and its Application to Quantum Mechanics," *IMA Journal of Applied Mathematics*, vol. 25, pp. 241-265, March 1, 1980 1980.
- [54] L. B. Almeida, "The fractional Fourier transform and time-frequency representations," *Signal Processing, IEEE Transactions on*, vol. 42, pp. 3084-3091, 1994.
- [55] H. M. Ozaktas and D. Mendlovic, "Fourier transforms of fractional order and their optical interpretation," *Optics Communications*, vol. 101, pp. 163-169, 1993.
- [56] D. Mendlovic and H. M. Ozaktas, "Fractional Fourier transforms and their optical implementation: I," *J. Opt. Soc. Am. A*, vol. 10, pp. 1875-1881, 1993.
- [57] D. Mendlovic, *et al.*, "Signal spatial-filtering using the localized fractional Fourier transform," *Optics Communications*, vol. 126, pp. 14-18, 1996.
- [58] H. M. Ozaktas, *et al.*, *The Fractional Fourier Transform: with Applications in Optics and Signal Processing*: John Wiley & Sons Ltd, January 2001.
- [59] A. Bultheel and H. Martinez Sulbaran, "A shattered survey of the fractional Fourier transform, <http://www.cs.kuleuven.be/~nalag/papers/ade/frft/index.html>," 2003.
- [60] A. Bultheel and H. E. Sulbaran, "Computation of the Fractional Fourier Transform," *Applied and Computational Harmonic Analysis*, vol. 16, pp. 182-202, February 2004.
- [61] D. S. Yeung, *et al.*, "Complete way to fractionalize Fourier transform," *Optics Communications*, vol. 230, pp. 55-57, 2004.
- [62] E. Leith, "Review of 'Systems and Transforms With Applications to Optics' " *Information Theory, IEEE Transactions on*, vol. 18, pp. 451-452, 1972.
- [63] T. Ran, *et al.*, "Image Encryption With Multiorders of Fractional Fourier Transforms," *Information Forensics and Security, IEEE Transactions on*, vol. 5, pp. 734-738, 2010.
- [64] Z. Nanrun and D. Taiji, "Optical Image Encryption Scheme Based on Multiple-parameter Random Fractional Fourier Transform," in *Electronic Commerce and Security, 2009. ISECS '09. Second International Symposium on*, 2009, pp. 48-51.

- [65] C. Vijaya and J. S. Bhat, "Signal compression using discrete fractional Fourier transform and set partitioning in hierarchical tree," *Signal Processing*, vol. 86, pp. 1976-1983, 2006.
- [66] S. Shankar and N. Srivastav, "Power Play: On the Notion of Fractional Quantum Fourier Transform," *Potentials, IEEE*, vol. 30, pp. 29-32, 2011.
- [67] B. Santhanam and M. Hayat, "On a pseudo-subspace framework for discrete Fractional Fourier transform based chirp parameter estimation," in *Digital Signal Processing Workshop and IEEE Signal Processing Education Workshop (DSP/SPE), 2011 IEEE*, 2011, pp. 360-363.
- [68] R. Shi, *et al.*, "A Novel SAR Signal Reconstruction Method from Non-uniform Sampling Associated with Fractional Fourier Transform," in *Measuring Technology and Mechatronics Automation (ICMTMA), 2011 Third International Conference on*, 2011, pp. 210-213.
- [69] G. Jianjun and S. Fulin, "A new cross-range scaling algorithm based on FrFT," in *Signal Processing (ICSP), 2010 IEEE 10th International Conference on*, 2010, pp. 2043-2046.
- [70] C. Xiaolong and G. Jian, "A fast FRFT based detection algorithm of multiple moving targets in sea clutter," in *Radar Conference, 2010 IEEE*, 2010, pp. 402-406.
- [71] C. Candan, *et al.*, "The discrete fractional Fourier transform," *Signal Processing, IEEE Transactions on*, vol. 48, pp. 1329-1337, 2000.
- [72] H. M. Ozaktas, *et al.*, "Digital computation of the fractional Fourier transform," *Signal Processing, IEEE Transactions on*, vol. 44, pp. 2141-2150, 1996.
- [73] P. Robertson and S. Kaiser, "Analysis of the loss of orthogonality through Doppler spread in OFDM systems," in *Global Telecommunications Conference, 1999. GLOBECOM '99*, 1999, pp. 701-706 vol. 1b.
- [74] C. Enqing, *et al.*, "Multi-tap equalization algorithm for the OFDM system based on the fractional Fourier transform," in *Communications and Networking in China, 2009. ChinaCOM 2009. Fourth International Conference on*, 2009, pp. 1-4.
- [75] R. O'Neill and L. B. Lopes, "Envelope variations and spectral splatter in clipped multicarrier signals," in *Personal, Indoor and Mobile Radio Communications, 1995. PIMRC'95. 'Wireless: Merging onto the Information Superhighway'. Sixth IEEE International Symposium on*, 1995, pp. 71-75 vol.1.
- [76] L. Xiaodong and L. J. Cimini, Jr., "Effects of clipping and filtering on the performance of OFDM," *Communications Letters, IEEE*, vol. 2, pp. 131-133, 1998.
- [77] V. Tarokh and H. Jafarkhani, "On the computation and reduction of the peak-to-average power ratio in multicarrier communications," *Communications, IEEE Transactions on*, vol. 48, pp. 37-44, 2000.
- [78] J. A. Davis and J. Jedwab, "Peak-to-mean power control in OFDM, Golay complementary sequences, and Reed-Muller codes," *Information Theory, IEEE Transactions on*, vol. 45, pp. 2397-2417, 1999.
- [79] A. E. Jones and T. A. Wilkinson, "Combined coding for error control and increased robustness to system nonlinearities in OFDM," in *Vehicular*

- Technology Conference, 1996. 'Mobile Technology for the Human Race', IEEE 46th, 1996, pp. 904-908 vol.2.*
- [80] S. H. Muller and J. B. Huber, "A novel peak power reduction scheme for OFDM," in *Personal, Indoor and Mobile Radio Communications, 1997. 'Waves of the Year 2000'. PIMRC '97., The 8th IEEE International Symposium on, 1997*, pp. 1090-1094 vol.3.
- [81] R. W. Bauml, *et al.*, "Reducing the peak-to-average power ratio of multicarrier modulation by selected mapping," *Electronics Letters*, vol. 32, pp. 2056-2057, 1996.
- [82] S. Das and P. Schniter, "Max-SINR ISI/ICI-Shaping Multicarrier Communication Over the Doubly Dispersive Channel," *Signal Processing, IEEE Transactions on*, vol. 55, pp. 5782-5795, 2007.
- [83] A. Solyman and J. J. S. S. Wise, "Low-Complexity LSMR Equalisation of FrFT-Based Multicarrier Systems in Doubly Dispersive Channels," presented at the ISSPIT 2011, Bilbao, Spain, 2011.
- [84] G. Taubock, *et al.*, "LSQR-based ICI equalization for multicarrier communications in strongly dispersive and highly mobile environments," in *Signal Processing Advances in Wireless Communications, 2007. SPAWC 2007. IEEE 8th Workshop on, 2007*, pp. 1-5.
- [85] P. B. Luca Rugini, and Geert Leus "Low-Complexity Banded Equalizers for OFDM Systems in Doppler Spread Channels," *EURASIP Journal on Applied Signal Processing*, vol. vol. 2006, Article ID 67404,, p. 13, 2006.
- [86] L. Rugini, *et al.*, "Simple equalization of time-varying channels for OFDM," *Communications Letters, IEEE*, vol. 9, pp. 619-621, 2005.
- [87] G. Liu, *et al.*, "Low-Complexity Iterative Equalization for Symbol-Reconstruction-Based OFDM Receivers Over Doubly Selective Channels," *Broadcasting, IEEE Transactions on*, vol. 58, pp. 390-400, 2012.
- [88] L. Guanghui, *et al.*, "Simple equalization of OFDM signal over doubly selective channels," in *Intelligent Signal Processing and Communication Systems (ISPACS), 2010 International Symposium on, 2010*, pp. 1-4.
- [89] A. Buttar, *et al.*, "FFT And OFDM Receiver ICS For DVB-T Decoders," in *Consumer Electronics, 1997. Digest of Technical Papers. ICCE., International Conference on, 1997*, pp. 102-103.
- [90] U. Reimers, "DVB-T: the COFDM-based system for terrestrial television," in *Broadcasting Convention, International (Conf. Publ. No. 428), 1996*, pp. 120-126.
- [91] R. Schafer, "Terrestrial transmission of DTVB signals-the European specification," in *Broadcasting Convention, 1995. IBC 95., International, 1995*, pp. 79-84.
- [92] B. Sklar. (2001). *Digital Communications Fundamentals and applications (2nd Edition ed.)*.
- [93] M. K. Simon and M.-S. Alouini, *Digital communication over fading channels* vol. 86: Wiley-IEEE Press, 2004.

- [94] C. J. William and C. C. Donald, *Microwave Mobile Communications*: Wiley-IEEE Press, 1994.
- [95] P. Dent, *et al.*, "Jakes fading model revisited," *Electronics Letters*, vol. 29, pp. 1162-1163, 1993.
- [96] RAPPAPORT, *Wireless Communication Systems*, 1996.
- [97] Z. Jing and W. Zulin, "ICI Analysis for FRFT-OFDM Systems to Frequency Offset in Time-Frequency Selective Fading Channels," *Communications Letters, IEEE*, vol. 14, pp. 888-890, 2010.
- [98] C. Yang-Seok, *et al.*, "On channel estimation and detection for multicarrier signals in fast and selective Rayleigh fading channels," *Communications, IEEE Transactions on*, vol. 49, pp. 1375-1387, 2001.
- [99] S. Ahmed, *et al.*, "Low Complexity Iterative Method of Equalization for OFDM in Doubly Selective Channels," in *Signals, Systems and Computers, 2005. Conference Record of the Thirty-Ninth Asilomar Conference on*, 2005, pp. 687-691.
- [100] T. Hrycak and G. Matz, "Low-Complexity Time-Domain ICI Equalization for OFDM Communications Over Rapidly Varying Channels," in *Signals, Systems and Computers, 2006. ACSSC '06. Fortieth Asilomar Conference on*, 2006, pp. 1767-1771.
- [101] R. Kumar and S. Malarvizhi, "Time-Domain Equalization Technique for Intercarrier Interference Suppression in OFDM Systems," in *Advanced Computing and Communications, 2007. ADCOM 2007. International Conference on*, 2007, pp. 391-396.
- [102] H. Dogan, *et al.*, "Low-complexity joint data detection and channel equalisation for highly mobile orthogonal frequency division multiplexing systems," *Communications, IET*, vol. 4, pp. 1000-1011, 2010.
- [103] A. A. A. Solyman, *et al.*, "Low-complexity LSMR equalisation of FrFT-based multicarrier systems in doubly dispersive channels," in *Signal Processing and Information Technology (ISSPIT), 2011 IEEE International Symposium on*, 2011, pp. 461-465.
- [104] G. H. Golub and C. F. Van Loan, *Matrix Computations*: Johns Hopkins University Press, 1996.
- [105] T. Hrycak, *et al.*, "Low Complexity Equalization for Doubly Selective Channels Modeled by a Basis Expansion," *Signal Processing, IEEE Transactions on*, vol. 58, pp. 5706-5719, 2010.
- [106] H. Hua and W. Le-nan, "Low Complexity LSQR-Based Block Decision Feedback Equalizer for OFDM Systems over Rapidly Time-Varying Channels," in *Communications and Mobile Computing (CMC), 2010 International Conference on*, 2010, pp. 438-441.
- [107] G. Taubock, *et al.*, "Low-Complexity ICI/ISI Equalization in Doubly Dispersive Multicarrier Systems Using a Decision-Feedback LSQR Algorithm," *Signal Processing, IEEE Transactions on*, vol. 59, pp. 2432-2436, 2011.
- [108] C. C. Paige and M. A. Saunders, "LSQR: An algorithm for sparse linear equations and sparse least squares," *ACM Transactions on Mathematical Software (TOMS)*, vol. 8, pp. 43-71, 1982.

- [109] D. C.-L. Fong and M. A. Saunders, "LSMR: An iterative algorithm for sparse least-squares problems," *SIAM J. Sci. Comp.*, vol. Mar 2011, 2011.
- [110] C. C. Paige and M. A. Saunders, "Solution of sparse indefinite systems of linear equations," *SIAM J.*, vol. Numer. Anal., 12 (1975), pp. 617-629, 1975.
- [111] G. Golub and W. Kahan, "Calculating the singular values and pseudo-inverse of a matrix," *Journal of the Society for Industrial & Applied Mathematics, Series B: Numerical Analysis*, vol. 2, pp. 205-224, 1965.
- [112] A. Stamoulis, *et al.*, "Block FIR decision-feedback equalizers for filterbank precoded transmissions with blind channel estimation capabilities," *Communications, IEEE Transactions on*, vol. 49, pp. 69-83, 2001.
- [113] I. Ivan and B. Muquet, "Reduced Complexity Decision Feedback Equalizer for Supporting High Mobility in Wimax," in *Vehicular Technology Conference, 2009. VTC Spring 2009. IEEE 69th*, 2009, pp. 1-5.
- [114] J. Wang and J. Wang, "Feature extraction method of fractional cosine and sine transform for speaker recognition," in *Electronics, Circuits and Systems, 2005. ICECS 2005. 12th IEEE International Conference on*, 2005, pp. 1-4.
- [115] H. Seung Hee and L. Jae Hong, "An overview of peak-to-average power ratio reduction techniques for multicarrier transmission," *Wireless Communications, IEEE*, vol. 12, pp. 56-65, 2005.
- [116] J. Radic and N. Rozic, "Soft decision PAPR reduction in OFDM," in *Systems, Signals and Devices (SSD), 2012 9th International Multi-Conference on*, 2012, pp. 1-3.
- [117] C. Rezgui, *et al.*, "A PAPR reduction technique based on Golay sequences and Fractional Fourier Transform for OFDM systems," in *Computing, Communications and Applications Conference (ComComAp), 2012*, 2012, pp. 383-386.
- [118] W. Sen-Hung, *et al.*, "A Low-Complexity SLM PAPR Reduction Scheme for Interleaved OFDMA Uplink," in *Global Telecommunications Conference, 2009. GLOBECOM 2009. IEEE*, 2009, pp. 1-5.
- [119] Z. Haixia, *et al.*, "Threshold method to reduce PAPR in wavelet based multicarrier modulation systems," in *Information Theory, 2005. ISIT 2005. Proceedings. International Symposium on*, 2005, pp. 1266-1269.
- [120] X. Dan, *et al.*, "PAPR Reduction Of FrFT-Based MB-OFDM Ultra Wide Band Signals," in *Wireless Communications, Networking and Mobile Computing, 2008. WiCOM '08. 4th International Conference on*, 2008, pp. 1-4.
- [121] Y. Ju, *et al.*, "Analysis of peak-to-average power ratio of a multicarrier system based on the fractional Fourier transform," in *Communications Systems, 2004. ICCS 2004. The Ninth International Conference on*, 2004, pp. 165-168.
- [122] L. H. B. a. A. D. Wyner, "Capacity of the Gaussian Channel with Memory: The Multivariate Case," *Bell Syst. Tech. J.*, vol. 53, pp. 745-778, May/June 1974.
- [123] S. M. Alamouti, "A simple transmit diversity technique for wireless communications," *Selected Areas in Communications, IEEE Journal on*, vol. 16, pp. 1451-1458, 1998.

- [124] J. Akhtar and D. Gesbert, "Partial feedback based orthogonal block coding," in *Vehicular Technology Conference, 2003. VTC 2003-Spring. The 57th IEEE Semiannual*, 2003, pp. 287-291 vol.1.
- [125] J. Akhtar and D. Gesbert, "Extending orthogonal block codes with partial feedback," *Wireless Communications, IEEE Transactions on*, vol. 3, pp. 1959-1962, 2004.
- [126] D. Agrawal, *et al.*, "Space-time coded OFDM for high data-rate wireless communication over wideband channels," in *Vehicular Technology Conference, 1998. VTC 98. 48th IEEE*, 1998, pp. 2232-2236 vol.3.
- [127] L. Ding-Bing, *et al.*, "Performance analysis of two-branch transmit diversity block-coded OFDM systems in time-varying multipath Rayleigh-fading channels," *Vehicular Technology, IEEE Transactions on*, vol. 54, pp. 136-148, 2005.
- [128] A. Vielmon, *et al.*, "Performance of Alamouti transmit diversity over time-varying Rayleigh-fading channels," *Wireless Communications, IEEE Transactions on*, vol. 3, pp. 1369-1373, 2004.
- [129] F. Kun, *et al.*, "CTH03-4: Alamouti Space-Time Coded OFDM Systems in Time- and Frequency-Selective Channels," in *Global Telecommunications Conference, 2006. GLOBECOM '06. IEEE*, 2006, pp. 1-5.
- [130] M. N. Hussin, *et al.*, "FrFT-based EO-STBC multicarrier system for transmission over doubly-dispersive channels," in *Wireless Communication Systems (ISWCS), 2012 International Symposium on*, 2012, pp. 686-690.
- [131] C. Toker, *et al.*, "Closed-loop quasi-orthogonal STBCs and their performance in multipath fading environments and when combined with turbo codes," *Wireless Communications, IEEE Transactions on*, vol. 3, pp. 1890-1896, 2004.